The University Of Sheffield.

Optimisation of Low NOx Hydrogen Micromix Combustor

Huanrong Lei

A thesis submitted in partial fulfilment of the requirements for the degree of

Doctor of Philosophy

The University of Sheffield

Faculty of Engineering

Department of Mechanical Engineering

July 2023

ACKNOWLEDGEMENTS

I would like to express my deepest gratitude to all those who have supported me on this journey.

First and foremost, I am always sincerely thankful to my supervisor Prof. Yang Zhang and Dr. Bhupendra Khandelwal, for their invaluable guidance, constant encouragement, and unwavering support throughout the duration of this research. Their expertise and insights have been instrumental in shaping this work and enhancing its quality.

I am also indebted to my colleagues in the office, Dr. Zongyou Zuo, Chenxing Ling, Wenjun Peng, Jinbei Tian, and those people who provided valuable assistance, insightful discussions, and constructive feedback during the course of this study.

I extend my heartfelt thanks to Dr Anis Haj Ayed and Gontzal Lopez Ruiz, who supported me a lot in understanding Micromix Combustion and modelling works. Your contributions have been significant in facilitating the smooth execution of this project.

I am grateful to my friends for their understanding, patience, and unwavering support during this journey. Your constant encouragement and belief in my abilities have been a source of motivation and strength.

Finally, I'd like to express my appreciation to my families, you should know that your love and encouragement were worth more than I can express on paper. You made me a better person and supported me in everything.

This project would not have been possible without the collective efforts and encouragement of everyone involved. Thank you all for being an integral part of this endeavour.

ABSTRACT

The growing environmental concerns have prompted a search for alternative fuel options, leading to the exploration of hydrogen as a promising alternative aviation fuel. Hydrogen's clean energy attributes, with emissions limited to H2O and NOx, make it an attractive candidate for sustainable aviation. However, its integration into gas turbines necessitates the modification of conventional combustors to accommodate hydrogen combustion.

The concept of micromix combustion has emerged as a promising and dynamic solution to address the challenges of safe hydrogen combustion. Aachen University has conducted extensive studies and experiments about micromix combustors in the last decades, and many researchers have also shown great interest in it. The results of these investigations have demonstrated the feasibility and potential of the micromix combustor concept as a viable and effective option for hydrogen combustion.

This project is dedicated to enhancing the performance of the micromix combustor, with a specific focus on improving its NOx reduction capability through geometric modifications of the burner. The optimization process of the micromix combustor is carried out in this thesis through comprehensive numerical simulations utilising ANSYS FLUENT.

Initially, a comprehensive literature review was conducted to assess and evaluate various numerical settings relevant to hydrogen combustion. Different numerical models were compared, and the most suitable settings were selected for subsequent investigations. Specifically, the turbulence model, combustion model, and kinetic mechanisms were thoroughly examined, and suggestions for the numerical model’s selection were made for micromix hydrogen combustion.

Following that, the geometric design of the micromix combustor was studied, involving the modification of parameters such as mixing distance, air gate height, and hydrogen injection pipe diameter. Simulation studies of the modified models were conducted. The results convincingly demonstrated the significant influence of geometric modifications on combustion performance. NOx emissions produced during combustion were successfully reduced by changing the internal geometry of the micromix combustor, and conclusions were drawn regarding the tendency of NOx emission variation with changes in geometric

parameters.

Beyond single micromix combustor elements, the combustion of multi-injection elements has also been studied. The burner was enlarged to reduce the number of elements; in this process, the effects of air gate width variation on flame size and NOx emission were studied. Additionally, a new MIC design was proposed to reduce NOx formation and eliminate the risk of flame merging between adjacent micromix injection elements.

In this project, applying hydrogen/ammonia blended fuel to the micromix combustor was attempted. The numerical simulation study was conducted for different fuel compositions, and the results demonstrated that the addition of ammonia into hydrogen could lower the combustion temperature and slow the burning velocity.

Overall, this thesis has demonstrated the promising potential for enhancing the NOx reduction capability of the micromix combustor through physical modifications. The optimization of the micromix combustor was successfully accomplished by altering the burner's geometry, and the feasibility of utilizing different fuel types in the micromix combustion concept was explored. These findings contribute valuable insights towards advancing cleaner and more efficient combustion technologies.

DECLARATION

I hereby declare that the work presented in this thesis is entirely my original work, except where otherwise indicated. This work has not been submitted for any other degree or qualification. Any contributions from others have been acknowledged. I understand the consequences of academic dishonesty and confirm that all necessary measures to avoid misconduct have been taken. I am solely responsible for the content of this work and its authenticity.

Publication

- H. Lei and B. Khandelwal, "Hydrogen fuel for aviation," in *Aviation Fuels*, Elsevier, 2021, pp. 237–270. doi: 10.1016/B978-0-12-818314-4.00007-8.
- H. Lei and B. Khandelwal, "Investigation of Novel Configuration of Hydrogen Micromix Combustor for Low NOx Emission," Jan. 2020. doi: 10.2514/6.2020-1933.
- P. F. Ghali, H. Lei, and B. Khandelwal, "A Review of Modern Hydrogen Combustor Injection Technologies for the Aerospace Sector," 2021, pp. 523–543. doi: 10.1007/978-981-15-5667-8_21.

NOMENCLATURE

A_{ref}	Reference area of single injection element
AGP	Air Guiding Panels
APU	Auxiliary Power Unit
BR	Blockage Ratio
CFD	Computational Fluid Dynamics
DLN	Dry Low NOx
DNS	Direct numerical Simulation
ED_n	Normalized energy density
E_{ref}	Reference thermal energy
EDM	Eddy Dissipation Model
EDC	Eddy Dissipation Concept Model
FR/ED	Finite Rate/Eddy Dissipation Model
JICF	Jet In Cross Flow
k	Turbulent kinetic energy
LDI	Lean Direct Injection
LEAF	Lean Azimuthal Flame
LES	Large Eddy Simulation
LHV	Low Heating Value
NO_X	Nitrogen Oxides
ppm	Parts-per-million
RANS	Reynolds-averaged Naiver-Stokes
RSM	Reynolds Stress Model

r	Momentum flux ratio
$\bar{S}_{NO}$	Mean turbulent rate of production of NO
u	Fluid Velocity
w_{NO}	Instantaneous molar rate of NO production.
y	Injection Depth
y_{crit}	Critical Injection Depth
Γ_k	Effective diffusivity of k
Γ_ω	Effective diffusivity of ε
ε	Dissipation rate of turbulence kinetic energy
k_f	Forward reaction rate constant
k_r	Reverse reaction rate constant
μ	Fluid Viscosity
ρ	Fluid Density
σ_k	Turbulent Prandtl number for k
σ_ε	Turbulent Prandtl number for ε
ω	Specific dissipation rate
Re_t	Turbulent Reynolds number

CONTENTS

LIST OF FIGURES

LIST OF TABLES

CHAPTER 1: INTRODUCTION

The aviation industry's growth has made air travel and transportation indispensable in modern life. However, the increasing frequency of air flights has raised significant environmental concerns due to the extensive use of traditional fossil fuels. Since the invention of the airplane, gasoline has powered reciprocating engines on aircraft, while jet fuel has been employed in turbo engines over the past few decades. The development of commercial aircraft has undoubtedly benefited the public, but it has also led to a substantial rise in fossil fuel consumption, causing severe global environmental impacts.

Presently, Kerosene and AVGAS are the most widely used aviation fuels, and their combustion results in substantial greenhouse gas emissions, including COx, NOx, and SOx. These emissions are released into the atmosphere, contributing to climate change. Statistics from Turkish airports show that approximately 6% of petroleum products are used as aviation fuels, with their burning responsible for about 3% of NOx and 2.6% of CO2 emissions from total anthropogenic sources [1]. In addition to environmental concerns, the consumption of fossil fuels poses economic challenges. Fossil fuels are non-renewable resources, and as we entered the 20th century, fuel prices began to rise rapidly. This situation calls for the exploration of new, clean alternative energy sources.

Indeed, apart from advancing existing combustion technologies and enhancing combustors, the adoption of alternative clean energy stands out as the most viable solution. The potential for further reducing emissions from current combustion methods is limited, making it crucial to address the issue at its source. Consequently, there has been a growing interest in developing and exploring alternative fuels. Initial investigations have explored various clean renewable energy sources, such as tidal power, solar power, hydrogen power, and wind power. However, among these options, hydrogen power appears to be the most promising for clean power applications in the aviation industry. In contrast to conventional fossil fuels, hydrogen combustion produces only water and nitrogen oxides as by-products, with no emissions of carbon/sulphur-contained gases. Moreover, hydrogen fuel offers numerous advantages compared to other conventional fuels.

Hydrogen fuel presents significant potential as an alternative fuel for the future, although it also comes with practical limitations. In recent research, ammonia (NH_3) has emerged as another viable alternative fuel and fuel additive. NH_3's carbon-free nature, along with its favourable storage and transportation properties, makes it a promising candidate for use in vehicular engines and turbines. However, there are substantial challenges to overcome for successful NH_3 combustion. These challenges include ensuring exceptional performance, durability, and reliability in its application as an alternative fuel, optimizing its combustion properties, and minimizing pollutant emissions. To address these challenges, a comprehensive understanding of NH_3 combustion characteristics, combustion enhancement methods, and strategies for optimizing NOx formation during combustion is essential.

The limited understanding of NH_3 combustion characteristics, the methods to enhance combustion, and the optimization of NOx formation have hindered the widespread adoption of NH_3 as a fuel. Therefore, it is crucial to develop a comprehensive understanding of the combustion and emission properties of pure NH_3 as well as its mixtures with other fuels. This knowledge will be vital for utilizing NH_3 effectively as a power source for transport vehicles, electricity generation, and industrial heating in future energy systems.

As depicted in Figure 1-1, NH_3 can be synthesized from various energy sources, such as wind power, nuclear energy, and fossil fuels with carbon capture and storage (CCS) technology. This process makes NH_3 fully CO_2-free and recyclable, making it a promising carbon-free fuel option with significant potential for the future.

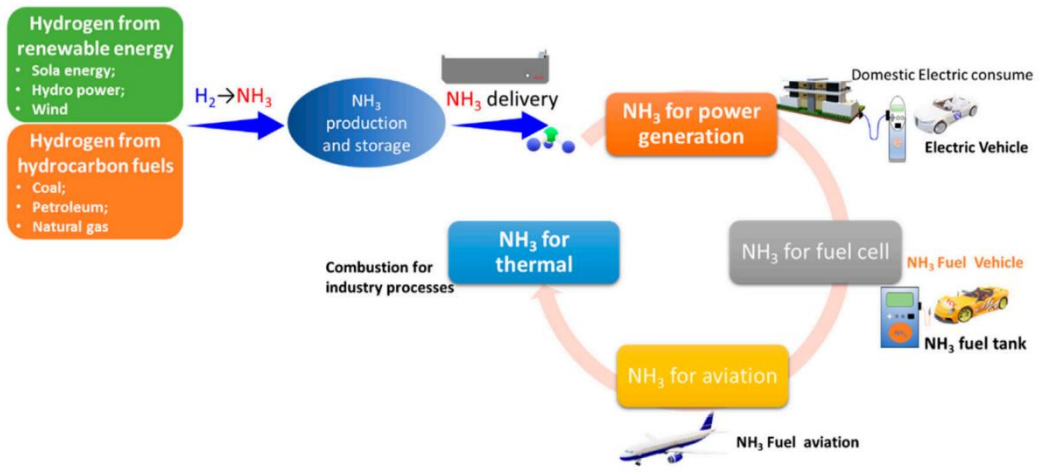

Figure 1-1.Application of NH_3 as a near-zero emission fuel system [2].

1.1 Hydrogen Fuel

1.1.1 Hydrogen fuel properties

During combustion, hydrogen reacts with air to produce only water vapour and nitrogen oxides (NOx). Unlike other fuels, hydrogen fuel does not produce harmful pollutants or particulate matter. The main challenge in hydrogen combustion lies in NOx formation, which is due to the high combustion temperature of hydrogen compared to conventional fuels. To mitigate NOx formation, suitable methods include controlling the combustion equivalence ratio or reducing the flame length[3].

Hydrogen fuel is not only a clean energy source but also boasts the highest energy density, with approximately 120 MJ/kg (excluding the radioactive element)[4]. In contrast, other aviation fuels such as methane and JET-A only have energy densities of about 50 MJ/kg [4], [5]. The low molecular weight of hydrogen gives it a high specific impulse, allowing 1kg/s of hydrogen fuel to provide 450 kg of thrust force. This property has made hydrogen a preferred fuel for space exploration, been used by NASA as the propellant for space shuttles and rockets since the 1970s [6]. Notably, the hydrogen used in rocket propellant is in solid form, as the density of gaseous hydrogen is too low for efficient rocket propulsion.

As indicated by previous studies, hydrogen has the lowest molecular weight among all elements, necessitating much larger storage tanks to hold the same weight of fuel. When comparing hydrogen fuel to conventional kerosene fuel, the volume of hydrogen required is three times larger to achieve the same energy content [6]. This means that if hydrogen fuels are to be used in existing aircraft, although the weight of the fuel tank could be reduced, the space needed for the fuel tank would be significantly larger compared to conventionally fuelled aircraft.

At present, employing solid hydrogen fuel in commercial aircraft is deemed impractical and economically unfeasible. The more viable option is to use hydrogen in its liquid form. However, the storage of liquid fuel presents a complex challenge. For the use of liquid hydrogen, NASA employs vacuum cryogenic tanks to store the fuel at temperatures lower than -423 degrees Fahrenheit [7]. While hydrogen fuel stands as a promising solution for environmental pollution and long-term development, the storage of hydrogen fuel on commercial aircraft remains a significant challenge that must be addressed.

1.1.2 Hydrogen production

In order to implement hydrogen fuels on a commercial scale, addressing the challenge of large-scale production becomes crucial. Before hydrogen-powered aircraft can be widely promoted, the production of hydrogen fuel on an industrial level must be resolved. The International Energy Agency (IEA) has already explored the production of hydrogen, and their findings indicate several feedstocks that can be utilized, including fossil fuels, water, or biomass [8]. Currently, approximately 50% of hydrogen is produced through steam reforming of natural gas, around 30% is reformed from oil/naphtha, 18% from coal gasification, and only 3.9% from water electrolysis, with the remaining 0.1% from other sources [9]. The primary large-scale production process involves producing hydrogen fuel from fossil fuels, which offers low costs and high efficiency. However, this process results in COx emissions as a by-product, undermining the primary objective of using hydrogen fuel for environmental benefits. Therefore, a cleaner method involves splitting hydrogen from water through electrolysis, which utilizes electric power to produce hydrogen. However, this process currently faces challenges due to its high costs, low efficiency, and reliance on electricity generated from fossil fuels.

From the simple water electrolysis method, various improved methods have been developed for hydrogen production, including high-temperature electrolysis, photolysis, and alkaline electrolysis. Among these, high-temperature electrolysis has shown promise as a technology for efficient large-scale hydrogen production [9]. The photo-electrolysis method is also a commercially viable option for large-scale hydrogen gas production, boasting high hydrogen splitting efficiency and relatively low costs. Moreover, photo-electrolysis utilizes solar energy for the production process, eliminating carbon oxide emissions. Establishing photolysis industries in regions with high solar energy potential, such as Algeria, could facilitate large-scale hydrogen production at reduced costs [10].

The basic concept of hydrogen production is illustrated in Figure 1-2 below. The process involves using feedstocks such as water or hydrocarbons, which then undergo an extraction process such as photolysis, electrolysis, or thermochemical methods [11]. During this extraction step, external energy is necessary to facilitate the release of hydrogen molecules. This external energy can be derived from various sources, including hydrocarbons, nuclear energy, or renewable sources. For instance, high-temperature electrolysis may utilize nuclear

energy as the external energy source, while photolysis relies on solar power [11].

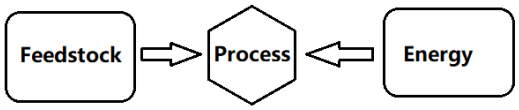

Figure 1-2.Hydrogen production progress

Based on the findings of the two studies [11], [12], photolysis appears to be the most efficient and cost-effective method for hydrogen extraction at present. Although the technology for large-scale hydrogen production as aviation fuel is not yet fully mature, there is significant potential for progress in the future. Moreover, the main focus of this project is on the application of hydrogen fuels and their utilization, rather than the concern of hydrogen fuel supply. Previous studies have already demonstrated the feasibility of industrially producing hydrogen as aviation fuel, indicating promising prospects for the supply of hydrogen for hydrogen-powered aircraft.

1.1.3 Hydrogen fuel storage

At room temperature, hydrogen exists in a gaseous state, but using hydrogen gas or hydride as aviation fuel is impractical due to the large volume and excessive weight of the storage tank[12]. Storing hydrogen in a solid or slush state is feasible, but it requires a significant amount of energy for pressurization and sub-cooling of the hydrogen. However, compared to liquid hydrogen, the density improvement is only about 20% (from 70.8 kg/m3 to 86 kg/m3), making solidification energetically inefficient. Thus, storing hydrogen in its liquid state is the most suitable solution for long-endurance aircraft applications.

To store hydrogen in a liquid state, high pressure and low temperature are necessary. Hydrogen must be cooled to -253°C (approximately 20K) in one atmosphere, or pressurized to 5000 to 10000 psi at room temperature [13].

Despite the advantage of higher energy content (2.8 times of kerosene) in the same weight of fuel, the complex hydrogen fuel supply system partly compensates for this benefit. However, it is anticipated that hydrogen could allow for a higher payload at a given Take-off Weight. On the other hand, for the same weight of hydrogen, the volume of liquid

hydrogen is four times larger than that of aviation kerosene. Consequently, hydrogen fuel requires a significantly larger fuel storage space compared to conventional fuels. Traditional wing storage designs would be too heavy for liquid hydrogen tanks, thus new tank layout designs are being considered to accommodate this unique challenge.

Hydrogen fuel tank configuration

To accommodate the large hydrogen tank in commercial aircraft, the conventional non-integral fuel tank structure is not suitable as the wing structure cannot support the weight of the hydrogen tank. Moreover, the larger volume of the hydrogen tank compared to the kerosene tank leads to increased frontal area and surface, causing higher drag force and affecting the aircraft's aerodynamics. Consequently, an integral tank design has been considered, where the tank is integrated into the aircraft structure.

One feasible approach for large commercial airplanes is to mount the integral tank on the top of the fuselage [14]. Integrating the fuel tank within the aircraft fuselage presents unique challenges in terms of tank shape and weight, especially considering the need to store liquid hydrogen at cryogenic temperatures (around 20K). The insulation and cryogenic devices for the tank are crucial factors in the tank design to ensure proper storage of liquid hydrogen. Therefore, the integral tank design proves to be more suitable for hydrogen-powered aircraft due to the large weight and volume of the cooling and pressurizing equipment required.

In the integral tank design, minimizing the frontal surface area is crucial to reduce weight and heat ingress into the fuel tank. With liquid hydrogen having an extremely low boiling point of -253℃, minimizing heat entry into the tank is essential to prevent fuel loss during storage [12]. The common design shapes for fuel tanks are spherical or cylindrical, mainly for insulation requirements [15], [16]. The spherical geometry is the simplest to design and manufacture, but it may have limited clearance with the existing airframe design. However, it offers the minimum surface area for a given volume, resulting in minimal passive heat conduction into the tank and reduced fuel loss. On the other hand, cylindrical fuel tanks are also widely used, but they have a larger surface area compared to spherical tanks of the same capacity. This means that more heat may be absorbed through the larger surface area, potentially leading to increased fuel loss. Additionally, the pressure inside a cylindrical tank is not evenly distributed, necessitating thicker and larger walls compared to spherical tanks [12]. The length of a cylindrical tank also raises concerns about weight balance due to

sloshing, making it less practical for commercial aircraft integration. As a result, for the same capacity, the weight of a cylindrical tank is greater than a spherical tank. Considering these factors, spherical tank designs appear to be more suitable for integral hydrogen fuel tanks in commercial aircraft.

1.2 Hydrogen powered aircraft

Over the long history of attempts to develop environmentally friendly airplanes over the years, hydrogen-powered airplanes are certainly one of the best options, and as mentioned above, the products of hydrogen combustion are very environmentally friendly compared to other fossil fuels. Hydrogen-powered airplanes have naturally been the target of research for many years.

The initial use of hydrogen power began with its physical properties, and the extremely low density of hydrogen made hydrogen balloons and airships the first applications for aircraft in the 19th century. However, due to the flammable nature of hydrogen, this led to one of history's most famous Hindenburg disasters, 35 passengers died in the airship burning accident. Since then, the hydrogen airship has fallen out of history.

However, the use of hydrogen as an energy source for aviation has not stopped, and in the 20th century, people gradually began to take advantage of the high energy density of hydrogen as a chemical property. In 1937, hydrogen was adopted as a fuel firstly on the simple Heinkel Strahltriebwerk 1 (HeS 1) engine, although the real flight test hadn’t been conducted, this engine burned the hydrogen fuel successfully which paved the path for research on hydrogen aircraft [17].

The debate over the first hydrogen powered air between Air Force B-57B and TU-155 has lasted for many years. People argued that the Air Force B-57B’s engine was not pure hydrogen fuelled. In 1955, under the support of NASA, a B-57B bomber was modified into hydrogen powered aircraft as Figure 1-3 shown below [8]. this bomber has two engines. One of the Curtiss Wright J-65 turbo engines has been modified to burn liquid hydrogen[18]. During the take-off stage, one engine combusted JP-4 aviation fuel and then the hydrogen engine started work after the altitude reached 16400m. The flight test of hydrogen B-57B has been tested three times, the third test was succussed in 1957, the bomber flight 17 mins with the velocity of approximately 0.75 Mach with hydrogen engine alone[19]. In the

experiments, the advantage of hydrogen engine has been found that the thrust could improve 2%~4% but with 60%~70% lower consumption of specific fuel [20]. It also revealed many problems about hydrogen powered aircraft, during the flight Hydrogen tanks are susceptible to pressure problems, additionally, due to the low density of hydrogen, flight endurance is a challenge of hydrogen aircraft development.

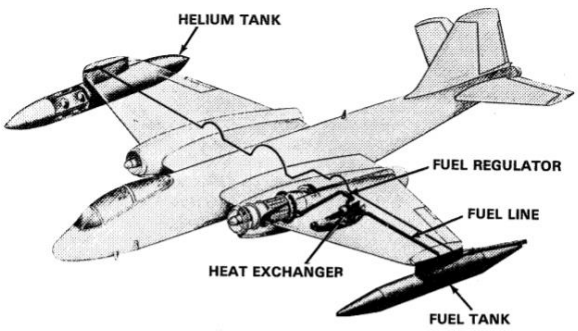

Figure 1-3.Configuration of B-57 hydrogen fuel aircraft [8]

1970s, the Oil Crisis drove for a new path, hydrogen powered aircraft were once again on the map. Soviet Union modified a Tu-154 to test with liquid hydrogen fuel, one of three NK-8 engines was redesigned to burn hydrogen fuel. To increase the endurance ability of Tu-155, partial passenger cabin has been removed and converted to hydrogen fuel storage tanks [21]. The firstly successful flight was achieved in 1988, the hydrogen engine was tested with a maximum speed of 900 km/h. Since then, several flights have been conducted and subsequently stopped due to the high developmental cost and the lack of liquid hydrogen facilities on the ground.

The successful flights of B-57B and Tu-155 have undoubtedly inspired people. In the year 2000, a project called “CRYOPLANE” started. This project focused on the investigation of liquid hydrogen as an alternative fuel for commercial aircraft. During this project, novel tank configurations and aircraft shapes were proposed, and the feasibility of applying hydrogen to conventional turbo engines was discussed. However, although the project believed that a hydrogen-powered commercial aircraft is feasible, it was discontinued due to practical reasons. The utilization of hydrogen fuel posed challenges due to its properties, and storage and transport became significant hurdles. Compared to other fossil fuels and alternative fuels, hydrogen fuel is unattractive [14], [22].

Research on hydrogen aircraft has shown that hydrogen fuel can be utilized as aviation fuel.

However, the development of hydrogen fuel storage has constrained the progress of hydrogen aircraft. Hydrogen has been proven to be a clean fuel with great potential; however, more time is required to support the development of hydrogen fuel technology.

1.3 Ammonia Fuel

1.3.1 Fuel properties

Compared to the in-progress research of hydrogen fuel, the use of ammonia as an alternative fuel has been studied for many years. In the aviation industry, ammonia can be employed as a hydrogen carrier and additive fuel.

Hydrogen fuel, as a clean energy source, can be generated from green sources, such as by electrolysis of water or by photolysis from solar energy. However, as mentioned in the last section, even if hydrogen can be produced cleanly on a large scale, the transport and storage of hydrogen fuel present the main challenges at present. The research on hydrogen fuel is not yet mature, and hydrogen transport pipeline systems are not constructed for most countries and regions. Under these circumstances, the cost of building hydrogen facilities is too high to be accepted. Additionally, due to the properties of hydrogen, storing hydrogen fuel always involves high risk. Therefore, the research and development of alternative methods of hydrogen storage have gained attention, leading to a consensus on the suitability of using ammonia as a hydrogen and energy carrier.

Ammonia as the hydrogen carrier, could produce carbon-free hydrogen directly by thermal cracking process [23], [24]. It provides the chance for hydrogen application to aviation fuels. As the research of ammonia indicated, ammonia has almost the greatest ability to carry hydrogen fuel. The hydrogen density of ammonia is higher than liquid hydrogen per unit volume [25]. Compared to the other potential carriers, as Figure 1-4 shows below, it demonstrates that the gravimetric and volumetric hydrogen densities for different potential carriers, liquid ammonia has the highest volumetric hydrogen density. Hydrogen's density is too small to store and transport, liquid ammonia has much bigger density than Liquid hydrogen (609 kg/m^3 > 71 kg/m^3) but about almost volumetric hydrogen density. By considering the risk and inconvenience of hydrogen fuel storage and transport, ammonia is a suitable carrier for hydrogen with excellent potential.

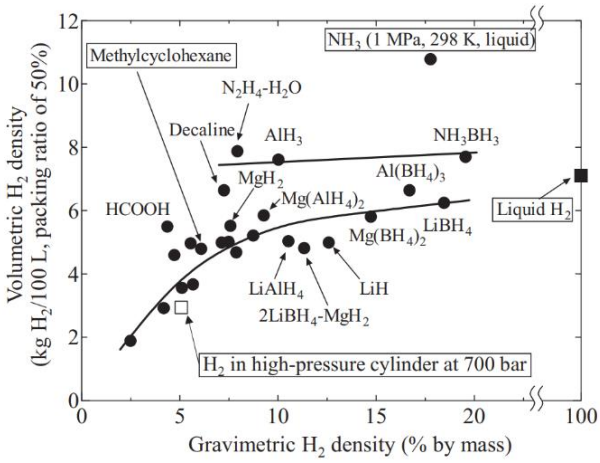

Figure 1-4.Gravimetric and volumetric H_2 density of hydrogen carriers [26]

In addition, ammonia could not only be used as a hydrogen carrier but also as an additive fuel. For pure hydrogen combustion, there is always a problem of flashback risk, due to the high reactivity and high burning velocity of hydrogen. The addition of ammonia into the hydrogen/air reaction could effectively enhance the safety of combustion [27]. Another significance of adding ammonia is the NOx reduction. Although hydrogen combustion could be considered as a clean reaction, low NOx emission is the main research direction of hydrogen fuel applications. The addition of ammonia could lower the flame temperature in the reaction zone, which is the key factor of NOx formation [28]. Although this advantage may be counterweighed by the high containing of N in ammonia. The NH_3/H_2 blended fuel still has a great potential to be used as the aviation fuel, the paper indicates that the NOx production of ammonia/hydrogen blends could be lower than 5ppm under the condition with pressure higher than 10 bar [29].

As Figure 1-5 below illustrates the energy density of liquid ammonia is even higher than that of gaseous natural gas, so ammonia is very good in the combustion system whether it is used as a fuel itself or as a carrier of hydrogen. Although the ammonia could be directly used as fuel, the lower burning velocity and the enormous amount of NOx produced make the blended fuel investigations demanded. The addition of other fuel such as hydrogen could increase the reaction of ammonia and oxidizer. Therefore, in the design of hydrogen combustor, ammonia could be considered as an additive fuel to control the NOx formation level and the supply source of hydrogen fuel. The combustion stability could be improved with the addition of ammonia fuel, and the risk of using hydrogen/ammonia blended fuel could be reduced with the slower burning velocity.

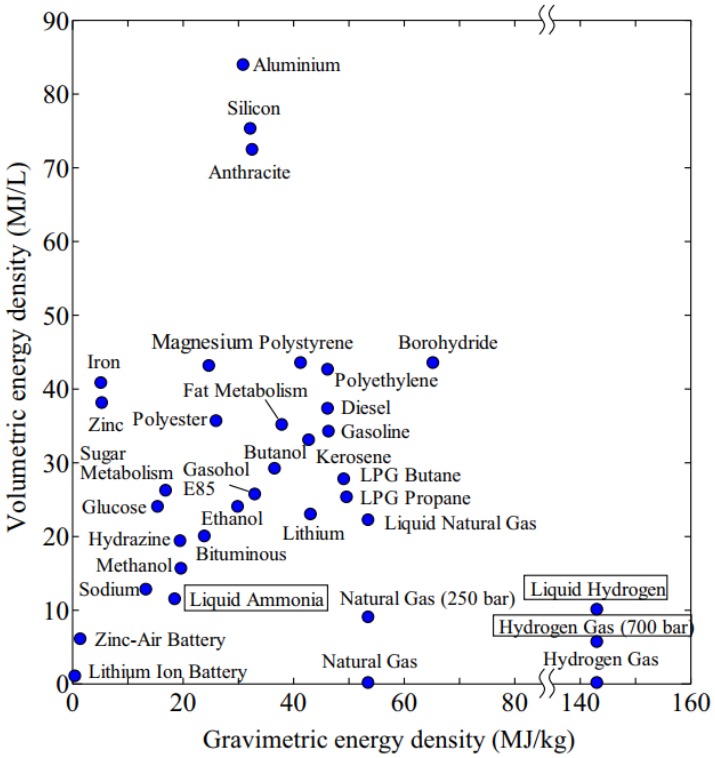

Figure 1-5.Gravimetric and volumetric energy density of combustible materials and batteries [30].

1.3.2 Ammonia production and storage

Over the past century, ammonia has found applications as a raw material in various industries, including manufacturing, agriculture, and power generation. As a result, the production, storage, and transportation of ammonia have become well-established fields. In the aviation fuel industry, ammonia holds significant research potential, with one of its key advantages being the low investment required. The existing mature ammonia industry can contribute to reducing research costs. Presently, the distribution infrastructure for ammonia handles over 100 million tons annually [31].

Traditionally, ammonia was primarily produced through the reaction of pure hydrogen and nitrogen under specific conditions [32]. However, obtaining pure hydrogen for ammonia production consumes significant energy, even with clean methods like photolysis and electrolysis. To address environmental concerns, recent research has focused on developing new technologies for green ammonia production. Studies suggest that ammonia can be produced using wind or solar power, significantly reducing energy costs compared to traditional fossil fuel consumption [33].

Regarding storage and transportation, ammonia has advantages over hydrogen fuel, as it poses a lower risk of explosion and can be stored more easily using cost-effective methods. Ammonia can be liquefied under room temperature and 10 bars, allowing for direct transportation through existing natural gas pipeline systems. In this mode of transport, the energy delivered with liquid ammonia is 1.5 times that of natural gas under the same conditions [34]. These factors contribute to the attractiveness of ammonia as a potential aviation fuel.

1.3.3 Ammonia/ Hydrogen combustor

The utilisation of ammonia fuel was attempted half a century ago. In 1966, the Solar Division of International Harvester Company investigated the ammonia-fuelled gas turbine engine, a Solar T-350 gas turbine engine was modified to operate ammonia fuel [35]. In 1967, Pratt examined the ammonia combustor and conducted a series of studies about it [36]. All these studies show that the combustion of ammonia is more difficult than hydrocarbon fuels. The combustion efficiencies are not satisfied. People found that due to the lower flammability of ammonia, additive fuels are required for ammonia combustors. After many decades, ammonia has been attempted with different fuels on the combustor. In 2015, Japanese researchers investigated a kerosene/ammonia blend fuelled micro gas turbine [37]. The results showed that the addition of ammonia could reduce the consumption of kerosene, but the high NOx formation level is still a problem. During this period, hydrogen has been considered of additive fuel to ammonia because of its physical properties.

At present, there is still no matured hydrogen/ammonia combustor technology in practical applications. Most ammonia/hydrogen combustion studies are based on the lab-scale swirl burner. In 2017, Hayakawa et al. investigated the stabilisation and emission of ammonia combustion in a swirl burner [38]. The results showed that the adopting of swirl burner design, the ammonia/air premixed flame could be stabilized without any additives. The researchers from National Institute of Advanced Industrial Science and Technology (AIST) in Japan further developed the ammonia combustor for power generation in 2019, they investigated a low-NOx ammonia/air non-premixed combustor and further reduced NO formation in the primary combustion zone and improved the combustion of hydrogen produced. Their findings prove that the ammonia combustion technology has the potential for future power generation [39].

In 2021, Franco et al. studied NH3/H2/air combustion in a swirl and bluff body stabilized burner [40]. They found that the NOx emissions would increase with the addition of hydrogen, but the stability of the flame would be increased with the addition of a fraction of hydrogen between 0.2 and 0.4. Their lab-scale combustor showed satisfactory performances which could be further improved for industrial applications.

Researchers also made improvements on the swirling combustion of NH3/H2. Ju's team published a paper of an experimental study on ammonia/hydrogen/air combustion with a plasma-assisted swirl burner [41]. The dielectric barrier discharge (DBD) plasma-assisted combustion technology has been applied to the ammonia/hydrogen blend combustion. As Figure 1-6 shows below, both laminar flame and swirl flame have been studied experimentally, the DBD discharge device was applied to the Bunsen burner and swirl burner. Their results showed that the DBD plasma could increase the laminar burning velocity and improve the kinetic process. In the swirling combustion, the flame structure could be changed by DBD plasma, and the flame volume and turbulent combustion velocity could be increased. For NOx formation, DBD would increase the NOx formation. Therefore, for the DBD plasma-assisted ammonia/hydrogen burner, more studies are required for the combustion of ammonia/hydrogen with plasma reactions.

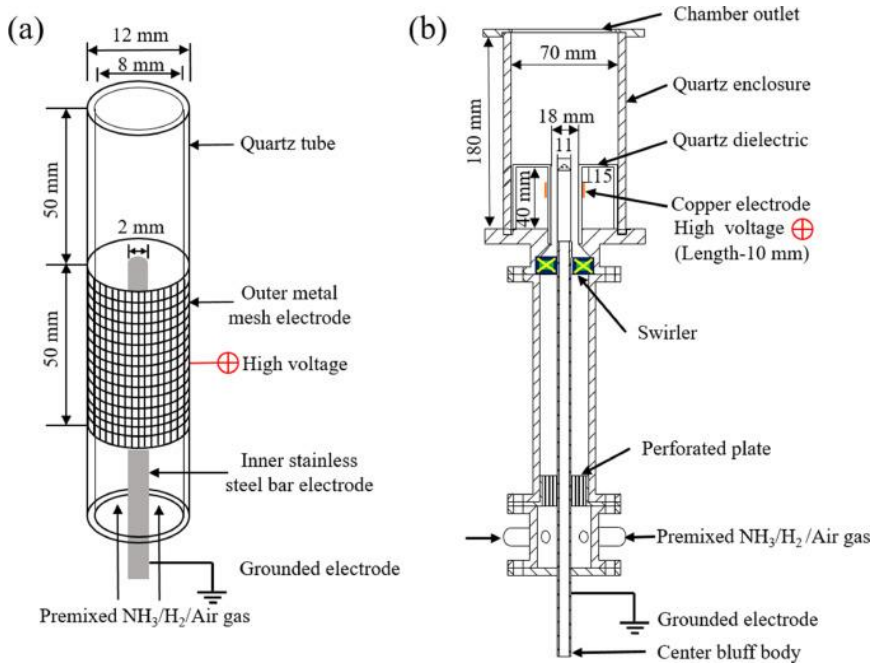

Figure 1-6. Schematic of the burner with DBD discharge, (a) the Bunsen burner;(b) the swirl burner[41].

All these studies show that there are not many existing hydrogen/ammonia burner

technologies, there is still a huge potential for development regarding the mixed combustion of ammonia/hydrogen/air. Applying ammonia-hydrogen blended fuel to a micromix combustor has a big investigable value.

1.4 Aim and Objectives

The main aim of this project is to study the micromix combustor design and further improve the NOx reduction capability. Based on the existing micromix combustor configurations, the geometry of the micromix burner would be modified to study the geometric effects on combustion performance. Based on the numerical study, the aim is to change the geometric parameters of the burner to achieve the purpose of reducing the NOx emission level.

Objectives

Identify the most appropriate numerical method for simulation study of micromix hydrogen combustors.

- To search a relevant micromix combustion experimental data for validation.
- To refine the meshing method to balance accuracy and practicality in numerical simulation.
- To evaluate and compare different numerical models including turbulence models, NOx models, combustion models. Select the most accurate settings for subsequent simulations.
- To search and analyse various combustion mechanisms for hydrogen and hydrogen/ammonia combustion. Select the most suitable mechanism for predicting combustion performance.

Study the geometric modification of burner effects on hydrogen micromix combustion.

- To investigate the impact of internal geometric parameters (e.g. mixing distance, air gate height, and hydrogen injection pipe) on NOx emissions and combustion performance.
- To summarize the trends of geometric parameters on combustion effects.

- With consideration of multi-injection elements combustion, to study the impacts of modification of micromix combustor, target to enlarge burner size and reduce flame merging risk.

Study ammonia/hydrogen blended fuel combustion in micromix combustor.

- To study of impact on NOx emissions of various fuel mixture fractions.
- To study of impact on combustion temperature of various fuel mixture fractions.

1.5 Thesis Outline

This thesis consists of seven chapters, including the introduction, literature review, four main result chapters and a conclusion chapter.

In Chapter One, the introduction about the alternative fuel background is given. The hydrogen fuel properties, production and storage are introduced, as well as the ammonia fuel. The historical application of the hydrogen fuel is reviewed for the hydrogen fuel powered aircraft. The demands for the new technology of hydrogen combustion are identified.

Chapter Two focuses on hydrogen combustion research, where relevant literature is reviewed to identify various types of hydrogen combustors. The primary focus is on addressing the main issue of hydrogen combustion, which is NOx emission, and exploring methods to reduce NOx emissions. The project employs numerical study methods to achieve its objectives. Mechanisms related to hydrogen combustion and hydrogen/ammonia blended combustion are reviewed and analysed. Additionally, various numerical settings are discussed to enhance the accuracy of Computational Fluid Dynamics (CFD) studies conducted in this research.

Chapter Three focuses on achieving an accurate numerical prediction of emissions and combustion performance in hydrogen combustion. Various numerical settings will be studied, compared, and discussed, including the turbulence model, NOx model, and combustion model. The hydrogen combustion mechanisms will also be compared and evaluated to identify the most suitable one for the research. To validate the numerical settings, the modelling results will be compared to relevant experimental data. The main objective is to select an appropriate numerical setup for hydrogen micromix combustion and evaluate the most suitable method for the subsequent numerical study.

Chapter Four is dedicated to the optimization of the detailed geometric parameters of the micromix combustor. This involves modifying various design parameters of the burner and simulating the new design configurations using ANSYS FLUENT software. The main focus is on evaluating the combustion performance and NOx emission levels for each design variant and comparing the results between different designs. The goal is to identify effective optimization methods that can enhance the performance of the low-NOx micromix combustion process. By systematically analysing and comparing the outcomes of different design iterations, the chapter aims to provide insights into the most promising design improvements for achieving lower NOx emissions.

In Chapter Five. Further research on the geometry design of micromix combustor element design and the interaction between multiple injection elements will be presented. For the micromix combustor design, the dimension of single element is important, it determines the number of burner elements and the overall manufacturing cost. In this chapter, possibilities for enlarging the micromix injection elements size will be studied aiming to reduce the flame merging risk and decrease the number of injection elements.

In Chapter Six, the preliminary study of applying hydrogen/ammonia blended fuel to micromix combustor will be presented. The combustion performance and NOx emission with various fuel mixture fractions are discussed in this chapter.

In the last chapter, the main findings of this project will be concluded, the recommendations of future works about this project and micromix combustion development will be given.

CHAPTER 2: LITERATURE REVIEW

The utilisation of hydrogen fuel in conventional combustors presents several challenges that need to be addressed before its practical implementation. This is mainly due to the distinct physical properties of hydrogen, which differ significantly from conventional fuels like Kerosene. Hydrogen has a high burning speed, large diffusivity, and a wide flammability range, leading to a higher risk of auto-ignition. In a conventional combustor, burning fuels typically generates a large-scale centre flame; however, with hydrogen fuel, there is a possibility of the flame burning back along the fuel injectors, which is known as flash-back.[42]. This phenomenon is more likely to occur during ignition when burning high flame speed fuels like hydrogen in conventional gas turbine combustion systems. Overcoming these challenges is essential to ensure the safe and efficient utilization of hydrogen fuel in existing combustors.[43].

Indeed, even if the self-ignition problem is resolved, the high emission of NOx remains another significant challenge in the application of hydrogen fuel. Conventional fuel combustors typically have a limited number of fuel injectors, leading to inadequate mixing of hydrogen and air. As a result, when combustion starts in the combustor, a high-temperature stoichiometric layer is formed in the combustion chamber, along with a large-scale flame. The concentration of high temperatures in the combustor contributes to the production of NOx emissions [44], [45]. As mentioned earlier, the only emission from hydrogen fuel is NOx, and the formation of NOx occurs when the flame temperature exceeds 1800K [46], Once this threshold is surpassed, the NOx formation rate increases with higher temperatures.

Indeed, the utilization of hydrogen fuel necessitates a new design concept for combustors that addresses the challenges of auto-ignition risk and high NOx emissions. This design concept should involve changes to the flame range, which may require smaller and multiple injector holes to improve fuel-air mixing. To reduce NOx emissions, the flame temperature in the combustor chamber must be decreased, along with the residence time of the reaction. Therefore, enhancing the intensity of fuel-air mixing and minimising the flame scale become a critical requirement in this design.

2.1 Hydrogen Combustor

2.1.1 LDI hydrogen combustor

To adapt hydrogen fuel for use in conventional combustors, the injectors play a crucial role. One of the approaches studied by Marek is the modification of a current lean direct injection (LDI) combustor injector [47]. The original design of this injector was based on premixed combustion, which had a high susceptibility to flashback. To address this issue, the injector was modified with multiple injection holes and quick mixing technology. The design aimed to reduce the risk of flashback by minimizing the mixing time and maximizing the mixing velocity, considering that the reaction rate of hydrogen is over 7 times that of conventional Jet-A fuel. Although the LDI injector is essentially a premixed combustion concept, it can also be seen as a type of non-premix concept. In this design, non-premixed air/fuel flows are injected separately and then mixed in small premix zones before combustion [47]–[51].

Previous studies have highlighted that NOx formation is highly influenced by the mixing of fuel and air [52]. The design of the fuel injector plays a critical role in achieving effective fuel-air mixing, which is a key factor in reducing NOx emissions. Another significant factor impacting NOx emissions is the flame temperature. To lower the peak temperature in the combustion chamber, several technologies have been proposed, and one of them is the Lean Direct Injection (LDI) combustion concept. LDI is a novel combustor design that significantly enhances fuel-air mixing to produce lean combustion mixtures. In this concept, the conventional fuel injector is replaced by multiple smaller injectors, creating multiple small burning zones in the chamber, and achieving rapid mixing [53].

To examine the function of the new LDI injector designs, an experiment was conducted in NASA Glenn Research Center [47], for this test the cell 23 of Research Combustion Laboratory (RCL-23) was modified to accommodate gaseous hydrogen fuel [54]. This test facility has completed experimental equipment to simulate different boundary conditions.

The test focused on the injectors, particularly measuring NOx emissions and combustion efficiency. Three gas probes were installed in the combustor chamber to collect the necessary data. The test rig, as shown in Figure 2-1 below, featured a modified fuel injector with a side injection design. Air flow entered the combustor from the front of the injector, while hydrogen was injected perpendicular to the air flow. The detailed design of the

injector, depicted in Figure 2-2 (a) and Figure 2-2 (b), served as the basic concept of the Lean Direct Injection (LDI) combustor. The injector panel comprised multiple rings, with air entering from the front holes and hydrogen injected along the rings' sides through the H_2 orifice. The gases then flowed through the rings, mixing inside. In comparison to conventional combustors, the hot mixed gas stream was divided into multiple smaller streams, reducing the risk of flashback and autoignition. The injection of hydrogen through two opposing holes improved the mixing intensity in the mixing tube.

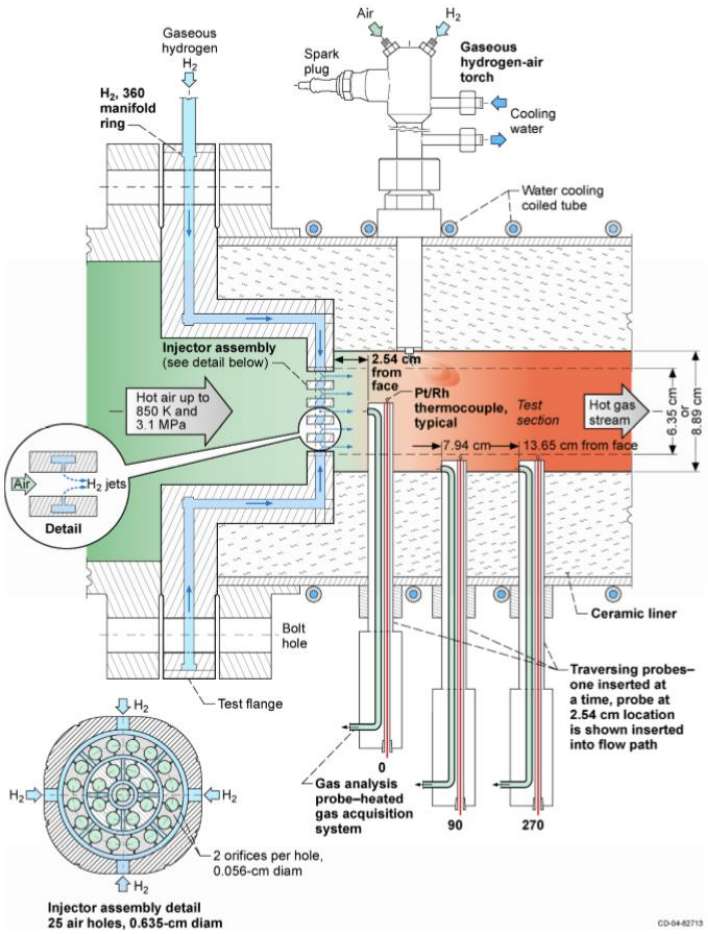

Figure 2-1.Schematic of NASA LDI combustor test rig [47].

In this experiment, the combustor chamber was equipped with three gas sample probes. As depicted in Figure 2-1, a specially designed hydrogen/air torch igniter was installed at the entrance of the combustor chamber. Water-cooling pipes were wrapped around the outside of the combustor chamber for cooling purposes. The three gas probes were positioned at distances of 2.54cm, 7.94cm, and 13.652cm from the injection surface, respectively. Only the first probe was inserted into the flow path, while the other two probes were slightly

above the inner surface of the chamber. Additionally, thermocouples were inserted through the probe into the hot gas stream to measure the temperature [47].

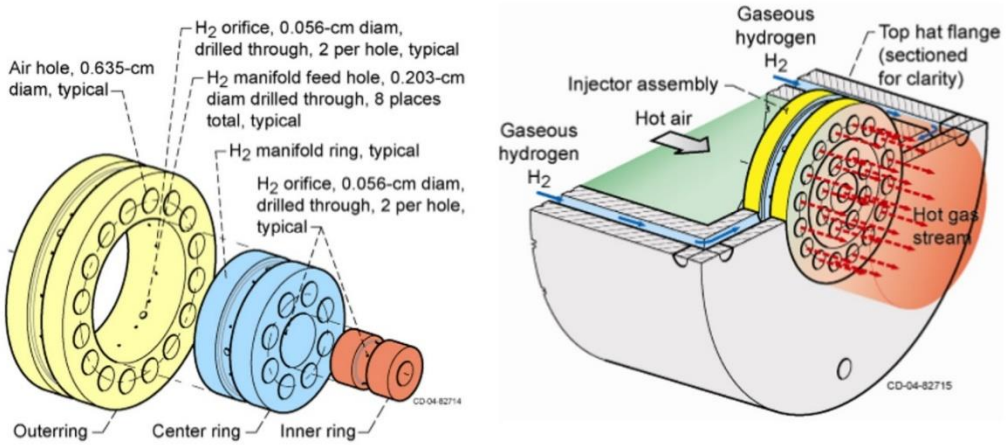

Figure 2-2. (a) Tree-piece injector brazing assembly detail -25 air holes total. (b) NASA low emissions LDI hydrogen combustor assembly[47]**.**

These total five injector designs are shown in Figure 2-3 below. The injector design in Figure 2-3 (a) is the NASA GRC (N1) injector, which was generated at NASA Glenn. The other four injectors in Figure 2-3 (b)(c)(d) were developed from NASA N1 injector and manufactured by experienced major fuel injector manufacturers. These manufacturers have experience in testing the configuration of rocket injectors and low-emission injectors.

The N1 injector configuration consists of 25 injection holes at the air entrance, with hydrogen gas injected from side holes in opposing directions. The crossflow of the jets helps improve mixing and gas penetration [55], [56]. The air and fuel pre-mix in a short distance before entering the combustion chamber. The air inlet has a diameter of 0.25 inches, and the hydrogen injection orifice has a diameter of 0.02 inches.

Figure 2-3 (b) shows the configuration of injector C1, where the simple air inlet has been replaced with a "snowflake" inlet, it has eight air injection holes arrayed around a central hydrogen jet pipe. This design is based on rocket injection technology and creates a rich region for ignition and flame holding near the face using four inner air injection holes. The rest of the air jets create the quench section.

The injector design C2 changes the jet hole shape of the jet holes to triangular which could reduce the size of the jet holes but increase the number of injection elements. Configuration

C3 adds a counter swirler to increase mixing. On the other hand, C4 has the same design as C3 but uses four small radial hydrogen jets instead of a central hydrogen hole.

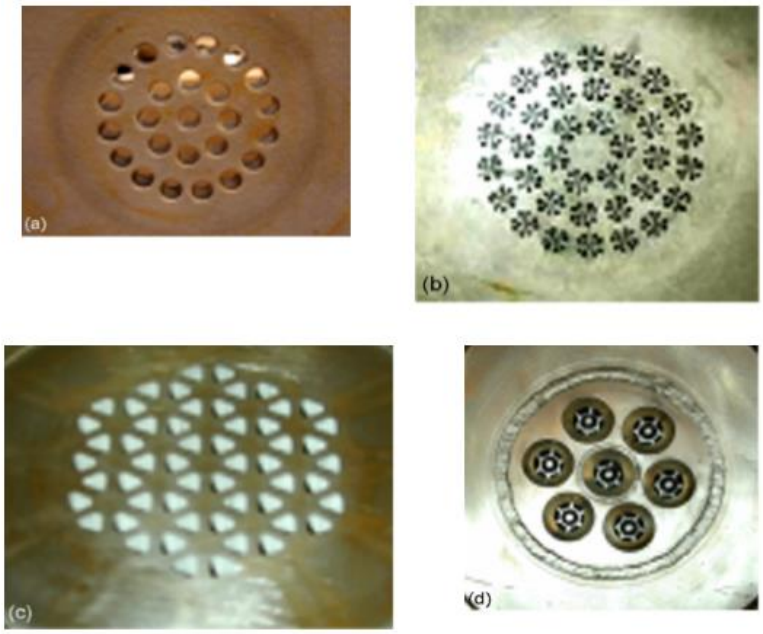

Figure 2-3.Four injectors tested. (a) NASA N1 injector. (b) Configuration C1. (c) Configuration C2. (d) Configuration C3 and Mod C4 [47]**.**

The NOx emission of all the injector configurations was plotted in Figure 2-4 below.

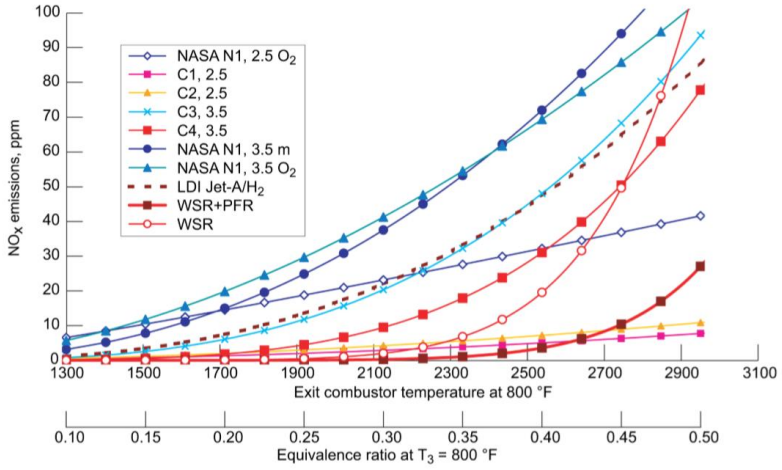

Figure 2-4. NOx emission of different injector designs [47]**.**

Experimental results of N1 injector showed that at the centreline of the combustor, the NOx emission was lower than Jet-A injector, but at the wall area, the NOx value was much higher. Also, with different liners the values are greatly different. In the 3.5-inch liner, the recirculation zones were larger than in the 2.5-inch liner, the residence times also get longer.

Hence the NOx emission is higher than 2.5-inch liner.

In the other injector designs, the C1 injectors were tested with different inlet temperature and pressure. It shows that the NOx emission with different positions is changed, for example at 1-inch position, the NOx is lower but at 3.125 point it grows to double of the Jet-A values. In addition, with higher inlet temperature, the NOx value increased. C2 design has the best performance at the initial. The NOx level was very low, but the cooling and durability affected the later data. The problem with this design is it is difficult to manufacture. C3 performance is very poor. C4 showed a relatively acceptable performance, the NOx values were almost half of the Jet-A over a wide range of equivalence ratios.

In a report by J. Goldmeer, the issue of high NOx formation during hydrogen fuel combustion was discussed [57]. It was noted that the traditional dry low NOx (DLN) system was not suitable to address this challenge directly. This configuration of highly mixed air/fuel in the small-scale injectors significantly reduces NOx emissions. Moreover, the velocity of the gas exiting the injector is higher than the flame speed, minimizing the risk of flashback. A key element of this design is the size of the injector, determining the quench distance of the flame. As the flame propagates through the geometry, it undergoes quenching[57]. Hence, the multiple small-scale injectors could effectively avoid the flashback of hydrogen combustion.

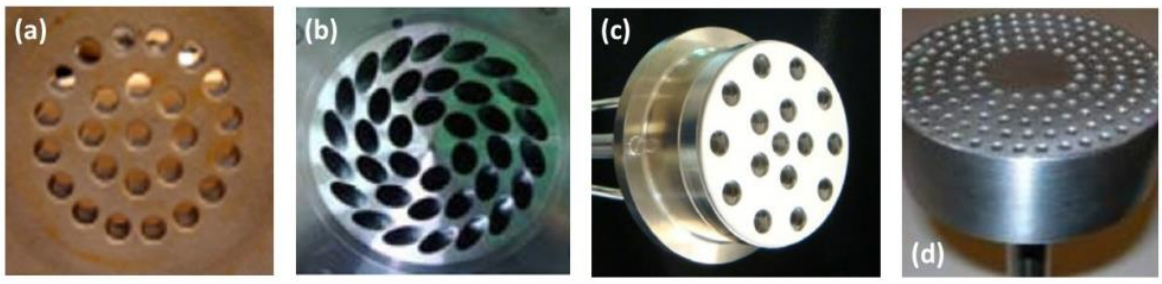

Figure 2-5. Multi-tube mixer concepts, left to right from NASA, Hitachi, Parker Hannifin, and GE Gas Power[57]**.**

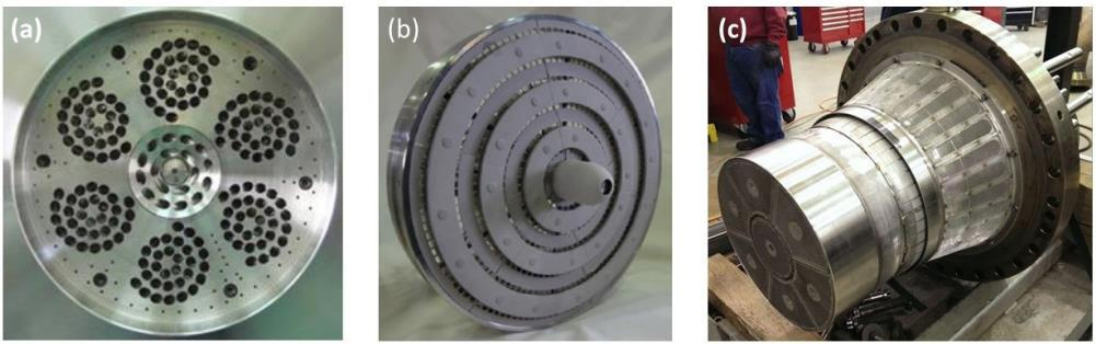

Figure 2-6.Full-scale multi-tube combustion systems used for lab testing and/or commercial operation (a) Mitsubishi Power, (b) Kawasaki Heavy Industries, GE Gas Power [57]**.**

Figure 2-5 and Figure 2-6 above show the multi-tube mixer of recent LDI hydrogen combustors, all these combustors adopted small-size fuel injectors, and the fuel and air achieve rapid mix by using this design. Also, the jet in cross flow (JICF) design has been used to improve the mixing intensity, the jet in of fuel/air flow sheared the primary flow and increased the mixing. This JICF design has also been used in micromix combustor design to improve the fuel/air mixing. The study of these LDI combustors has proven that the miniaturized flame approach could effectively reduce the potential risk of flashback which makes the hydrogen combustion possible.

The overall conclusion from these studies is that the NOx emission is related to the injector configurations. Different injectors showed various emission performances, but the NOx levels were all lower than Jet-A. From the results, it could be found that more injection points could provide a lower level of NOx, but the manufacturing techniques limited the design of the injectors, for a high amount of injection holes design, it might be difficult to build [47]. The concept of the LDI combustor is closely similar to micromix combustor, the multiple injector elements instead of conventional injectors, also the injector configuration designs do affect the NOx emission from combustion. It shows the potential of using multiple small injectors which is further investigated in the micromix combustion concept.

2.1.2 LEAF hydrogen combustor

Lean Azimuthal Flame (LEAF) combustor is a novel concept hydrogen combustor which is could be used on gas turbines. As Figure 2-7 shows below, this concept is based on the opposed of air and fuel injection directions, the air jets are injected at high velocity against the net flow and fuel flows which could create a highly turbulent toroidal reaction zone[58].

The air jet into the reaction chamber could been involved in the recirculation of combustion products which results in the increasing of turbulence and mixing [59].

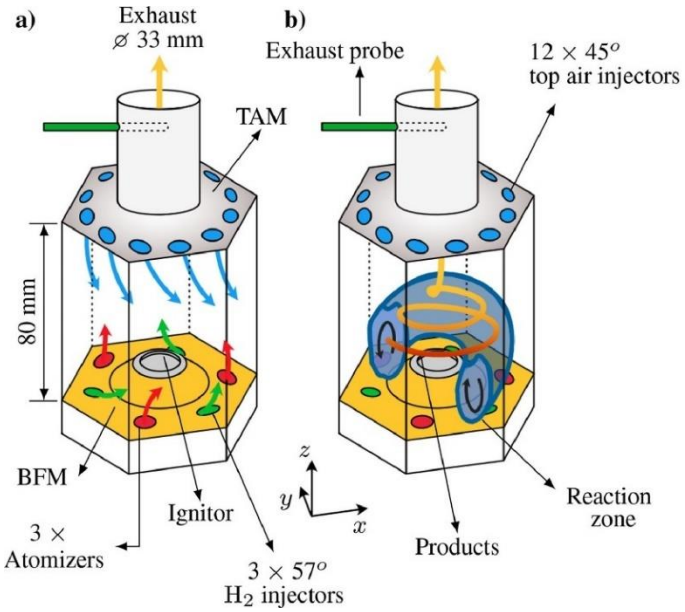

Figure 2-7. Sketch of LEAF combustion [58].

The LEAF combustor had just been proposed in recent few years which is still an idea that has not been fully studied. The different fuel was tested and the hydrogen addition fuel has been studied on it. As the researchers from this project Dr Pedro de Oliveira said, the results obtained from this project have shown that the LEAF combustor could be fuelled by 100% hydrogen [60]. This project was studied by the University of Cambridge and supported by European Commission, Figure 2-8 below shows the lab-scale test burner used in this new project from ETH Zurich. The fuel tested on this combustor was from kerosene, Jet-A to hydrogen, the results show that this new concept combustor has versatility on different fuel types. The tests carried out by the University of Cambridge and ETH Zurich both proved that the pure hydrogen fuel could be combusted in this burner with a low NOx emission level.

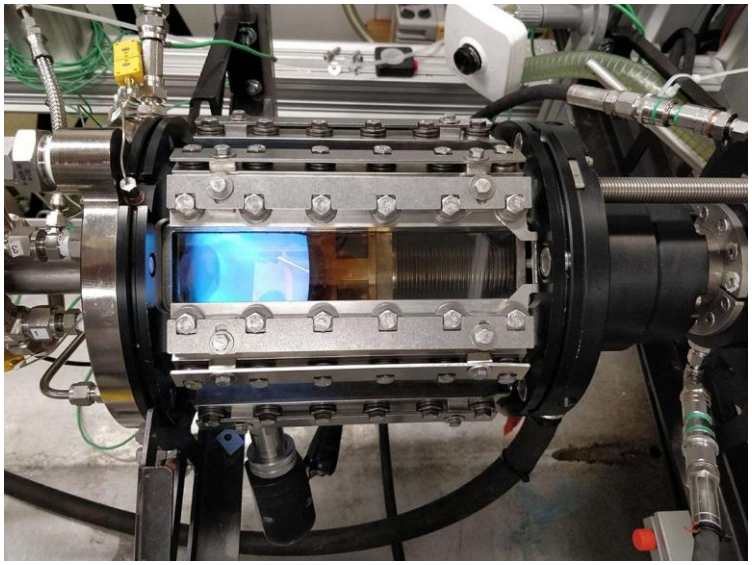

Figure 2-8. LEAF concept at ETH Zurich operated with kerosene and hydrogen [60]**.**

Although the lean azimuthal flame concept is a totally different design from the micromix combustor, it also indicates the future of hydrogen combustion and NOx emissions. The mixing of air and fuel is an important point of hydrogen combustion. This LEAF design is still under development, but it has proven the potential of 100% hydrogen could be used as an aviation fuel in the future, maybe in the next few years more and more research on this concept will emerge, which will further open up the research and application of hydrogen fuel on gas turbine.

2.1.3 Micromix combustor

Fach-hochschule (FHA) Aachen University started the hydrogen combustion study since 1988, FHA successfully converted a small shaft gas turbine engine, KHD T216, into a gaseous hydrogen-powered engine[61]. Building upon this achievement, in July 1994, FHA collaborated with DASA, BGT, ASA, and Sundstrand to work on an Auxiliary Power Unit (APU) GTCP 36-300 of A320. The focus of this research was to convert the conventional A320 APU into a hydrogen-powered APU [44]. While the previous gas turbines designed for burning fossil fuels worked well in a pre-mixing configuration due to the physical properties of natural gas, the highly combustible nature of hydrogen and air mixture posed a high risk of premature burning. To address this challenge, FHA developed a new combustion concept. In this innovative micromix concept, the number of air/fuel mixing zones was significantly increased. The design aimed to minimize the scale of mixing and

maximize the intensity of the air/fuel mixing, to reduce the risk of flashbacks and improve combustion efficiency[44].

In the Micromix combustor concept, the conventional air inlet is replaced by a ringed panel, featuring a large number of injection holes arranged on the main cross-section of the combustor. This design transforms the conventional large-scale flame into multiple miniaturized diffusion flames, aligning closely with the idea of the LDI combustor discussed earlier. By using multiple combustion units, the NOx formation level is significantly reduced, and the risk of flashback is minimized. This modification of the combustor successfully achieves its design purpose. Thousands of hydrogen/air mixture gases enter the chamber and burn into miniaturized diffusion flames, leading to a considerable reduction in the risk of self-ignition. The number of injection holes in principle can be virtually unlimited, even reaching molecular sizes. A combustor inlet section could potentially have millions of air/fuel inlets. The increased number of injectors reduces the scale of mixing zones, allowing for a more thorough and efficient mixture of air and fuel, ultimately contributing to improved combustion performance.

Compared to conventional combustors using fossil fuels, the NOx emissions from hydrogen combustors are considerably lower, but there is still room for further reduction. During hydrogen combustion, nitrogen in the air reacts with the flame, leading to the formation of NOx. To reduce the NOx emission of the hydrogen combustor, the flame temperature needs to be controlled. Additionally, the efficiency of air/fuel mixing plays a significant role in determining the combustion temperature and NOx formation. The micromix concept combustor effectively addresses this issue. By utilizing multiple injectors, the conventional large flames are split into miniaturized diffusion flames, resulting in a substantial increase in the number of local mixing zones. This maximizes the overall mixing intensity of hydrogen and air. Moreover, the improved stirring of fuel and air in the micromix concept combustor generates increased turbulence and eddy breakdown, leading to rapid mixing of local stoichiometric combustion zones. As a result, the residence time of the flame is reduced, and the formation of NOx is decreased[62].

Indeed, while increasing the number of injection holes can enhance mixing intensity and reduce NOx emissions, there are limitations to consider. The miniaturization of flames cannot be taken to an unlimited extent due to two primary factors. Firstly, manufacturing

technology poses a limitation. As the number of injectors increases, their size decreases, reaching a point where existing manufacturing techniques are unable to produce components of such small sizes. Secondly, pressure drop becomes a critical challenge. In modern combustors, the pressure loss should not exceed 3%-4% to maintain efficient operation. The flow energy is utilized to stir the fuel and air, so excessive pressure drop can adversely affect the overall mixing intensity. Therefore, there is a practical limit to the number of injection holes that can be used in the design, taking into account both manufacturing capabilities and the need to maintain acceptable pressure drop levels. Balancing these factors is essential to achieve optimal combustion performance with reduced NOx emissions.

The research findings of the micromix combustion concept by FHA were applied to a practical GTCP 36-300 combustor, and further studies were planned to explore NOx reduction and micromix improvements. This APU was built by AlliedSignal and used for experimental purposes [44]. In this research, the configuration of the combustor has been modified to a hydrogen operated combustor. The schematic comparison between the conventional combustor and the micromix concept combustor of the A320 APU is shown in Figure 2-9, It shows that the inlet section of the original fossil fuel combustor has been replaced with a multiple-hole inlet. The miniaturized injection holes at the combustor inlet guide the air/fuel mixture to burn in numerous miniaturized flames, significantly increasing the mixing intensity of the reactants. Additionally, the shortened flamelet length reduces the residence time in high-temperature regions, contributing to the reduction of NOx emissions[63].

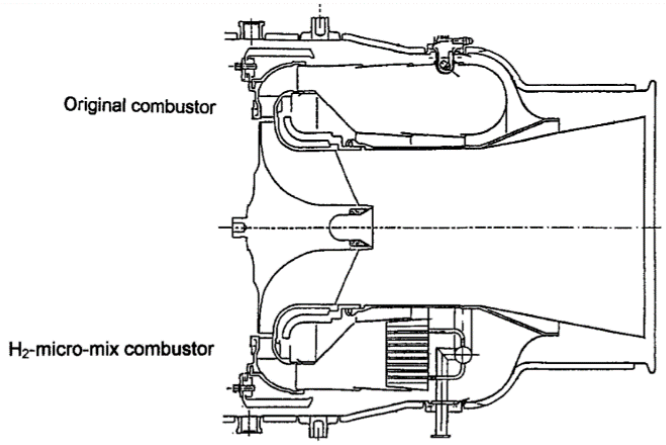

Figure 2-9.The comparison between convention and micromix combustor [44]**.**

In Figure 2-10 shown below, the previous annular combustor inlet was transformed into a ring shape. The combustor consists of two main parts: the hydrogen-segment ring, which contains a large number of micro hydrogen injection holes evenly distributed on it, and the air guiding panels (AGP), consisting of multiple AGP gates corresponding to each hydrogen injector. These modifications enabled the combustor to burn with a thermal loading power of 1.6 MW. Within the combustor chamber, a total of 1600 miniaturized diffusion flames were created, greatly enhancing the mixing of the reactants and promoting efficient combustion.

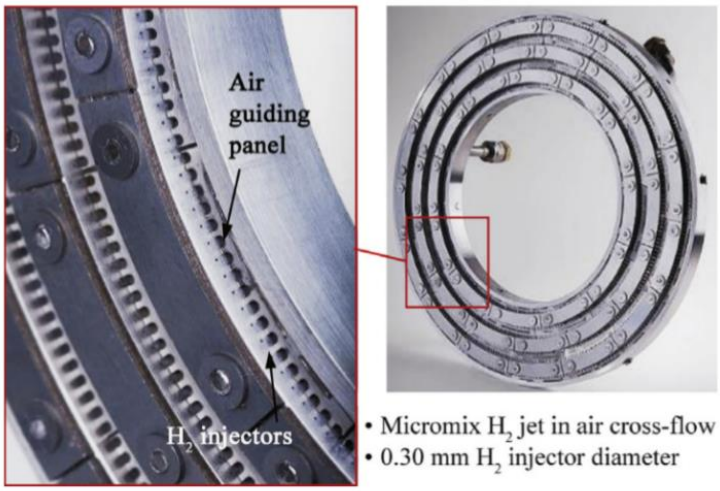

Figure 2-10.Hydrogen micromix injector design [64]**.**

The Air Guiding Panel (AGP) structure plays a crucial role in the micromix concept, and extensive research has been conducted by Funke et al. [61], [63]–[66]. It has shown that the splitting of large-scale flame to micromix flames could lower the residence time of NOx and result in the reduction of NOx level during the combustion [63], [67]. Numerical CFD studies have been conducted to explore the effects of AGP on combustion performance[61], [63]–[66], [68].

The function of the Air Guiding Panel (AGP) is illustrated in Figure 2-11 below, o enhance the mixing ability of the injectors, a new injection method was developed, as shown in Figure 2-11 (b). In this method, hydrogen was injected perpendicularly into the airflow, which accelerated and intensified the mixing of hydrogen and air. This design leads to a reduction in NOx emissions based on combustion principles. The AGP design involves an important parameter known as the Blockage Ratio (BR), which influences the degree of

mixing, flame shape, and other factors related to combustion performance.

Furthermore, the AGP design also affects the injection penetration of fuel into the air stream. As depicted in Figure 2-11 (b), the hydrogen injection depth y, plays a crucial role. If the hydrogen injection depth exceeds the critical injection depth y_{crit}, the fuel will penetrate the shear layer of the AGP vortex, leading to the injection of fuel into the inner vortex. This can result in high temperatures in the vortices region, leading to an increase in NOx emissions [64]. On the other hand, the critical injection depth is influenced by the height of the air gate, which is determined by the AGP design. If the fuel is injected too shallow into the air stream, it can result in insufficient mixing and an increase in NOx formation.

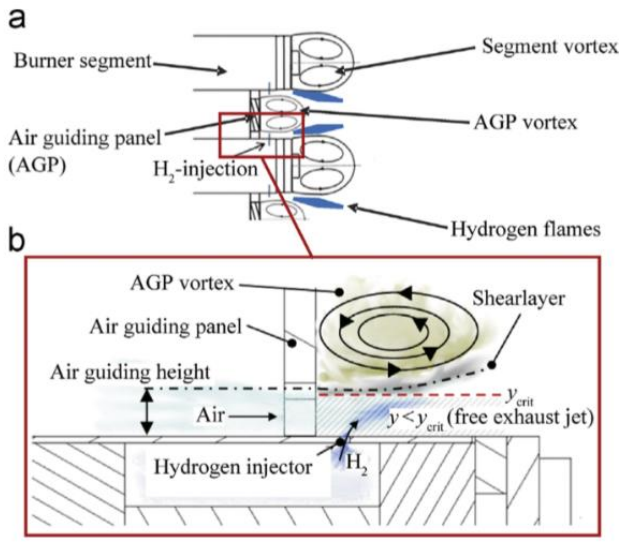

Figure 2-11.Hydrogen cross-flow injection concept [64]**.**

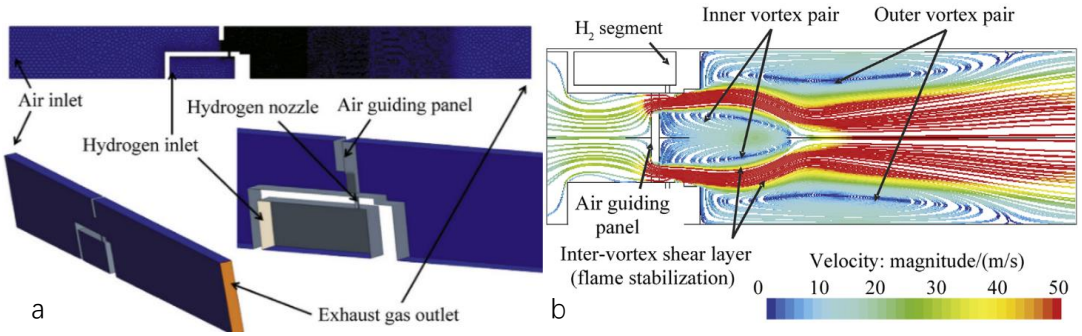

Figure 2-12.-(a) CFD model of micromix combustor. (b) Gas recirculation in the chamber [68]**.**

In their numerical study, Funke et al. [68] investigated the combustion performance of the micromix concept combustor with different BR and geometries of AGP. They discovered that the height of the AGP has a direct influence on the formation of vortices within the

combustor. As depicted in Figure 2-12 (b) two types of vortices are observed: the inner vortex formed as the air flows through the AGP and contracts in the air gate, and the outer vortex created by the recirculation of hot gas downstream of the hydrogen segment. The simulation results show that the air/fuel combustion takes place along the inter-vortex shear layer which is established between the inner/outer vortex. By adjusting the AGP dimension, the size of the vortex could be increased which increases the length of the vortex shear layer and reduces the amount of NOx emissions.

Overall, Funke et al. [68] have shown a high-quality study on the AGP geometry effect on NOx emission, the main objective of this investigation is the gas recirculation in the combustor chamber. By numerical calculation, the gas dynamic behaviour could be directly predicted, the different geometry effects on the vortices formed in the combustor chamber were studied clearly. The studies by Funke et al. [66] have proved that the NOx emission could be effectively reduced about 80% by adjusting the flame profile, it can be achieved by adjusting the injector geometry. The modification of the burner geometry could positively influence the vortex shear layer length which means the combustion zone length and the residence time could be affected. In the paper of Funke et al., the energy density of a single micromix injector has been studied [69]. The study focused on increasing the energy density by increasing the overall size of the single injector element, the NOx emissions have remained at a relatively low level as well.

These papers indicate the path of the physical approach of NOx reduction, the geometric modification could effectively improve the combustion performance of the micromix combustor, which is also been focused in this thesis. In addition, the modification could be further investigated, the increasing of energy density is a path with research potential.

The fundamental geometry of the micromix combustor design investigated was based on a previous study conducted by Ying Chun Li et al. at Cranfield University as well [6]. Their research provided the essential concept of the hydrogen micromix burner and explored various injection methods. The initial design of the combustor featured a main air inlet and four perpendicular hydrogen injection holes. Ying Chun et al. modified the injection method to include two hydrogen jets with two air injectors. They studied two different injection configurations: the first one involved hydrogen injection through four radial injectors, and the second one utilized hydrogen and air injection from two opposite holes. These injection

variations were investigated to assess their impact on the micromix combustion performance.

The results indicated that the different injection methods had a significant impact on the combustion performance and emissions within the chamber. The simulation data revealed distinct temperature distributions between the two injection methods. The second injection method, involving two hydrogen and two air injections, notably reduced the flame length in the chamber. This reduction in the high-temperature zone not only decreased the level of NOx emissions but also made it feasible to reduce the size of the chamber. The modification of the injection method proved to be effective and efficient. In conclusion, this study demonstrated that adjusting the injection method could effectively influence combustion performance, leading to varied flame shapes within the chamber, improved chamber modifications, and extended material lifespan of the chamber.

2.2 Hydrogen Combustion Mechanism

In the numerical simulation of pure hydrogen combustor, the hydrogen-air combustion mechanism is a significantly important part. To obtain an accurate prediction of hydrogen combustion, it highly relies on the precision of the chemical mechanism [70]. Numerous detailed hydrogen combustion mechanisms have been developed and validated with experimental data in previous studies. Examples of such mechanisms include GRI-Mech 3.0, Li's mechanism, and Ó Conaire's mechanism. Among these, GRI-Mech 3.0, developed by the Gas Research Institute (GRI), is widely known and used. The latest version, GRI-Mech 3.0, includes 26 reversible reactions for hydrogen combustion[71]. These mechanisms are commonly employed in research and simulations of hydrogen combustion processes.

Ó Conaire's hydrogen combustion mechanism is widely used in research due to its extensive validation and accuracy. The mechanism was developed based on a large number of experiments conducted by Ó Conaire et al., which involved ignition delay time measurements, flame speed measurements, and burner-stabilized flames. The original hydrogen mechanism used in this research was taken from Mueller et al. [72] The previous paper by Marinov et al. [73] had developed a detailed kinetic mechanism to simulate the sock tube and flame speed. Ó Conaire further refined it to develop a detailed kinetic

mechanism suitable for elevated pressure combustors. A series of comprehensive experiments has been selected to validate the H_2/O_2 combustion mechanism. In total 6 experimental aspects have been studied to evaluate the kinetic mechanism which are listed as follows:

1. The ignition delay times measurement.
2. The flame speed measurements.
3. The high-pressure speed measurement.
4. The very lean Hydrogen/Air and Hydrogen/Air/CO_2/He flame speed measurements.
5. The burner-stabilized flame profile.
6. The comprehensive flow reactor data.

After this series experiment, an enhanced hydrogen combustion mechanism has been developed which is shown in Table 2-1 below. It consists of 19 reversible elementary reactions. It achieved an overall improvement with all the experiments conducted compared to the original kinetic mechanism by Mueller. Compared to the previous works, this hydrogen/air mechanism could provide a more accurate prediction. As conclusion, Ó Conaire et al. [74] were confident that this enhanced hydrogen mechanism could provide a better performance against existing models (2003) for a wider range of physical conditions [74].

	Reaction	A	n	E_a
	H_2/O_2 chain reactions			
1	$H + O_2 = O + OH$	1.91×10^{14}	0.00	16.44
2	$O + H_2 = H + OH$	5.08×10^{4}	2.67	6.292
3	$OH + H_2 = H + H_2O$	2.16×10^{8}	1.51	3.43
4	$H_2 + M = H + H + M$	2.97×10^{6}	2.02	13.4
H_2/O_2 **dissociation/recombination reactions**				
5	$O + O + M = O_2 + M$	4.57×10^{19}	-1.40	105.1
6	$O + H + M = O_2 + M$	6.17×10^{15}	-0.5	0.00
7	$O + H + M = OH + M$	4.72×10^{18}	-1	0.00
8	$H + OH + M = H_2O + M$	4.50×10^{22}	-2	0.00
Formation and consumption of HO_2				
9	$H + O_2 + M = HO_2 + M$	3.48×10^{16}	-0.41	-1.12
	$H + O_2 = HO_2$	1.48×10^{12}	0.6	0.00
10	$HO_2 + H = H_2 + O_2$	1.66×10^{13}	0.00	0.82
11	$HO_2 + H = OH + OH$	7.08×10^{13}	0.00	0.30
12	$HO_2 + O = OH + O_2$	3.25×10^{13}	0.00	0.00
13	$HO_2 + OH = H_2O + O_2$	2.89×10^{13}	0.00	-0.5
Formation and consumption of H_2O_2				
14	$HO_2 + HO_2 = H_2O_2 + O_2$	4.2×10^{14}	0.00	11.98
	$HO_2 + HO_2 = H_2O_2 + O_2$	1.3×10^{11}	0.00	-1.629
15	$H_2O_2 + M = OH + OH + M$	1.27×10^{17}	0.00	45.5
	$H_2O_2 = OH + OH$	2.95×10^{14}	0.00	48.4
16	$H_2O_2 + H = H_2O + OH$	2.41×10^{13}	0.00	3.97
17	$H_2O_2 + H = H_2 + HO_2$	6.03×10^{13}	0.00	7.95
18	$H_2O_2 + O = OH + HO_2$	9.55×10^{06}	2.00	3.97
19	$H_2O_2 + OH = H_2O + HO_2$	1.0×10^{12}	0.00	0.00
	$H_2O_2 + OH = H_2O + HO_2$	5.8×10^{14}	0.00	9.56

Table 2-1. Revised H_2/O_2 Reaction Mechanism of Li [75]**.**

In 2006, Jochen et al. wrote a paper about different reaction mechanisms for hydrogen combustion for gas turbines [76]. They investigated a wider range of hydrogen combustion mechanisms and selected some most relevant mechanisms based on the degree of validation. The mechanism of Li et al. [75], Ó Conaire et al. [74], the San Diego mechanism [77], [78], GRI-Mech 3.0 and Leeds mechanism [71] have been paid more attention. The author conducted a series of comparisons among these five hydrogen combustion mechanisms. These kinetic mechanisms have been compared from ignition delay time calculations and laminar flame speed these two aspects.

For the ignition delay time experiments, the mechanism of Li et al. [75] and Ó Conaire et al. [74] have shown better performance with experimental data. For the flame speed tests, the San Diego mechanism [78] showed a good agreement with the experiment at about 10 atm, the better performance was obtained by the kinetic mechanism of Li and Ó Conaire. Li's mechanism has the best predictions on it. Overall, the mechanism of Li et al. [75] and Ó Conaire et al. [74] showed the best performance on the prediction of hydrogen combustion.

More comparisons of detailed mechanism steps have been discussed by Jochen et al. [76]. For example, the differences of reaction steps R1 and R9 have the impact on the laminar flame speed, the reaction step difference might give different predictions. Li's and Ó Conaire's mechanisms both have 19 reversible reactions, most reactions are kept the same, just several different steps have been updated by them. Li found that the reaction R9 was very sensitive to the consumption of species in a flow reactor, which is a key factor of prediction hydrogen combustion, this reaction has been updated by Li. [76]. As conclusion, the study showed that the mechanism of Li and Ó Conaire could provide an accurate prediction of hydrogen combustion under a gas turbine, but Li's mechanism included more up-to-date data which could provide the best performance for the hydrogen combustion prediction.

A similar assessment of different hydrogen reaction mechanisms has also been studied by Weydahl et al. in 2011 [70]. This study included more kinetic mechanisms than Jochen's work. The comparison of the included mechanism is shown in Table 2-2 below. The mechanism of GRI-Mech, Davis, Konnov, Leeds, San Diego, Li and Ó Conaire have been studied and compared.

With the in-depth study of the hydrogen-oxygen reaction mechanism, more advanced reaction mechanisms are proposed every year. These hydrogen mechanisms are based on the investigation of the existing reaction mechanisms, and the improvements are made based on the previous results to further enhance the accuracy of hydrogen combustion predictions. The experiments under different conditions are undertaken to make the mathematical speculation closer to practical hydrogen combustion. In 2008, an improved H_2/O_2 mechanism was proposed by Hong and his team. The study of this mechanism was based on the shock tube and laser absorption measurements [79].

As the paper of Hong et al. mentioned in the detailed hydrocarbon mechanism, the elementary reactions of H, O, OH, HO_2, H_2O, H_2O_2 are very important. These reactions are almost included in all the stages of hydrogen combustion reaction. Indeed, the existing mechanism never stops the investigation about these reactions. In the last years, several studies focused on the H_2/O_2 reactions and developed the corresponding detailed parameters. However, as the paper from Konnov [80] mentioned there are still many uncertainties about the reaction of HO_2 and H_2O_2. Although the hydrogen combustion mechanism has been studied by many different researchers, the well-known mechanisms such as Li [81] and O'Conaire [74] are widely validated and used, there are some arguments about the reaction of HO_2 radicals. In the paper of Konnov et al. mentioned that in some mechanisms the reaction step is adopted with different reaction equations. As the example shown below, the reaction (2.2) is replaced by the reaction (2.1) compared to Mueller's mechanism [72]:

$$H + HO_2 = H_2O + O \tag{2.1}$$

$$H + HO_2 = OH + OH \tag{2.2}$$

These are the uncertainties which still existed in the mechanism studies. Konnov and his research team made the research on this point. The ignition, oxidation, flame velocities and flame structure of hydrogen combustion are studied based on the considerations of the HO_2 and H_2O_2 uncertainties.

The study of uncertainties in the hydrogen combustion mechanism has inspired Hong. Further studies of H_2/O_2 reaction combustion have been made with the consideration of the remaining uncertainties. Hong et al. explained that most of the previous hydrogen combustion experimental studies were conducted under low-pressure and high-temperature conditions, to get a more thorough understanding of the mechanism. The updated

mechanism by Hong et al. was validated with the specialized experimental conditions. As the conclusion of the paper of Hong et al.[79], the updated mechanism was optimised with the shock tube/laser absorption experiments, the specialized conditions such as the high diluted hydrogen oxidation, the decomposition of H_2O_2 combustion temperature and the instantaneously heated H_2O and O_2 mixture. After several experiments, more accurate rate constants in the reactions which contain H_2O_2, HO_2, and OH radicals have been proposed. The new mechanism showed a good agreement with the experiments about the H_2 oxidation, H_2O_2 decomposition. In addition, this mechanism has validated, the most common requirements such as the ignition delay time, laminar flame speed etc. Although the deeper investigation of the reaction of HO_2 and H_2O_2 radicals mentioned about still required, this mechanism has made improvements in these aspects.

As mentioned above, the reaction mechanism of hydrogen combustion has been widely used and studied. In addition to the several commonly used reaction mechanisms mentioned before, many scholars committed to carrying out the kinetic mechanism and improving on the basis of them. Zsély has been studying and upgrading the hydrogen combustion mechanism since 2005. The paper published in 2005 by Zsély et al. was improved and updated on the basis of the Leeds Methane Oxidation mechanism [82]. Their work was validated with three hydrogen oxidation and two wet CO bulk experiments. In this project, only the hydrogen-related reactions are focused. In their research, Zsély et al. analysed the uncertainties of kinetic parameters and the heat of formation data in the updated mechanism. In the experimental and calculation comparison, the ignition delay data showed good agreement between simulation and experimental data, there are some uncertainties of ignition delays, but it shows small deviations after the time correction. However, the flame velocity always presents some deviation. The calculation results are larger than the experimental data, this is because of the uncertainties mentioned before. Zsély et al. also indicated that although the temperature and concentration of hydrogen oxidation have a relatively good agreement with the measured data in the flow reactor by Yetter et al.[83] the uncertainty of the enthalpy of formation OH still caused the uncertainty of OH concentration calculated [82].

After the paper was published in 2005, Zsély contributed to perfecting the reaction mechanism of hydrogen for decades. The researchers in Eötvös University (ELTE) completed a very detailed comparison of the hydrogen combustion mechanism[84] in 2014.

In their evaluation work, a large set of experimental results was prepared for the comparison of existing hydrogen reaction mechanisms. The datasets include the combustion temperature and pressure with different equivalence ratios in different experiments. Olm et al. aim to compare all the well-known reaction mechanisms of hydrogen in the 21st century.

Based on these experimental data, a total of 19 mechanisms were validated, the accuracy of different mechanisms under different experiment types and conditions was studied and analysed. In this paper, to evaluate the accuracy of calculated data, a specific function was defined. The equation shown below is the tool used to compare the performance of different mechanisms.

$$E_i = \frac{1}{N_i}\sum_{j=1}^{N_i}\left(\frac{Y_{ij}^{sim} - Y_{ij}^{exp}}{\sigma\left(Y_{ij}^{exp}\right)}\right)^2 \tag{2.3}$$

$$E = \frac{1}{N}\sum_{I=1}^{N} E_i \tag{2.4}$$

Where $Y_{ij}\begin{cases} y_{ij} & if\ \sigma\left(y_{ij}^{exp}\right) \approx constant \\ \ln y_{ij} & if\ \sigma\left(lny_{ij}^{exp}\right) \approx constant \end{cases}$

Which N is the number of the datasets, N_i represents the number of data points in the ith datasets. Value of y_{ij} could be defined as the jth data in the ith data sets. σ means the standard deviation. In this function, the error function values E_i and E determine the accuracy of the mechanism, if the values of the error function close to unity it means this mechanism shows good agreement between simulation and experiment.

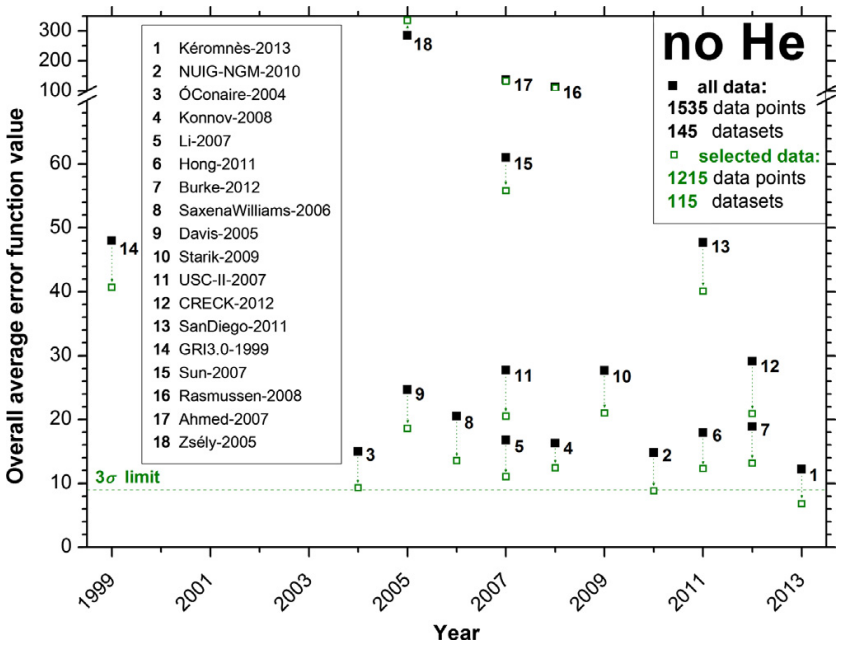

Figure 2-13. Overall performance of the mechanisms [84]**.**

Olm et al. concluded that based on the comparison shown in Figure 2-13, the reaction mechanism of hydrogen by Kéromnès[85] has the best performance among all the tested mechanisms. The widely used mechanism by Ó Conaire[74] also showed good agreements, konnov's and Li's mechanisms [75], [80] have good accuracy as well. The mechanism updated by Zsély in 2005 has bad agreements between simulation and experiments. In this project, the comparison results of different hydrogen combustion mechanisms from this paper will be taken into account while the mechanism selection for the micromix hydrogen combustion simulation.

In Kéromnès' paper, the mechanism of the oxidation process of syngas mixtures was studied in 2013 [85]. In this paper, both the experimental and numerical method have been taken to study the detailed mechanism of syngas under different pressure ranges and temperatures. The test was conducted from the equivalence ratio of 0.1 to 4.0. It's a very comprehensive study of syngas oxidation with variable experimental conditions relative to gas turbine conditions. In the result section, the conclusion involves the hydrogen needs attention. Kéromnès et al. stated that the oxidation stages $H_2 + H\dot{O}_2 \leftrightarrow \dot{H} + H_2 0_2$ and $H_2 0_2(+M) \leftrightarrow \dot{O}H + \dot{O}H(+M)$ are the most important for the prediction ignition delay time under high-pressure and high-temperature conditions. These reactions could improve the reactivity under rich fuel conditions but inhibit the reactivity of flame speed with lean burn. The production of $H\dot{O}_2$ radicals dominated this characteristic, during the formation of $H\dot{O}_2$, $\dot{O}H$

radicals will be formed or consumed. As the paper concluded that the new mechanism from Kéromnès updated some key reaction rate constants and showed a better prediction ability on high-pressure and high temperature compared to several previous studies.

On the basis of the hydrogen reaction mechanism from Kéromnès, the research team from Eötvös University (ELTE) had made the optimisation of the combustion mechanism based on both the direct and indirect experiments data in 2015[86]. They published a paper about the optimisation of the mechanism in 2015, by combining the comparison method discussed before[84]. In 2013, Olm et al. collected a large set of experimental data and made the analysis of different 19 mechanisms. In all those mechanisms the direct measurements were adopted to update the parameters, the indirect measurements were also used which is improving the prediction accuracy by tuning the parameters. Although the parameters used in the existing could provide relatively good performance on the combustion prediction, the mechanism predicting accuracy is different with different experimental conditions.

Compared to the kinetic mechanism optimisation method in the last decades, the mechanism development described in this paper has some differences. In the past, from the first optimisation work by Frenklach and Miller[87] to the optimisation done by Kéromnès et al.[85], majority of the previous mechanism updates select a target first and then optimise the targeted parameter by experiments and calculations. In the paper from Eötvös University (ELTE), a huge number of datasets have been collected for optimisation purposes. In addition, they updated all Arrhenius parameters in their mechanism in 11 reaction steps and produced a new method for the response surfaces generation and global parameters estimation [88].

For convenience purposes, in the project, the new optimised mechanism by T. Varga et al. will be recorded as mechanism ELTE-2015. The results and conclusions in the paper [86] indicated that compared to the other existing mechanisms, the new ELTE-2015 mechanism has the best overall performance. The research shows that the updated 30 Arrhenius parameters and third body collision efficiency parameters improve the prediction accuracy markedly. In different experiments such as the ignition delay time, flame speed etc. the performance of ELTE-2015 showed good agreement with the experiments.

After a systematic study of the hydrogen reaction mechanism, a simple evaluation of the pros and cons of the hydrogen reaction mechanism was made from the description in the

literature. In this project, the above-mentioned mechanism will be used for the simulation of hydrogen micromix combustion, and different reaction mechanisms will be adopted in the simulation to compare with the experimental result. The most appropriate reaction mechanism is then used for subsequent hydrogen combustion simulations work. Since different reaction mechanisms are optimized under different experimental conditions, some reaction mechanisms are optimized for low-temperature and low-pressure hydrogen combustion. Some of the mechanisms are only tested in lab studies. Although the recent mechanism considered about applying for the gas turbine, the new concept of micromix combustion still needs more research to find an appropriate mechanism for the simulation study purposes.

	Reaction	GRI-Mech	Davis	Konnov	Li	Ó Conaire	San Diego	Leeds
(1)	$H + O_2 = O + OH$	$2.65 \cdot 10^{16}, -0.7,$ 17041	$2.64 \cdot 10^{16}, -0.7,$ 17041	$2.06 \cdot 10^{14}, -0.1,$ 15022	$3.55 \cdot 10^{15}, -0.4,$ 16599	$1.91 \cdot 10^{14}, 0.0,$ 16440	$3.52 \cdot 10^{16,}$ $-0.7, 17070$	$9.76 \cdot 10^{13}, 0.0,$ 14821
(2)	$O + H_2 = H + OH$	$3.87 \cdot 10^{4}, 2.7,$ 6260	$4.59 \cdot 10^{4}$,2.7 6260	$5.06 \cdot 10^{4}, 2.7,$ 6290	$5.08 \cdot 10^{4}, 2.7,$ 6290	$5.08 \cdot 10^{4}, 2.7,$ 6292	$5.06 \cdot 10^{4}, 2.7,$ 6291	$5.12 \cdot 10^{4}, 2.7,$ 6277
(3)	$OH + H_2$ $= H + H_2O$	$2.16 \cdot 10^{8}, 1.5,$ 3430	$1.73 \cdot 10^{8}, 1.5,$ 3430	$2.14 \cdot 10^{8}, 1.5,$ 3450	$2.16 \cdot 10^{8}, 1.5,$ 3430	$2.16 \cdot 10^{8}, 1.5,$ 3430	$1.17 \cdot 10^{8}, 1.3,$ 3635	$4.52 \cdot 10^{8}, 1.6,$ 18401
(8a)	$H + OH + M$ $= H_2O + M$	$2.20 \cdot 10^{22}, -2.0,$ 0.0 $H_2O = 3.65$ $H_2 = 0.73$ $AR = 0.38$	$4.40 \cdot 10^{22}, -2.0,$ 0.0 $H_2O = 6.3$ $H_2 = 2.0$ $AR = 0.38$	$6.06 \cdot 10^{27},$ $-3.3, 120770$ $H_2O = 0$ $H_2 = 3.0$ $N_2 = 2.0$ $O_2 = 1.5$	$3.80 \cdot 10^{22},$ $-2.0, 0.0$ $H_2O = 12$ $H_2 = 2.5$ $AR = 0.38$	$4.50 \cdot 10^{22},$ $-2.0, 0.0$ $H_2O = 12$ $H_2 = 0.73$ $AR = 0.38$	$4.00 \cdot 10^{22},$ $-2.0, 0.0$ $H_2O = 12$ $H_2 = 2.5$ $AR = 0.38$	$5.53 \cdot 10^{22},$ $-2.0, 0.0$ $H_2O = 2.55$ $N_2 = 0.4$ $O_2 = 0.4$ $AR = 0.38$
(9a)	$H + O_2(+ M)$ $= HO_2$ $(+M)$ $H + O_2 = HO_2$	$2.80 \cdot 10^{18}, -0.9,$ 0.0 $H_2O = 0$ $H_2 = 0$ $N_2 = 0$ $AR = 0$	$5.12 \cdot 10^{12}, 0.4,$ 0.0 [6.3 $\cdot 10^{19}, -1.4, 0.0]$ $F_e = 0.5$ $O_2 = 0.85$ $H_2O = 12$ $H_2 = 0.75$ $AR = 0.4$	$4.66 \cdot 10^{12,}$ 0.4, 0.0 [5.7 $\cdot 10^{19}, -1.4, 0.0]$ $F_e = 0.5$ $O_2 = 0$ $H_2O = 0$ $H_2 = 1.5$ $AR = 0$	$1.48 \cdot 10^{12}, 0.6,$ 0.0 [6.4 $\cdot 10^{20}, -0.17, 5248$ $F_e = 0.8$ $O_2 = 0.78$ $H_2O = 11$ $AR = 0$	$1.48 \cdot 10^{12}, 0.6,$ 0.0 [3.5 $\cdot 10^{17}, -1.4, -1120$ $F_e = 0.5$ $O_2 = 0.78$ $H_2O = 14$ $H_2 = 1.3$	$4.6 \cdot 10^{12}, 0.4,$ 0.0 [5.7 $\cdot 10^{19}, -1.4, 0.0]$ $F_e = 0.5$ $O_2 = 0.85$ $H_2O = 16$ $H_2 = 2.5$ $AR = 0.7$	2.10 $\cdot 10^{18}, -0.8, 0.0$ $O_2 = 0.4$ $H_2O = 0$ $H_2 = 0.75$ $N_2 = 0.67$ $AR = 0.29$
(10)	$HO_2 + H$ $= H_2 + O_2$	$4.48 \cdot 10^{13}, 0.0,$ 1068	$5.92 \cdot 10^{5}, 2.4,$ 53502	$1.05 \cdot 10^{14,}$ 0.0, 2047	$1.66 \cdot 10^{13}, 0.0,$ 823	$1.66 \cdot 10^{13,}$ 0.0, 820	$1.66 \cdot 10^{13}, 0.0,$ 823	$4.28 \cdot 10^{13}, 0.0,$ 1048
(11)	$HO_2 + H$ $= OH + OH$	$8.40 \cdot 10^{13}, 0.0,$ 635	$7.48 \cdot 10^{13},$ 0.0 ,295	$1.90 \cdot 10^{14}, 0.0,$ 875	$7.08 \cdot 10^{13}, 0.0,$ 295	$7.08 \cdot 10^{13,}$ 0.0, 300	$7.08 \cdot 10^{13}, 0.0,$ 295	$1.69 \cdot 10^{14},$ $0.0, 883$
(13)	$HO_2 + OH$ $= H_2O + O_2$	1.45 $\cdot 10^{13}, 0.0, -500$	$2.38 \cdot 10^{13}, 0.0,$ -500	$2.89 \cdot 10^{13},$ 0.0, -500	$2.89 \cdot 10^{13},$ 0.0, -497	$2.89 \cdot 10^{13,}$ 0.0, -500	$2.89 \cdot 10^{13},$ 0.0, -497	$2.89 \cdot 10^{13},$ 0.0, -500
(13d up)	$HO_2 + OH$ $= H_2O + O_2$	$5.00 \cdot 10^{15},$ 0.0,	$1.00 \cdot 10^{16},$ 0.0,	$9.27 \cdot 10^{16},$ 0.0,				

		17330	17730	17500				
(14)	$HO_2 + HO_2 = H_2O_2 + O_2$	$4.20 \cdot 10^{14}$, 0.0, 12000	$3.66 \cdot 10^{14}$, 0.0, 12000	$1.03 \cdot 10^{14}$, 0.0, 11040	$4.20 \cdot 10^{14}$, 0.0, 11982	$4.20 \cdot 10^{14}$, 0.0, 11980	$3.02 \cdot 10^{12,}$ 0.0, 1386.2	$4.22 \cdot 10^{14}$, 0.0, 11957
(14d up)	$HO_2 + HO_2 = H_2O_2 + O_2$	$1.30 \cdot 10^{11}$, 0.0, -1630	$1.30 \cdot 10^{11}$, 0.0,-1630	$1.94 \cdot 10^{11}$, 0.0, -1409	$1.30 \cdot 10^{11}$, 0.0, -1629	$1.30 \cdot 10^{11}$, 0.0, -1629		$1.32 \cdot 10^{11}$, 0.0, -1623,
(15a)	$H_2O_2(+M) = OH + OH(+M)$	$7.04 \cdot 10^{13}$, $-0.4, 0.0$ $[2.3 \cdot 10^{18} - 0.9 - 1700]$ $H_2O = 6$ $H_2 = 2$ $AR = 0.7$	$1.11 \cdot 10^{14}$, $-0.4, 0.0$ $[2.0 \cdot 10^{17} - 0.58 - 2293]$ $H_2O = 6$ $H_2 = 2$ $AR = 0.7$	$1.00 \cdot 10^{14}$, $-0.4, 0.0$ $[2.4 \cdot 10^{19} - 0.8\ 0.0]$ $F_e = 0.5$ $H_2O = 0$	$2.95 \cdot 10^{14}$, 0.0, 48430 $[1.2 \cdot 10^{17}0.00$ 45500] $F_e = 0.5$ $H_2O = 12$ $H_2 = 2.5$ $AR = 0.64$	$2.95 \cdot 10^{14}$, 0.0, 48400 $[1.3 \cdot 10^{17}0.0$ 45500] $F_e = 0.5$ $H_2O = 12$ $H_2 = 2.5$ $AR = 0.64$	$7.04 \cdot 10^{13}$, $-0.4, 0.0$ $[2.3 \cdot 10^{18} - 0.9 - 1700]$ $H_2O = 6$ $H_2 = 2$ $AR = 0.7$	$7.23 \cdot 10^{13,}$ $-0.4, 0.0$ $[5.6 \cdot 10^{19} - 0.76\ 0.0]$ $H_2O = 6.5$ $N_2 = 0.4$ $O_2 = 0.4$ $AR = 0.35$
17	$H_2O_2 + H = H_2 + HO_2$	$1.21 \cdot 10^{7}$, 2.0, 5200	$6.05 \cdot 10^{6}$, 2.0, 5200	$1.70 \cdot 10^{12}$, 0.0, 3755	$4.82 \cdot 10^{13}$, 0.0, 7950	$6.03 \cdot 10^{13}$, 0.0, 7950	$4.79 \cdot 10^{13}$, 0.0, 7950	$1.69 \cdot 10^{12}$, 0.0, 3747

Table 2-2. Overview and comparison of reaction rate coefficients for the most important H2/O2 reactions [70]

2.3 NOx Emission Formation

Using hydrogen and ammonia as aviation fuels offers the advantage of being carbon-free, addressing concerns about carbon emissions and their impact on the environment. However, the combustion of these fuels can still lead to the production of NOx emissions, which need to be addressed. Regardless of the type of combustor used, NOx will be generated during combustion. Therefore, to effectively reduce the NOx emissions from hydrogen combustion, it is crucial to study and understand the factors that may influence NOx formation.

Several factors can affect the generation of NOx, including the temperature of combustion, the duration of residence, the mixing of air and fuel, the type of fuel used, the pressure inside the combustion chamber, and the temperature at the inlet. Numerous research papers have explored the impact of these variables on NOx formation, the results will be discussed later [46], [89]–[92].

2.3.1 Combustion temperature

The combustion temperature is a critical factor that significantly influences the conversion ratio of NOx. Extensive experimental and numerical studies have consistently demonstrated that NOx is predominantly produced in the high-temperature regions of the flame. Research has shown that when the combustion temperature exceeds 1800K, the formation rate of NOx increases rapidly [46]. In a study by Nakata et al. [93]. shown that when burning other types of fuels, the NOx production will be affected by the reaction temperature. Figure 2-14 illustrates the NO mole fraction under various reaction temperatures. The plot clearly indicates that the mole fraction of NO produced varies with changes in temperature, rate of NO formation raised with higher temperature. Below 2000K, the NO formation remains relatively constant at a mole fraction of 10^-4, but as the reaction temperature rises, the formation rate increases significantly. On the other hand, if the reaction temperature can be kept below 800K,

the amount of NO produced can be greatly reduced, even approaching negligible levels [46].

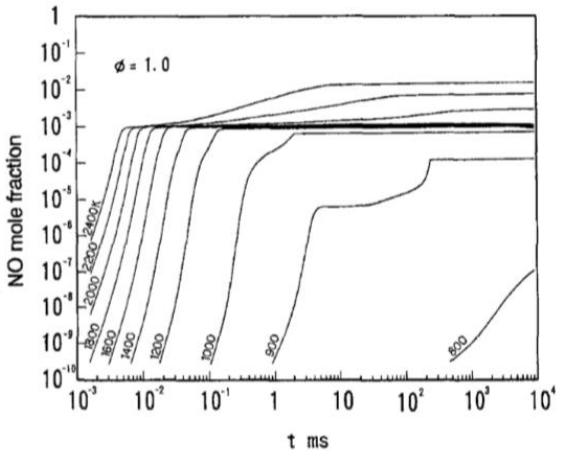

Figure 2-14.Effect of reaction temperature on NO formation [18].

2.3.2 Mixing intensity

In addition to the combustion temperature, the intensity of air and fuel mixing also plays a significant role in the formation rate of NOx. The impact of secondary-air mixing conditions has been investigated in the study conducted by Nakata et al. [46], [93]. During the test, the results of a combustor in 1990 were compared with the same combustor but with modifications to facilitate the mixing of secondary air. The comparison is depicted in Figure 2-15, where the triangle represents the results with secondary air mixing. It can be observed that with improved secondary air mixing, which leads to a slower mixing process, the intensity of air and fuel mixing is enhanced, resulting in a reduction in the amount of NO formation.

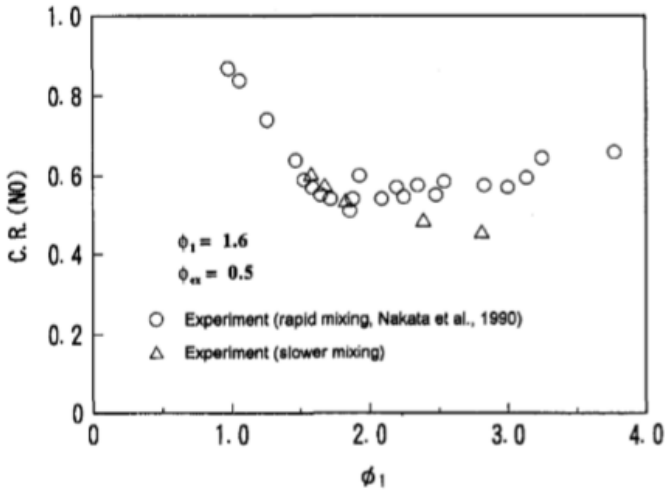

Figure 2-15. Experimental NO emission comparison of the tested combustor [46]**.**

2.3.3 Resident time

During combustion, not only the temperature but also the residence time of the reaction can influence the formation of NOx. Previous studies on NOx formation during combustion have shown that NOx emissions increase with longer combustion residence times [92], [94]. In a study conducted by Steele et al.[92] they modelled NOx formation at constant combustion temperatures but varied residence times and pressures. The results in Figure 2-16 (a) indicate that when the combustion temperature remains constant, a longer residence time leads to an increase in the amount of NOx produced. The plotted curves also reveal that increasing the pressure results in a higher rate of NOx formation[92]. Another study from Lefebvre also mentioned about the influence of combustion residence time, based on the results from Anderson's investigation [95], the NOx formation amount during the propane combustion with residence time changing has been plotted in Figure 2-16 (b) [94]. Figure 2-16 (a) below demonstrates the NOx emission amount increase with the increase of residence time which shows a similar tendency in Figure 2-16 (b) [94]. Additionally, the curve in Figure 2-16 (b) indicates that at very lean premixed combustors, such as an equivalence ratio of 0.4, NOx formation does not vary with residence time.

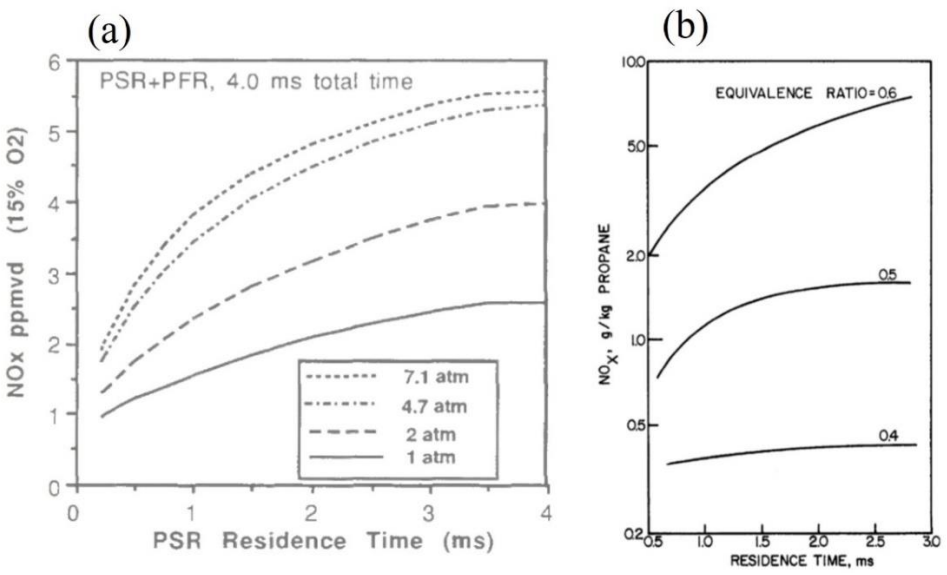

Figure 2-16. (a) PSR residence time effects on NOx[92]**. (b) NOx emission against residence time**[94]**.**

However, the dependence of NO formation on residence time is not that absolute, in the paper of Lee et al. studied the effect of temperature and residence time on NOx decomposition and formation in thermal reactor. The SNCR technology was used to reduce the NOx formation during combustion. The conclusion indicates that the NOx formation rate would decrease with the residence time at some specific condition [96]. Another paper from Rutar et al. in 1988 stated a similar conclusion about the NOx dependency on residence time [97]. The relation between NOx formation and residence time and inlet temperature was investigated in this paper, the experiments were conducted with the jet-stirred reactor at 6.5 atm, in the experiments the fuel used is methane and the combustion temperature is maintained at about 1803K. As Figure 2-17 The results show that the NOx formation level reduced between the residence time 0.5ms to 2.5ms and reached the lowest point at 2.5ms. The paper indicates that this situation may be related to the stirred reactor, at residence time 2.5 to 4ms, the gases are enriched and cause the reactor temperature to rise, this could be the reason of the NOx increase.

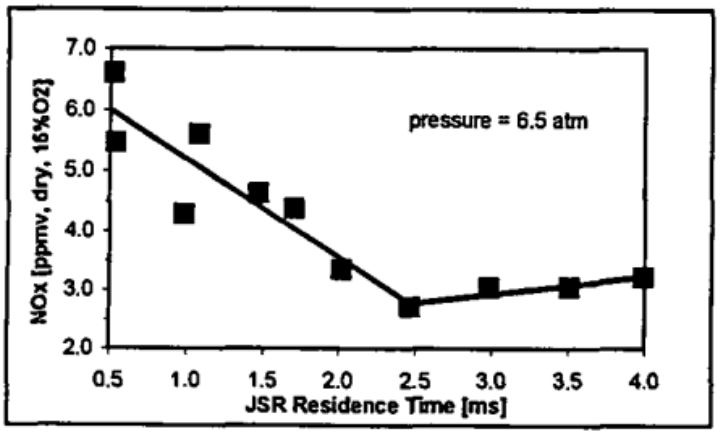

Figure 2-17. NOx formation against JSR residence time/ms [97]**.**

2.3.4 NOx formation type

During all the combustion which includes the nitrogen atoms, the NOx is produced. Generally, the NOx emission includes most NO and a minor degree of NO_2 and N2O. In this project, the NOx emission prediction of hydrogen combustion is achieved by the post-process tool of the software Fluent. The NOx prediction depends on the combustion simulation, the NOx transport equations are solved based on the prediction of the reaction solution which means that the temperature and flow field during combustion must be predicted to a very high degree of accuracy if accurate NOx emission modelling needs to be obtained. There are mainly three types of NOx formation in Fluent which are thermal NOx, prompt NOx and fuel NOx.

2.3.4.1 Thermal NOx formation

Thermal NOx is the nitrogen oxide formed during high temperature combustion, which is highly dependent on the temperature. The formation steps of thermal NOx are widely used by extended Zeldovich mechanism. The extended Zeldovich mechanism used to govern the thermal NOx produced could be represented in the following equations [62]:

$$O + N_2 \rightleftharpoons N + NO \tag{2.5}$$

$$N + O_2 \rightleftharpoons O + NO \tag{2.6}$$

$$N + OH \rightleftharpoons H + NO \tag{2.7}$$

During the combustion, large amounts of thermal NOx formation are produced once the temperature of the reaction zone reaches 1800K. With the temperature increase, the thermal NOx production rate increased exponentially when the temperature was beyond 2200K. The atom bond of Nitrogen and oxygen molecules breaks in the high temperature condition and the atoms form NO during this stage. In the fuel-lean condition, sufficient oxygen atoms make the NO formation rate become equilibrium, the equation shown below is valid for most combustion examples, the extremely fuel-rich condition is not included, the NO formation rate could be expressed as:

$$\frac{d[NO]}{dt} = 2k_{f,1}[O][N_2]\frac{\left(1 - \frac{k_{r,1}k_{r,2}[NO]^2}{k_{f,1}[N_2]k_{f,2}[O_2]}\right)}{\left(1 + \frac{k_{r,1}[NO]}{k_{f,2}[O_2] + k_{f,3}[OH]}\right)}\left(\frac{mol}{m^3} - s\right) \tag{2.8}$$

In the equation above, $k_{f,1}$, $k_{f,2}$, $k_{f,3}$ is the forward reaction rate constant, the reverse rate constant is expressed as $k_{r,1}$, $k_{r,2}$ and $k_{r,3}$. These constants is expressed below:

$$k_{f,1} = 1.8 \times 10^8 e^{-38370/T}, \qquad k_{r,1} = 3.8 \times 10^7 e^{-425/T},$$

$$k_{f,2} = 1.8 \times 10^4 T e^{-4680/T}, \qquad k_{r,2} = 3.81 \times 10^3 e^{-20820/T},$$

$$k_{f,3} = 7.1 \times 10^7 e^{-450/T}, \qquad k_{r,3} = 1.7 \times 10^8 e^{-24560/T},$$

The formation rate of NO could be calculated by the equation above, the concentrations of the atoms and molecules in the expression are required.

2.3.4.2 Prompt NOx formation

The second route of NOx formation during the combustion is so-called “Prompt NOx” formation, this formation mechanism was first built by Fenimore [98]. The formation mechanism of prompt NOx is complex, this type of NOx is formed in some special

conditions, such as short residence time, low combustion temperature and fuel-rich conditions [99]. In most combustion, the prompt NOx is only a small proportion of total NOx emissions.

Current studies generally agree that the intermediate product CH_i is source of formation of prompt NOx. In the hydrocarbon flame, the prompt NOx produced via the reactions below:

$$CH + N_2 \rightleftharpoons N + HCN \tag{2.9}$$

$$N + O_2 \rightleftharpoons NO + O \tag{2.10}$$

$$HCN + OH \rightleftharpoons CN + H_2O \tag{2.11}$$

$$CN + O_2 \rightleftharpoons NO + CO \tag{2.12}$$

The formation of prompt NOx usually occurs in high equivalence ratio conditions, it is more dependent on fuel and air amount not temperature. The formation level of prompt NOx is related to the number of carbon atoms in fuel, therefore, in this project, the prompt could be neglected because the combustion of hydrogen fuel is a carbon-free process.

2.3.4.3 Fuel NOx formation

Fuel NOx usually formed when the bonded nitrogen contained in the fuel, this type of NOx mostly been produced during liquid or solid fossil fuel combustion. It is mainly produced in coal combustion because coal normally contains at least 1% nitrogen by weight.

The fuel nitrogen reacts in high temperatures and lead in the NOx increases. The detailed formation mechanism of fuel NOx is too complex, until now there are many researchers working on this field and a simplified approach of fuel NOx formation shown below (Figure 2-18) was agreed generally. Briefly, the route of nitrogen

contained in fuel convert to NOx is mainly dominated by the combustion and the initial concentration of nitrogen-bound compounds in fuel. In this project, hydrogen fuel is investigated, the fuel NOx will not be studied for the hydrogen combustions.

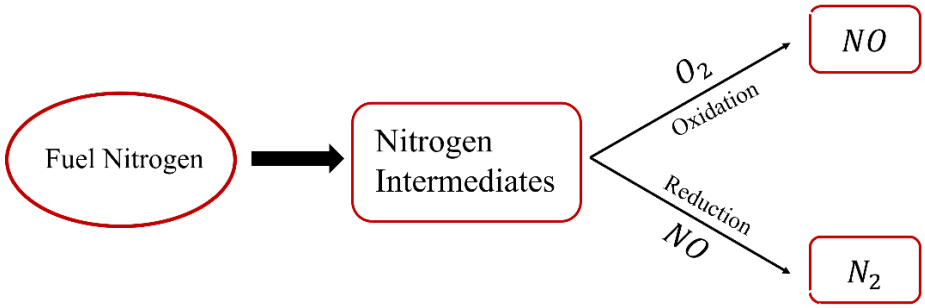

Figure 2-18. Simplified fuel NOx formation model.

2.4 Ammonia/Hydrogen Mixture Combustion Mechanism

Ammonia, as a benign hydrogen carrier, also has the potential to be used as an alternative fuel. Although the low burning rate of ammonia, stringent ignition conditions, and so on, make it difficult for ammonia to be used as an aviation fuel at present. However, it has the potential to be used as a blended energy source with hydrogen. On the one hand, the hydrogen could be cracked from ammonia, on another hand the high combustion velocity of hydrogen makes it an excellent combustion promoter. The combustion of ammonia/hydrogen fuel blends has been a topic of interest for many years and is even more popular as an alternative fuel than hydrogen alone.

In the current research, a detailed kinetic model that accurately predicts the details of the combustion of fuel blends is extremely important in order to better target the application of ammonia-hydrogen fuel blends. A large number of ammonia combustion mechanisms and mechanisms for ammonia-hydrogen mixtures have been developed in the last decades.

In 1989, in the paper by Miller and Bowman on the chemistry of nitrogen in combustion [100], a brief review of the previous nitrogen combustion chemistry was given and the steps of NOx generation were described in detail, in which the oxidation of ammonia was also discussed in detail, with the specific pathway of ammonia oxidation shown in the following Figure 2-19. It can be seen that the involvement of ammonia has a great impact on the generation of NOx.

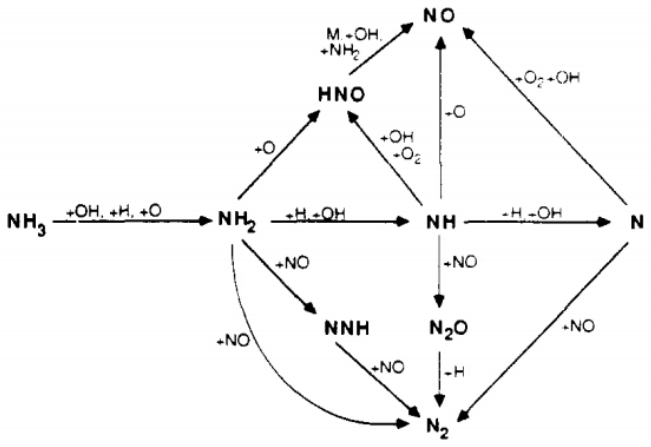

Figure 2-19. Reaction path diagram for the oxidation of NH_3 in flames [100]**.**

Later in 1993, a detailed study on the reaction mechanism of ammonia combustion was been carried out [101], although this article was more focused on the reaction mechanism of laminar flame, but still had a detailed introduction to the production and conversion of ammonia in combustion. Lindstedt et al. improve an ammonia combustion mechanism with 21 species and 95 reactions, this mechanism could be used in the wider temperature range. As this paper indicated that the NO formation path is more dependent on the combustion conditions, the reaction between NH and OH is important for all the flame types. But in hydrogen flame with ammonia conditions, the Zeldovich mechanism[102] becomes more important, in this type of combustion condition, the reaction of NO with N takes the primary position.

These two articles are very helpful for the subsequent chemical kinetic modelling studies [103]–[106]. Skreiberg et al. established an ammonia oxidation mechanism

which considered the presence of hydrogen, carbon monoxide and methane in 2004 [106], this model has shown good accuracy in the prediction of combustion. However, this paper more targeted on the combustion below 1400K. In the many years that followed, reaction mechanisms continued to be developed for ammonia combustion [107]–[109]. This paper wouldn't been discussed detailly here.

There are two mechanisms important for the following ammonia/hydrogen combustion research. The first one is from the paper by Konnov[110], he developed the mechanism of small hydrocarbon and ammonia oxidation, it showed good agreements on the NOx emission prediction. His mechanism refined the understanding of ammonia chemistry and improved the accuracy of computational models used to simulate ammonia-related processes. This mechanism has been widely used in the prediction of ammonia combustion and NOx emissions, also is the basis for many mechanisms' development. Konnov and this research team published another in 2019 [111], in this paper the combustion of $NH_3/H_2/CH_4$ fuel mixtures was studied. As the results of this research, the reduced combustion mechanism of ammonia/hydrogen is provided which included 213 reactions and 28 species.

Another mechanism is from Mathieu and Petersen [112], the paper published in a 2015 study about the combustion details of ammonia flame and the combustion with hydrogen blends. In this research, the laminar burning velocity and ignition delay of ammonia and hydrogen blended fuel were tested, the results stated that the addition of hydrogen could effectively enhance the burning velocity of NH_3, also, the increase of the H_2 addition ratio could reduce the ignition delay time of ammonia fuel and improve the combustion of ammonia. This mechanism was shown to be the most promising NH_3/H_2 combustion mechanism under practical conditions.

Hua Xiao et al. studied hydrogen/ammonia combustion in gas turbines in 2017[113]. In their paper, the combustion mechanisms of ammonia were comprehensively reviewed and analysed, they found that although the mechanisms of NH_3/H_2

combustion have been developed for many years and numerous research has targeted on this topic, the applicability of the mechanism for practical gas turbine combustion of ammonia-based fuels still requires more research on it, especially under the industrially related conditions. Therefore, their team targeted on the gas turbine application optimised the existed mechanism, the ignition delay time, burning velocity, NOx emission all these aspects are investigated to provide a reliable mechanism for hydrogen/ammonia blended fuel reaction. This mechanism was based on Mathieu's previous work[112], it has been modelled for different test conditions. After a set of experimental comparisons, the reduced mechanism has shown better performance than the Mathieu mechanism and a great improvement compared to Duynslaegher's mechanism [103]. For the NO prediction accuracy, as Figure 2-20 shows below, the NO production has been compared with different mechanisms and measured data with the equivalence ratio 0.5. The burning velocity prediction of NH_3/H_2 fuel mixtures has been compared as well, from Figure 2-21 it could be found that the mechanism from Hua Xiao's team showed a very agreement with the experimental data. Although Mathieu mechanism also presents an accurate prediction, the computational costs are different. The ammonia/hydrogen combustion mechanism was reduced in this paper into three mechanisms, in mech 3 only 23 species and 76 reactions are included, it's no doubt saved lots of computational sources. The reduced mechanism still could provide relatively accurate predictions for NH_3/H_2 fuel combustion.

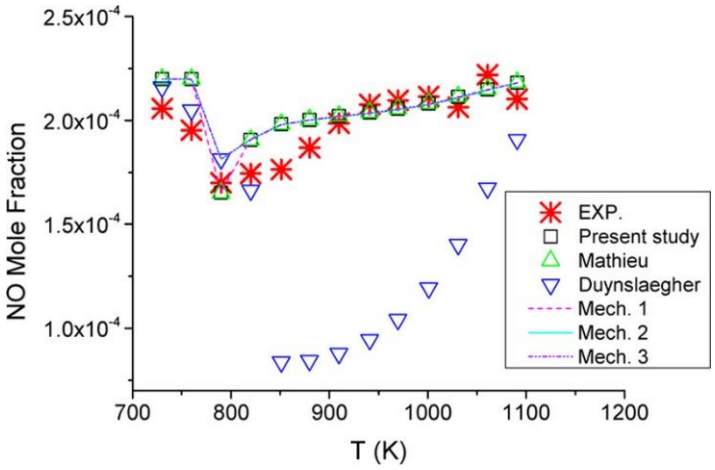

Figure 2-20. NO prediction of hydrogen-oxygen-nigrogen in jet stirred reaction [113]**.**

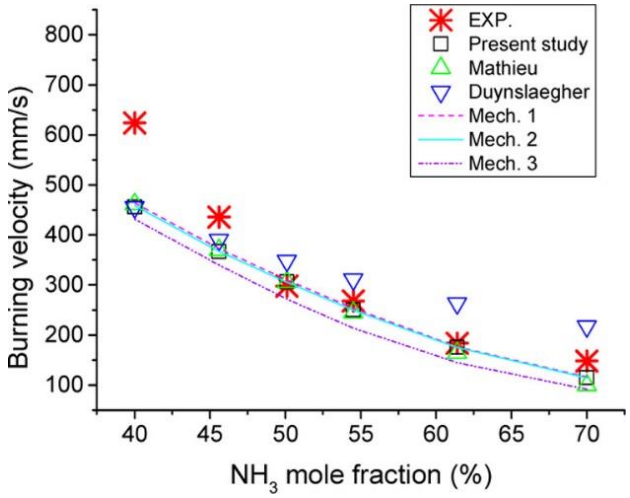

Figure 2-21. Burning velocity comparison of different NH_3 fractions under equivalence ratio 0.8[113]**.**

In year 2021, Kévin Bioche et al. conducted a detailed comparison of existing ammonia/hydrogen combustion mechanisms. The mechanisms were compared from different aspects with different hydrogen mole fractions, such as the ignition delay time with different initial temperatures and the burning velocity. The mechanism from Zhang's team had the best performance for all aspects [114]. Then, on the basis of Zhang's mechanism, the detailed kinetic model was reduced. In the comparison of Zhang mechanism and the reduced mechanism, the reduced model provided good predictions in flame speed and ignition delay time. Then the reduced model by

Kévin Bioche was used in the LES numerical study of NH_3/H_2 fuel combustion, the results showed its reliability in 1-dimension and 3-dimension simulation studies. This mechanism has 21 species and 122 reactions which means compared to the detailed kinetic mechanism from the others, enormous computational savings can be made. However, although this mechanism was developed closest to now, the reliability of this reaction mechanism needs to be verified by more research due to the lack of experimental studies in this paper.

For this thesis, all the mechanisms reviewed above have shown very good accuracy as well as applicability, but due to the limitations of computational source and the study time in this project, the reduced mechanism 3 from Hua Xiao's work would be used to investigate the hydrogen/ammonia combustion in micromix combustor. The compact mechanism which only has 23 species, and 76 reactions is very suitable for this project.

2.5 Research Gap

The existing studies about hydrogen combustion in gas turbines are insufficient to support the use of hydrogen in aircraft combustors. In particular the research on the micromix combustor, this new concept of hydrogen combustion still has great potential to dig out. First of all, for the hydrogen micromix combustion, most of the works on based on the experiments from Aachen University. The experience about numerical study is insufficient and not well concluded, the suggestion of the turbulence models, combustion models are not given. Secondly, the present research on micromix combustors is mainly focused on the overall configuration, the detailed geometrical parameters of a single injection element should be focused more on it. For instance, in the previous study, the air guiding panel was studied, in their work the overall geometry of the burner was adjusted to study the effect of the blockage ratio. In this project, the internal structure will be studied in greater depth. Furthermore, it could be found that the research on micromix hydrogen combustors is mainly focused on individual injection element, the potential of changing the existing structure of the entire micromix

combustor is still big, the research on this aspect is lacking. In this project, the combustion among multiple injection elements will be investigated and modifications will be made to enhance the combustion performance. Except the existing hydrogen micromix combustion, the other alternative fuels haven't been applied to the micromix combustor, in this project, the hydrogen/ammonia blended fuel will be studied.

CHAPTER 3: MICROMIX COMBUSTION SIMULATION SETTING STUDY AND VALIDATION

3.1 Micromix Burner Geometry Introduction

The origin of the micromix combustor was from Aachen University of Applied Sciences, as described in Chapter Two, numerous studies have been conducted since the last century, with the micro-injection concept being proposed during this period. These approaches have shown promise in effectively reducing NOx emissions by employing high mixing intensity. However, the premixing method used in these approaches carries the potential risk of flashback, especially considering hydrogen's high reactivity, which could lead to ignition within the premixing zone. In response to this challenge, Aachen University of Applied Sciences (AcUAS) proposed the DLN-Micromix combustion principle, which combines the benefits of high mixing intensity and the micro-injection concept.

The Micromix combustion concept comprises two key technologies. The first involves miniaturizing the injection components, while the second focuses on improving the intensity of air/fuel mixing. As demonstrated in previous papers by Funke, the research group at Aachen University of Applied Sciences (AcUAS) successfully transformed the APU Honeywell/Garrett GTCP 36-300 into a micromix concept combustor. In Figure 3-1 below, it can be observed that the traditional main air-inlet chamber has been replaced with thousands of micro injections. This innovative micro injection design has proven to significantly reduce NOx emissions in both laboratory tests and industrial gas turbine tests [47], [115].

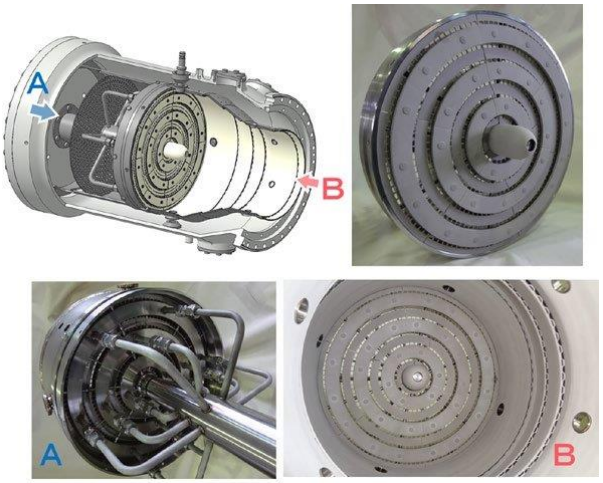

Figure 3-1. The design of hydrogen micromix combustor design [116].

To enhance the mixing of air and fuels, the jet-in-crossflow mixing method has been employed. As depicted in Figure 3-2 shown below, hydrogen fuel is injected perpendicularly into the airflow. This injection technique effectively enhances the mixing intensity inside the chamber. The introduction of gaseous hydrogen into the airflow leads to the formation of inner and outer vortices within the chamber. Between these vortices, a shear layer is created where the reaction takes place. The miniaturized flame is developed and stabilized along this shear layer. This design allows for significant reductions in chamber temperature and NOx emissions. Moreover, the use of multiple flamelets ensures excellent stability and eliminates the risk of flashback.

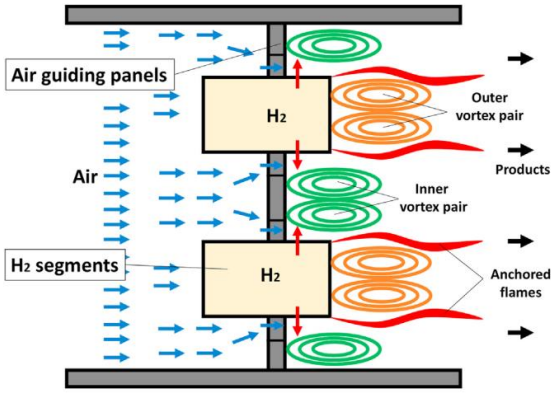

Figure 3-2.Schematic view of the MCP showing the jet in crossflow, vortex formation and flame anchoring [117].

In this chapter, further studies of the micromix combustor are based on this design concept. Due to the inherent dangers involved in conducting hydrogen combustion experiments and considering practical limitations, the optimization of the micromix combustor cannot be tested experimentally. Instead, the investigations into burner geometry will be conducted numerically using the software ANSYS fluent (version 2021 R2). Moreover, the focus of combustion simulation will be on a single injection element, as this approach significantly saves computational resources and time.

Before proceeding with the simulation of different micromix combustor geometries, it is essential to validate the numerical settings with experimental data. In this chapter, various numerical parameters will be studied and evaluated to determine the most suitable settings for the subsequent works. This validation process ensures the accuracy and reliability of the numerical simulations in the project.

3.2 Boundary Conditions of the Reference Experiment

Due to the limitations in experimental conditions, this project will not include any experimental data. Instead, the results obtained will be validated using Ayed's paper and thesis [66], [118]. In Ayed's experiment on micromix combustion, a small-scale test burner was constructed in the lab, as the actual modified APU rig was not utilized. The lab test burner's configuration was simplified but retained the same geometry as the single injection element in the micromix combustor.

As Figure 3-3 shows below, the number of injectors was reduced, and the curved array of injectors was changed to a linear arrangement for the lab test. This adjustment was acceptable for the lab-scale testing, considering that in the modified APU rig, the injectors are positioned very closely, and the angle between the central axes of injectors can be neglected. The emissions of NOx in the experiment were measured using an exhaust gas probe.

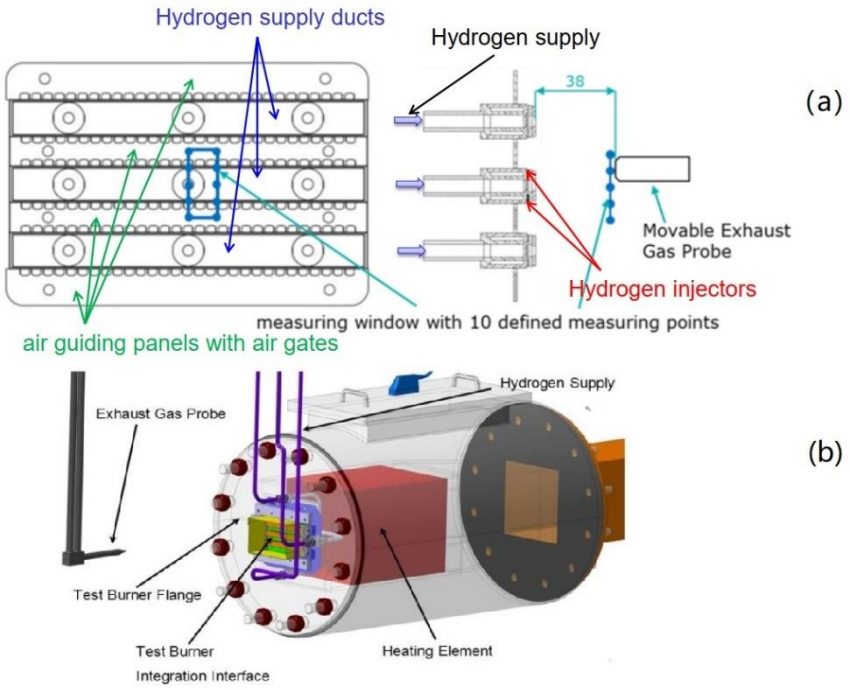

Figure 3-3. (a) the schematic of the injector elements array. (b) 3D drawing of the test rig. (figure modified from [118]**)**

In the reference experiments, the air is blown through the heating element, where it is heated to the designated temperature. The exhaust gases are then extracted using a movable gas probe positioned 38mm behind the hydrogen injectors. These extracted gases are supplied to the analysis system ABB Advanced Optima AO2020, and the level of NOx emissions is determined using Eco Physics CLD 700EL.

To measure the NOx emission accurately, the exhaust gas flows through an internal hot pipe and particle filters, resulting in the measurement of dry NOx. The CLD 700EL instrument used in the experiments offers a measuring accuracy of 0.1 ppm [118].

To create a simulation model that accurately aligns with the real test rig, it is essential to clarify the parameters of the single test rig. As depicted in Figure 3-4, the simulation domain corresponds to the reference area (Aref), allowing the dimensions of the model to be defined accordingly. Two critical parameters that need to be clarified are the distance between two air gates (dAGP) and the height of the air guiding panels (DAGP),

as they directly impact the air blockage ratio (BRAIR). The air blockage ratio is a crucial factor that significantly affects the combustion results. The importance of the air guiding panel (AGP) design will be discussed in the next chapter. In the validation simulation, the combustion performance of a single injector element shown as Aref will be studied.

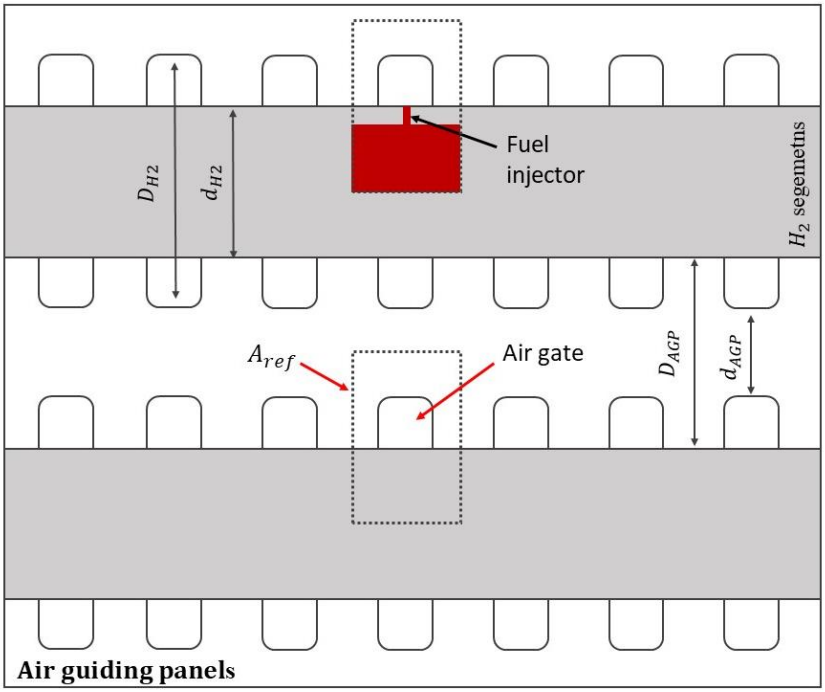

Figure 3-4. Annotation of the upper view of the test burner.

From the simplified schematic drawing of the test rig demonstrated in Figure 3-4, the single injector element in the dash-line is a four-sided symmetrical design. Therefore, to save the computational source and time, in this project, the single injector element will be modelled. Four sides in X and Y directions would be defined as symmetry planes, except these four symmetry planes, inlets and outlet, the other boundaries will be defined as walls. According to Ayed's paper[66], the dimensions of the single injector can be obtained through calculations, and these dimensions are illustrated in the drawings presented in Figure 3-5. The geometry shown below is the flow domain in the combustor, it is just a cut slice of the flow domain of the entire test burner. In the micromix combustor, the air flows through the air guiding panel, where it is accelerated.

Simultaneously, hydrogen fuel from the hydrogen segment enters the fuel injector and is jetted into the crossflow of air. Considering one injection element, its size is extremely small, and the corresponding combustion zone is confined within a domain of approximately 3 mm * 10 mm. In the experimental burner, the diameter of the hydrogen injection pipe has the diameter 0.3 mm.

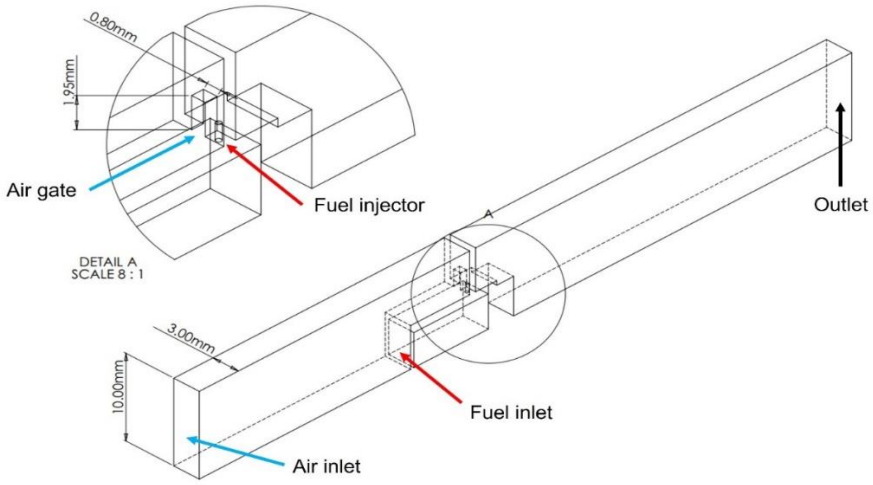

Figure 3-5.Isometric showing of single hydrogen micromix combustor element.

According to Ayed's paper, the combustion test was performed under atmospheric conditions, with the inlet air being preheated to 550K before being introduced into the test combustor. The hydrogen's temperature, on the other hand, remained at room temperature. In practical scenarios, the control over parameters is limited, and only the inlet velocity of air through the air gate and the hydrogen flow rate through the injector hole can be adjusted. Specifically, the inlet gas velocity is adjusted to maintain an equivalence ratio of 0.4. The detailed boundary conditions are listed in Table 3-1 below.

Boundary conditions	Value
Air velocity in the air gate	100 m/s
Air inlet temperature	550 K
Hydrogen velocity in the injector	206 m/s

Hydrogen inlet temperature	300 k
Operation condition	1 bar

Table 3-1.The boundary of the experiment (ϕ=0.4).

For the simulation, the magnitude of the air inlet velocity and the hydrogen inlet velocity needs to be calculated based on the area of the air gate and the air inlet, respectively. The normalized energy density (ED_n) of the burner is 6.7 MW/m^2, representing the thermal power design demand and referring to the energy of the designed combustor zone. Different normalized energy densities would impact the geometry and boundary conditions of the micromix burner.

$$ED_n = \frac{E_{ref}}{A_{ref} \times P_{ref}} \left[\frac{MW}{m^2 bar}\right] \tag{3.1}$$

Which E_{ref} is the reference thermal energy of a single injection element, A_{ref} is the front view area of single injector combustion which is labelled in Figure 3-4 shown above.

For the validation case, the reference thermal energy could be defined with the experimental boundary conditions.

$$E_{ref} = \rho_{H2} \cdot q_{H2} \cdot \dot{v}$$

$$E_{ref} = \rho_{H2} \cdot q_{H2} \cdot \left(u \cdot A_{H2\,injector}\right) \tag{3.2}$$

In this case, the normalized energy density ED_n is 6.7 MW, the low heating value of gaseous hydrogen q_{H2} is $120 \times 10^6\ J/kg$. The density of hydrogen under atmospheric pressure is $0.0808\ kg/m^3$. The velocity of air in the air gate and hydrogen in the inject pipe is already given with the equivalence ratio 0.4, with the defined size of the air inlet and air gate, the thermal power is kept at a fixed value, to the change the air/fuel ratio, the speed of intake air will change accordingly.

In the real test rig, the hydrogen combusts with air, not pure oxygen, so the nitrogen must be included. In the combustion reaction, each kmol of oxygen is accompanied by 3.76 kmols of nitrogen. The general reaction equation of hydrogen and air combustion is listed below, from the equation and according to the molar mass of gases, the stoichiometric air-to-fuel ratio could be determined [119].

$$H_2 + \frac{1}{2}(O_2 + 3.76N_2) \rightarrow H_2O + 1.88N_2 \tag{3.3}$$

$$\left(\frac{A}{F}\right)_{mass} = \left(2.38\frac{kgmole\ of\ air}{kgmole\ of\ H_2}\right)\left(\frac{28.8\frac{kgair}{kgmol}air}{2\frac{kgH_2}{kgmolH_2}}\right) = 34.3kg\frac{air}{kg}H_2 \tag{3.4}$$

At the stoichiometric condition, the ratio between the air and fuel is 34.4. For different equivalence ratios, the value of the required air mass flow rate could be calculated, and then the air inlet speed is determined.

For this validation work, the simulation will repeat with different equivalence ratios, the changes in the air inlet velocity under different air-to-fuel conditions are listed in Table 3-2.

Hydrogen inlet mass flow rate $\dot{m}_{H_2}\ [kg \cdot s^{-1}]$	Equivalence Ratio ϕ	Air gate velocity $\dot{u}_{airgate}\ [m \cdot s^{-1}]$	Air inlet velocity $\dot{u}_{air}\ [m \cdot s^{-1}]$
$ED_n = 6.7\ MW$ $\dot{m}_{H_2} = 1.176 \times 10^{-6}$	0.3	134.40	6.99
	0.35	115.20	5.99
	0.4	100.80	5.24
	0.45	89.60	4.66
	0.5	80.64	4.19
	0.54	74.67	3.88

Table 3-2. Air inlet velocity with various equivalence ratio.

In the experiment and simulation, most of the hydrogen combustion is conducted with fuel-lean conditions, which could provide lower temperatures and lower NOx emissions. The validation simulation will mainly work under the condition with an equivalence ratio of 0.4 which keeps consistent with the reference experiment. In addition, in this project, the solid wall parts are not modelled, because the heat transfer would not have much impact on the fuel tank and other structures. In the real test rig built in Aachen University, the heat shield made of Hastelloy X is applied to prevent heat transfer to the stainless-steel burner body [65]. As Figure 3-6 shows below, on the front surface of the burner, the heat shield is mounted internally between the fuel tank and the combustion chamber. The air-filled cavities are designed between the heat shield and the burner body. Therefore, the conjugate heat transfer would not affect the temperature of the other parts of the burner.

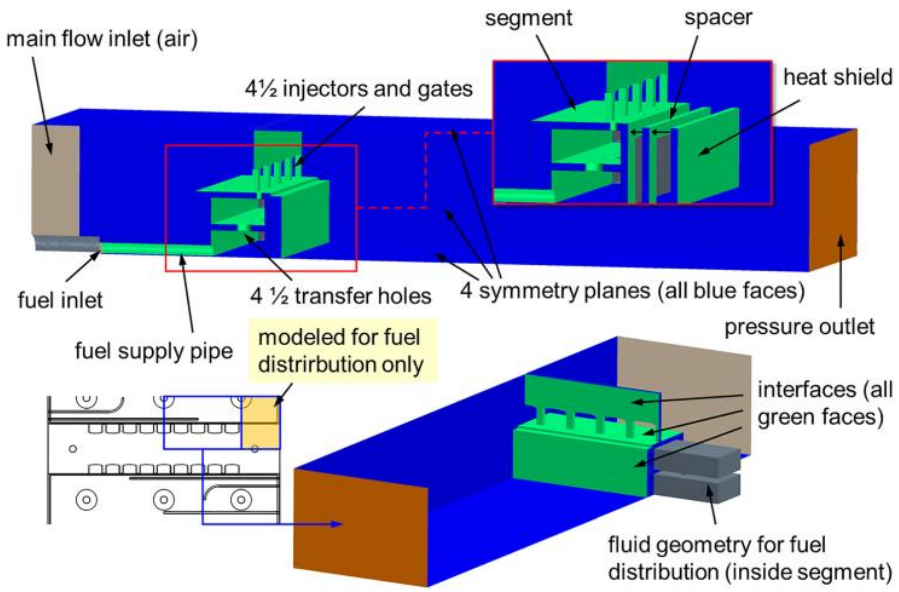

Figure 3-6. Computation domain of burner with heat shield[65].

3.3 Reference Experimental Data

To ensure the accuracy and reliability of the micromix combustion simulation, it is essential to compare and validate the numerical predictions against experimental data.

However, in this project, conducting actual hydrogen combustion experiments poses inherent risks and practical limitations. Therefore, the reference experimental data used for validation is sourced from the papers and thesis of Ayed [66], [118]. In these papers, the combustion performance at the design point (equivalence ratio Φ=0.4) was thoroughly studied both experimentally and numerically. The NOx emissions resulting from these experiments were recorded and compiled in Table 3-3. This reference data will serve as a benchmark for the validation simulation, allowing for a comprehensive assessment of the numerical model's performance and its agreement with real-world combustion behaviour.

	EDM	ED-FR	EDC	Measurement
NO emission [ppmv @ 15% O_2]	6	0.65	1.02	1.3

Table 3-3.Numerical calculation and experimental NOx emission of the baseline burner.[66]

In this study, the main study will be conducted with the Ansys Fluent calculation, the numerical settings need to be studied and developed. Therefore, for validation and comparison purposes, the experimental data would be used. To make the comparison more convincing, the measured NOx emissions at different equivalence ratios are required. From Figure 3-7 in Ayed's paper, the measured data could be extracted, for this study, the emission data at equivalence ratios of 0.3, 0.35, 0.4, 0.45, 0.5, 0.54 are extracted and listed in Table 3-4 below.

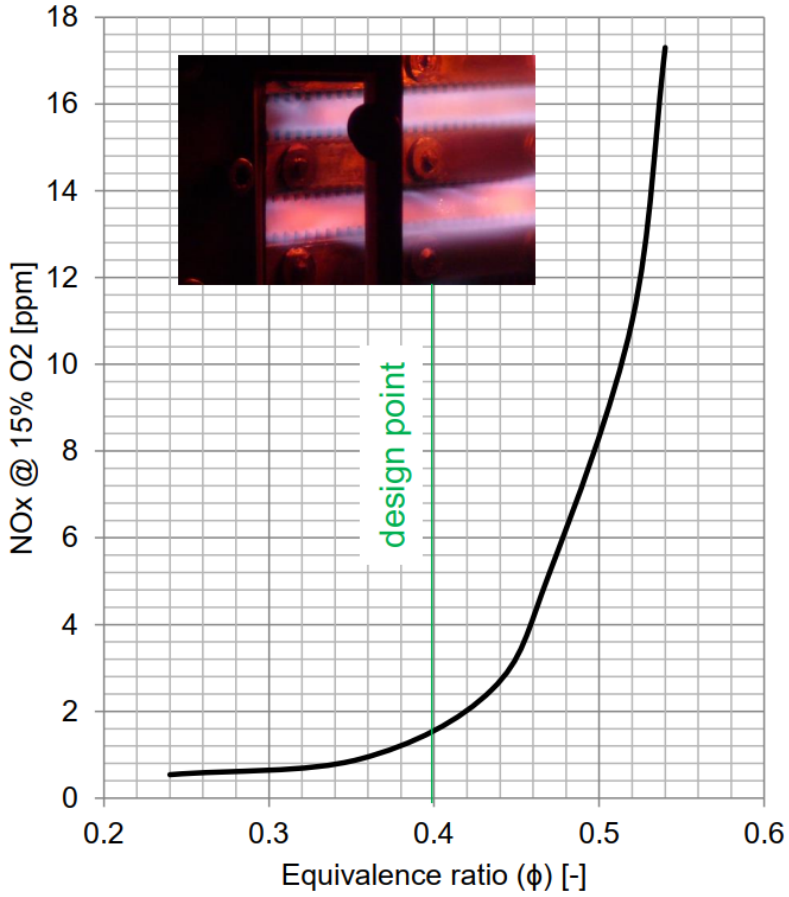

Figure 3-7. Measured NOx emission of the basic burner with different equivalence ratios [118].

Equivalence Ratio	0.3	0.35	0.4	0.45	0.5	0.54
NOx emission [ppm @ 15% O2]	0.75	0.9	1.33	3.2	8.2	17.2

Table 3-4.Experimental NOx emissions extracted with different equivalence ratios.

As the data shown above, the units used for the NOx emission is in [ppm], "Parts-per-million" which is the commonly used unit for the emission concentration. In the fluent, the NOx emission amount is always calculated as the mole fraction or mass fraction. To unify the unit, the equations demonstrated below are used to convert the NOx from mole fraction to ppm.

$$NOx_{general}\,[ppm] = X_{NOx}[mole] \times 10^6 \qquad (3.5)$$

$NOx_{general}$ $[ppm]$ is the value of the NOx emission directly converted from the calculated value, X_{NOx} $[mole]$ is the mole fraction obtained from Fluent. However, considering the oxygen concentration in the experiment is 15%, the values of the NOx in ppm need to be further corrected with the steps below.

$$NOx_{Correct}\ [ppm] = NOx_{general}\ \cdot \frac{21 - 15}{21 - X_{O2} * 100} \tag{3.6}$$

$$NOx_{dry}\ [ppm] = NOx_{Correct}\ \cdot \frac{1}{1 - X_{H2O}[mole]} \tag{3.7}$$

In the following studies, the NOx emission will be presented in the unit [ppm].

3.4 Numerical Setting Evaluation

3.4.1 Mesh strategy

In CFD simulation, meshing is a crucial and essential step that significantly influences the accuracy of the calculation results. The size and quality of the mesh directly impact the calculation accuracy of flow dynamics in Fluent.

To achieve reliable and precise results, it is imperative to draw a mesh that satisfies both quality requirements and result accuracy, tailored to the specific conditions of the model. For the 3D flow domain in this project, various mesh shapes can be adopted, with different cell shapes available for consideration. These cell shapes are illustrated in Figure 3-8, showcasing the available options for meshing the flow domain.

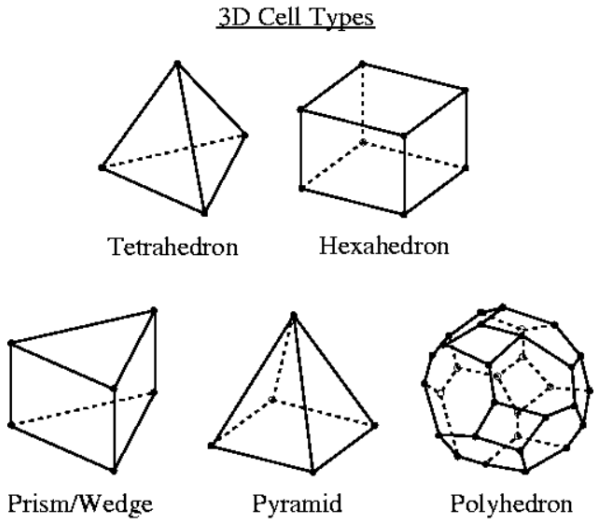

Figure 3-8. Various mesh cell shapes in 3D case [99].

These cell shapes have their advantages and disadvantages. The meshing can be divided into two types. The first one is an unstructured mesh. In a 3D mesh, this type of mesh is formed with different shape elements; it could be a hexahedron, a prism, but most commonly tetrahedrons [120]. Compared to a structured mesh, the unstructured mesh offers more flexibility as it can be hybrid with different shapes, and the nodes' distribution is random. This type of mesh has higher adaptability with irregular and complicated domains. The disadvantage is that the generation of unstructured mesh is more random and not easy to control. Additionally, calculations with an unstructured mesh always require much higher computational power.

Structured meshing involves having all internal nodes in the mesh elements with the same adjacent cells, resulting in hexahedral cell shapes. The structure of this mesh type ensures that nodes are distributed on grid lines of each layer, forming a uniform grid in a rectangular area topologically. On each layer, the number of nodes remains consistent.

Using a structured mesh offers several advantages. Firstly, it saves computational resources, and secondly, it typically results in higher mesh quality. This higher quality is due to the mesh shapes being hexahedrons, which helps maintain low cell skewness. Consequently, structured meshing often provides more accurate results for the same

domain compared to unstructured meshing. The accuracy of numerical predictions is primarily reliant on mesh quality, irrespective of whether the meshing is structured or unstructured. Therefore, the focus should be on controlling mesh quality based on specific simulation requirements to achieve accurate results.

In this project, a high-quality mesh was produced using the structured mesh method for all subsequent simulations with software ICEM, it is a user-friendly meshing tool which could generate a high-quality mesh with a relatively low effort. The geometry of the flow domains in this project is structural, therefore, ICEM is very suitable for this project. As discussed above, structured meshing offers significant computational savings while delivering reliable performance in calculations. Additionally, since the flow domain in the micromix combustor has a rectangular outline, structured mesh cells can easily fit the boundary of the region, further enhancing the accuracy and suitability of the mesh for the simulation.

For the meshing strategy, the cell density varies across different regions, as shown in Figure 3-9 the reference micromix burner. The flow domain is meshed using structured hexahedron cells, while the crossflow air stream and the combustion reaction zone have increased mesh density to capture the flow intricacies accurately. Conversely, near the outlet, the cell width is larger, reducing the number of mesh elements in this less critical region to save computational costs.

In the illustrated case (Figure 3-9), there are approximately 2.3 million mesh elements, which constitutes a relatively fine mesh. However, such a large number of mesh cells might lead to unnecessary computational expenses. To address this, for the validation case, the mesh density will be adjusted, ranging from 500,000 to 3,000,000 mesh elements. A mesh independence study will be conducted to determine the most suitable mesh strategy that strikes a balance between accuracy and computational efficiency.

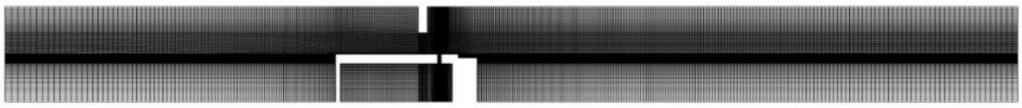

Figure 3-9.The general view of the mesh at the mid-section at ZY plane.

The detail of burner meshing is demonstrated in Figure 3-10, the example work shows quite fine meshing, and the variation of mesh density at different regions could be observed clearly. On the horizontal axis of this figure, the mesh density was increased for the potential flame occurrence area. Also, near the hydrogen injector region, the meshing will be finer because the flow behaviour at this zone is significantly impactive to the simulation result. The hydrogen flow jet into the cross-air flow and the interaction between two axis motions is the key point of the mixing intensity improvement in micromix design. Therefore, the mesh density at this region has to be higher to ensure prediction accuracy. In addition, as the mesh details shown in the red rectangle labelled, the grid number at the near-wall region increased to improve the performance of the near-wall modelling. For all the near wall parts, the mesh density at the near wall sections is increased, and the grid size is around 0.01mm for the finest case to calculate the flow dynamics better between the flow domains and the wall surface. With the range of the y+ value in 1~5, the near wall section mesh is good enough. For this project, the SST $k-\omega$ turbulence model was used, therefore, in the viscous sublayer near the wall surface, it will automatically use the low-Re formulation. The near-wall calculation greatly affects the accuracy of the solutions. In the near wall space, accurate calculations of the flow are important which determines the flow dynamics of wall-bounded turbulence [99]. The mesh strategy of the mesh in this project will adjust depending on the specific conditions.

For the boundary conditions, four sides of the computational domain were defined as

symmetry, because the flow domains are symmetric in X direction and Y direction, therefore using symmetry for those sides is good enough for this project. The periodic plane is not used because there is no rotate flow in the flow domain which would cross through the boundaries.

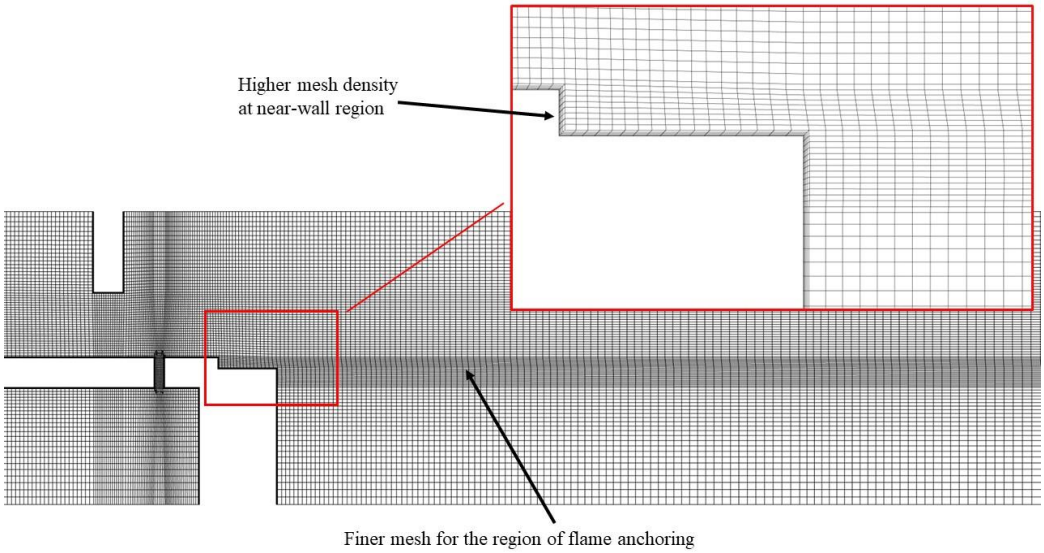

Figure 3-10. The detailed mesh of flow interaction zone.

3.4.2 Mesh independence

To determine a reasonable mesh density that offers reasonably accurate simulation results while minimizing computational costs, a mesh independence study is essential. In this section, the boundary conditions and parameters of the basic validation model are applied to conduct the mesh independence simulation.

For the basic micromix combustor geometry, the meshing strategy is based on the description from the previous section. The air/hydrogen reaction region is meshed with finer mesh elements, as shown in Figure 3-10 above. Following this meshing outline, the same burner model is meshed with four different element densities. The mesh densities for these cases range from 500,000 to 2,500,000 elements, and the

corresponding data in the chamber is recorded in Table 3-5 below.

Distance from AGP	Mesh 850,000	Mesh 1,350,000	Mesh 1,890,000	Mesh 2,300,000
Facet Average temperature / K				
6 mm	1264.85	1245.37	1244.43	1167.23
8 mm	1403.16	1347.57	1349.49	1265.76
10 mm	1546.05	1499.13	1492.20	1437.70
12 mm	1614.23	1600.55	1604.60	1596.49
14 mm	1636.26	1628.73	1635.72	1635.92
16 mm	1631.86	1625.15	1631.30	1627.82
Area-Weighted Average Mole fraction of Pollutant (*10^6)				
6 mm	1.816	1.979	2.149	2.032
8 mm	1.822	1.993	2.161	2.052
10 mm	1.834	2.035	2.199	2.115
12 mm	1.934	2.181	2.361	2.290
14 mm	1.995	2.226	2.417	2.349
16 mm	1.967	2.185	2.367	2.290
Outlet	1.333	1.464	1.581	1.524

Table 3-5. Temperature and NOx data for mesh independence study.

To validate the independence of the mesh counts, the location of the air guiding panel on the Z-axis was set as the origin point, the hydrogen fuel injected at the location 2mm, then the data on the section plane every 2mm was recorded as Figure 3-11 shown below. The facet average temperature along the chamber on XY-Plane is monitored. In addition, the area weight average mole fraction of NOx emission on those cross sections is recorded as well.

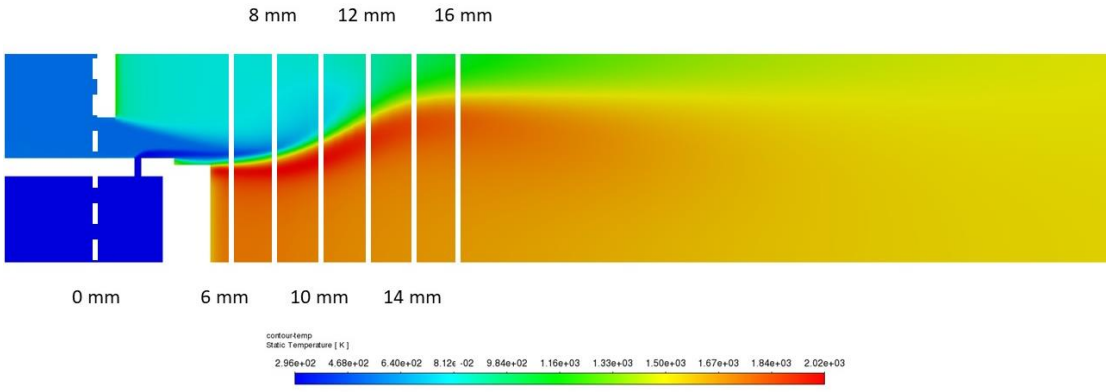

Figure 3-11.The indication of the data recording position along the chamber.

As shown in Figure 3-12, the facet average temperature along the Z-axis with different mesh counts was plotted. From the length of 6mm to 16mm, where the flame exists, there are no significant differences in temperature between the different mesh densities. Particularly for mesh cell counts between 1,000,000 to 2,000,000, the temperature curves are overlapping, indicating that predictions within this range provide almost identical results.

Furthermore, the distribution of NOx in the burner was recorded at each position and plotted in Figure 3-13. The NOx emission data represents the pollution of the reference burner at an equivalence ratio of 0.4, with the Y-axis representing the average mole fraction multiplied by 10^6. The plot shows that, with different mesh densities, the NOx emission varies within a small range of 0.05×10^{-6}, demonstrating a very high degree of overlap. Notably, the prediction of NOx produced with a mesh count of 2,000,000 is slightly lower than the other mesh cases.

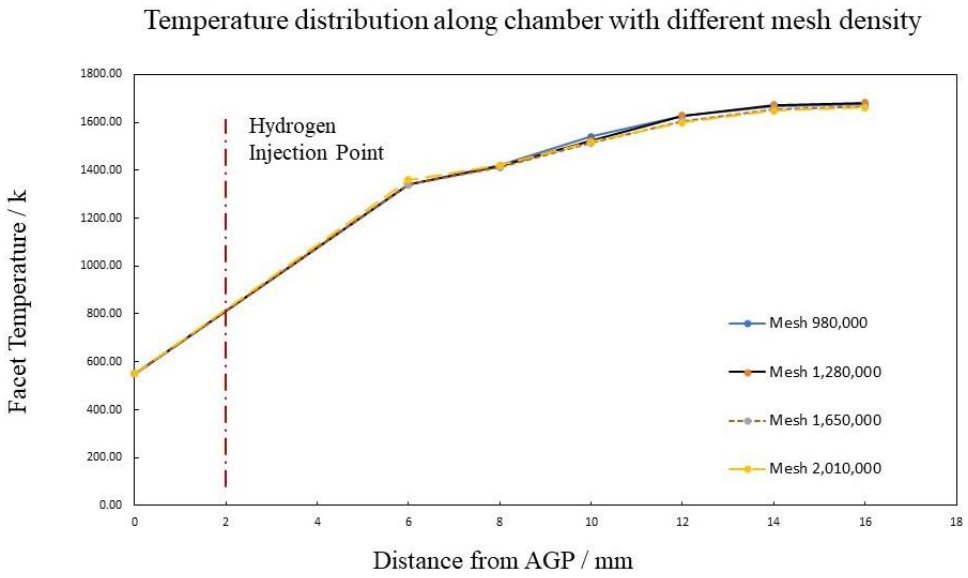

Figure 3-12. Temperature distribution along the Z-axis with different mesh density

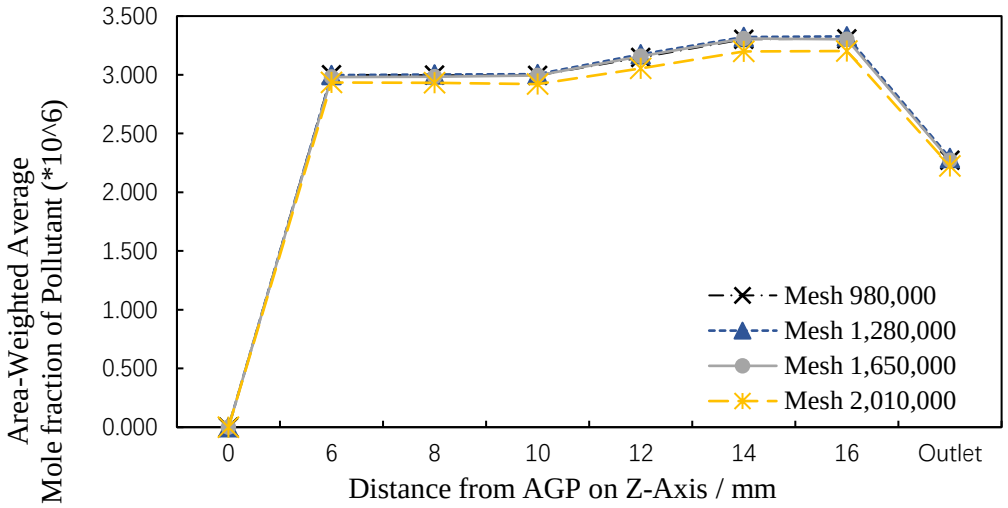

Figure 3-13.The NOx emission along chambers with different mesh densities.

Considering the mesh independence study results for temperature and NOx, it is evident that a mesh number over one million is acceptable. To strike a balance between prediction accuracy and timesaving, it is reasonable to control the number of mesh elements around 1,500,000 for the follow-up simulations. This mesh density has been shown to provide relatively accurate predictions for temperature and NOx distribution

in the micromix combustor, making it a suitable choice for subsequent analyses.

By using a mesh density of approximately 1,500,000 elements, the simulations can deliver accurate and reliable results without excessive computational costs. This optimized meshing strategy ensures the efficiency of the simulation process while maintaining a reasonable level of accuracy in predicting temperature and NOx emissions within the micromix combustor.

3.4.3 Turbulence model selection

Despite the small size of the single burner, flow dynamics significantly impact the combustion performance within the chamber. As previously mentioned, the formation of vortices dictates the flame shape, necessitating an accurate prediction of flow dynamics. In numerical calculations, choosing an appropriate turbulence model can greatly improve prediction accuracy.

To obtain simulated data that closely match experimental results, it is essential to acknowledge that there is no single turbulence model that can be universally applicable to all flow types. In the context of the numerical work in this project, several factors must be taken into account, including the desired level of accuracy, the availability of computational resources, and the time constraints. Therefore, evaluating different turbulence models becomes necessary to identify the most suitable one for the specific simulation scenario.

Although large eddy simulation (LES) and direct numerical simulation (DNS) models could provide highly accurate predictions of the flow dynamics, the detailed turbulence information could be captured with high precision. The key disadvantage of those models is the exorbitant computational source requirements. Especially DNS model, the numerical cost of DNS simulation is proportional to the turbulent Reynolds number (Re_t), which results in the cost being prohibitive for high Reynolds numbers turbulence calculation. Compared to the LES and DNS model, the Reynolds-averaged Navier-

Stokes (RANS) model such as k − ε model, k − ω model. The research between the LES and RANS models was taken by many researchers, the paper stated that although the LES model provided the closest results compared to the experiment, the k − ω model showed good predictions as well[121]. For the researchers, they need to make trade-offs between accuracy and computational cost. In this project, after taking into account the cost of time and computing source, as well as the specific requirements of the burner simulation, the RANS model will be used. Specifically, Reynolds Stress model, realizable k − ε models and SST k − ω model will be discussed and decided.

The realizable k − ε model is an advanced model based on the standard k − ε model, compared to the standard model, the realizable model could provide a more accurate prediction of the spreading rate of planar and round jets. Moreover, the function of predicting rotation, separation and recirculation is enhanced with realizable k − ε model. The development of k − ε model is based on two ways, a new formulation for the turbulent viscosity is included in the enhanced model, another reason is for the dissipation rate ϵ a new transport equation is used.

In addition to the epsilon model, another viscous model with good performance is the shear-stress transport (SST) k − ω model. Compared to the standard k − ω model, the transport of the shear stress of turbulence is considered and refine the constants. Furthermore, this model effectively combines the advantages of near-wall region prediction of the k − ω model and the free-stream independence of the k − ε in the far field together. The blending function is variable with different calculation zones, at the near-wall region, the standard k − ω model will be activated to give a relatively accurate prediction. For the region away from the walls, the calculation will be carried out with the transformed k-epsilon model. The improvements of the SST model have a finer prediction and make it more reliable.

The transport equations of SST k − ω model is shown below [99], compared to the equation of the standard k − ω model shown before, the model constants are different,

in addition, the term cross-diffusion D_ω was added to blend $k-\varepsilon$ and $k-\omega$ model.

$$\frac{\partial}{\partial t}(\rho k)+\frac{\partial}{\partial x_i}(\rho k u_i)=\frac{\partial}{\partial x_j}\left(\Gamma_k \frac{\partial_k}{\partial x_j}\right)+G_k-Y_k+S_k \tag{3.8}$$

$$\frac{\partial}{\partial t}(\rho \omega)+\frac{\partial}{\partial x_i}(\rho \omega u_i)=\frac{\partial}{\partial x_j}\left(\Gamma_\omega \frac{\partial_\omega}{\partial x_j}\right)+G_\omega-Y_\omega+D_\omega+S_\omega \tag{3.9}$$

$$D_\omega=2(1-F_1)\rho\frac{1}{\omega\sigma_{\omega,2}}\frac{\partial_k}{\partial x_j}\frac{\partial_\omega}{\partial x_j} \tag{3.10}$$

To better understand the performance of different turbulent models, a simple validation simulation comparison has been conducted for the viscous model selection. The boundary conditions used were the same as the experiments mentioned in the last section, for the comparison, the combustion model selected is the Finite-Rate/Eddy Dissipation model (FR/ED). The turbulent models discussed above were compared, which are realizable $k-\varepsilon$ model, *SST* $k-\omega$ model and Reynolds Stress Model.

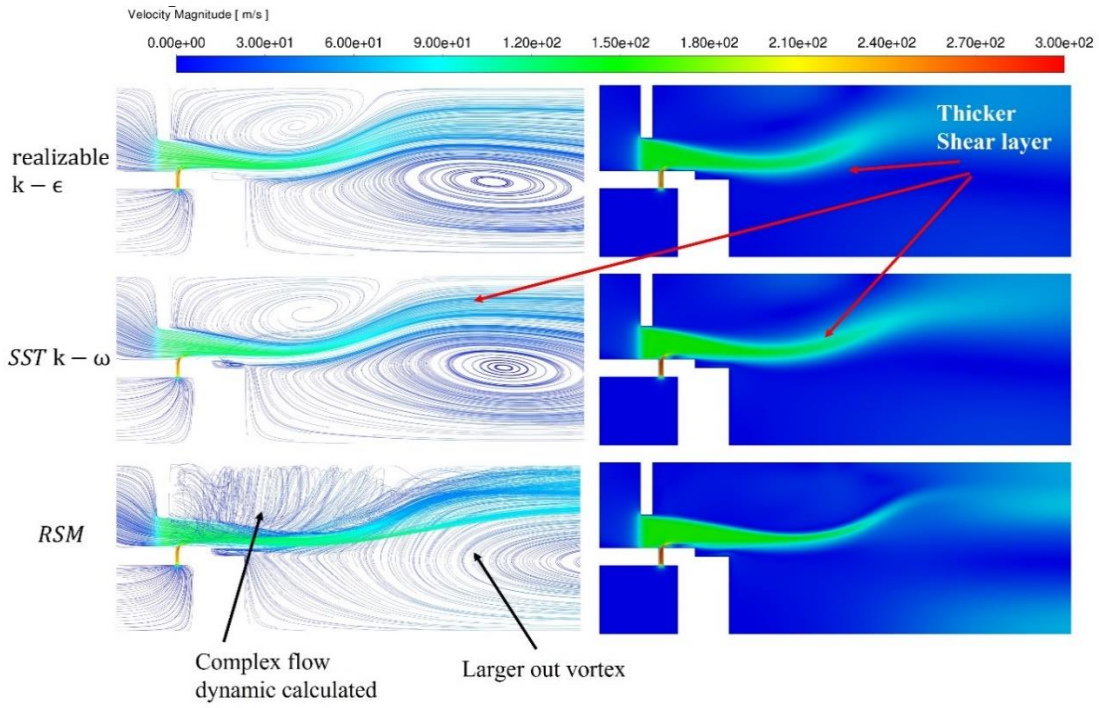

Figure 3-14. Flow comparison between turbulence models.

Figure 3-14 displayed the flow dynamic in the combustor from the different turbulence models, the pathline and the velocity contour on the centre plane along the Y-Z direction. For the same boundary conditions, the calculated flow behaviour among three different viscous models presented big differences. It could be found that the vortex structure displayed in Figure 3-14 between the 2-equation RANS equation models and RSM model are different. The 2-equation models have similar flow dynamics, and the inner and outer vortices have similar size and shape. The RSM predicts the inner vortex in a different way, the streamline of air/fuel mixed flow has different flow directions and presents a more complex inner vortex structure, the gas flow recirculates on the X-Y plane and forms the inner vortex. Compared to RSM model, realizable $k-\varepsilon$ model and SST $k-\omega$ model's inner vortex stabilized on the Y-Z plane and formed a very typical micromix vortex structure. The shear layer between the vortices in realizable $k-\varepsilon$ model and SST $k-\omega$ model is thicker than RSM model.

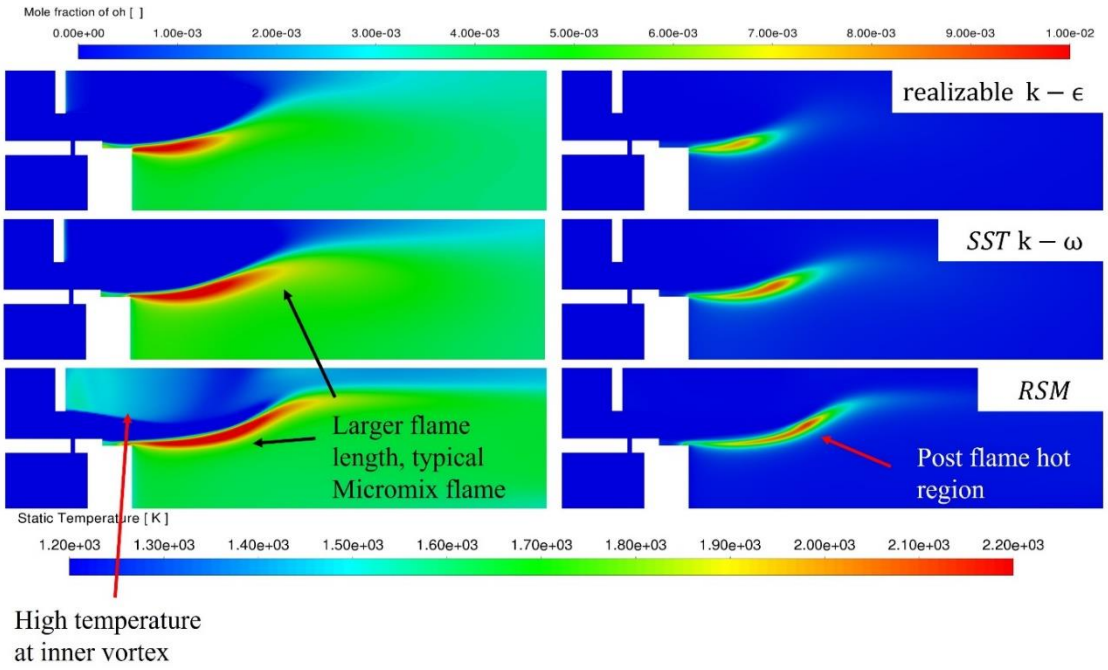

Figure 3-15. Temperature and OH contour comparison between turbulence models.

The combustion performance of the selected turbulence models is demonstrated in Figure 3-15. The temperature distribution is shown on the left, RSM and SST $k-\omega$

model both predicted the flame shape more close to the typical Micromix flame than realizable $k-\varepsilon$ model. The high temperature region and flame size in the realizable $k-\varepsilon$ model's result are too small compared to the experimental flame shape. The larger hot region in RSM model and SST $k-\omega$ model may lead to higher NOx emission in the calculation. One thing needs to be noticed is that the high temperature at the inner vortex in RSM model, this might be because of the difference of the inner vortex structure shown in Figure 3-14.

The NOx emission at the outlet of the burner has been calculated. The corrected dry NOx emission in ppm of realizable $k-\varepsilon$ model, SST $k-\omega$ model and RSM model are 0.77, 1.09, 0.78 respectively. Compared to the experimental emission data 1.3ppm, SST $k-\omega$ model provided the closest result, the flame shape and flow structure calculated by this model are relatively accurate to simulate the hydrogen micromix combustion.

Overall, by considering the simulation results discussed above and the computational power availability, RSM model was removed from consideration, it will cost several times over the other two models but with similar performance on combustion prediction. For these two-equation RANS models, even though both models are fine and suitable, a limitation of the realizable $k-\varepsilon$ model makes the SST $k-\omega$ win in the selection which is when the computational domain includes the rotating and stationary fluid zone, the realizable $k-\varepsilon$ will produce non-physical turbulent viscosities. After comprehensive consideration and comparing the results of the preliminary simulation of the basic burner, the SST $k-\omega$ model was chosen which could provide great prediction, but less computational source required. In the subsequent simulation works, SST $k-\omega$ model will be used in the study of optimization of Micromix combustor design.

3.5 NOx Model Analysis and Selection

3.5.1 Theoretical NOx model discussion

In this project, the primary objective is to optimize the design of a Low NOx micromix combustor, with a focus on reducing NOx emissions. Therefore, the selection of the appropriate NOx model in Fluent software is of paramount importance.

As mentioned earlier, there are two types of NOx produced in hydrogen combustion: thermal NOx formation and prompt NOx formation. Prompt NOx is generated in low-temperature, rich burn conditions and contributes only to a small portion of the overall NOx emission during combustion. The major pollutant is thermal NOx, which is highly dependent on the combustion temperature. To predict the formation of NOx, Fluent employs the extended Zeldovich mechanism, which involves two reactions for NO formation from nitrogen and oxygen at high temperatures, and a third reaction involving the hydroxyl radical [62].

The equations (3.11) and (3.12) illustrate the formation of NO under high-temperature conditions. The high temperature during combustion provides the necessary energy to break the triple bonds of nitrogen, which is why NOx levels tend to increase rapidly when temperatures exceed 1800K. Additionally, when the combustion temperature surpasses 2200K, the thermal NOx production rate doubles for every 90K. The third equation supplements the NOx formation under fuel-rich conditions.

$$O + N_2 \rightleftharpoons N + NO \tag{3.11}$$

$$N + O_2 \rightleftharpoons O + NO \tag{3.12}$$

$$N + OH \rightleftharpoons H + NO \tag{3.13}$$

The NOx emission value would vary greatly with the different NOx model selection. For the NOx model, the turbulence-chemistry interaction model is quite important to

the result, the NO concentration in Fluent is calculated by computing the time-averaged NO formation rate at each node. To obtain the mean turbulent flow, the probability density function (PDF) method is applied which is especially useful to describe the turbulent reaction rate. In Ansys Fluent, the temperature and species mass fraction could be considered to predict the NOx emissions by changing the turbulence interaction model. As known that the NOx emission is highly dependent on the temperature, to predict a more accurate NOx emission the effect of fluctuations of temperature must be taken into account.

When the turbulent reaction rate of NOx production considered, the equations below will be used.

$$\bar{S}_{NO} = \int \rho w_{NO}(V_1) P_1 (V_1) dV \tag{3.14}$$

$$\bar{S}_{NO} = \iint \rho w_{NO}(V_1, V_2)\, P(V_1, V_2) dV_1 dV_2 \tag{3.15}$$

Where V_1 , V_2 means the normalized temperature or the species concentrations. In this project, only the temperature fluctuations are modelled in the NOx emission. As the preliminary simulation works, for the hydrogen combustion the species mass fraction would not affect the results obviously, it could be neglected. Therefore, the equation (3.14) above is used, the turbulent rate of NOx production is integrated at every node and iteration. Hence, to evaluate the suitable NOx model, the numerical setting would be studied with “none” which is no consideration of turbulence interaction and “temperature” for the normalized temperature solution at each node.

As mentioned above, the majority of NOx emission produced is thermal NOx, for the thermal NOx calculation, the equation (3.16) shown below could clear the formation of the NO in the combustion.

$$\frac{d[NO]}{dt} = 2k_{f,1}[O][N_2]\frac{\left(1-\frac{k_{r,1}k_{r,2}[NO]^2}{k_{f,1}[N_2]k_{f,2}[O_2]}\right)}{\left(1+\frac{k_{r,1}[NO]}{k_{f,2}[O_2]+k_{f,3}[OH]}\right)}\left(\frac{mol}{m^3}-s\right) \quad (3.16)$$

Based on the equations, it is evident that the concentration of radical O/OH plays a dominant role in the rate of NO formation. Following the principle from Zeldovich, the NOx formation can be post-processed if the temperature, O atom, and OH radical are assumed to be in equilibrium. This method of NOx formation calculation is employed in Fluent. However, when assuming the O atom concentration to be at equilibrium, the prediction of NOx formation tends to be lower by approximately 30%.

It is important to note that there is no definitive conclusion regarding the exact impact of radical concentrations on NOx emission calculations, as this area lacks extensive studies. However, some research has indicated that both O atoms and OH radicals have a significant effect on NOx production, with O atoms in particular, playing a crucial role in the process.

In the numerical calculation of the thermal NOx, the impact of O atom and OH free radical was included in Fluent. Because the thermal NOx formation is always after the combustion, the NOx emission could be decoupled and calculated with the assumption of the reaction equilibrium. The assumption made of the O atom and radical OH dominates the NOx emission prediction given by Fluent.

For O atom [O] concentration, there are three assumptions:

1. Equilibrium assumption, this approach could simplify the calculation but it may cause the NOx formation under predicted 28% [99].
2. Partial equilibrium approach, compared to the equilibrium approach, this method considers the third body reactions. The O atom concentration will be higher with this method.
3. Instantaneous, in the Fluent, the O atom concentration could be directly

predicted from the local O-species amount.

By comparing these three approaches theoretically, the Equilibrium and Partial equilibrium approaches could simply assume the concentration of the O-atom, then the NOx formation could be processed with the calculations. However, the NOx prediction with Equilibrium approach would be lower than expected, in addition, the Partial equilibrium method has limitations on the thermal NOx prediction. Although the Instantaneous method requires more computational sources it could provide a more realistic prediction.

The OH radical is another factor which may affect the thermal NOx prediction, Fluent includes three approaches:

1. Compared to the effect of the O atoms, the free radical OH could be neglected, hence in the numerical calculation the OH radical could be excluded which is a reasonable assumption.
2. Partial equilibrium approach, the concentration of OH radical would be taken into account when using this approach, the OH fraction is dependent on the O atom and H_2O mole fraction.
3. Instantaneous, this approach is similar to the O atom's method. Which could give a good prediction, but a higher numerical source is required.

3.5.2 NOx model evaluation

To evaluate the NOx models and select the most proper numerical method for the NOx emission prediction. Series micromix combustion simulation with the basic burner was studied, the NOx emission was calculated with different combinations of NOx models mentioned above. The simulation results were compared with the reference basic burner data presented before.

The study of the NOx emission with different NOx models is through two groups, the

first group considers the turbulent interaction of the normalized temperature, and the second group excludes the effect of the turbulence. The detailed combinations of NOx models are shown in Table 3-6 below. For the convenience of recording, a different combination of the NOx model is abbreviated with three letters, as the example, the abbreviation "**TIP**" stands for the "T (turbulence interaction) – I (instantaneous approach for O-atom) – P (partial equilibrium approach for OH radical)".

Turbulent interaction of Temperature (T)	Instantaneous **(I)**	Partial equilibrium **(P)**	Equilibrium **(E)**
Instantaneous **(I)**	TII	TPI	TEI
Partial equilibrium **(P)**	TIP	TPP	TEP
None **(N)**	TIN	TPN	TEN
No turbulent interaction (N)	Instantaneous **(I)**	Partial equilibrium **(P)**	Equilibrium **(E)**
Instantaneous **(I)**	NII	NPI	NEI
Partial equilibrium **(P)**	NIP	NPP	NEP
None **(N)**	NIN	NPN	NEN

Table 3-6.The detailed combination of NOx models.

All the data demonstrated in this part are simulated with the basic burner geometry at the equivalence ratio of 0.4. To find the suitable thermal NOx model, different numerical approaches of O-atom and OH radical free were selected and the NOx emission data at the outlet of the burner. The recorded data is in the unit of mole fraction, to compare with the experimental data, the emissions would be corrected with the oxygen concentration and the water concentration and then converted to the unit [ppm].

3.5.3 Result of NOx model evaluation

As Table 3-7 shown below, the exhausted NOx emission data recorded in [ppm] at the outlet of the micromix combustor are listed, the difference of [O] atom model selection

is shown horizontally, and the effect of [OH] radical change is listed vertically.

Group 1. The turbulent interaction of temperature included **(T)**.			
[O] atom / [OH] radical	Instantaneous **(I)**	Partial equilibrium **(P)**	Equilibrium **(E)**
Instantaneous **(I)**	TII - 1.09	TPI -2.35	TEI - 1.973
Partial equilibrium **(P)**	TIP - 1.08	TPP - 2.27	TEP - 1.96
None **(N)**	TIN - 1.09	TPN - 2.34	TEN - 2.03
Group 2. No turbulent interaction considered **(N)**.			
[O] atom / [OH] radical	Instantaneous **(I)**	Partial equilibrium **(P)**	Equilibrium **(E)**
Instantaneous **(I)**	NII - 0.36	NPI -0.34	NEI -0.29
Partial equilibrium **(P)**	NIP - 0.36	NPP - 0.33	NEP - 0.29
None **(N)**	NIN - 0.36	NPN - 0.33	NEN - 0.29

Table 3-7.NOx emission data in [ppm] at the outlet of the micromix combustor with different NOx models.

By comparing the data listed in group 1 and group 2, the result shows that the turbulent interaction of temperature directly affects the NOx emission prediction. In group 2, all the NOx model selections predicted the NOx emission excessively lower than the reference value 1.3 from the experiment. Therefore, it reflects that the turbulent interaction of temperature is essential to post-process prediction. The comparison between the “Partial equilibrium” (P) and “Equilibrium” (E) of [O] approach of both groups verified the theory above. The partial equilibrium model is slightly higher than the equilibrium approach. The NOx value in group 1 displayed the more reasonable results; for the same [O] atom approach, the NOx emission predicted with different [OH] approaches showed almost the same value. Based on the theoretical analysis mentioned before, compared with the impact of different [O] atom calculation

approaches, [OH] radical models have almost negligible changes in NOx emission, which means the selection of this radical would not affect the calculation of NOx emission.

For the detailed [O] atom model, the results in group 1 show that the (P) and (E) approaches both over-predicted the emission amount of NOx; in the first column, the instantaneous (I) approach has much lower NOx which is closer to the experimental data. Based on this point, the conclusions of the NOx model selected could be settled. For the [O] atom approaches, significant differences are presented between the instantaneous predictions and the other two approaches. Only the "Instantaneous" method predicted the acceptable value of the emission, when using (P) and (E) approaches, the calculated amount of the NOx emission is far from the measured data.

Figure 3-16 below directly demonstrates the emission with different NOx models compared to the measured data. The bar chart indicated that the instantaneous approach of [O] atom predicated the NOx values around 1.09 which are the most closed. The (P) and (E) both have the excessive calculated NOx which has about 1ppm and 0.7ppm gap compared to the measured value respectively. It proves the importance of the "Instantaneous" approach. With the equivalence ratio increasing, the prediction of "**TII**" setting will be closer to the experimental data, and the differences of the other setting will become bigger. As the conclusion of the NOx model evaluation, the temperature turbulence interaction would be included for further simulation works, and the "instantaneous" approach is adopted for both [O] atom and [OH] radical. Although more computational resources will be consumed, it is acceptable if the calculation result could be more accurate. Therefore, the combination of the NOx mode used in this project will be "**TII**".

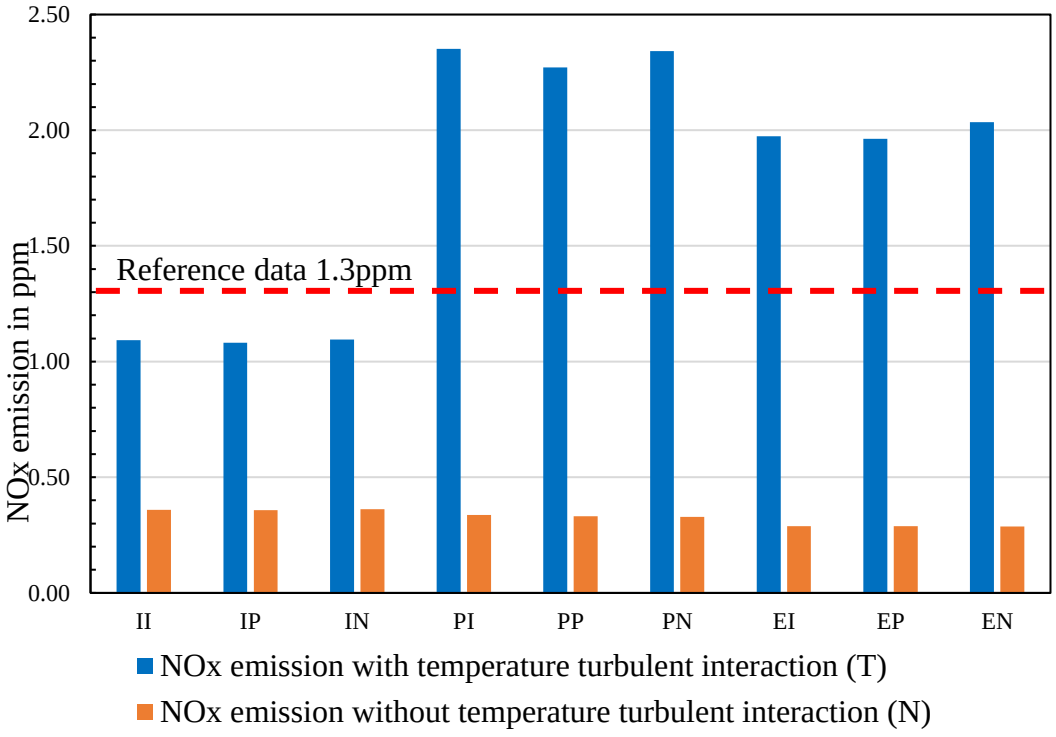

Figure 3-16. The NOx emissions simulated with different NOx model settings.

3.6 Hydrogen Combustion Model & Mechanism Selection

As the study of hydrogen oxidation progresses, simulations have become a valuable tool to save time and reduce economic costs. Simulations allow for a more detailed and realistic analysis of hydrogen combustion, including flame behaviour and pollutant emissions. To achieve accurate and efficient simulations, it is essential to use appropriate hydrogen reaction mechanisms.

In this project, all simulations of hydrogen combustors will utilize detailed reaction mechanisms to enhance the accuracy of predictions for flame temperature and NOx pollutant generation. In the previous section 2.2, various hydrogen combustion mechanisms were analysed in detail by reviewing extensive literature and evaluating existing mechanisms. However, relying solely on literature is not sufficient to draw

conclusive findings. Therefore, in this section, different hydrogen reaction combustion mechanisms will be applied and evaluated through simulations of micromix hydrogen combustion with the basic burner.

The results obtained using different reaction mechanisms will be compared with experimental data from the paper[66]. This comparison will enable the researchers to identify the most suitable reaction mechanism for subsequent simulations and design optimizations of the low NOx micromix combustor.

By thoroughly assessing and selecting the most appropriate hydrogen reaction mechanisms, the project aims to improve the overall performance and accuracy of the simulations, leading to more reliable predictions and a better understanding of hydrogen combustion behaviour.

In this section, there are 7 different optimised hydrogen reaction mechanisms have been selected based on the conclusion of the literatures on these mechanisms. The choice of these mechanisms covers a long time range. The first choice is the Ó Conaire's mechanism[74], this one has been widely used for many years, it shown good agreement with the test data in the low temperature range. The reaction mechanism from Zsély et al. [82] published in 2005 also been selected, this mechanism was updated from the Leeds methane reaction mechanism, although it performed not that well in the author following assessment in 2014[84], in the optimisation work the uncertainties of the kinetic parameters has been considered. Kéromnès et al.[85]'s reaction mechanism published in 2013 provide a satisfactory performance in high pressure and high temperature conditions, hence the Kéromnès-2013 reaction has also been selected. Creck-2012[122] and Hong 2011 [79] mechanisms are also applied in this section, the importance of key elementary reactions has been analysed in detail in their studies. In addition, the recently published hydrogen reaction mechanism ELTE-2015[86] from Eötvös University and Li-2015 from Xiaoyu Li et al. [123] were selected. ELTE-2015 mechanism was updated based on Kéromnès, it optimised Arrhenius parameters which

is very important when using the Finite-Rate chemistry reaction model. The latter publication from Li et al. reduces the uncertainty bound of model parameters and provides a reliable prediction at laminar flame speed.

3.6.1 Preliminary comparison of mechanisms

The selected mechanisms for the validation purpose are shown in Table 3-8 below, in the table, the number of reaction steps and applied species are listed. The usage of the Ar/He element was noted as well, it could be found that as the development over time, the species of noble gases also been considered in the reaction mechanism.

Mechanism	No. of species	No. of reactions	Ar/He	Reference
Ó Conaire-2003	10	21	x/-	[74]
Zsély-2005	10	32	x/-	[82]
Hong-2011	12	25	x/-	[79]
Creck-2012	11	33	x/x	[122]
Kéromnès-2013	12	33	x/x	[85]
Li-2015	11	25	x/x	[123]
ELTE-2015	12	30	x/x	[86]

Table 3-8.The summary of selected hydrogen reaction mechanism.

For the validation of the micromix combustion, the simulation of hydrogen combustion by using these mechanisms in the basic burner geometry will be compared against the experimental data shown in Table 3-8 above. For different mechanism test cases, the NOx pollutant emissions of hydrogen combustion with variable equivalence ratio from 0.3 to 0.54 will be recorded.

In the Table 3-9 shown below, it demonstrates the NOx emissions (in ppm) of hydrogen combustion in the basic burner while the combustion happened when the equivalence ratio is 0.4. It’s a preliminary comparison of different mechanisms with the reference

value 1.3. In this section, by considering the accuracy and correctness, the costs of computational source and time will be regardless. The model selection the NOx model used for all simulations is "TII" and the combustion model used is Eddy dissipation concept (EDC) and Finite-Rate/Eddy dissipation (FR/ED) respectively.

Mechanism	**EDC**	**FR/ED**	**Reference Value**
Ó Conaire-2003	2.66	1.03	1.3
Zsély-2005	2.65	1.03	
Hong-2011	0.94	4.21	
Creck-2012	2.09	0.88	
Kéromnès-2013	1.98	1.11	
Li-2015	1.74	1.05	
ELTE-2015	1.63	1.09	

Table 3-9.NOx emission simulation comparison with different mechanisms with Φ=0.4.

In Table 3-9 the NOx emissions in ppm calculated could be compared directly. With the selection of the combustion model FR/ED, most mechanisms' simulation results are all close to the reference value in a range of 0.3, which shows good agreement with the experimental model. When using the EDC model as the combustion model, the accuracy of the NOx emission prediction ability among the mechanisms shows a difference. Comparing all the mechanisms selected, ELTE-2015 and Li-2015 mechanisms provide relatively close results with the EDC model applied. For these two mechanisms, the FR/ED model shows a very good agreement with the reference experimental value. In addition, the calculated data of the Hong-2011 group is also noticeable, the simulation result with this mechanism shows an unusual trend compared to the other mechanisms. A higher NOx has been produced with FR/ED model, but the NOx formation amount calculated by EDC model is only 0.94 ppm, which is close to the reference data. Therefore, the mechanism of Li-2015, ELTE-2015 and Hong-2011 will be learned more deeply.

3.6.2 Evaluation of selected mechanisms

The mechanisms were constantly optimised with the development of time. The newest mechanisms provide the best performance are expected. Therefore, in this section, the mechanism of Li and ELTE will be focused and conduct more simulation work with the different equivalence ratios. Also, the mechanism from Hong will be studied as well, it shows a noticeable result in the preliminary comparison. The numerical prediction of the NOx emission is compared in the range from equivalence ratio 0.3 to 0.54 for these three selected kinetic mechanisms.

The operation conditions will remain the same as well as the fuel inlet amount to keep the thermal power of combustion the same. The NOx emission prediction results comparison of Hong-2011, Li-2015 and ELTE-2015 mechanisms are directly shown in Figure 3-17, the emission of NOx rising with the decrease of air/fuel ratio.

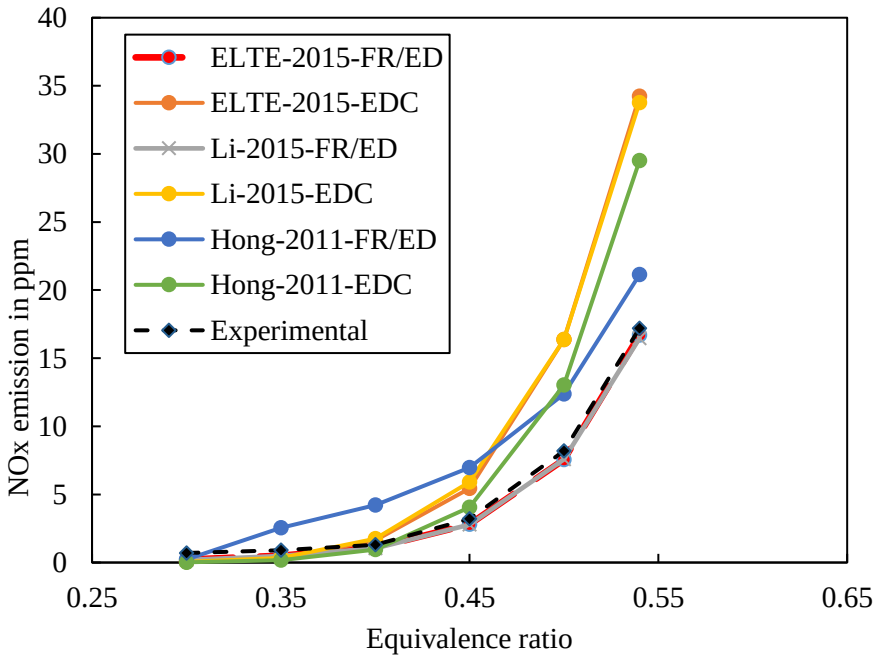

Figure 3-17. NOx emission prediction with selected mechanisms.

For the Hong-2011 mechanisms, the curves in the figure show an unexpected trend, the calculated NOx emission of EDC and FR/ED models are both greatly deviated from

the experimental results. The temperature contour in Figure 3-18 and the OH distribution contour in Figure 3-19 also show the performance difference between Hong-2011 and the other two selected mechanisms. When using FR/ED model, the high temperature region predicted by the Hong-2011 mechanism is bigger, and the flame length is longer as well. On the contrary, the predictions with the EDC model show an opposite result, the hot region is much smaller with a contour range of 1200K~2200K. In Figure 3-20, the NO formation contour comparison displayed a big difference, with FR/ED model the prediction by the Hong-2011 mechanism has bad performance. Compared to the other mechanism the NO formation was over-predicted. Therefore, the Hong-2011 mechanism would not be applied to the following simulation works.

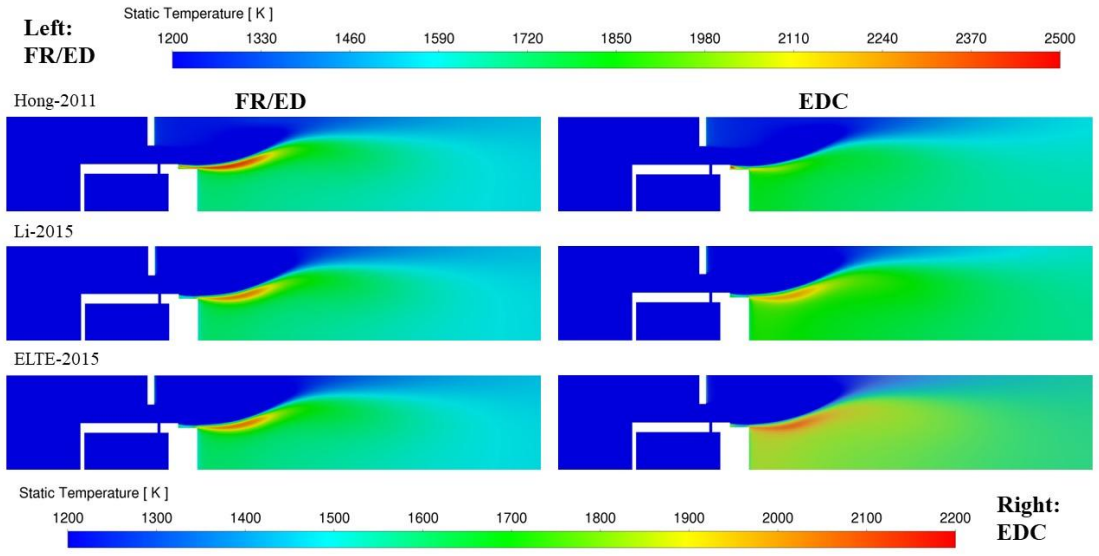

Figure 3-18. Temperature contour with different mechanisms

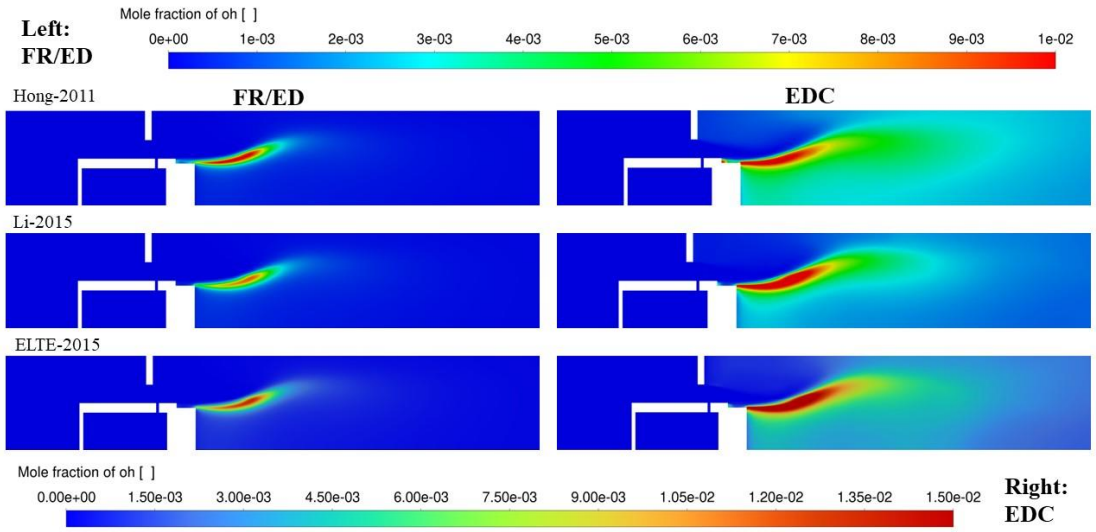

Figure 3-19.OH mole fraction contour with different mechanisms

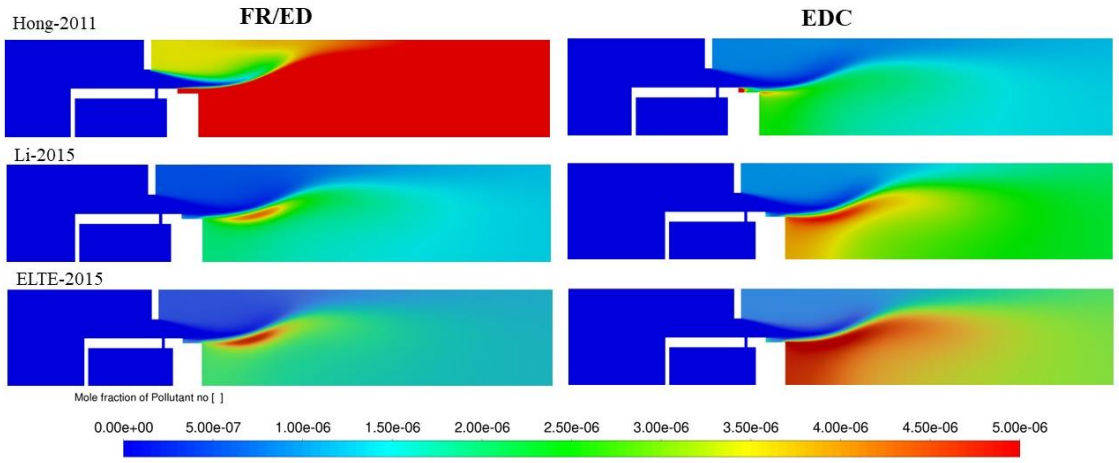

Figure 3-20.NO distribution contour with different mechanisms

In Figure 3-17, the ELTE-2015 mechanism and Li-2015 mechanism displayed an almost trend both with EDC and FR/ED models. The curves with different combustion models of these two mechanisms are overlapped. The FR/ED model of them presented a great agreement with the experimental data, with the equivalence ratio increase, the predictions maintained an accurate level. The prediction EDC model of ELTE-2015 and Li-2015 mechanisms show increasing differences with the equivalence ratio increased. Figure 3-20 displayed the NO distribution contour in the chamber, the high

concentration NO region predicted by ELTE-2015 is slightly bigger than the Li-2015 mechanism, which matches the NOx emission calculated. The NOx emission by ELTE-2015 mechanism is 1.09ppm which is closer to the measured data compared to Li-2015.

Overall, for the selected mechanism, both the ELTE-2015 and Li-2011 performed well with the NOx prediction, the simulation results are both in good agreement with the measured data. For the further study, both these two mechanisms are feasible. To decide on a mechanism for the following work, the ELTE-2015 mechanism is selected. Because the ELTE-2015 mechanism was specially optimised for hydrogen combustion, the OHEX (excited state) sub-mechanisms were included. By contrast, the Li-2015 mechanism is developed for H_2/CO combustion. In addition, the emission results calculated by ELTE are slightly more accurate.

3.6.3 Selection of combustion model

In this project, to simulate the combustion of hydrogen/air, the detailed mechanisms are evaluated and selected. It could more accurately describe the species' reaction during the combustion. Therefore, the species transport model would be applied for this project. Through the previous literature reviews on this subject, the finite rate eddy dissipation (FR/ED) model and eddy dissipation concept (EDC) model will be studied and discussed.

With the selected mechanism ELTE-2015, the numerical calculation of outlet NOx emission is shown in Table 3-9 and Figure 3-17. From the results above, it could be found that the predictions by FR/ED model are more accurate than the EDC model. Especially when the equivalence ratio increases, the results difference between EDC prediction and measure data becomes larger, with Φ=0.54 the predicted emission is doubled compared to experimental data. On the contrary, the numerical result by FR/ED model keeps a very good agreement with the measured data, the discrepancies were kept under ± 1ppm.

Theoretically, as expected, EDC model could provide more accurate predictions compared to the other species transport models, but the predictions show a contradictory result. After large sets of simulation work, the predictions by FR/ED model show very good reliability. For this situation, the initial guesses are the FR/ED combine the finite rate model and eddy dissipation model, and the reaction rate of hydrogen combustion is very high which is suitable for the EDM model. Also, the chemistry solver is another potential reason, the numerical calculation of micromix hydrogen combustion is steady combustion, the Relaxation to Chemical Equilibrium model is applied as the chemistry solver, the solver makes the species react towards chemical equilibrium does not react completely, which is matching the experimental measurement conditions. At present, the application of EDM and FR/ED model is mostly in industrial simulation works, which could give acceptable accuracy of the prediction of the industrial combustion but with relatively low consumption of the computational source. The accuracy of the EDC model needs more work on it, the experimental data is required for comparison which is certainly unfeasible. Hence, it is unable to give an accurate conclusion on which model is more accurate at this stage.

Anyway, although the NOx emission predicted point to the FR/ED model is more accurate, the EDC model would be applied as well to study the micromix geometry modification. For the geometric modification study, the trend of NOx emission variation with the dimension changes is the most important point. Therefore, the accuracy of both EDC and FR/ED models is acceptable as long as they can clearly reflect the NOx emission reduction/increase with the geometry optimisations. In the following studies, the EDC model will be used together with FR/ED model, to double verify the NOx emission variation trendy with burner configuration changes.

CHAPTER 4: THE MODIFICATION OF MICROMIX BURNER GEOMETRY

In Chapter Three, the numerical settings used for the micromix combustor geometry study were validated with the reference experimental data from Aye[66]. The performance selection of the viscous model and combustion model showed good agreements with the realistic experimental condition, it proves that the numerical settings studied for this project are trustable for the subsequent CFD study of hydrogen micromix combustor design.

In this chapter, the geometry of the single micromix combustor element will be modified, the optimisations are based on the basic burner studied in the last chapter. The change of the design is aimed at reducing the NOx emissions of a single injection element but maintaining the thermal density the same. Hence, the dimension of the injection element will remain the same, which the front size will be 3 mm * 10 mm, the other geometry detail will be updated to investigate the NOx emission variations.

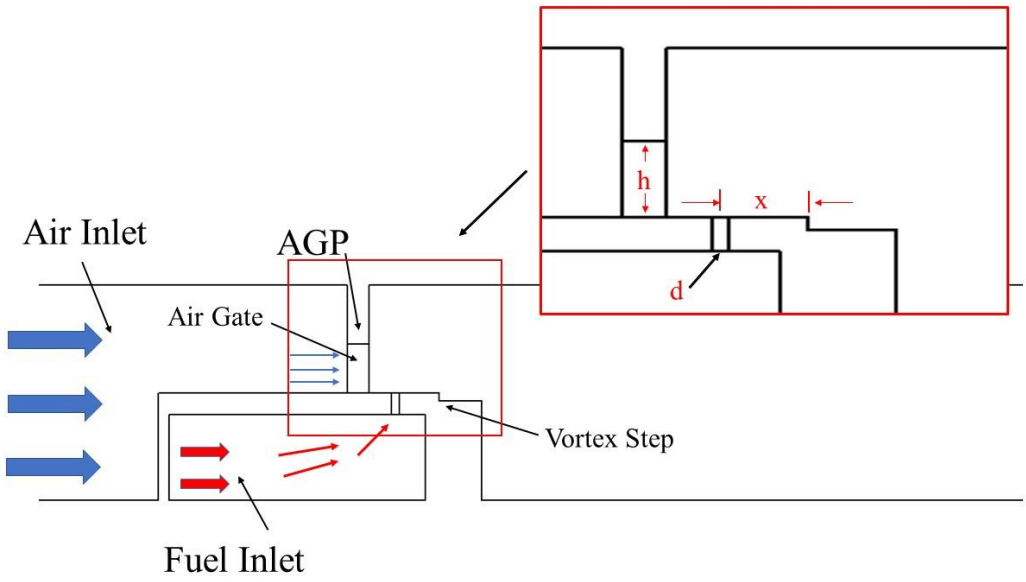

Figure 4-1. The annotation of the micromix combustor geometry.

To optimize the performance of the hydrogen micromix combustor, there are some design points could be improved, which are shown in Figure 4-1 above. From the experience and theories [65], [117], [124], the dimensions of the mixing field could affect the mixing intensity effectively which will contribute to the amount of NOx emission formation. In this section, there are three main geometry parameters will be investigated, which are the height of the air channel (h), the mixing length of the air and fuel (x) and the diameter of the hydrogen injector (d). In the following study, the simulation work will focus on the modification of these parameters, main research objective is to investigate the effect of geometric shape changes on NOx pollutant emission for the purpose of low NOx emission hydrogen micromix combustor design.

4.1 The Effect of the Mixing Distance On NOx Emission

From the last chapter and the previous studies, it could be observed that the flame usually occurs behind the point of the vortex step, before this point the hydrogen fuel and air are mixing intensively. Then the reaction happens in the mixtures, the flame profile anchored along the shear layer formed by the vortices in the chamber. The simulation result of the basic burner is shown in Figure 4-2 below, the temperature contour and the velocity pathline are demonstrated. From the velocity pathline the flow dynamics in the chamber is displayed clearly. By combining Figure 4-1 shown above it can be seen that the air stream enters the combustor and flows through the air gate and accelerates, the hydrogen fuel injected perpendicularly into the air stream. Then vortices form in the chamber, the upward impact of the fuel stream promotes the formation of the inner vortex, the flame occurs in the shear layer formed between the inner vortex and outer vortex, it could be assumed that the shape of the shear layer affects the flame profile. The outer vortex was formed because of the recirculation of the hot gas downstream of the flame.

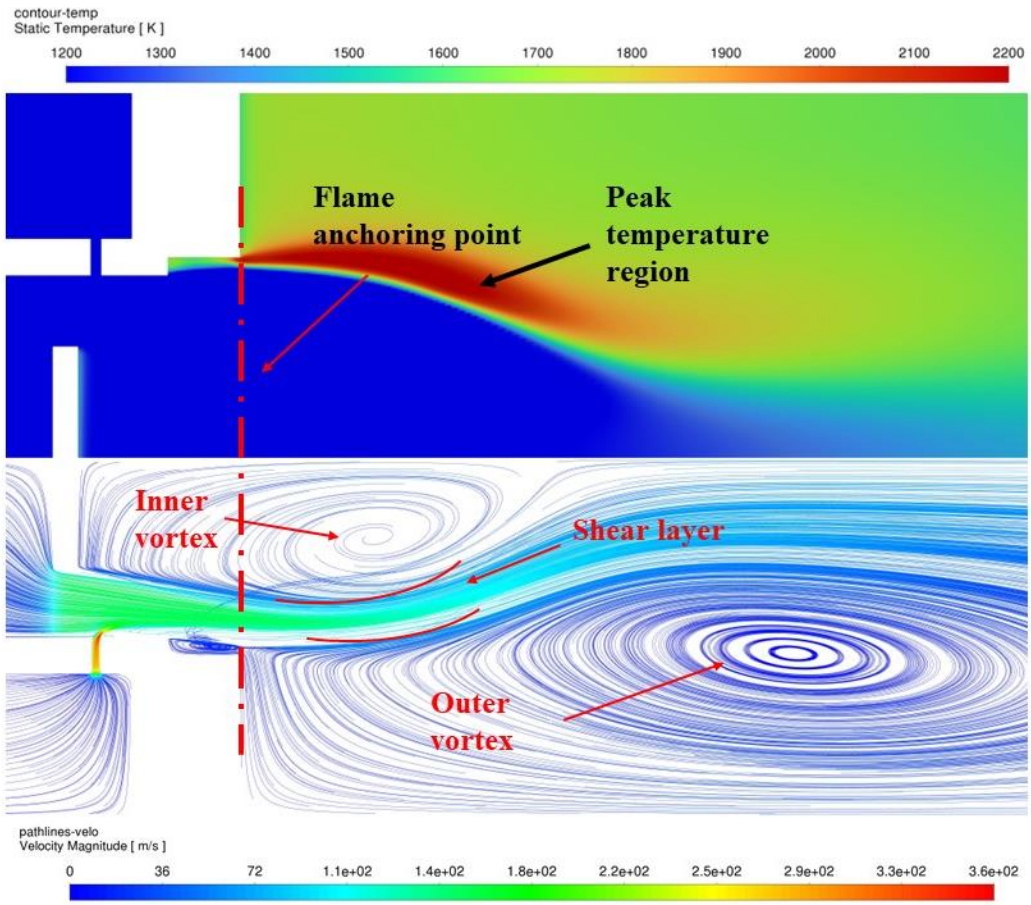

Figure 4-2. The temperature contour and velocity pathline of the basic burner.

As known that the NOx formation is strongly related to the mixing intensity and the flame temperature. Therefore, this section is focused on improving the mixing of hydrogen and air. If the fuel stream and air stream remain the same, the injection depth of the hydrogen fuel would not change. Based on this point, disregarding the influence of the other factors, just improve the mixing by changing the mixing distance x shown in Figure 4-1. The flame would stabilize after the flame anchoring point, then before the mixture ignited, the longer distance should provide a better mixing ability. There are three different mixing distance geometries are studied to compare the emission reduction ability, the detailed dimensions of the geometries are shown in Figure 4-3.

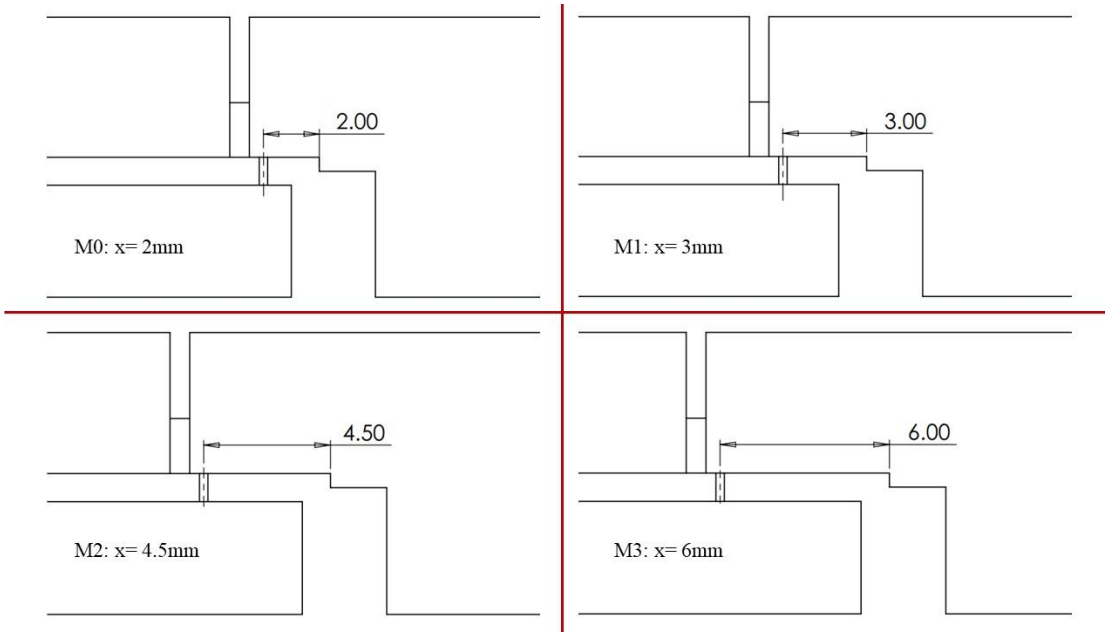

Figure 4-3. The designs of mixing distance study.

M0 is the design of the basic burner, it will be considered as the design prototype, the mixing distance will be increased from 2mm to 6mm. Because this study only conducts numerically, the cost of the manufacturing is saved, the length of the mixing area could be tested with a wide range. The mixing distance is varied for these four cases, to maintain the accuracy of the numerical calculations, for all these cases, the mixing distance part will keep the similar mesh density. Hence, with the increase of the mixing distance, the mesh cell number would also increase.

There are some points that need to be noticed:

- The energy density for all the combustor designs is kept at 6.7MW, therefore, for the same air gate size and hydrogen pipe diameter, the velocity of the gas streams is maintained the same at the specific equivalence ratio.
- The mixing distance is defined as the point from the hydrogen injection pipe to the vortex step. To compare the influence of the mixing distance x, the other dimension will remain the same as the basic burner.

- The combustion model used for this part is the FR/ED model, although there are some arguments about the accuracy of combustion model EDC and FR/ED, the main purpose is studying the NOx variation trend. Therefore, even though the simulated result may not perfectly match the real measurements, the performance of the design medication still could be observed by comparing the trend of the emission.

4.1.1 Results of variable mixing distance designs

The combustion performances of the hydrogen fuel of design cases M0~M3 are simulated by using the software Fluent 2021 R2. The results are compared from the aspects of temperature distribution, NOx emission in ppm and distribution and the flow dynamics inside the chamber. The emission of NOx for these cases is plotted in Figure 4-4. By considering the arguments of the combustion model in the last chapter, both EDC and FR/ED models have been applied to simulate the NOx emission for M0-M3 cases. From the plotting the trend of the NOx emissions change could be intuitively observed, as the mixing distance increases, the NOx emission drops rapidly, especially in the range of the length from 3mm to 6mm. In the results of the FR/ED model simulation group, the NOx emissions were reduced about 40%, this value is even bigger in the EDC model's prediction which is about 50%. Initially, the downward trend was not that significant from 2mm to 3mm, the NOx emissions difference between reference case M0 and M1 was only 0.05ppm, the change of mixing distance is not effective. Then after the mixing distance extended to 4.5mm, the NOx was decreased greatly. In the comparison of the findings of the figure plotted, both the combustion models showed the NOx emission trend that the design objective was achieved, the results support the idea that the NOx emission could be reduced by enlengthening the mixing distance.

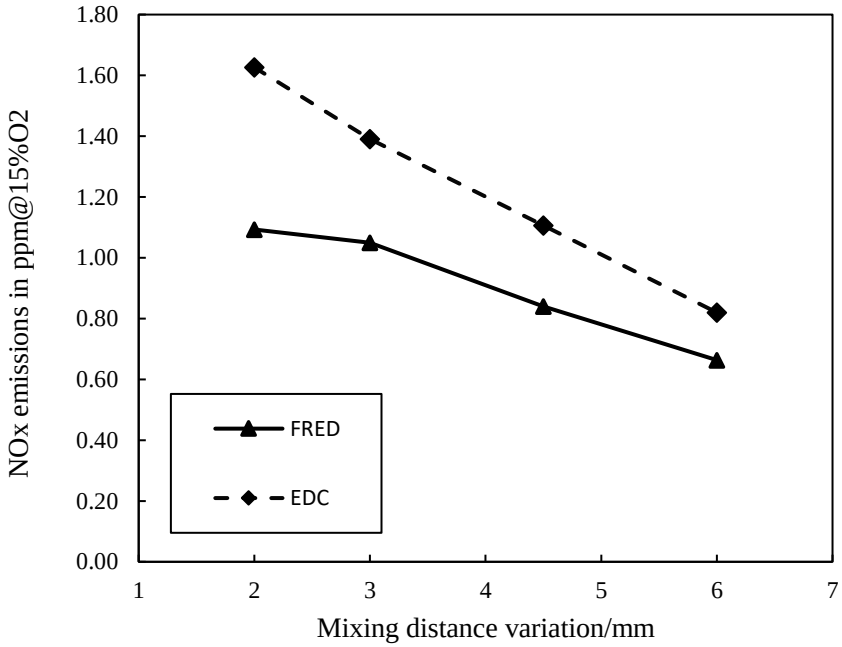

Figure 4-4. The effects of mixing distance on NOx emission

Figure 4-5 presents the results obtained from calculations of mixing distance cases M0-M3, the flow structures inside the micromix combustor are clearly demonstrated. In this typical micromix burner structure, the vortices formation is significant to the fuel-air mixing and flame stabilization. The intent of these designs is to increase the mixing intensity of the fuel and air, the pathline of velocity shown below confirms that the longer mixing distance could effectively increase the vortex size formed in the chamber. The size of the inner vortex keeps growing from cases M0 to M3, and the difference between M1 and M2 is not that obvious which coincides with the results above, the length of the mixing distance longer than 3mm improves the size growth of the vortex.

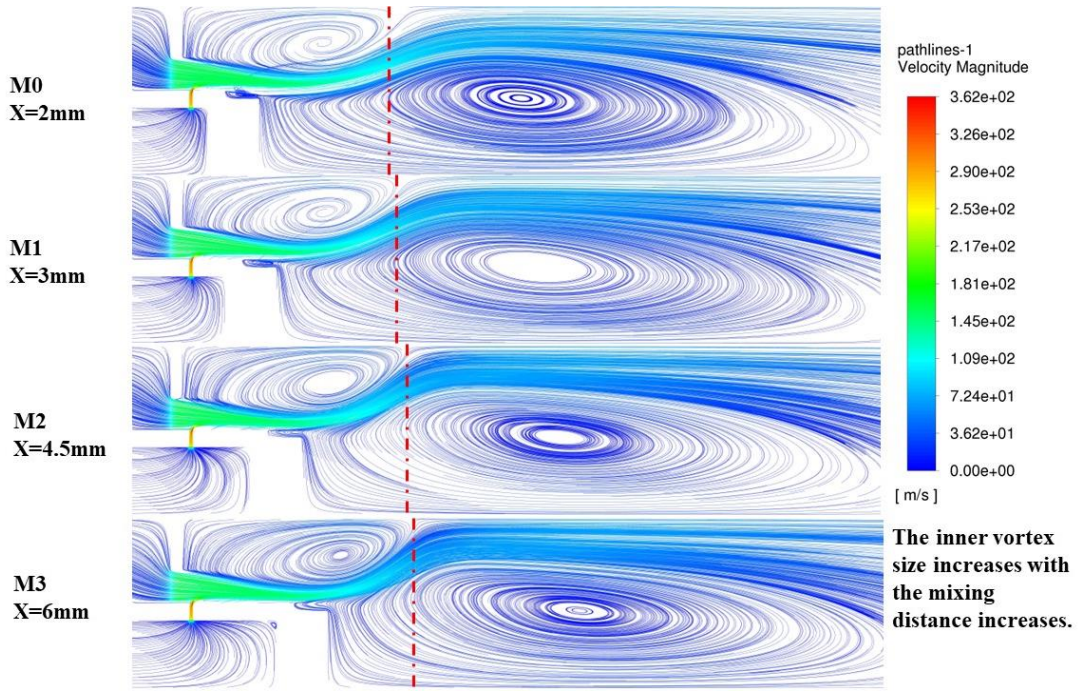

Figure 4-5. The vortex structure change of the micromix combustor designs.

In accordance with the results presented in Figure 4-7, the NOx emissions concentration decreased dramatically from case M0 to M3, with the mixing distance increases, the NOx peak area gets narrow. As can be seen from the NOx distribution contour, the high NOx emission formed along the shear layer where is the flame anchored range, the shrinkage of the high NOx field indicates that the NOx emission amount has been reduced. The Figure 4-6 shows below also proves that the extension of the mixing distance effectively improves the mixing intensity of fuel/air, the local equivalence ratio inside the chamber shown below in the gray-scale contour, it could be found that in case M3 the colour at the inner vortex is darker than the other cases, which means that hydrogen and air have better mixing in this region. In addition, the vorticity magnitude contour line is shown in Figure 4-6 as well, it shows that the vortices size in longer mixing distance cases is larger, and more fuel/air gas is involved in the inner vortex.

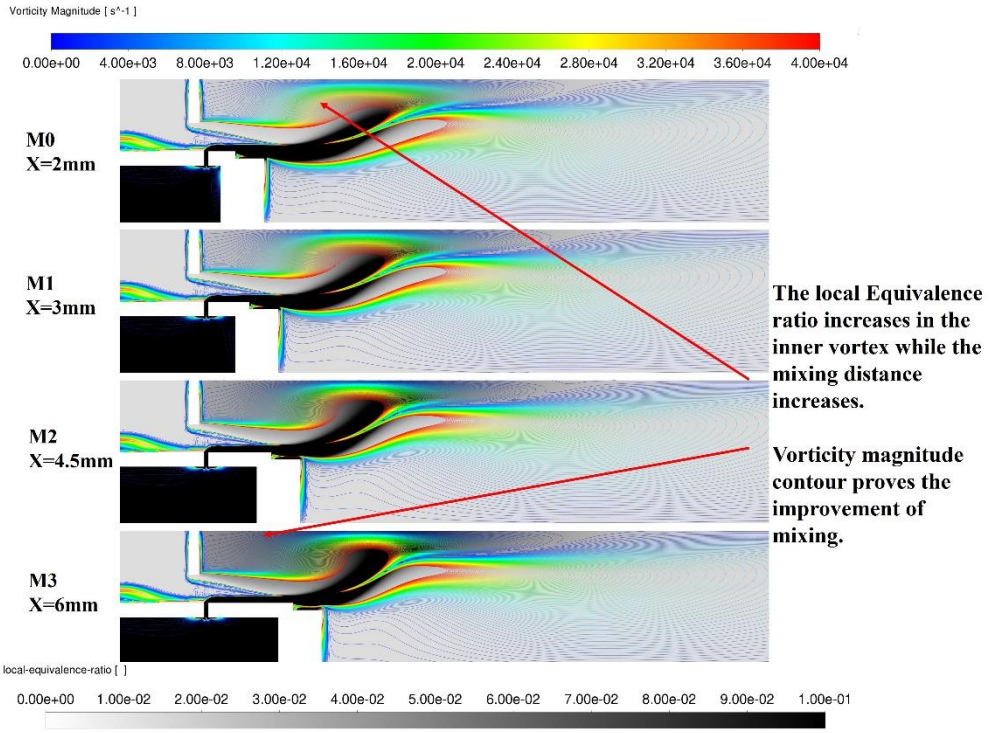

Figure 4-6.Local equivalence ratio and Vorticity magnitude contours with the mixing distance

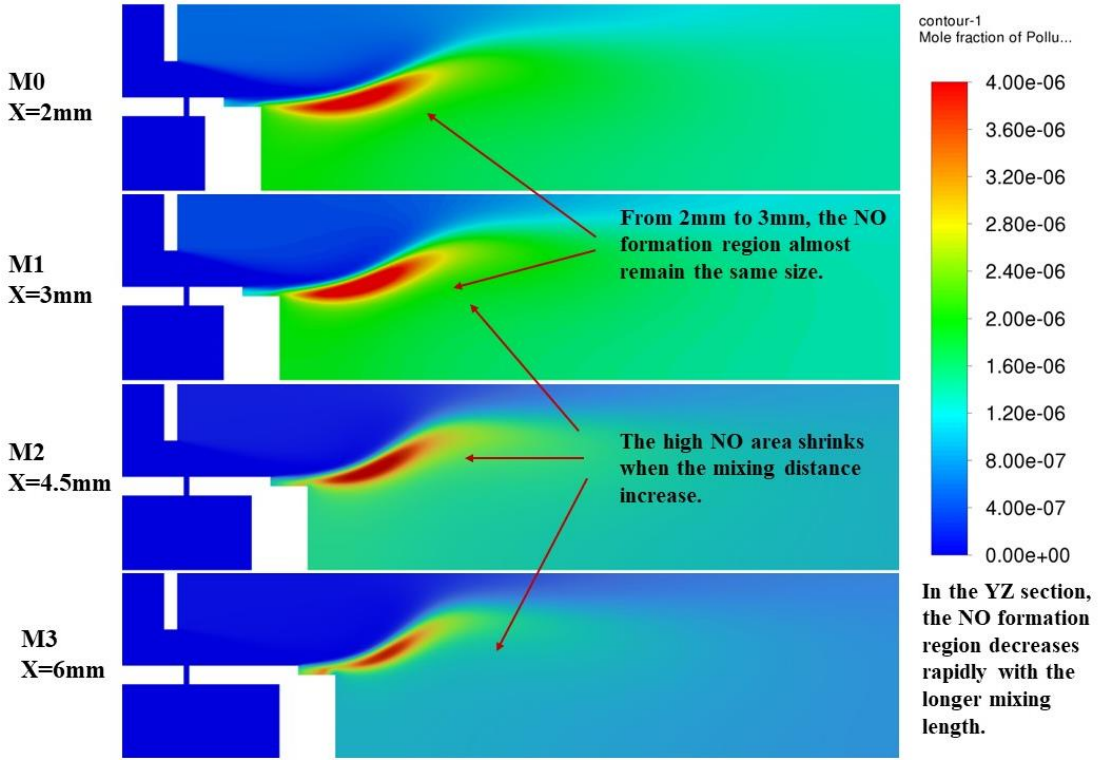

Figure 4-7. NOx emission reduced with the mixing distance variation.

Figure 4-5 and Figure 4-7 reflect that the larger the vortex size, the lower NOx pollutants are produced. It could be deduced that the extension of the mixing distance did functional for the NOx emission reduction, this could be considered that the increase of the vortex size does improve the mixing ability. With the growth of the recirculation area, more gases participate in the strong turbulent movement, which resulted in more species being involved in the vortex, the fuel and air got sufficiently mixed. The vortex increases the interface area of the mixture flow which leads to the improvement of mixing. Another possibility which helped in the NOx emission is the gas velocity increased in the vortex with the extended mixing length, the speed at the edge of the vortex is slighter higher when the size grows bigger. But the velocity change is too minor, this statement requires more work to prove it.

The design cases with A/F ratio change

To further study the NOx emission reduction ability of the mixing distance design cases, the hydrogen micromix combustion should be tested with different operation ranges. At lean fuel conditions, the NOx emission was reduced compared to the basic burner design. In order to verify more deeply, the cases have been simulated with different equivalence ratios, for comparison purposes, the fuel inlet amount will still be 1.213m/s but the volume of the inlet air will be adjusted. The numerical calculation was completed by using FR/ED model, the NOx emission predictions in ppm are listed in Table 4-1. This data has been plotted in Figure 4-8 to compare the NOx emissions differences between case M1 to case M4 under variation air/fuel ratio conditions.

Equivalence ratio	M0 x=2mm	M1 x=3mm	M2 x=4.5mm	M3 x=6mm
0.3	0.21	0.19	0.18	0.16
0.35	0.51	0.49	0.41	0.33
0.4	1.09	1.05	0.84	0.66
0.45	2.81	2.53	1.98	1.53

0.5	7.57	6.66	5.36	4.38
0.54	16.70	15.19	12.07	11.55

Table 4-1. The NOx emission of variation mixing distance with different A/F ratios.

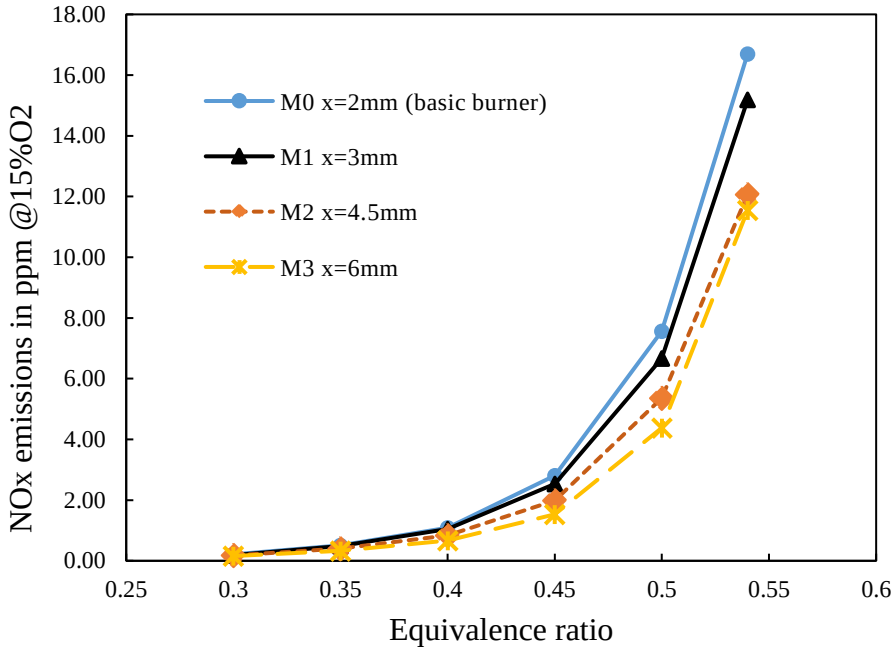

Figure 4-8. NOx emission at different equivalence ratios of modified cases.

The curves in the graph above clearly show the NOx reduction performance discrepancy with the mixing distance change, it can be seen intuitively that when the mixing length is extended, the NOx emissions are reduced, especially when the inlet air is less at high equivalence ratio, the effect on NOx emissions reduction is particularly obvious. In all modified cases, the M3 case has the lowest emissions at each equivalence ratio point among all the cases. Compared to the original design case M0, the decline of the NOx emission is even greater than 5ppm at the equivalence ratio $\phi = 0.54$. It is noticeable that, at the high equivalence ratio $\phi = 0.54$ the longest mixing distance case M3 has similar emission compared to case M2, this finding points out that it is not feasible to increase the length of the mixing one-sidedly, the excessive extension may reduce the efficient NOx emission reduction. On the other hand, the long

mixing distance may increase the heating area of the chamber wall which has the risk of material failure.

The overall performance of modified cases showed great NOx reduction ability at high equivalence, these reflect that the NOx emission reducing ability could be better when the fuel fraction increased. The reason for this phenomenon may be due to the mixing intensity is playing an important role under rich fuel conditions, when the fuel/air increases, incomplete combustion often occurs in the combustion chamber when excess fuel is injected, which causes an increase in temperature and a dramatic increase in NOx emissions. Therefore, in this case, it is particularly important to improve the mixing strength to help the fuel mix with the air adequately, which then improves the efficiency of combustion and reduces temperature and emissions.

4.1.2 Conclusion of mixing distance designs

The results discussed above confirm the association between the geometry modification of the mixing distance and the NOx emission. The simulation results of different cases seem to be consistent with the theory mentioned before, that the NOx emission is related to the mixing intensity of fuel and air. The optimisation of the design geometry considering this theory, the design's main objective is to improve the mixing of the flow streams in the chamber but maintain the thermal power the same. The geometry modifications did achieve the study aim, the mixing distance extended resulted in the enlarger of the vortices size formed in the chamber, the peak flame size and the NOX emissions were greatly reduced by the improved mixing intensity. In the optimized designs, the hydrogen fuel injected perpendicular to the air stream has longer distance to mixing with oxidizers before the flame started, the updating of the low NOx micromix combustor is successful. At the equivalence ratio of 0.4, the NOx emission has been significantly reduced from the design case M0 to M3, the simulation results applied with FR/ED model indicate that the NOx decreased from 1.09 ppm to 0.663 ppm when the mixing distance increases 4mm. The geometric variation may cause the

practical micromix burner has a thicker hydrogen segment and increase the burner weight, but the great reduction of the NOx emission makes this design still have the potential in future research.

4.2 The Effect of Air Gate Height Variation

In the last section, it has proved that the NOx emissions are related to the mixing distance, in the case M0 to M3, the air stream through the air gate remains the same compared to the reference design of the basic burner. The results support that even the velocity of the fluids entering the chamber doesn't change, the reduction of emission still could be achieved by changing the geometry design. In this part, the investigation of the effects of air speed entering the mixing area on NOx emission will be focused on.

For most of the previous studies by Funke et al.[63], [65] which involved the air guiding panel height effects put more attention to the overall structural changes, the hydrogen segments dimension is changed to achieve the research aims. This section of the project will only be focused on the air gate height and the relative speed variations.

The height of the air gate is important to the micromix combustor designs, the overall dimension of the micromix combustor element would remain the same compared to the basic burner. Air enters the front section of the micromix combustor and then accelerates when flows through the air gate, hence the height of the air gate is an important parameter to the air gas in the mixing section. The front area of the air inlet would be the same while the air gate height change, the total amount of air entering is constant under the same equivalence conditions.

4.2.1 Overview of air gate height designs

The air gate height of the basic burner design is 1.95mm, to study the effect of the height change, the air gate height was changed in both directions. There are 5 modified

cases in total, the dimensions varied from 1.5mm to 2.4mm as Figure 4-9 presented below, including the original basic burner 6 design was studied and the simulation of these cases was conducted by ANSYS Fluent 2021 R2, the viscous model used is still the shear-stress transport (SST) k − ω model, and both EDC and FR/ED combustion model are applied. Therefore, the geometry modification could be compared with the last mixing distance section.

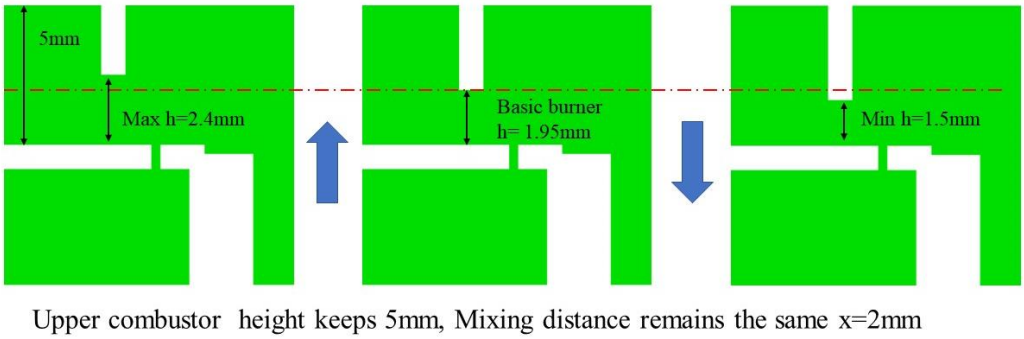

Figure 4-9. The indication of air gate height variation.

The reason why the air gate height is the changing of the height will cause the blockage ratio (height of upper section/height of air gate) different, which would influence the turbulence flow dynamic inside the chamber. Because in order to maintain the same thermal power, the fuel and air amount would not change under the specific equivalence ratio for all design cases. The importance of the air gate height is the fuel/air mixing intensity could be affected when the fuel stream is injected into the air stream, the injection depth of the fuel can be totally different with different heights. The equation shown below indicates the importance of the airflow. Its velocity would vary with the height of the air gate.

$$r = \frac{\rho_{H2} V^2{}_{H2}}{\rho_{air} V^2{}_{air}} \tag{4.1}$$

$$y \sim \alpha \cdot d_{H2} \cdot \sqrt{r} \tag{4.2}$$

Where V is the velocity of gases mixing, which is the air velocity through the air gate

and hydrogen velocity being injected in. r is the momentum flux ratio, it decides the injection depth y. From the paper [125], the value of α could be defined as 2, hence the preliminary calculation of each case could be calculated. The injection depth is essential to this micromix combustor jet-in design, the excessive injection may penetrate the air flow and cause the hydrogen fuel directly enter the inner vortex directly.

The brief of cases H0 to H5 are listed in Table 4-2 below, the air velocity through and momentum flue ratio are presented as well. The reference air gate dimension is 0.8mm(w) * 1.95mm(h), in this section only the effect of the gate height has been investigated, for all the cases the width of the air gate will not change.

Case	Air gate height	Air velocity (m/s)	Momentum flux ratio
basic burner- H0	1.95mm	100.00	0.53
H1	1.50mm	130.00	0.32
H2	1.65mm	118.18	0.38
H3	1.80mm	108.33	0.46
H4	2.25mm	86.67	0.71
H5	2.40mm	81.25	0.81

Table 4-2. Design case information.

It could be seen that with the increase of the air gate height, the momentum flux ratio grows as well, it deepens the length of the hydrogen fuel penetration.

4.2.2 Result of numerical study of air gate design case.

The boundary conditions are the same for all the design cases H0 to H5, the NOx emission in ppm plotted in Figure 4-10 could directly demonstrate the performance of each case design. Both EDC and FR/ED models are applied to study the trend of different air gate height's NOx emissions. It is very obvious that when the air gate height increases the NOx emission increase rapidly. In the comparison between case

H0 and case H5, the air gate height increased 0.45mm but the NOx amount at the outlet is three times higher in FRED model results. The NOx emission with EDC model shows a similar tendency, the slight increase in the height of the air gate can lead to a multiplicative increase in the production of emissions. The NOx increasing exhibits a slow trend from case H1 to H3, but when the height is higher than 2mm, the pollutant increases abruptly, compare the NOx emission between case H0 and case H4, the air gate height increased 0.3mm but the NOx emission doubled. For both combustion models' predictions, the results show that the NOx emissions are acceptable if the air gate height could be kept below 2mm.

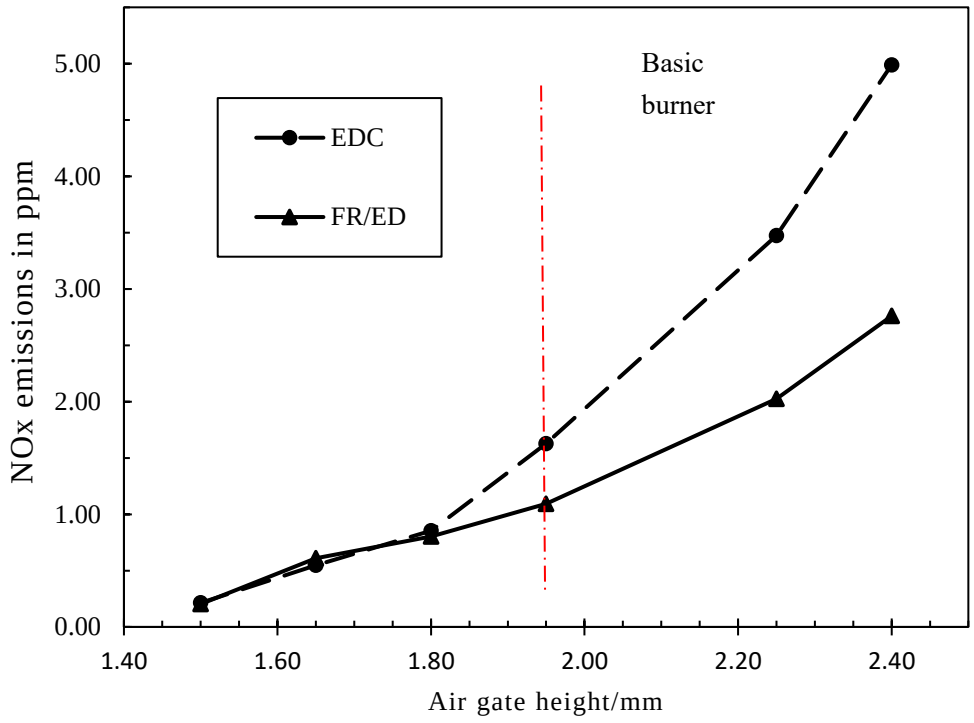

Figure 4-10. NOx emission changes with the air gate height variation.

The temperature distribution contour of these 6 cases is displayed in Figure 4-11 and Figure 4-12 below, from the contour it can be seen that with the height of the air gate increase, the NOx emissions reduction becomes worse. The height decrease group in Figure 4-11 shows a good performance of temperature reduction, the area of the high-

temperature zone is shrinking which corresponds to a significant reduction in nitrogen oxide emissions, the flame shapes of the cases H1-H3 are maintained a good typical micromix flame shape. The high-temperature zone distributes along the shear layer between the inner and outer vortex which maintains the chamber temperature relatively low.

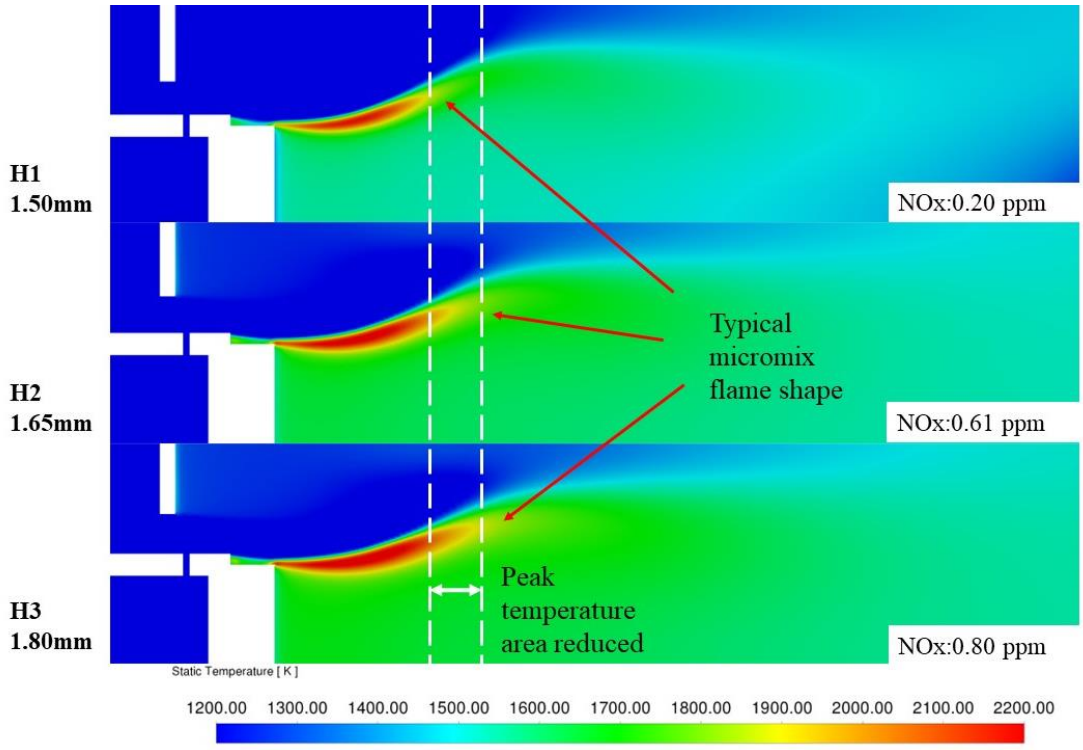

Figure 4-11.Temperature distribution in height decrease groups H1, H2, and H3.

By contrast, the gate height increase group demonstrate the results which are not expected. Compared to the basic burner design H0, as the height of the air gate increases, the size of the high-temperature region inside the chamber also gradually increases, and the length of the hot flame grows sharply and thickens at the gate height of more than 2mm. It can be seen that the heat of the flame has spread into the outer vortex which undoubtedly increases the downstream recirculated air temperature and makes the outer vortex unable to play a good cooling role.

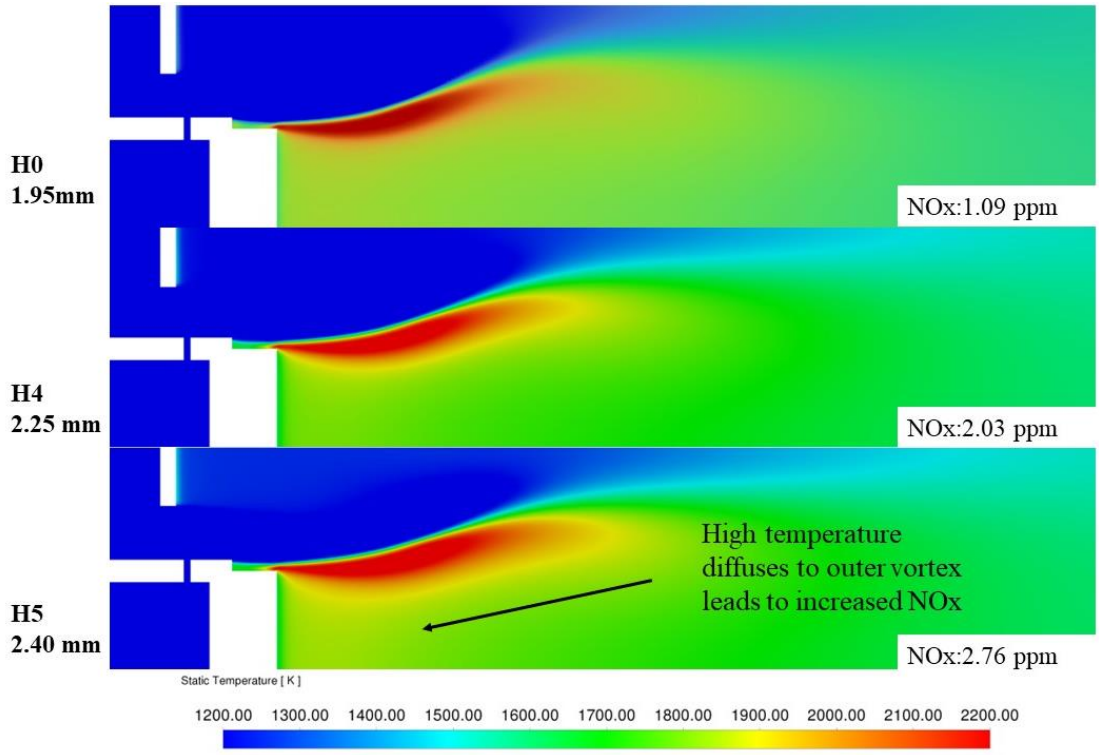

Figure 4-12. Temperature distribution in height increase group case H0, H4, H5.

To better understand the impact of air gate height on emissions reduction capacity, the typical modified cases will be compared and discussed. Among these six cases, case H5 presents the worst performance, the NOx emission produced in this case is more than ten times higher than the best design H1. The temperature contour has illustrated the reason why the NOx formation amount could increase such an amount. Figure 4-13 shown below displays the comparison of the NOx formation and temperature distribution of case H5, from the colourmap it can be seen that the pollutant distribution exactly matches the temperature contour, when the high temperature penetrates into the outer vortex, a large amount of NOx is formed and the residence time of NOx increased due to the bigger high-temperature zone which leads to the NOx emissions exponentially.

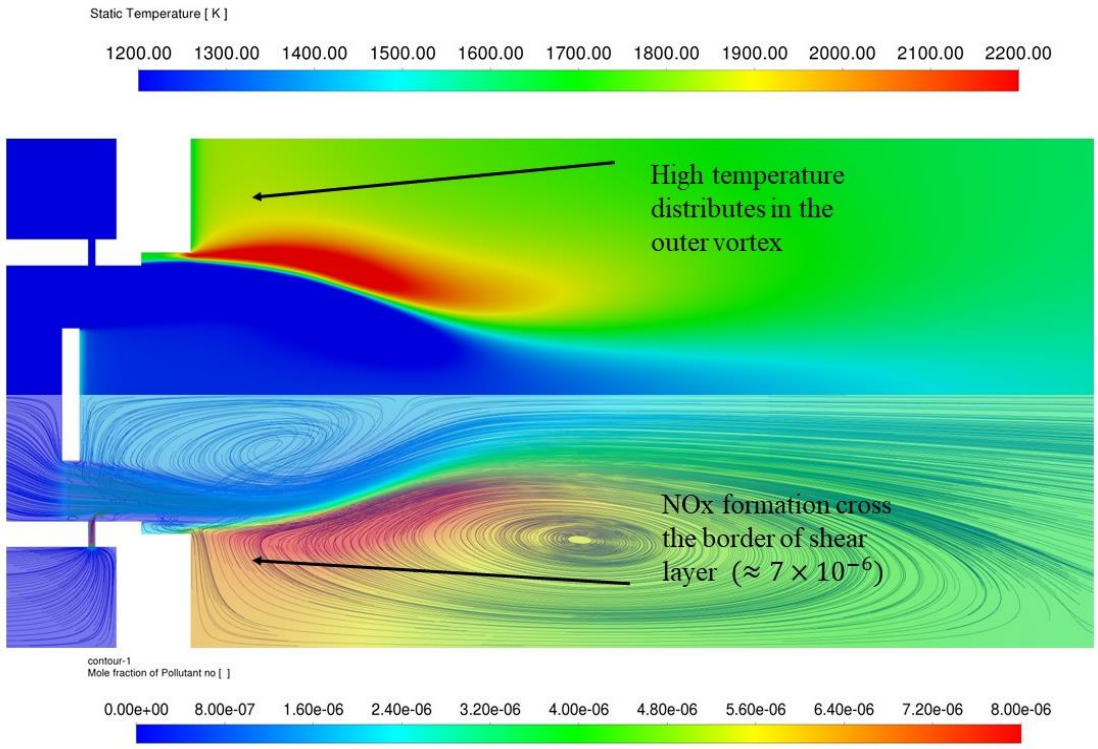

Figure 4-13. NOx and temperature distribution of case H5.

In addition, in Figure 4-14 the velocity pathline of cases H1 and H5 have been compared, it demonstrates that the higher air gate drives the inner vortex size smaller, the width of the inner vortex in the H5 case decreased, as mentioned before the mixing intensity could be affected by the vortex size changes which may contribute to the NOx emission increases. Another reason that would lead to higher NOx production could be because of the velocity in the outer vortex. In case H5 the velocity at the edge of the outer vortex is lower than in case H1, this makes the gas of the vortex into the shear layer slower, the cooling air is difficult to lower the temperature in the combustion zone.

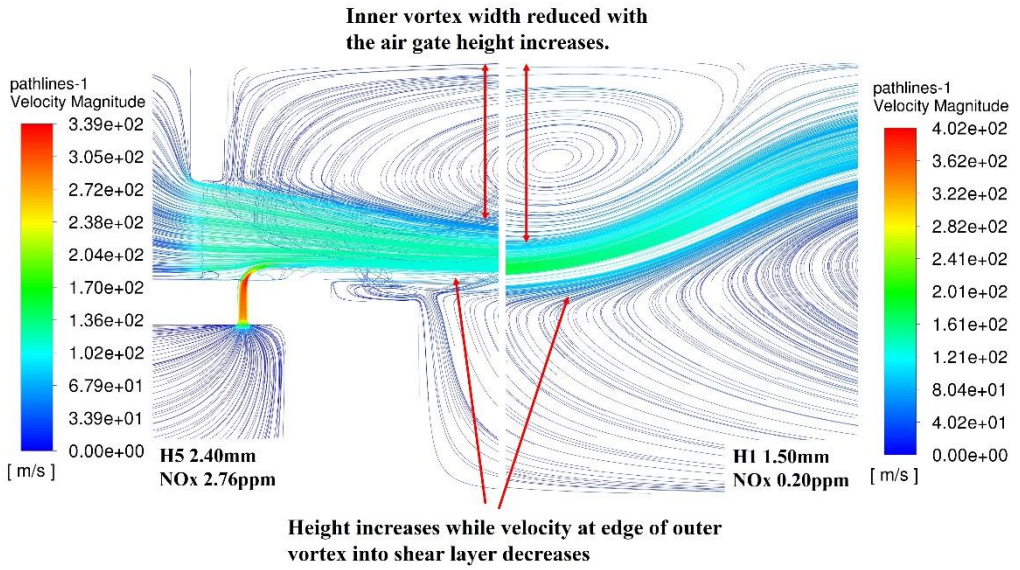

Figure 4-14. The pathline comparison between cases H1 and H5.

Figure 4-15 below demonstrates the difference of mixing of the fuel/air between cases H1 and H5. This figure demonstrates the local equivalence ratio contour in the gray-scale and vorticity magnitude in bgr-scale. From the figure, it could be found that with the lower air gate, in the inner vortex region, the contour colour of case H1 is lighter than case H5, which means that the local equivalence ratio is higher and more fuel has been involved in that region, the fuel and air has better mixing in the inner vortex. The vorticity value further proves this point, the vorticity value is higher in case H1, which means the lower air gate could provide better mixing ability between fuel/air.

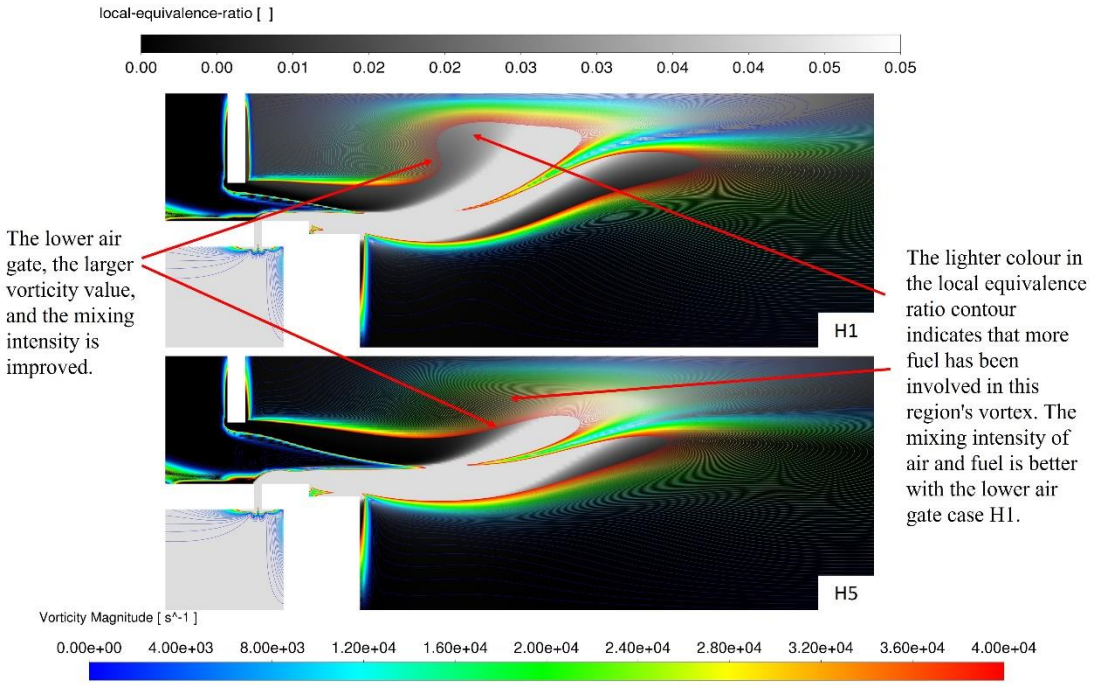

Figure 4-15. Local equivalence ratio and Vorticity magnitude contours of case H1&H5.

Overall, the flow dynamics changes in the micromix combustion chamber finally led to the combustion temperature variation which is the main factor that affects the NOx formation. According to the theory [46] NOx is always formed with high combustion temperature, hence the temperature variation between cases is quite important. The temperature in the flame region of different design cases is different, to better observe the temperature variation in the chamber, the X-Y facet maximum temperature is plotted in Figure 4-16. The cross sections on the Z axis along the chamber are set every 1.5mm from the air gate, the starting point of the record is the flame started position (4mm from the air gate), therefore the temperature of the flame is recorded.

The curves clearly illustrate how the air gate design affects the peak temperature in the combustor, except the temperatures at the ignition point are close, the temperatures distributed along the chamber are lower with the small air gate. For the peak temperature region which is about from 5.2mm to 11.5mm, the temperature at each position of design H5 (2.4mm) is about an average of 50K higher than the reference basic burner H0. Compared to the best performance case H1 (1.5mm), the temperature

dropped greatly at each point, the average difference of each point could be about 200K. Then at the downstream of the flame, the temperature has been reduced significantly between case H5 and H1, which is about 400K.

It could confirm that the temperature of micromix combustion could be reduced by changing the air gate height which is essential to the low NOx design. The results of these cases demonstrate a great ability of temperature reduction. In addition to the decrease in peak temperature, one more thing can be found in the curves that the flame length is shortened from case H6 to case H2, at the position of Z=19mm, the maximum temperature of case H1 has dropped to 1625K, which almost lower than the NOx formation temperature, by contrast, the temperature in H1 still over 1900K, the NOx continuously formed in this area. The other AG height cases showed a similar trend, with the height reducing, the temperature in the chamber would be decreased.

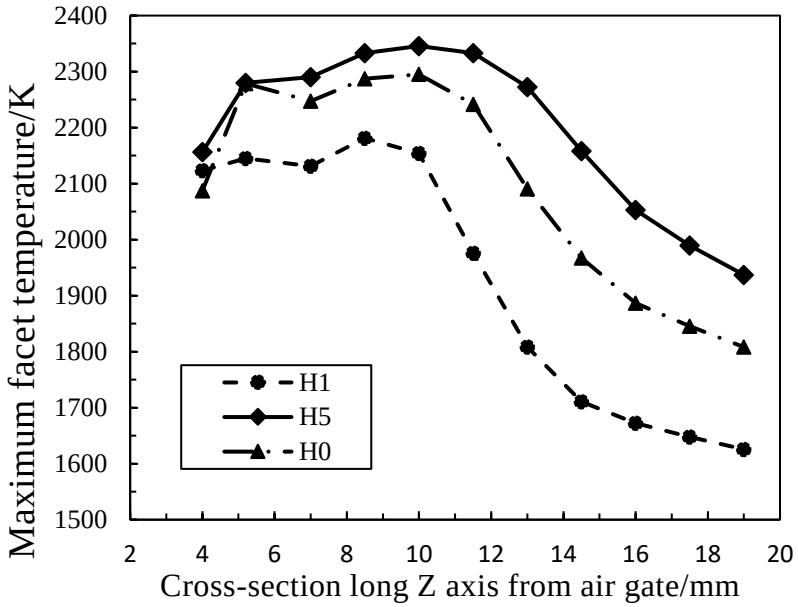

Figure 4-16. The comparison of maximum temperature along the chamber between cases H0, H1, and H5.

4.2.3 Discussion

The comparison of the findings with the air gate height case confirms the injection

depth and momentum flux ratio theories make sense. The air gate height variation design drives the velocity of the air stream through the channel changes, from the equation it can be seen that the velocity of the hydrogen injected speed will remain constant, with the height increase the velocity of air decreases. By applying equation (4.1) shown above, the momentum flux ratio increased at higher air gate, which will lead to the injection depth increases. According the theory of the jet-in cross flow from the papers [66], [126], [127], the injection depth should be guaranteed less than the critical injection depth y_{crit}. If the momentum flux ratio is too big, the risk of the hydrogen penetration into inner vortex would cause the fuel to enter the recirculation region, the residence time of the mixture will be extended, and the NOx formation would increase significantly in the hot region. There is also a minimum limitation of the fuel injection depth, if the injection distance is too short, the hydrogen cannot enter the cross-airflow deep enough, the mixing could be decreased, the NOx formation will be intensified. Also, the combustion may happen near the lower surface of the air channel, which could reduce the lifespan of the combustor.

For all the air gate cases H0 to H5, the injection depth could be directly evaluated by the equation (4.2) shown above, it is obvious that with the lower gate height, the injection depth will reduced. As the experience, the longer injection penetration could improve the mixing intensity and lower the NOx emissions. The result shows a total opposite trend, the biggest injection depth case H6 provides the worst NOx reduction ability. This does not imply that the results of the simulation contradict the theory, because in the previous study the dimension of the upper section of the combustor chamber but maintained the air gate height was the same to study the injection depth effect, the thickness of the air stream would be the same as the gate height constant. The critical injection depth y_{crit} is determined by the air gate height, therefore, y_{crit} for each air gate height case in this study is variable.

To study the effects of penetration distance of the fuel injected, the ratio of injection

depth to the thickness of air flow should be considered. The fuel injection depth of the best case H1 and worst one H5 are deeply investigated, the penetration distance of fuel in both cases is compared. By studying the hydrogen species contour shown below (Figure 4-17), it can be seen from the comparison, although the injection distance in H1 is only 0.25mm, smaller than the depth in H5 0.35mm the penetration ratio is more important for the fuel and air mixing. Even though the fuel injected distance of H5 is longer, the thicker air stream controlled by the air gate makes the depth of the hydrogen penetrated air shallower proportionally, the result of the NOx emission proved this which H6 has 2.76 ppm and H1 only produced the NOx 0.20 ppm.

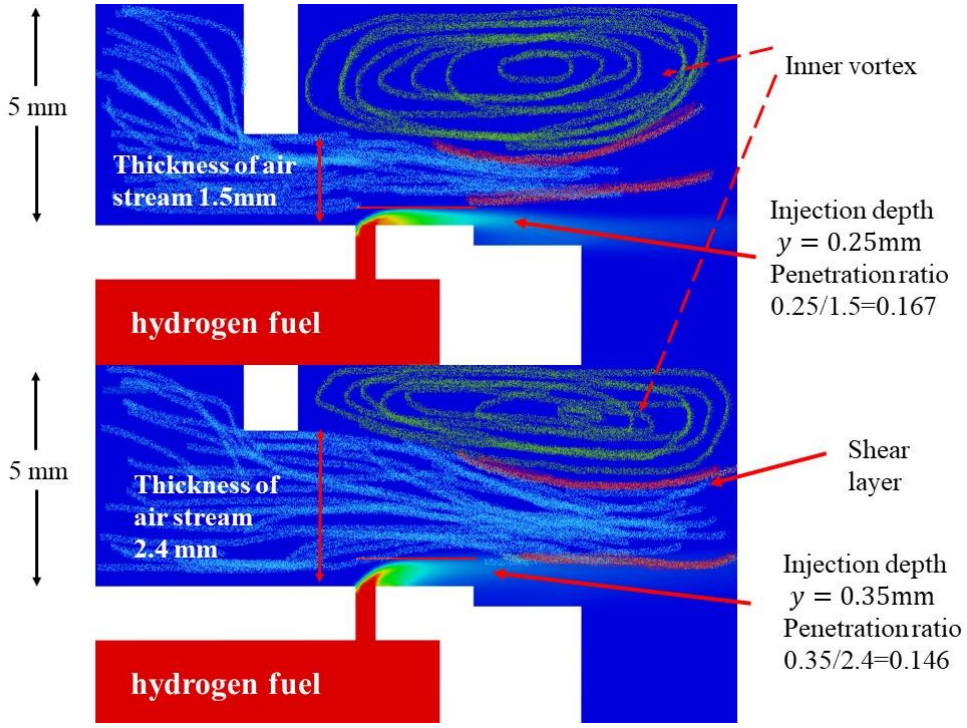

Figure 4-17. Hydrogen injection depth comparison between H2 and H6.

4.2.4 Conclusion of air gate height design

In conclusion, the results demonstrated above confirm that the jet-in cross-flow theory by Recker et al.[63], [125] is valuable for the micromix combustor design. The NOx emission produced in each case confirms that the higher air gate will have more NOx

formation during the combustion. This is mainly due to two reasons, firstly the higher air gate will squeeze the width of the inner vortex size which will lead to the weak mixing of air and fuel, at this circumstance the NOx formation would be higher. Another factor is the higher air gate height may cause the lower penetration ratio, the less injection depth relative to the thickness of air stream makes an insufficient mixing before the ignition position, the region of NOx formation is extended and the residence time increase causes the rising of the NOx formation amount. The potential of low air gate design has been demonstrated, after the comparison, NOx emissions are reduced by about 80% compared to the original design H0. For more in-depth learning, the low gate design requires more research in the future, as the small air gate may reduce the thickness of the shear layer and contribute to the shrinking of the NOx formation region, which is expected, but the excessive low air gate may cause the fuel-air mixing near the wall section, the high temperature of the wall could cause the combustor failure and more cooling agent required. However, for practical usage of this design, the present research is insufficient, the boundary conditions for realistic situations are different. The pressure condition would affect the performance of the design in this section, for the same geometry the pressure variation would make the velocity of air and fuel different which leads to the injection depth varying.

4.3 Effect of Hydrogen Injection Diameter Change

In the micromix combustion concept, an important idea is the hydrogen fuel injection method changed to the perpendicular jet-in cross-flow method, the hydrogen fuel is injected into the air stream vertically which increases the interaction between fuel and oxidiser. In this concept, the flame length and the thickness are related to the recirculation gas flow dynamic in the Z-Y plane of the chamber. As the results discussed in the sections previously, the vortex size and shape determine the shear layer formed in the gap between the two vortices. Except for the fame structure on the Z-Y plane, the width of the high-temperature region created by flame is significant as well.

In this section, how the hydrogen injection hole diameter affects the NOx emission during the combustion will be studied by redesigning the fuel injector diameter. In the cases studied before, the attention has been put on the airflow dynamic, the hydrogen injected velocity remains the same for all the designs. The effect of hydrogen velocity variation will be focused. Also, for the same burner out appearance, the width of the chamber will be the same but with changed hydrogen diameter would affect the flame width.

In the previous studies by other researchers [68], [117] the hydrogen injector diameter of the micromix combustor also been involved, in those studies the burner dimensions also modified with changes in normalised energy density. The purpose of this variation is because the diameter changes have the risk that the flame merges with neighboured injection elements. In this project, the study concentration will be put on diameter and NOx emissions themselves with the same energy density and dimensions. Also, the flame merging situation will also be concerned to make sure the design is in an available operation range.

4.3.1 Overview of the hydrogen diameter variation cases

The hydrogen injection diameter design cases will be studied in two directions, in the preliminary study, two cases are studied and compared to the basic burner. Case D1 decreased the injector diameter of the reference burner from 0.3mm to 0.24mm, Case D2 studied the NOx emission with the larger hydrogen injector which has the diameter of 0.4mm. All the other geometric parameters of all the cases remain the same. The premise of the diameter design cases is listed below.

- For better comparing purposes, the normalised energy density will not change which means the inlet air amount and the fuel inlet amount will still be the same with the previous cases.

- The combustor outline dimension will remain unchanged which allows the velocity of the air inlet and hydrogen inlet to be constant compared to the cases studied before under the same equivalence ratio. As the diameter of the hydrogen injectors changes the velocity of the hydrogen gas intersecting the air stream will be different.
- The boundary conditions of the gases inlet are kept the same, the inlet pressure and temperature of air still be 1 bar and 550K.
- To observe the NOx variation trend, both the EDC and FR/ED models will be applied, also the viscous model will be SST k − ω model.

As the schematic (Figure 4-18) of the design cases D1 and D2 shown below, only the diameter of H_2 injector changed, the position of the injector kept the same distance from the air gate as well as the mixing distance. To better understand the temperature and NOx emission distribution in the burner, the cross-section panel along the Z axis was established to cover the flame range, the panels set every 2mm from the position of -7mm.

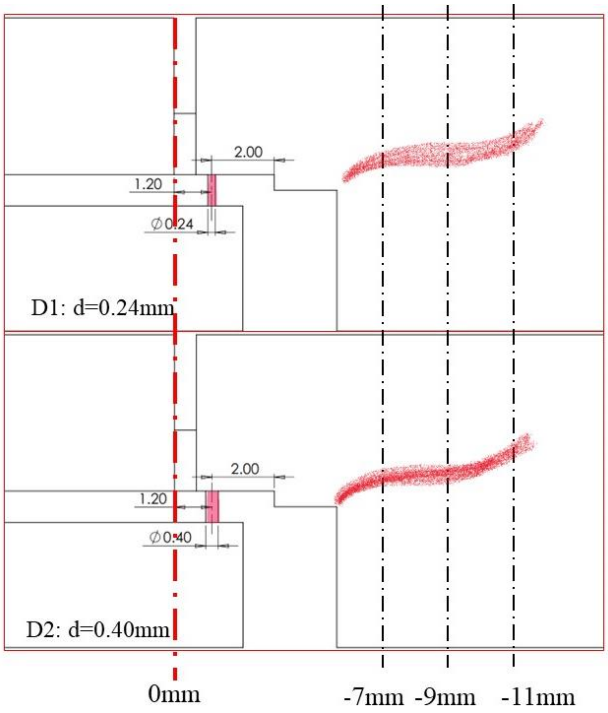

Figure 4-18.Schematic of injector diameter design cases D1, D2.

4.3.2 Result and discussion of the H_2 diameter designs

The initial case studies were focused on these two cases, the simulation results of cases D1 and D2 showed the combustion performance when the diameter decreased and increased respectively. Preliminarily, the boundary condition of the combustion simulation was set with the equivalence ratio of 0.4 only, thus the emission result could be directly compared with the reference burner data. For case D1, with a smaller injector size, the emission decreased from 1.09ppm to 0.85ppm in FR/ED model group and 1.62ppm to 1.17ppm in EDC group. By contrast, with the diameter of the hydrogen injector increased to 0.4mm, the NOx emission increased 0.07ppm with FR/ED model. The NOx formation variation is slight between these cases, the emission reduction effect is not particularly obvious. As mentioned before, the objective in this section also includes the effect of flame width with the injector diameter changes.

Figure 4-19 and Figure 4-20 display the temperature and OH species distribution along

the chamber, the simulation results are displayed on the cross-sections. If the starting position of the flame is defined as -5.2mm, the positions of each established panel start from -7mm and cover the length of the flame ends at -15mm. (In different cases, this length is variable). From the contour, although the peak temperature in both cases is almost the same, the high-temperature zone size has significant differences. With the increased hydrogen injection diameter, the width of the high temperature field is extended, it leads to the NOx increasing by extending the residence time in the chamber.

In the combustion simulation, the flame shape image cannot be directly obtained from Fluent, in the experimental works the species of OH* and OH have always been used to study the flame structure. The papers indicate that the OH* could provide a more accurate result of flame shape [128], [129], however, the mechanism used doesn't include the species OH* in reactions, the OH species would be used to define the flame shape in this project. By combining the OH contour below, the flame shape can be roughly observed. The diameter increases leads to the flame width increase between D1 and D2, the flame in case D2 is too wide which is already close to the edge of the injection element. It causes the risk of the flame merging between the next injection units which will result in the rapid increase of NOx emissions. The miniaturized flame produced in single element merged, at this point, the meaning of the micromix combustion concept is lost. Another potential reason of the NOx formation difference is the cooling gases, as the annotations on the figure indicated that in case D1, the flame anchored along the centre of the chamber, the space between the edge of the chamber allows the cooling gases downstream flow around the flame, the NOx products could be taken away fast and reduce the residence time. Also, the space wrapped flame could be cooled and reduce the temperature in that region. This has also been demonstrated in the temperature and OH contour, in the cross-section at 13mm position, which is the end of the flame tip. In case D1, cooling air flow through the sides of the peak-temperature region, conversely, the combustion in D2 forms a high-temperature zone connecting the two sides of the burner. The wide flame of case D2 displayed in Figure

4-20 illustrates that the flame near the single combustion zone, as know that the wall of this burner is the symmetry panel, the wider flame increases the risk of the flame merging with the neighboured combustion zone. The thousands of micromix flames would connect and form the flame ring which will render the micromix design meaningless.

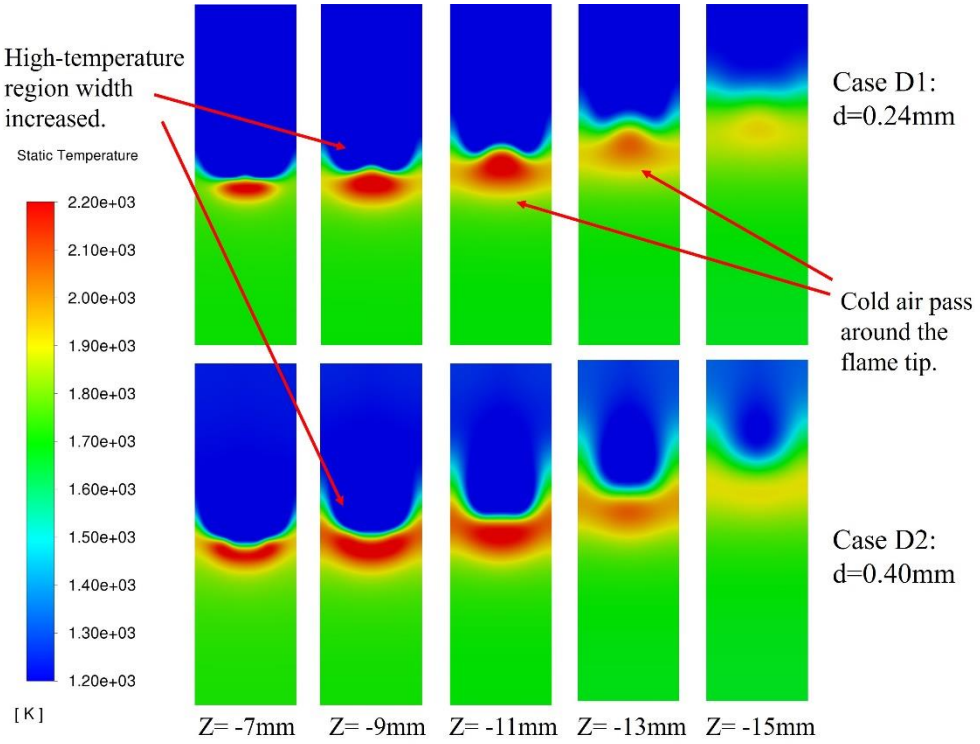

Figure 4-19. Temperature contour of cross-sections comparison between D1 and D2.

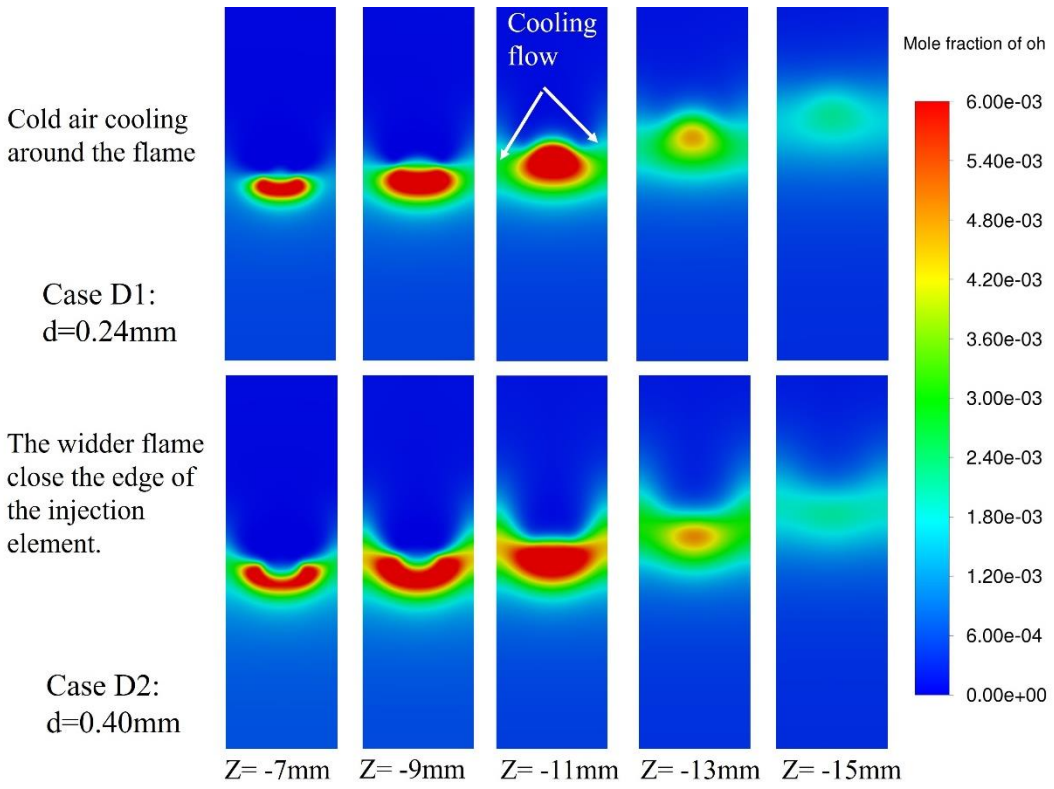

Figure 4-20.OH distribution contour of cross-sections comparison between D1 and D2.

The effects of the flame width on NOx emissions can be observed more visually in the NOx distribution contour shown below in Figure 4-21. It can be seen that as the diameter of the hydrogen injector increases, the high-temperature region becomes wider. Correspondingly, the high concentration of NOx region enlarged as well, the presence of the wider hot region prevents the oxygen and nitrogen from leaving the combustion region as quickly as possible which increases the residence time and leads to higher NOx. However, as mentioned before, the NOx only increased slightly with the diameter increase. The emissions controlled in 1.5 ppm is very acceptable for the micromix design. Hence, the focus of the design should be more on the flame merging risk.

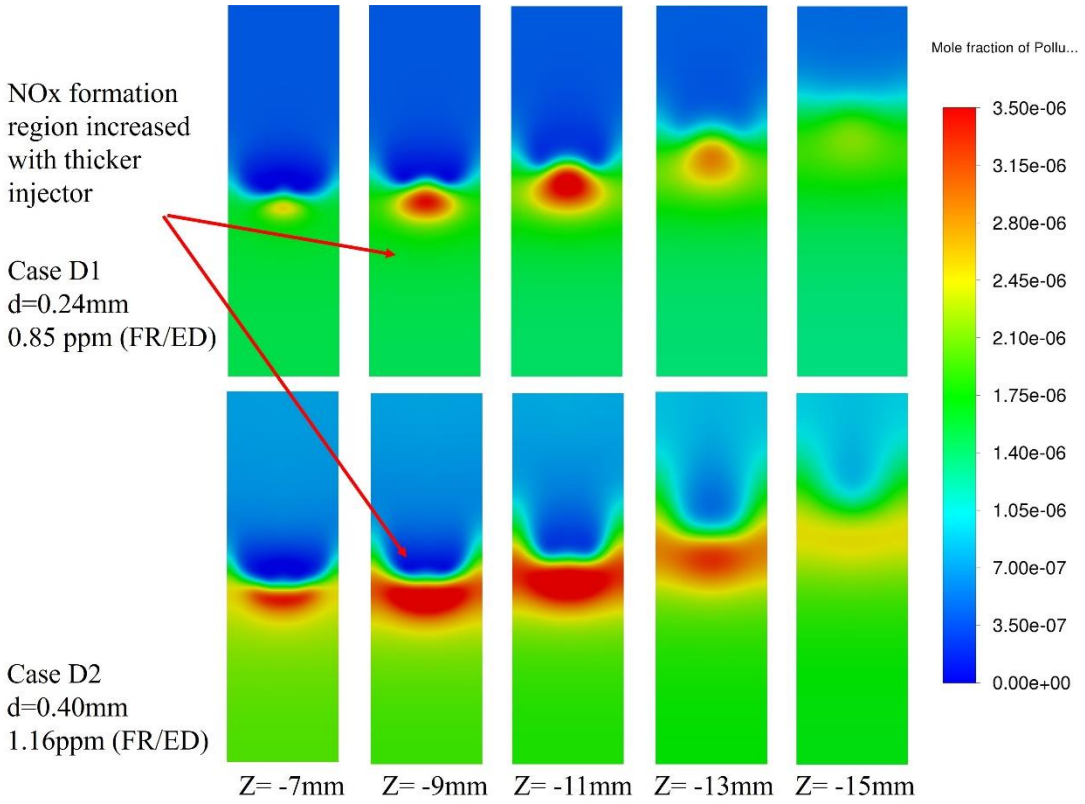

Figure 4-21. NOx distribution along the chamber with varied hydrogen injector diameter design.

In this section, only two modified models are compared, for further verifying purposes, the diameter of the hydrogen injector is increased to 0.50mm and simulated as named Case D3. The calculated NOx emission with the different equivalence ratios is shown in Figure 4-22 below, the results are compared to the basic design with $d_{H2} = 0.3$mm. Based on the experience before, the NOx emissions of this burner should be increased with the larger hydrogen injector in expectation. However, the plotting in the graph clearly demonstrates a contrary trend. When the low equivalence ratio lower than 0.4, the NOx emissions of the reference burner (named D0) are slightly lower than modified case D3, but when the air inlet amount decreased, the NOx production in case D3 reduced compared to the reference data. In particular, with the lower air/fuel ratio, the emission differences between cases can be even greater.

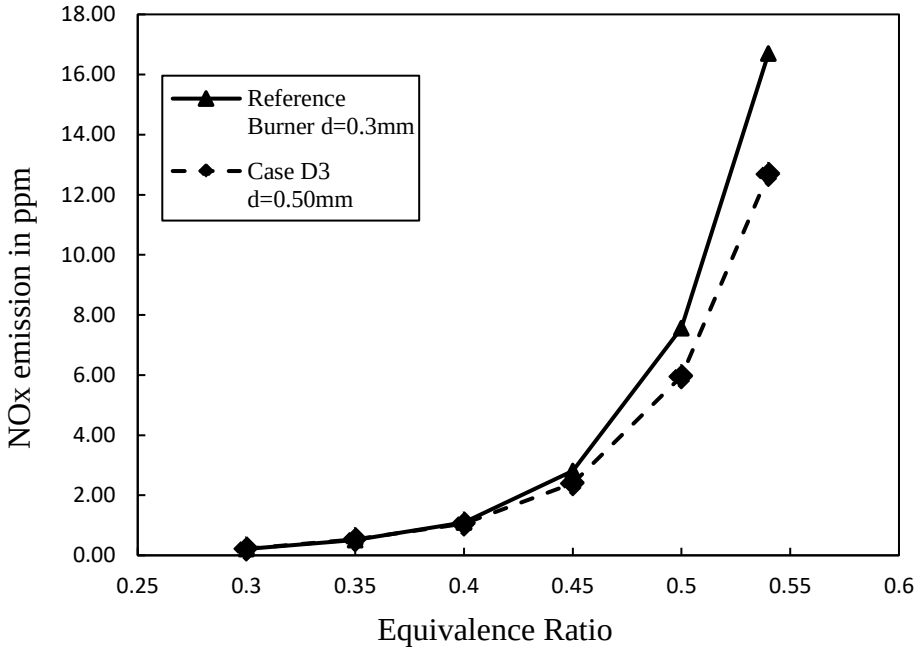

Figure 4-22.NOx emission of case D3 compared to reference burner.

Such numerical results are undoubtedly confusing because according to the theory of the injection momentum flux ratio and depth, the smaller diameter would provide a better penetration ability which could improve the mixing intensity and reduce the NOx. By observing the flame contour at the -11mm position of the chamber (shown in Figure 4-23), it can be found that at the high equivalence ratio, the flame region in D3 and D0 are both too wide which filled up the cross-section of the chamber, but when the combustor operated under Φ=0.4, the OH species distribution of D3 cases shown better shape than original cases. The preliminary guess is that at the lower air condition, the flame width almost occupies the entire Z-axis of the chamber, the peak temperature is almost the same in these cases, at this point the mixing intensity of the air and fuel is important to the NOx formation.

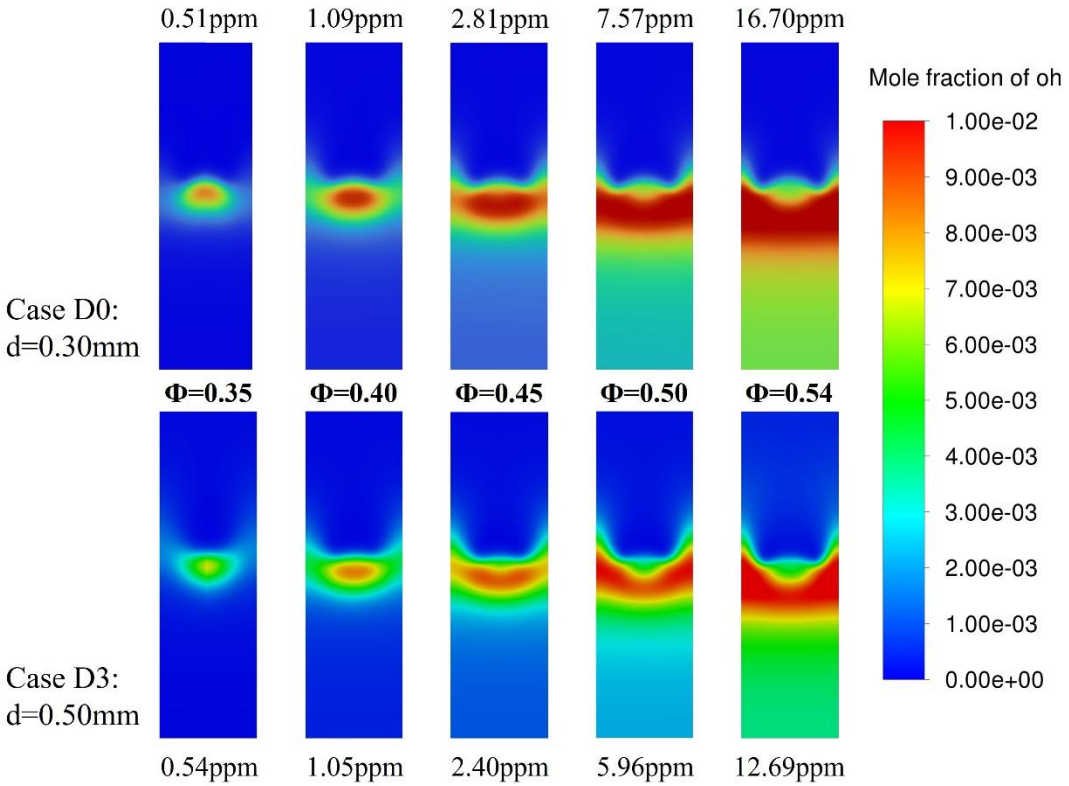

Figure 4-23.OH contour comparison between D0&D3.

The dynamic velocity pathline calculated by Fluent displays an interesting phenomenon that the enlarged hydrogen injector provides more lifting force to the air stream, although the injection depth decreased slightly, the width of the lifted air stream increased by increasing of fuel injector size. In the reference burner D0, the air stream was lifted from the midline of the chamber and formed the inner vortex from the middle to the sides. The larger injection diameter provides a better lifting capability, wider air stream forms the vortex more intensively. As Figure 4-24 demonstrated below, the velocity pathline under Φ=0.54 is shown. With high equivalence ratio, the flow dynamics difference is more obvious, the pathline in case D3 has the bigger inner vortex, more gases have been lifted into the inner vortex and increase the mixing intensity. The mixing of the air and fuel has been improved and contributed to the NOx reduction.

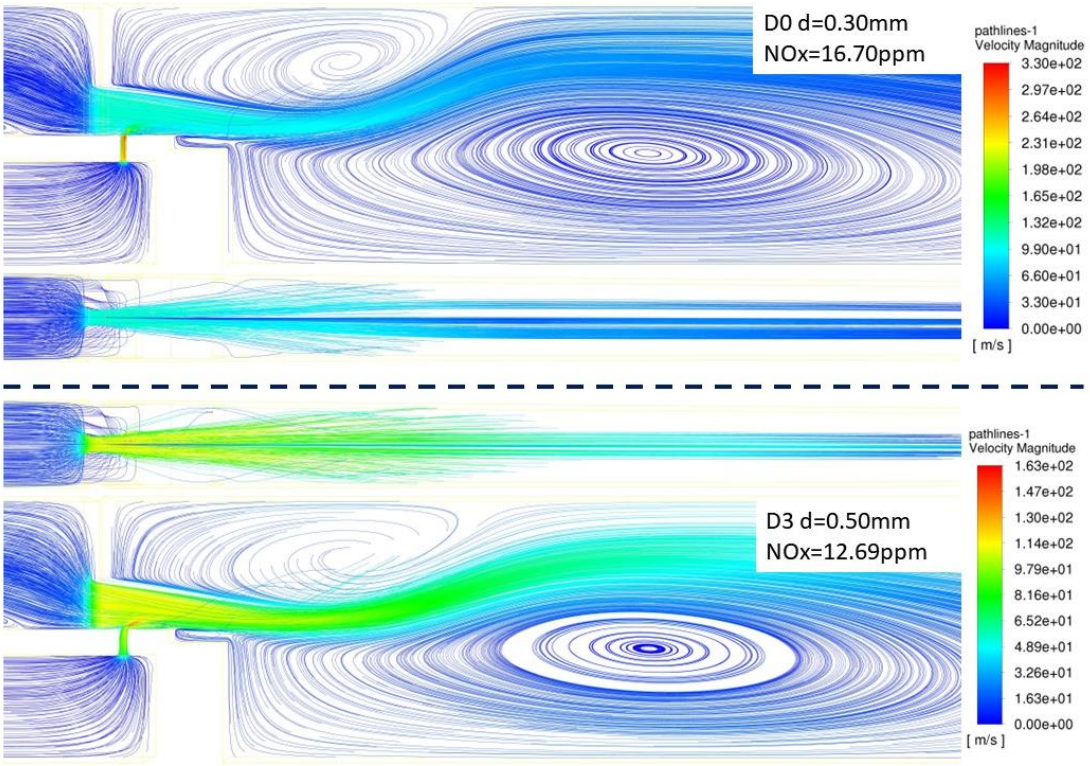

Figure 4-24. Pathline comparison between case D0&D3 at Φ=0.54.

Although the NOx emission has been reduced with the fuel injector diameter variation, these types of combustion should be avoided in micromix combustion, the excessive width of flame risked in the flame merge and NOx emission increased. This conclusion is more based on speculation, more detailed experiments and simulation works are required in the future to verify its correctness.

4.3.3 Conclusion of hydrogen diameter effects on NOx emission and flame width

The modifications of the hydrogen diameter discussed above show the objective of NOx emission reduction could achieved by the change the injection size. From the numerical results of cases D1 and D2, it can be found that although the NOx emission reduction is slight, the injector size still has an impact on the pollutant emitted. The mixing intensity has been improved of micromix combustion because the injection

depth of fuel has been increased, the more mixtures are involved in the vortex which contributes to the reduction of NOx emissions. Also, in the thinner hydrogen injector case, the lateral cooling air flow through the flame could reduce the temperature of the adjacent area and lower the NOx formation. This speculation is inconclusive, case D3 shows an opposite result with prediction which is unexpected. However, for all the diameter cases, the NOx emission changes are not very dramatic, the flame width difference inside the chamber deserves more attention.

Hence, another study point of this section is the flame width. With the certain width of the chamber and air gate, the H_2 injector diameter has a big impact on the flame width at low equivalence ratio, during the combustion the thickness of the hydrogen stream could affect the flow dynamics inside the chamber, the high temperature region size could be effectively changed with different injector design. The comparison of the results of cases D1 and D2 reflects that with the thicker hydrogen stream, the flame width could be increased greatly if the air stream size remains the same.

To further support the presumption made before, a developed case D3 employed the injector diameter 0.48mm has also been studied. However the results were not expected, the NOx decreased with the high equivalence ratio which is abnormal. By analysing the flow dynamics and temperature in the chamber, another conclusion has been deduced that the larger injector may have weaker penetration, but the model is in 3 dimensions, the lifting effect of the air stream in the lateral direction should also be considered.

Also, when the size of the injector increased, the flame width had no bigger difference compared to the basic burner at less oxidizer conditions, the flame had already connected the sides of the combustor zone.

The investigation of the hydrogen injector design is insufficient, more design case studies are required for more practical applications. The thinner injector has shown the potential of slim flame width maintenance, which could support the micromix combustor operated in a wider equivalence range but without the risk of flame merging.

However, the diameter cannot be continuously decreased. As know 0.24mm is already a very small dimension for fuel injector, such a design has very high requirements for the level of industrial manufacturing, which will undoubtedly increase the industrial cost. In addition to this, the condition of purity of the fuel is critical, although the fuel used in the micromix combustion is hydrogen gas, but as long as there are minor impurities can easily lead to the injection port being blocked and thus affect the operation of the combustion chamber.

As the performance of case D3 shows, the increasing of diameter size showed results which suggest that the NOx emissions could be reduced with the larger injector, which is worth further focus. If the NOx could be reduced with the larger injector diameter, the manufacturing difficulties and costs could be reduced. For deeper research on it, the flame width should be ensured at a safe range, then the NOx emission reduction capability could be compared.

4.4 Summary of Micromix Combustor Geometric Modifications

The main objective of this chapter is to investigate the effect of micromix burner geometry optimisations on NOx abatements. In this chapter the single injection element geometry has been studied in detail, the mixing distance, the air gate height and the hydrogen injector diameter have been modified respectively with multiple cases. The optimisations of these parameters have achieved the target successfully, the NOx emission has been reduced in serval cases significantly.

Firstly, the mixing distance of the air and hydrogen streams is studied, the extension of the mixing distance provided a better mixing chance to fuel and oxidiser, the flow dynamics have been improved due to the enlargement of the inner vortex size. More gases participate in the mixing stage, the NOx emission could be reduced because of the enhancement of mixing intensity. It gives the fuel a better chance to mix with more

air which allows the mixture to reach a lean burning condition before the ignition point. With the extension of the mixing distance of 4mm, the NOx emission could be reduced about 40%. This result greatly encourages the mixing distance design, although when the mixing distance increased to a certain value the NOx reduction is not that efficient, this design could still be applied to the micromix combustor, the manufacturing could be easily achieved with relatively low cost. The air gate heigh design modifications also performed well on NOx emission reduction. In this section, the hydrogen fuel injection depth has been focused on, the different air gate design proves that the NOx emissions could be effectively reduced with the lower air gate height, the air flow stream will be accelerated and improve the mixing intensity which could help the combustor burns leaner. Also, with the decrease of the air gate height, the penetration ratio could be higher by measurement. In the air gate height design cases, the air velocities are changed. If the air stream stays the same, the hydrogen velocity increase could also help in the penetration distance, in the hydrogen injector diameter cases. However, the NOx only reduced slightly in these cases, the improvement is not that obvious. But in this chapter, the effects of the flame width are studied preliminarily, which shows the importance of micromix design. In conclusion, with the changing of the burner geometry, the flow dynamics have been affected significantly. The shape change of the vortices formed near the flame anchoring region could determine the flame shape and the NOx formation zone. The performance of these modifications supports that the NOx produced with the micromix combustion could be reduced without changing any operation conditions. All the design cases also show the limitations, to apply these designs on industrial micromix combustors, further investigations are required. Especially in the hydrogen diameter design, when the diameter increases over 0.50mm, the NOx emission is reduced which is good but the flame width in the burner produces the risk of flame merging. To better understand the diameter design impact, the air gate design needs to be modified, like increasing the air gate width to ensure the high temperature could be cooled by the lateral air flows or widening the burner to prevent

the merging of flames. At less air condition, the flame is too wide for burner width of 3mm in all designs, hence, in the next chapter, the further design of scaling the burner will be studied to make the micromix burner could be operated in wide range without risk of flame merge, also the combustion of multiple injection elements should be concerned.

CHAPTER 5: FURTHER MODIFICATIONS AND STUDY OF MULTI-INJECTOR COMBUSTION

In the last chapter, the flame width effect is discussed, with the equivalence ratio increase, the overly wide flame has the risk of flame merging. Therefore, the aim of this chapter is to study the effects of burner width variation and reduce the potential risk of merged flame. In addition, the NOx emissions reduction capability is also demanded.

Previously, the studies about the micromix burner were focused on the single injector elements, zooming out on the entire burner the configurations optimised are just a small part. In reality, the manufactured micromix burner has 1600 injectors arrayed on it. The simplified drawing of the injectors arrangement is shown in Figure 5-1 (a) below, the single elements distributed on the inlet panel as a ring shape. Figure 5-1 (b) displays the structure of the single injector, the fuel supplied inside the ring panel and injected into the cross-air flow through the air gate.

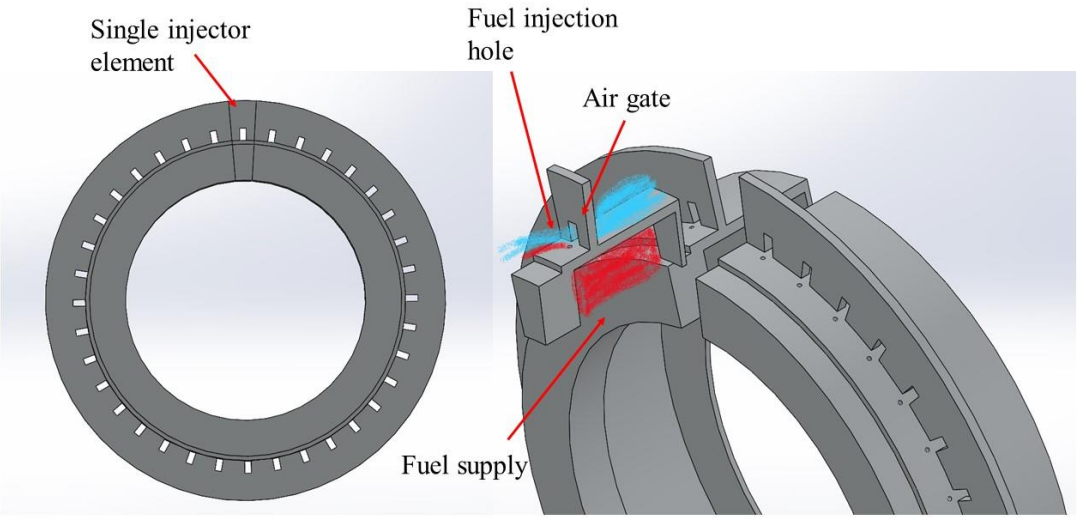

Figure 5-1. (a) The drawing of the simplified front panel. (b) Single injector annotation.

The basic burner has the dimensions 3mm*10mm and 0.3mm for the hydrogen injection hole, to manufacture the injector elements in such a size would be very complex and high-costed. Hence, if the injector scale and hydrogen hole size could be increased the difficulty of manufacturing can be reduced. The following study will be focused on the burner size and the interaction of neighboured injector elements.

5.1 Initial Burner Width Modifications

5.1.1 Overview of burner width increasing

The previous study of the basic burner focused on the NOx emission, which achieved a good performance after the geometry modification. However, for this 3mm*10mm dimension burner, when the equivalence ratio increased to 0.54 the OH contour showed that the flame inside the combustion zone would expand to the sides wall (symmetry plane), the flame would merge together with less air condition. The iso-surface of OH distribution inside the combustion zone of the basic burner shown in Figure 5-2 below displays the phenomenon of flame merging. It could be clearly seen that when the

equivalence at 0.54, the flame of three injector elements have contact with each other, which causes the NOx emission ascending, more seriously, to a high risk of flashback.

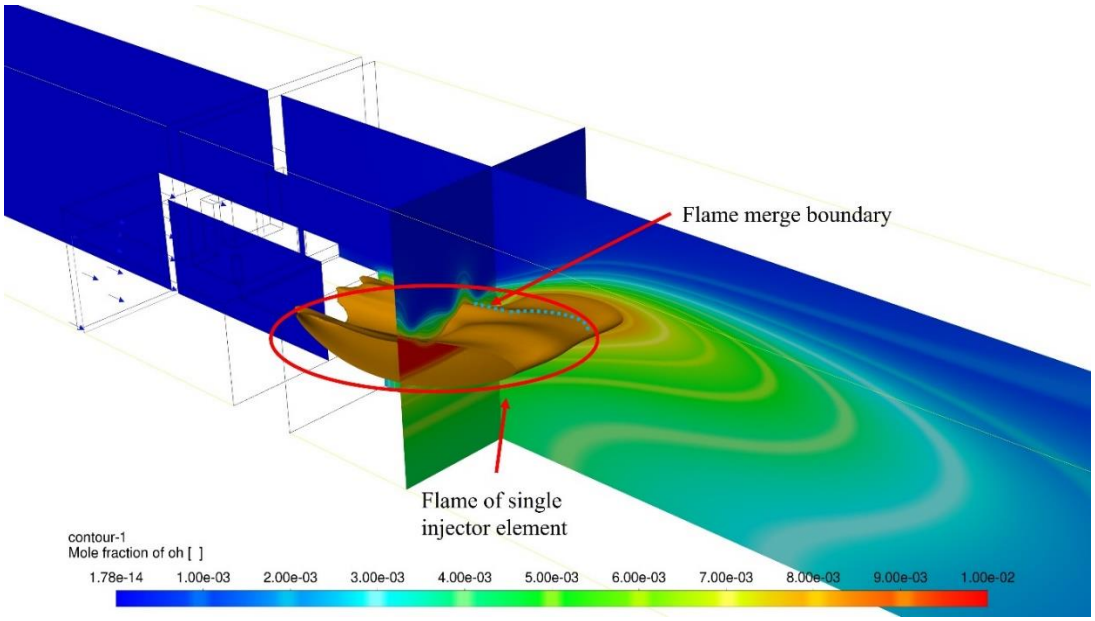

Figure 5-2. Flame merge in basic burner under Φ =0.54.

To avoid the flame connection the burner width will be modified, if the flame size remains the same, increase the burner width more space will be supplied around the flame. However, keeping the energy density constant in this part is a very critical point. The energy density (ED) of the injector element is related to the energy input in this section and the reference area A_{ref} of this injector. As equation (3.1) shows in Chapter 3, when the burner becomes wider, the area increases, hence the fuel flow rate should increase as well to maintain ED as constant.

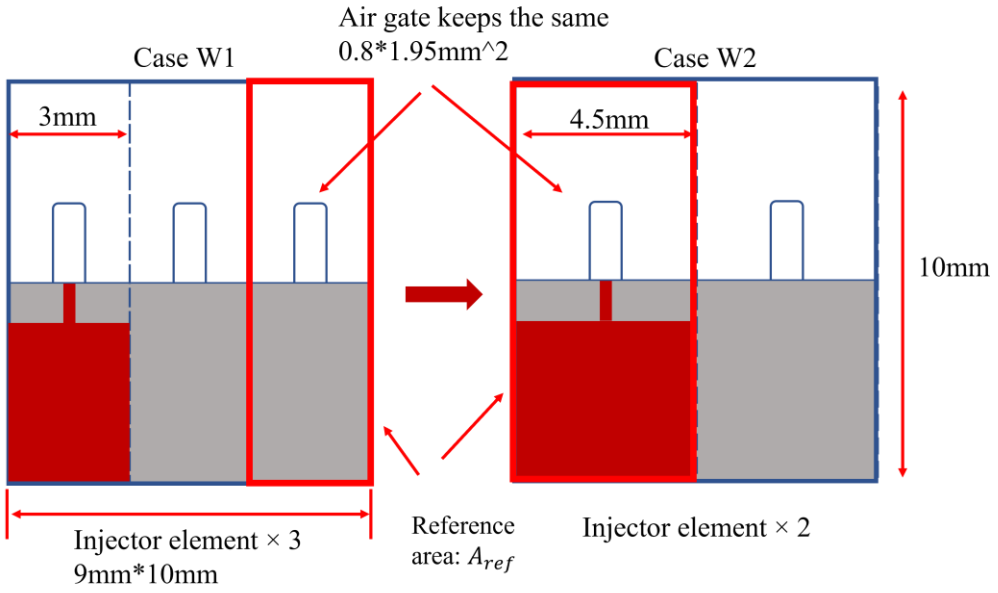

Figure 5-3. Injector width increasing cases W1&W2.

The initial modification of the burner is increasing the width from 3mm to 4.5mm. As Figure 5-3 displayed above, for the same space 9mm*10mm, the basic burner W1 could arrange three injectors side by side, but the improved design W2 just needs two injectors. The advantage of this design is the reduction of manufacturing costs. For example, a micromix combustor needs 1600 injectors with design W1, if the burner width increased like W2, the number of the micromix burner would reduce about 33%.

With the larger reference area, to maintain the energy density the same, the fuel mass flow rate required for single injector W2 has to be 1.5 times than W1. Although the burner width increased, to study the effects of the burner, the size of the air gate wound not change, the hydrogen injection hole diameter is 0.3mm. In the reference area 9mm×10mm, two 4.5mm burner W2 are arranged on it. In assumption, the air gate and mixing distance will stay the same with the basic burner, hence, if the modification of burner width could not affect the flame shape, this design could effectively avoid the flame merging.

5.1.2 Result of the initial burner width modification

The initial comparison of the flame size affected by burner width was conducted between 3mm basic burner W1 and 4.5mm burner W2. Except the fuel inlet amount increased, the other boundary conditions are the same. Since the basic burner, W1 has a good flame condition with an equivalence ratio of 0.4, therefore, to study flame interactions the simulation was conducted under the condition ϕ =0.54.

The OH distribution contour of cases W1 & W2 was calculated and compared. For more visual observation of the flame interaction of these two designs, a cross-section panel at the position Z=-11mm was established. As Figure 5-4 below displayed, the flame interaction is clearly shown. In Figure 5-4 (a) the flame is completely merged, forming a large-scale flame. By contrast, the modified design W2 performed well, two distinct flames were produced. The distance between flames is clear which eliminates the risk of flame merging.

The maximum combustion in case W1 is approx. 2450K, in case W2 which is about 2370K. The flame merging only caused the temperature to rise about 80K; however, the emissions of NOx increased exponentially. The predicted NOx in W1 is 16.8ppm which is more than 5 times of wider burner design W2 (3.3ppm). This clearly shows the disadvantages of flame contact, although the temperature is close, the total amount of NOx emission is unacceptably increased due to the flame merging.

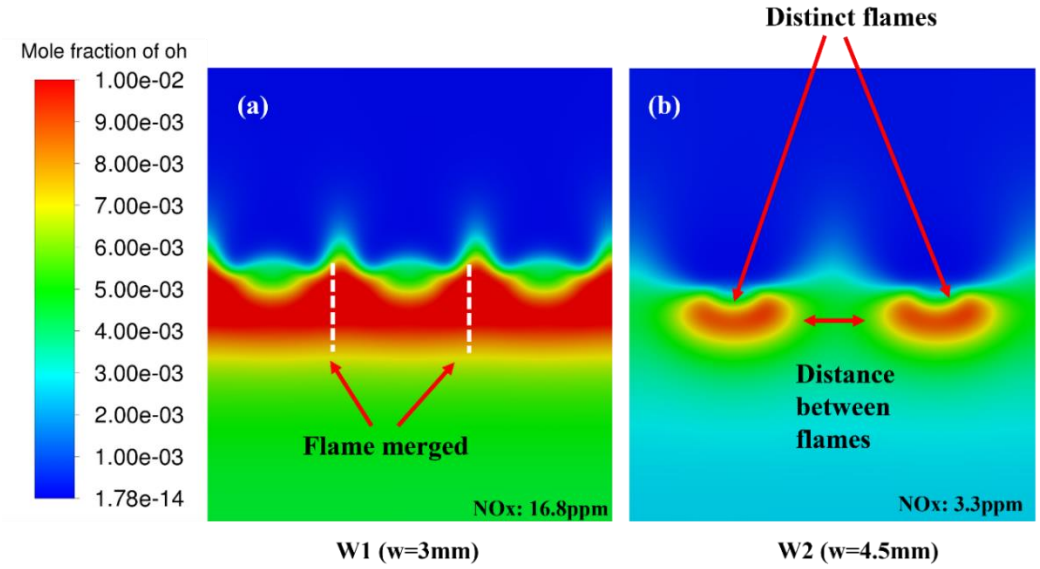

Figure 5-4. OH contour comparison between W1&W2 on the Z-axis (Φ =0.54).

However, this still does not confirm that a simple widening of the burner is a perfect solution. Figure 5-5 below illustrates the potential drawbacks of case W2, the OH distribution contour is produced on the Z-Y plane. The contour shows that in the basic burner W1, the flame thickness and length are both larger than in case W2, it does reflect the improvements of the modified design, but the flame angle needs to be concerned. When the burner reference area increases but the size of the air gate remains the same, this inevitably increases the air stream velocity through the gate at the same inlet velocity.

The accelerated air flow meets the perpendicularly injected hydrogen fuel, then the lifting force is given to the mixed gas stream and forms the vortex. However, in case W2, the air velocity is much larger than the basic burner, the fuel injected could not efficiently lift the air stream up. Also, the penetration depth of fuel is reduced as well. The results reflected in the OH contour, the flame angle variation is obvious. In case W2 the flame swings downwards, the less-lifted flame has a smaller angle between the upper and lower adjacent injection elements. The flame close to the wall part may damage the combustor wall, also the flame size is too small which may have the

potential to be extinguished. Of course, the size of the flame will reach the extinguishing limit which requires further experimental study to verify.

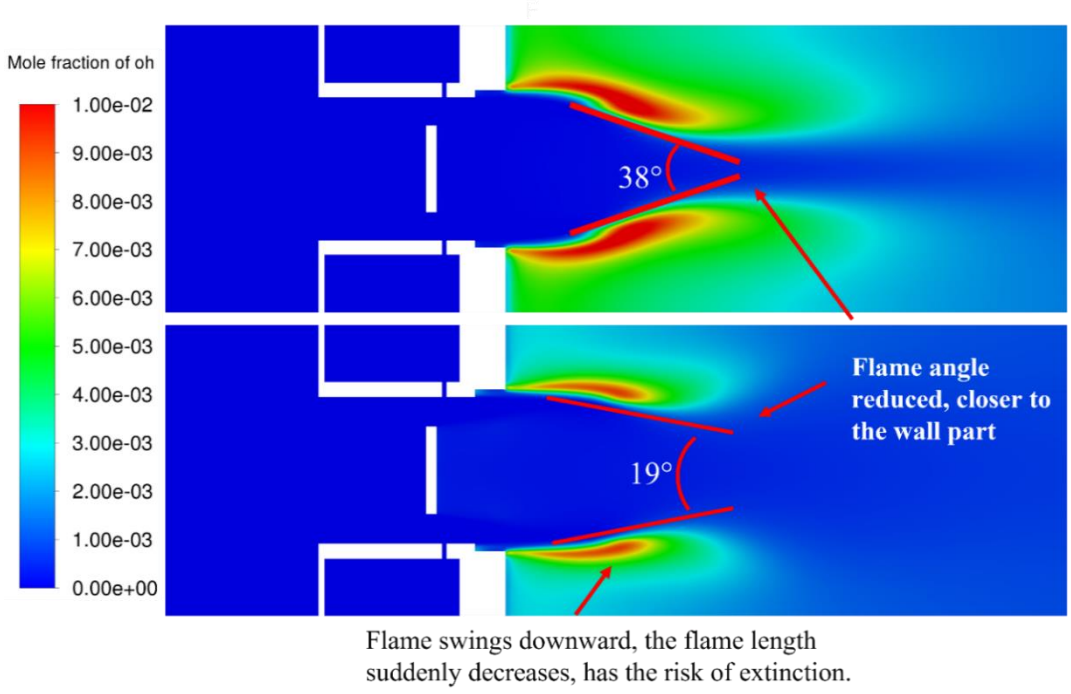

Figure 5-5.Flame structure comparison between W1&W2.

5.1.3 Further study about the widened burner

Since the results of air gate height studies in the last chapter, the design of height-reduced air gate could be further applied and studied for the widened burner models. The discussion about the air gate designs has shown that the lower air gate could effectively increase the width of the inner vortex and reduce the NOx emissions of combustion. Therefore, in the initial attempt for the 4.5mm width design W2, the air gate would be reduced to 1.5mm to further verify the air gate design, also the inner vortex shape and size might affect the flame angle due to the micromix flame anchoring along the shear layer between the vortices.

By considering the downward swing of the flame because of the increasing air velocity in the widened burner. The reduced height of air gate would further worsen this

situation, hence while reducing the height, the air gate will be widened to keep the total area constant and thus maintain the downstream air flow at the same velocity. The air gate width has been increased to 1mm the AG area is kept as $1.5mm^2$ ($\approx 1.56mm^2$ because of the complexity of manufacturing). This design is named as W3-1 (Figure 5-6).

In addition, the numerical results of widened burner W2 reveals that the input energy promotion causes the hydrogen injection velocity to increase rapidly. In case W2, the hydrogen injecting speed reaches 309m/s, which is too high. The excessive injection speed is undoubtedly a burden on the burner, and considering the stability of the entire micromix combustor, the kinetic energy generated by high-speed injection is likely to have a negative impact. Section 4.3 has discussed the hydrogen diameter, the results show an unexpected finding. As predicted, the smaller hydrogen hole should have better NOx reducing capacity, but the 0.5mm diameter injection hole shows good performance as well. Hence, the design W3-1 has been further modified with the larger hydrogen injection diameter of 0.5mm.

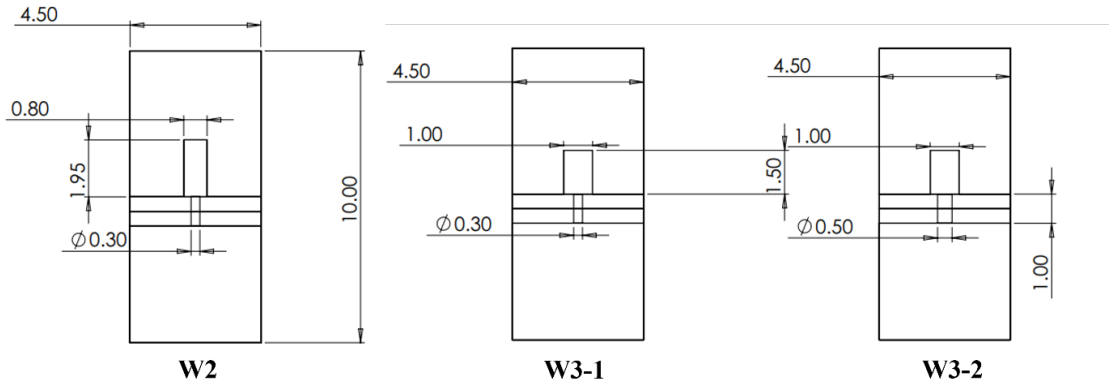

Figure 5-6. Schematic of further modified burner W3-1&W3-2

The simulation results of the widened cases are shown below, in Figure 5-7, from the OH contour the flame structure inside the combustion zone could be directly observed. The OH distributed on cross-section panel Z=-9mm position shows that the flame for all these widened burners has a distinct outline, the risk of merge is avoided.

Since the design purpose is applying the advantages of a shorter air gate, the OH distribution reflects this modification can be considered functional. The comparison between case W2 and W3-1 proves it, when the air gate height was reduced to 1.5mm, the NOx emission reduced about 18%. Additionally, the flame tail is lifted, the velocity pathline shown in Figure 5-8 below supports this point.

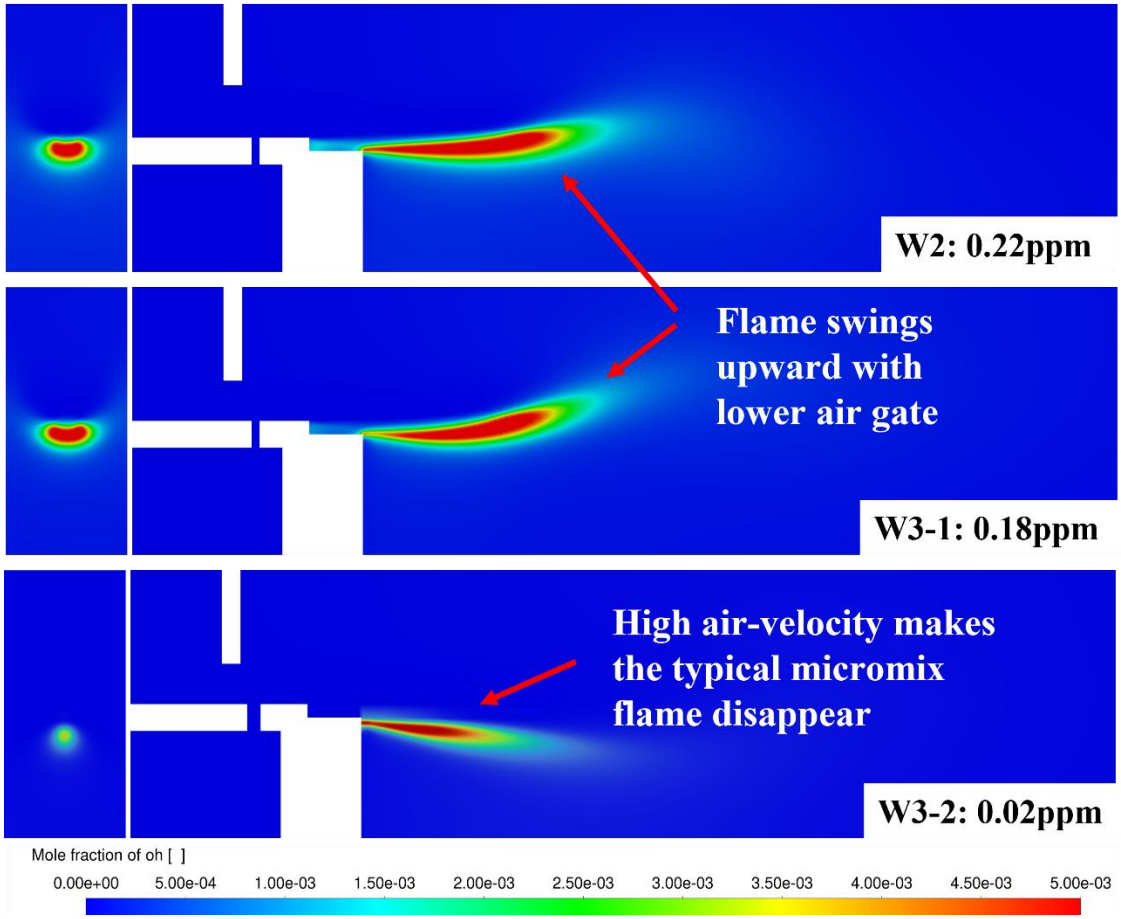

Figure 5-7.OH distribution contour comparison Φ=0.4

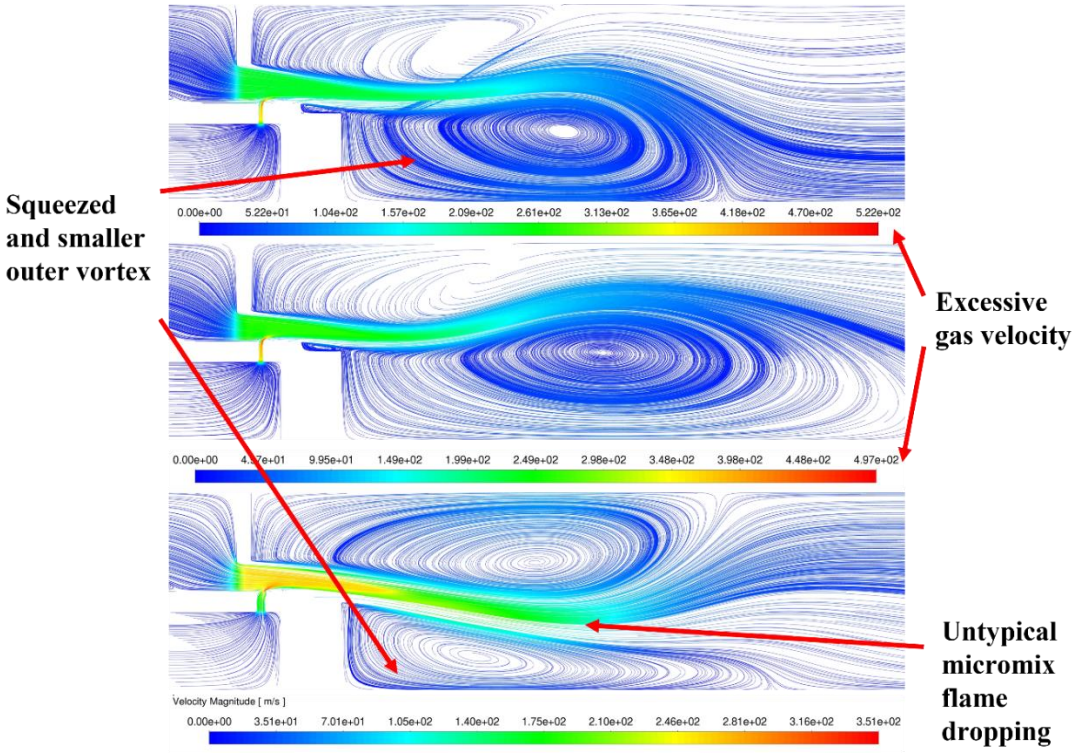

Figure 5-8. Velocity pathline of modified cases Φ=0.4.

Combining Figure 5-7 and Figure 5-8, it demonstrates the micromix flame position and angle are affected by the shear layer between the inner and outer vortex. The shear layer depends on the vortices inside the combustion zone, the shear layer decides the angle of the flame, as well as the size and position. The pathline difference between case W2 and W3-1 shows the reason that reducing air gate height is effective in improving the flame orientation. The outer vortex of case W1 has been squeezed and compressed, the size of the vortex becomes smaller and the shear layer cannot be greatly lifted, resulting in the flame swinging downwards. For similar air velocity, the shorter air gate in W-2 provides a good flow dynamic inside the combustion zone, the end of the flame is lifted. Need to be concerned that the peak velocity of W2 and W3-1, the highest velocity of hydrogen injection reaches approximately 500m/s, which is undoubtedly too high for an injector element of this scale which may not be feasible for practical conditions.

The same problem of case W1 happens to W3-2, the velocity pathline displays the

compressed outer vortex. Although the air gate height is 1.5mm, the 0.5mm diameter hydrogen injection hole reduces the fuel stream velocity. On the one hand, this is good, the high inject velocity of hydrogen is greatly reduced from 309m/s to 111m/s, this speed is acceptable for the micromix burner. On the other hand, the decelerated hydrogen stream is difficult to reach the ideal penetration depth, moreover, the air stream could not be lifted up by the slow hydrogen stream when air velocity is too high. This leads to bad vortices formation and unstable shear layer.

Figure 5-7 clearly displays the unexpected micromix flame structure of case W3-2, the flame length is too short, at position Z=-9, the flame almost disappeared. The position of the flame is too low and too close to the wall section. Although the NOx emission is extremely reduced in this case, this is because the size of the flame is too small and the possibility of potential flame extinction.

5.1.4 Conclusion

The results of the modified widened burner proved that the lower air gate could improve the flow dynamics inside the chamber. The large air guiding panel provides better room of the development of the vortex and enhances the shear layer stability. The disadvantages of cases W2 and W3-2 show the importance of the vortices structure inside the chamber, in the following improved cases, the flow behaviour demands more focus on it. The gases velocity requires more attention as well. For the fuel injector, with the burner dimensions enlarged, the increase of energy input causes the hydrogen stream velocity to increase to an unrealistic condition. Therefore, for the 4.5mm burners, the hydrogen injector must be enlarged as well to keep the fuel injection velocity within a realistic situation.

However, it can be found that the high-speed airflow has a devastating impact on the typical micromix vortices. The flow dynamic and the OH contour of W3-2 reveal that, with the larger injection hole, the hydrogen injection velocity is too slow, with the

current size of the air gate the fuel stream could not effectively lift the high-speed air stream. The mixed gases will be directed to the larger space in the lower part of the chamber.

Therefore, for the following designs, there are some criteria that need to be met:

- To prevent the jet in velocity of hydrogen fuel in the thin pipe from being too high, also, to prevent the hydrogen pipe from blockage due to the impurity of the fuel. An enlarged fuel injector is necessary.
- Based on the first point, the research is targeting to slow down the air stream velocity by increasing the air gate size. The attempts are focused on keeping the same air gate height but increasing the width.
- The relationship between the flame width also needs more studies to prevent the flame merging risk.
- Lastly, for all the cases, the main purpose of the optimisation of micromix combustor is to reduce the NOx emissions of combustion.

Overall, the burner needs to be further modified to provide a relatively good performance of combustion and the flow behaviour must be maintained as a typical micromix combustion. At the same time, the combustion emission has to be kept as low as possible.

5.2 Air Gate Size Study

5.2.1 Effects of air gate width on flame size

5.2.1.1 Overview of the air gate width cases

Based on the conclusions mentioned in the last section, the hydrogen injection hole size must be increased, otherwise, the supersonic injection speed may cause the fuel injection failure. Hence, all the 4.5mm burner designs would employ with the larger

fuel injector such as a 0.5mm diameter. To effectively reduce the velocity of cross-air stream, enlarging the air gate is the most direct method.

In this section, the effects of air gate width on flame size will be simply studied. A series of cases are simulated to investigate the relationship between flame and gate width. Only the width of the air gate will be studied in a targeted manner. Based on the 0.5mm burner W3-2, the air gate width has been increased from 1mm to 1.8mm gradually, the gate height is kept as 1.5mm. As known that the combustion performance in the 1mm burner W3-2 is unsatisfactory this is mainly because of the small gate size, in the expectation, the larger burner could provide a better vortices shape and flame stability.

The first optimisation step is focused on the air gate width. For the original design, the air stream through the gate for the 4.5mm burner is about 157m/s. The simulation of these wider air gate burners is operated with the equivalence of 0.4. The air stream velocity and injection depth calculations are shown in Table 5-1 below. The penetration depth calculation of the original basic burner (3mm, $d_{h2} = 0.3mm$) is listed as well. From the table, it could be found that when the hydrogen diameter is increased to 0.5mm, with the enlarged energy input, the momentum flux ratio and injection depth are much smaller compared to the basic burner. The flame's downward swing could be attributed to it. With the 0.5mm hydrogen injector, the air gate width must be at least 1.65mm to maintain a close injection depth. By considering the air gate height is reduced to 1.5mm, the penetration ratio could be achieved when the air gate width reaches 1.35mm. (Penetration ratio is the injection depth over critical depth.)

Air gate width	Air stream velocity (m/s)	Momentum flux ratio	Injection depth/α	Penetration ratio
basic burner	100	0.534	0.219	0.112
1mm	157	0.063	0.125	0.084
1.2mm	131	0.091	0.151	0.100
1.35mm	116	0.115	0.169	0.113
1.4mm	112	0.123	0.176	0.117
1.5mm	104	0.142	0.188	0.125
1.65mm	95	0.171	0.207	0.138
1.8mm	87	0.204	0.226	0.151

Table 5-1. Boundary conditions and injection depth calculation of width study cases $\boldsymbol{\Phi = 0.4}$.

As concluded that the increasing of air gate area could help on the up-lifting of the flame, compared to the 1mm width case (W3-2), the widened burner eliminates this drawback. Figure 5-9 displays the position of the flame in the burner, the cross-section is located at the Z=-13mm which is the position of the flame tail, the cross-section of the OH contour chosen for this position allows a more visual and effective observation of the flame uplift.

5.2.1.2 Result and discussion of gate width study

The OH distribution clearly demonstrates the flame centre position shifting with the air gate's width increase. For better comparison purposes, the flame position of case W3-2 is also displayed. The OH distribution at the position Z=-9 was adopted because the flame is too short and can't be seen at the Z=-13 position. The white dash line is at the centre of flame of 1.2mm case, with the air gate becoming wider, the flame size is larger and has been lifted. These results confirm that with the larger air gate, the hydrogen fuel injector has better penetration depth, the outer vortex size grows larger and lifts the

shear layers. The shear layer provides a better space for flame anchoring and growing.

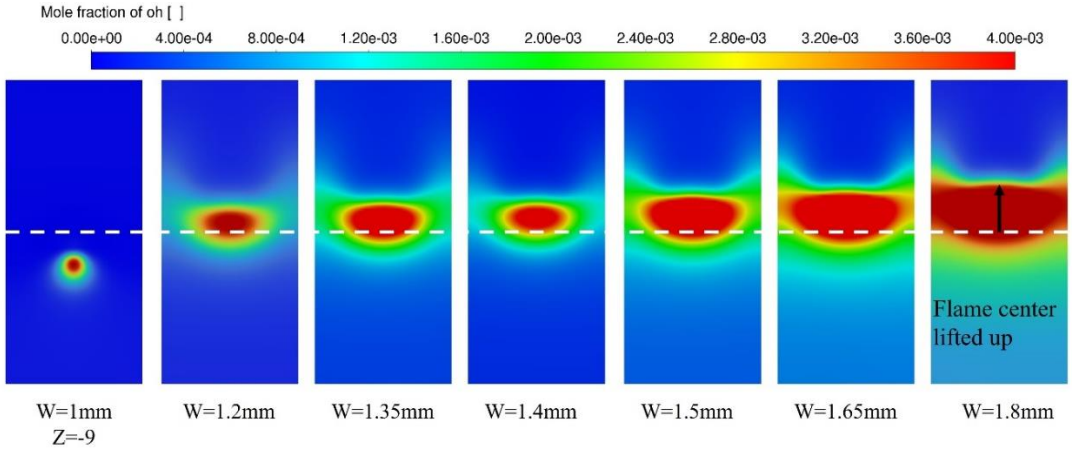

Figure 5-9. Flame size growing with the air gate width increasing. (Z=-13)

However, although the flame has been effectively lifted by using wider air gate, the OH contour indicates that the flame would become larger with wider gate. It could be found that when the gate width is 1.2mm, there is still cold air wrapped around the flame, increasing the cooling capacity as well as preventing the flame from contacting each other. As the width of the air gate, it can be clearly seen that the size of the flame becomes larger at the same position on the Z-axis. Especially when the width exceeds 1.5mm, the flame gradually touches the boundary of the burner sides. In 1.8mm design, the flame has moved up but the sides of the flame have come into contact with the flame in the adjacent burner.

The plotting of the facet maximum mole fraction of OH shown in **错误!未找到引用源。** shows the boundary of the flames. The minimum value of the OH fraction is determined as 0.004, which is the maximum value of colormap label. The curves illustrate the size of the flame from air gate width 1.2mm to 1.8mm. Could be found with the widest gate 1.8mm, the flame distributed from -2.25mm to 2.25mm on the X-axis which means the width of flame has filled the entire burner and merged. When the width is below 1.5mm, the flame width increase is not that obvious, the flames stay in

the range of about ±1.1mm~±1.5mm.

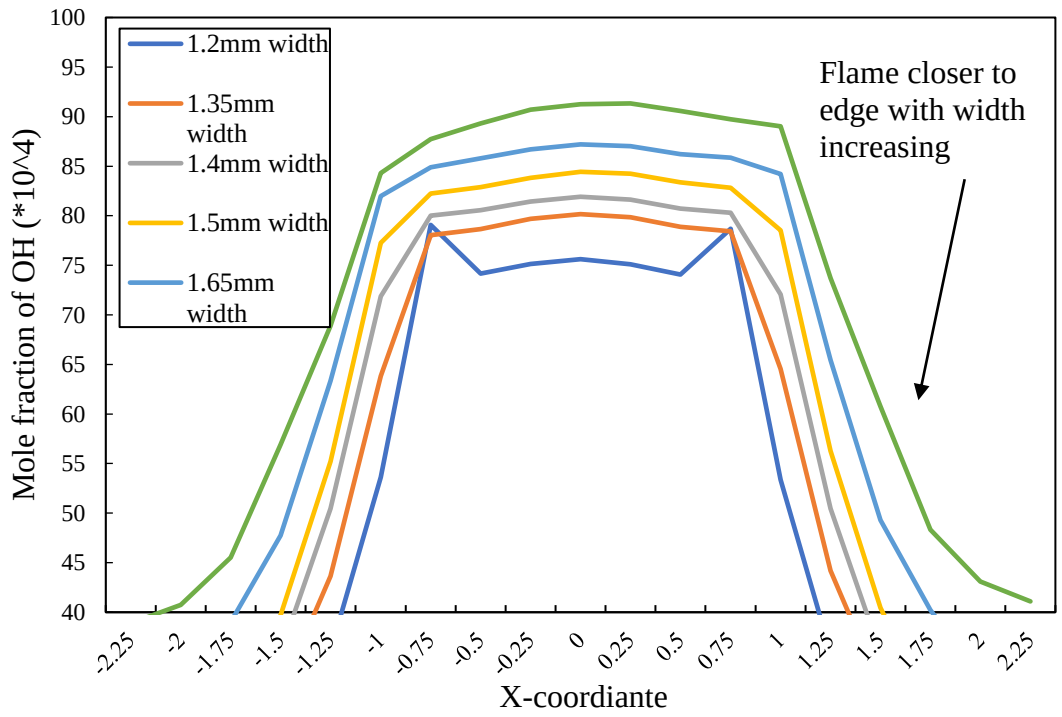

Figure 5-10.OH mole fraction along the X-axis of the chamber of widened air gate designs.

Since the peak temperature and flame size increase, the NOx emission would rise with wider air gate theoretically. The NOx emission of these cases is predicted, the Figure 5-11 plots NOx amount in ppm at the outlet of the burner. From the trend of the curve, it could be found that more NOx has been emitted with the increase of the air gate width. Using 1.3ppm as the baseline for the design, the NOx emission data verified the discussion above, when the burner width is under 1.5mm, the NOx emission is acceptable. The 1.65mm design and 1.8mm design have the 1.71ppm and 2.42ppm respectively, these modifications make the pollution even worse. As the overall aim of the micromix combustor design, the NOx reduction capacity is a key factor in assessing burner modifications. The over-wide air gate design would cause negative effects on

the combustion performance.

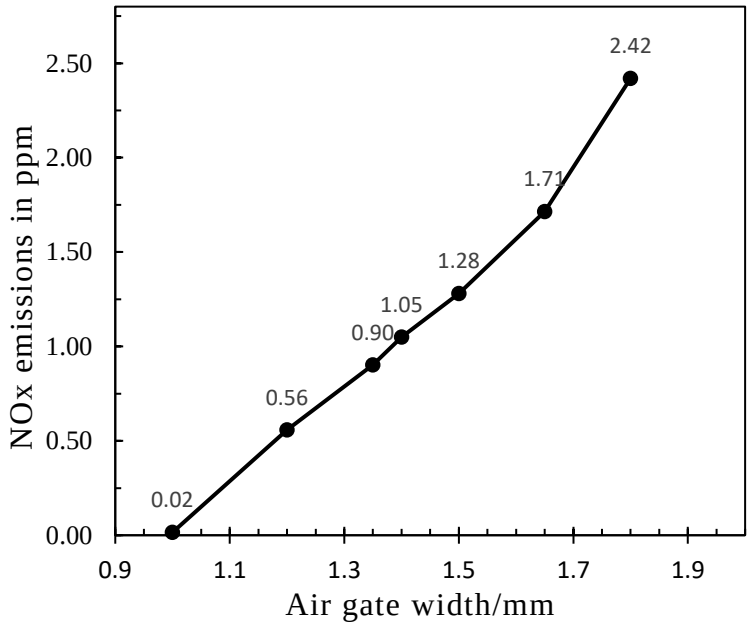

Figure 5-11. NOx emission variation with the air gate width changes.

5.2.1.3 Conclusion

As the conclusion, from the above results, it is not advisable to simply increase the width of the air gate. Although the main purpose of this section is to investigate the effects of gate width on flame size, it is also to study whether enlarging the air gate and reducing the air stream velocity can have positive effect on combustion performance when increasing the hydrogen injection hole diameter. After the analysis about the gate width study and combining the conclusion from the last chapter, one key solution to reduce the NOx emission is to increase the air stream velocity and then improve the mixing intensity. However, in this chapter, the hydrogen injector diameter must be increased with the greater energy input, since reducing the hydrogen fuel velocity the injection depth would be decreased as well.

There is a dilemma point occurred:

To keep the injection depth effective as the basic burner, the air velocity has to slow

down since the lower fuel injection velocity of larger hydrogen hole diameter. To reduce the air stream velocity, the air gate size needs to increase. The lower air gate could provide a better penetration ratio and improve the vortices formation in the burner. Therefore, increasing the air gate width could achieve this goal with lower gate. However, the wider air gate would increase the flame width and cause the risk of flame merge.

Therefore, the 4.5mm burner needs further optimisation to find a balance between these drawbacks, the increase of the air gate size would not only focus on the width, but different height-width-ratio of the air gate should be investigated. In conclusion, the hydrogen diameter must be increased, there is no doubt about it. The air gate size needs to be enlarged for it, the balance between the height and width and the hydrogen diameter will be focused.

5.2.2 Study about the gate size ratio effects on micromix combustion and NOx emissions

5.2.2.1 Design parameters of different gate sizes

With plenty of studies about air gate, it could be found that the air gate size variation could directly affect the flow dynamics in the combustion chamber and contributes to the changes in temperature and flame size. The NOx formation during the combustion is highly dependent on the temperature and hot region size.

This section will focus on the air gate aspect ratio studies, different design parameters effects on NOx emissions will be compared. For this purpose, there are five different air gate designs have been modelled. The design parameters are shown in Table 5-2 below. As the parameters presented in the table, all the air gate case has larger area than the basic burner 1.56 mm^2, the reason for this design is based on the conclusion presented in the last section. Due to the larger hydrogen pipe diameter, the air gate size

has to be increased to prevent the flame from down-swing. For cases AG 1, AG 2 and AG 4, the area of the area gate is kept almost the same, for these cases, the research point is the aspect ratio effect on the emission and combustion performance when the air gate area maintains the constant. Case AG 3 and AG 5 limit the width of air gate in 1mm and have less area than the other cases. An additional case AG 5-2 study about the aspect ratio of air gate, it has exactly the same area compared to AG 6, only the width and height exchanged.

Case name	Width / mm	Height/ mm	Area/ mm^2	Air velocity/ms^{-1}	Momentum flux ratio	Injection depth
AG 1	1.20	1.65	1.98	119.13	0.110	0.166
AG 2	1.30	1.55	2.02	117.06	0.114	0.169
AG 3	1.00	1.80	1.80	131.04	0.091	0.151
AG 4	1.45	1.40	2.03	116.19	0.115	0.170
AG 5	1.00	1.60	1.60	147.42	0.072	0.134
AG 5-2	1.6	1.00	1.60	147.42	0.072	0.134

Table 5-2. Design parameters of air gate.

In the previous studies, the air/fuel ratio changes relying on increase/decrease the air inlet amount, the fuel inlet amount keeps the constant for all cases under different equivalence ratios. By considering the larger hydrogen injector could not provide enough lifting force, in this section, the equivalence ratio variation will be achieved by changing the hydrogen fuel inlet mass flow rate. Based on this change, when the burner operated at high equivalence ratio, more hydrogen fuel would be input to the burner, the energy input would increase as well. It could further verify the micromix burner performance with the energy density increasing conditions.

For this 4.5mm single micromix element, the boundary conditions of different

equivalence ratios are shown in Table 5-3.

Equivalence ratio	Hydrogen inlet mass flow rate (kg/s)	Hydrogen inlet temperature (K)	Air inlet velocity (m/s)	Air inlet temperature (K)
0.3	1.3237E-06	300	5.24	550
0.35	1.5443E-06			
0.4	1.7649E-06			
0.45	1.9855E-06			
0.5	2.2061E-06			
0.54	2.3826E-06			

Table 5-3. Boundary conditions at different equivalence ratios.

5.2.2.2 Result and Discussion

For these air gate cases, the main target is to examine the NOx emission reduction capability, the NOx emission at the outlet was recorded. To better understand the NOx reduction ability of different designs, all the cases were simulated with different equivalence ratios in the range of 0.3¬0.54. The prediction of the NOx is plotted in Figure 5-12 below, the unit of emission is converted to ppm.

As Figure 5-12 demonstrated, the NOx emissions for these five cases have obvious differences. In general, all the cases demonstrated the great NOx reduction ability compared to the baseline design. The highest NOx produced among these cases is 5.23ppm (AG 4) when the equivalence ratio is 0.54. Overall, the emission reduction capabilities demonstrated by these five designs are gratifying, demonstrating strong emission reductions despite increasing input energy. It reflects that the larger diameter of the hydrogen injection pipe employed by 4.5mm combustor element has the potential to produce lower NOx than the original 3mm element.

For more information, case AG 5 provided the best performance on the NOx reduction compared to the other cases, the emission at $\phi = 0.54$ is several times lower than the other models, although the energy input for $\phi = 0.54$ has reached 285 J/s which is

doubled basic burner 141J/s), the NOx exhausted remain well within the 1.5ppm. (Compared to the 3mm basic burner which is 17ppm.) The NOx emissions of cases AG 2 and AG 4 are the highest of these cases, the emission curves plotted of these two cases are almost overlapped, it reflects that the NOx emission mainly depends on the air gate area. It dominates the air stream velocity which mixes with the hydrogen fuel, the mixing intensity is primarily affected by it. The mixing intensity difference leads to the NOx reduction capability discrepancy of the designs. The NOx emission curves of AG 3 and AG 5 prove that the smaller air gate design could effectively reduce NOx pollution from combustion.

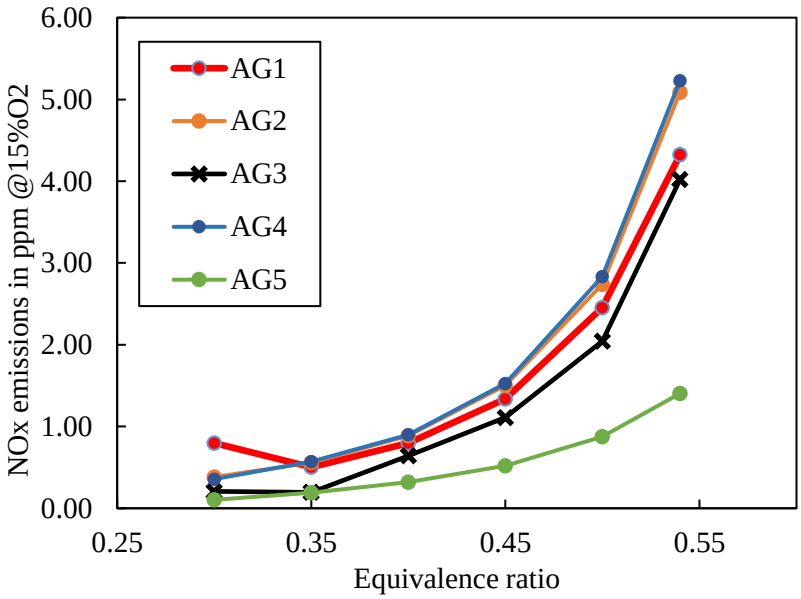

Figure 5-12. The NOx emission of different AG design cases.

Regarding the combustion performance inside the chamber, Figure 5-13 demonstrates the OH distribution of these designs. From the left to the right, the operation loading increases, as the OH mole fraction contour illustrated that for all the designs, the flame size is in an acceptable range for this 4.5mm width burner at $\phi = 0.4$, however, when the equivalence ratio over 0.45 the case AG 1, 2, 4 is shown a trendy that the flame starting contact with the sides of the combustion zone and has the risk of merge with

the adjacent combustion elements. This potential risk is obvious when $\phi = 0.54$ which coincides with the NOx emissions plotting in Figure 5-12. As expected the design of AG 5 provides the best performance of flame size, in the operation range from $\phi = 0.3 \sim 0.54$, the flame width is in a good range. The cold air vortices wrap above and below the flame and provide cooling effects to the hot areas.

For all the cases, the OH is spread to the lower part of the burner, which means that the heat reaction-diffusion to the outer vortex. The temperature in the lower part is much higher than in the upper part. It could be clearly observed in case AG 1-4, the temperature in the outer vortex affects the cooling of the combustion zone. Also, the high temperature may affect the wall material's life span.

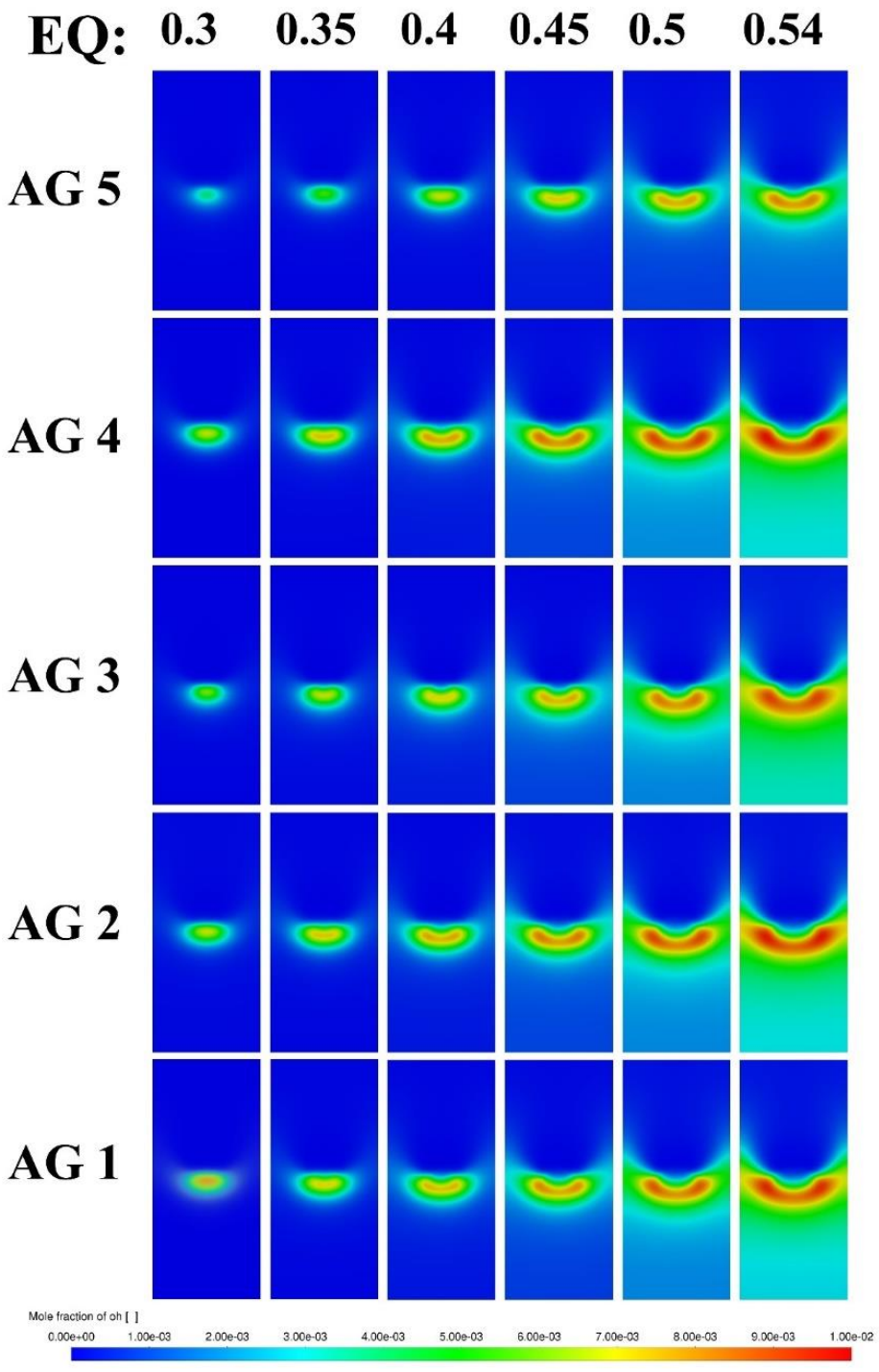

Figure 5-13. OH distribution comparison at the cross-section plane Z=-11 with equivalence ratio increasing.

5.2.3 Secondary modification of case AG 5

To better understand the effect of the air gate aspect ratio, the design AG 5 was further modified into AG 5-2. As Figure 5-14 shows, the width and height of the air gate were exchanged. In the previous section, the conclusion has revealed that the area of air gate would dominate the NOx emissions of combustion. Therefore, in this secondary modification, the area maintains the same and the aspect ratio changes. The air gate height has been reduced to 1mm, and the width increased to 1.6mm.

These two designs were simulated under the design point $\phi = 0.4$ and fuel rich condition $\phi = 0.54$. The NOx emissions and temperature would be compared. In addition, the velocity pathline has also been calculated to study the flow behaviour inside the combustion zone. As the prediction, the wider air gate of AG 5-2 should have negative impact on flame size, the height-reduced air gate may have the potential that the fuel flow would over penetrate the air stream.

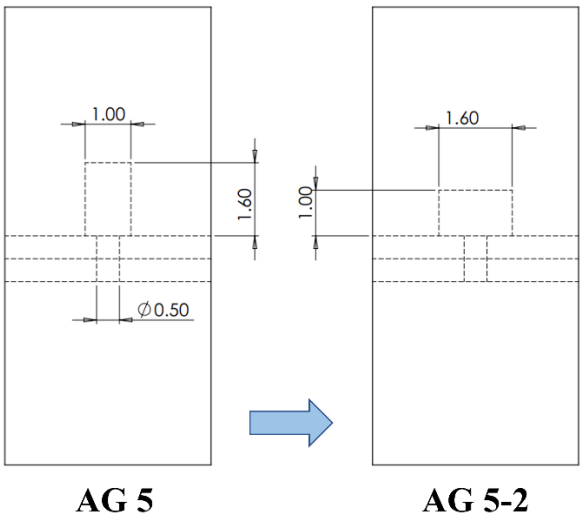

Figure 5-14. Schematic drawing of secondary modification.

5.2.3.1.1 Result and Discussion

Firstly, the NOx emission of these two designs is compared, as expected, the amount

of NOx produced at the outlet is almost the same. For case AG 5 and AG 5-2, the NOx emission is 0.32ppm, 0.25ppm and 1.4 ppm and 1.59ppm at equivalence ratio 0.4 and 0.54 respectively. This result is expected before the simulation, which further proves that the NOx emission primarily depends on the air gate area if the other geometric parameters are kept as constant. These two modified designs both show a good NOx reduction capability, the emission has been controlled to a very low level which both met the design target. At $\phi = 0.4$, the NOx emission of case AG 5-2 is slightly lower than AG 5, the initial speculation is that although the air velocity and hydrogen fuel velocity are the same, the lower air gate could increase the penetrate ratio. The hydrogen flow is injected into thinner air stream, the fuel has the chance to mix with more air flow which provides a better mixing. That could be the reason for lower NOx produced, however, this is just a subjective presumption which needs more modelling work and experiments to verify.

The NOx emissions amount of these two burners are almost the same, the combustion reaction and flame profile inside the chamber will be compared and analysed. Figure 5-15 and Figure 5-16 show the combustion condition at the design point and fuel rich point. The temperature and OH contours are created to make the contrast between case AG 5 and AG 5-2.

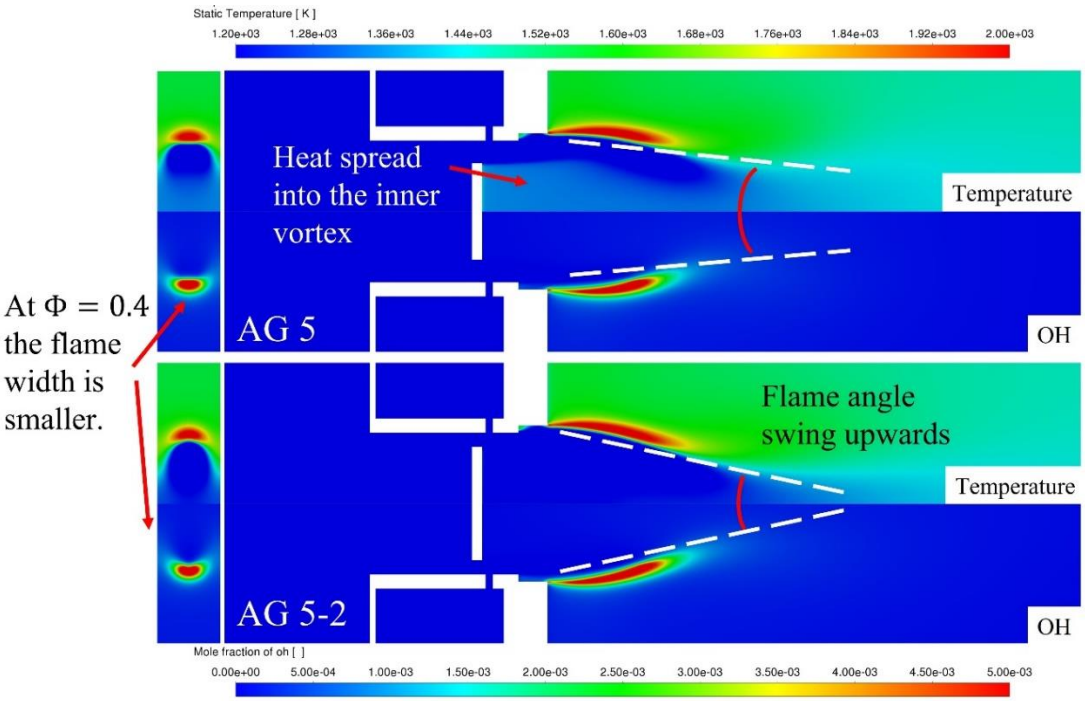

Figure 5-15.Temperature and OH contour comparison at $\phi = 0.4$.

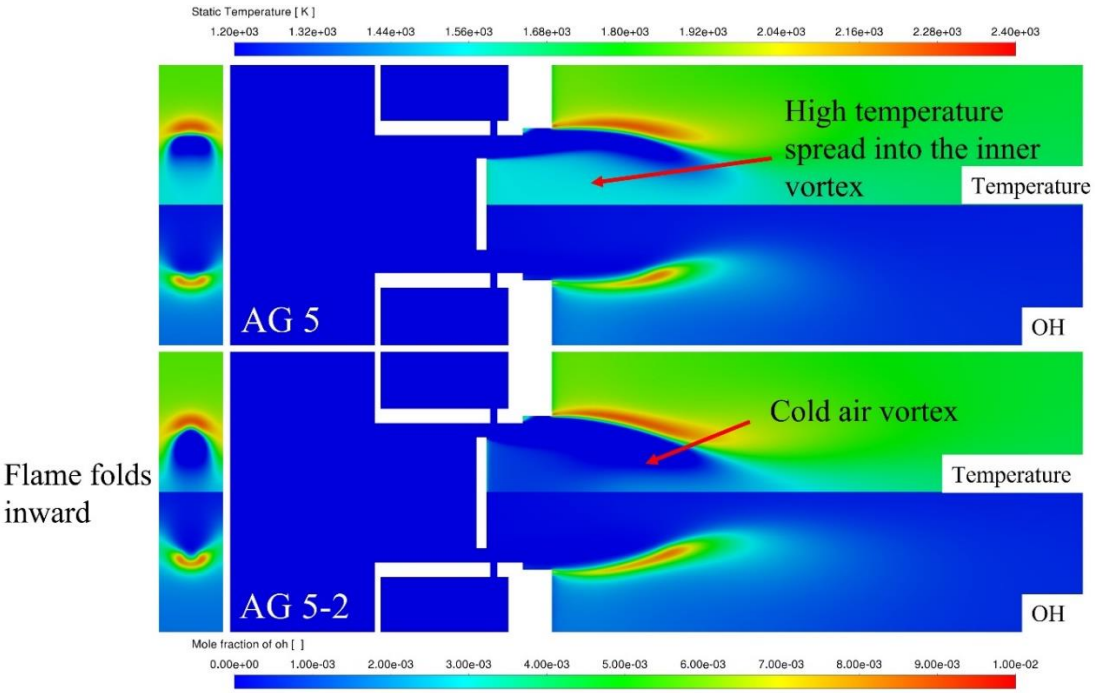

Figure 5-16.Temperature and OH contour comparison at ϕ =0.54.

From the temperature contour at $\phi = 0.4$ and $\phi = 0.54$ it could be observed that the main hot region is both allocated along the flame position, the hot gas recirculated into

the outer vortex the lower part of the burner zone is stable about the temperature 1550K at $\phi = 0.4$, the outer vortex temperature of AG 5-2 is slightly 20K lower than AG 5. This difference is very tiny which cannot be clearly observed from the contour. The reason for this situation could be because the outer vortex size of AG 5-2 is much larger than AG 5, which is demonstrated in the velocity pathline Figure 5-17, the larger vortex allows more downstream gas to participate in the cooling stage.

In the modified design AG 5-2, the temperature level of the inner vortex has clear differences compared to AG 5. The cyan colour region in Figure 5-16 of AG 5 indicates that the heat spread into the inner vortex region, the temperature is approx. 1500K which is not very high but considering the air gate panel is a thin plate the material damage needs to be concerned.

By combining the OH contour and temperature contour, it could be found that for these two designs, the flame is distinct at low equivalence, it avoids the flame merging risk. At the condition $\phi = 0.54$, both designs have the flame size increasing but still acceptable for this 4.5mm design. With the lower air gate design (AG 5-2), the high temperature of flame has the trendy to fold inwards at high equivalence ratio, the air gas of the inner vortex pressed the shear layer where the flame anchored along. This prevents the high temperature penetrates to the inner vortex and fold the flame inwards. From Figure 5-15 it could be directly observed that the lower air gate effectively increased the outer vortex size and lifted the flame upwards, it helps the inner vortex structure stabilisation. The OH cross-section contour at Z=-11 position shows that the lifted flame is folded inwards and allows more cold air flow to surround the flame. It not only decreases the merging of the flame but also helps the cooling of the hot region. Theoretically, the NOx emission could be reduced because of the air cooling which is finally reflected in the emission difference (0.25ppm to 0.32ppm).

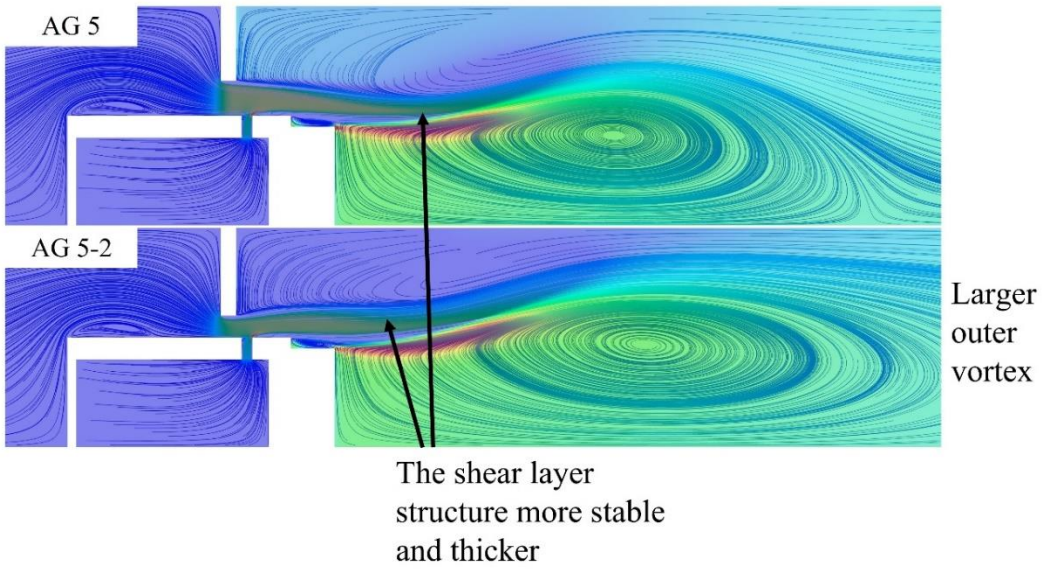

Figure 5-17. Velocity pathline comparison at $\boldsymbol{\Phi = 0.54}$.

Figure 5-17 above demonstrates the flow dynamics changes inside the burner. The case AG 5-2 employed the lower air gate to make the air stream flow pass the gate thinner compared to AG 5. However, after the air mixed with the hydrogen fuel, the stream developed into a thicker shear layer. This might because the hydrogen fuel injected into the air with a higher penetration ratio. The lifting force by hydrogen effectively enlarges the outer vortex size and contributes to the flame upswing. The pathline also indicates the defect of these designs, due to the large hydrogen injector diameter, the slow hydrogen stream could not provide enough uplift effect, the inner vortex formation is not stable. The gas flows into the inner vortex partially helps the formation of the vortex structure, part of the gas flows along the shear layer. This problem has been improved in the modified design AG 5-2 but is still not solved.

Overall, from these comparisons, it reveals that for both cases the flame width increased and stabilised about the similar size when the equivalence ratio increased, which reflects that with the same air gate area, the gate width won't affect the flame thickness. For the specific air gate area design, the aspect ratio could clearly affect the flow

dynamics inside the chamber and finally lead to the flame position and angle. The flame shape may be affected but more research is required on it. The NOx emission has a slight difference, it could be considered as the verification of the conclusion of gate height design in the last chapter. With the given gate area, the lower air gate could help on the vortex's formation inside the combustion area, also improve the flame size and position.

5.2.3.2 Conclusion of Air Gate Size Design

In this section, the air gate size and aspect ratio were studied, since the study about the air gate width in section 5.2.1, the conclusions indicate that to enlarge the size of the air gate, it is undesirable to simply widen the air gate. At the same gate height, the wider air gate will directly affect the width of the flame thus causing the flame to contact with the sides of the combustion zone, ultimately causing the adjacent flame to merge resulting in high NOx emissions and risk of flashback. Hence, this section focused on the effects of air gate area on emission and flame size for different aspect ratios. Through a series of modelling, it is found that the area of the air gate actually has a decisive effect on emissions and flame width. In the comparison of case AG 1-5, it was found that the same or similar size air gate would produce close NOx emissions, as well as the flame size. Therefore, the key point of the air gate enlargement is to find an acceptable gate area, then the flame size would be controlled in a predicted range.

For the established air gate size, the aspect ratio would further affect the flow dynamics inside the combustion zone, the inner and outer vortex size would be directly controlled by the gate design. As mentioned previously the structure of these two vortices is an important factor in the NOx formation and flame behaviour, therefore, the air gate design has the potential to improve based on the aspect ratio. The basic study about the air gate aspect ratios in this section has proven that for the given size, the lower air gate could change the flame size and angle which is essential to the multiple micromix combustion elements study.

5.3 Multi Injection Elements with Side Cooling Design

5.3.1 Side cooling design introduction

The modifications and methods discussed above aimed to reduce the NOx formation of the hydrogen combustion and maintain the risk of flame merging as low as possible. As described before, at fuel-rich conditions, the flame size would increase and have the tendency to border on each other, as well as the hydrogen pipe diameter increasing. By considering the combustion of adjacent combustion elements, the flame has to be limited in a safe range and make sure the distinct flame shape during combustion. Therefore, except the modification of air gate geometry, another method was proposed to reduce the flame merging during multi-injection elements interaction.

The idea of this design was inspired by the dilution air inlet of the conventional combustor design. In the conventional combustor, the dilution air jet could improve the combustion efficiency and help cool the exhaust gas temperature before the turbine stage. In the micromix combustor design, the large combustion zone is split into thousands of miniaturized combustion fields. The miniaturized combustion zone arrayed next to each other in the ring shape, provides the space for the cooling air design.

In this new side cooling design, one of the adjacent injection elements is modified to the cooling and dilution air channel. As the schematic drawing shown in Figure 5-18 (a) below, for a normal micromix combustor as shown in the red square, the adjacent injector has been converted to the cooling air chamber (blue border), it has the same air gate design as the combustor chamber but no fuel pipe design. The drawing in Figure 5-18 (b) clearly shows the differences between the previous design, the fuel pipe being removed from the cooling air chamber, the air stream flow through the cooling channel wouldn’t mix with the fuel stream, it will participate into the cooling of the high temperature and eliminate the flame merging risk.

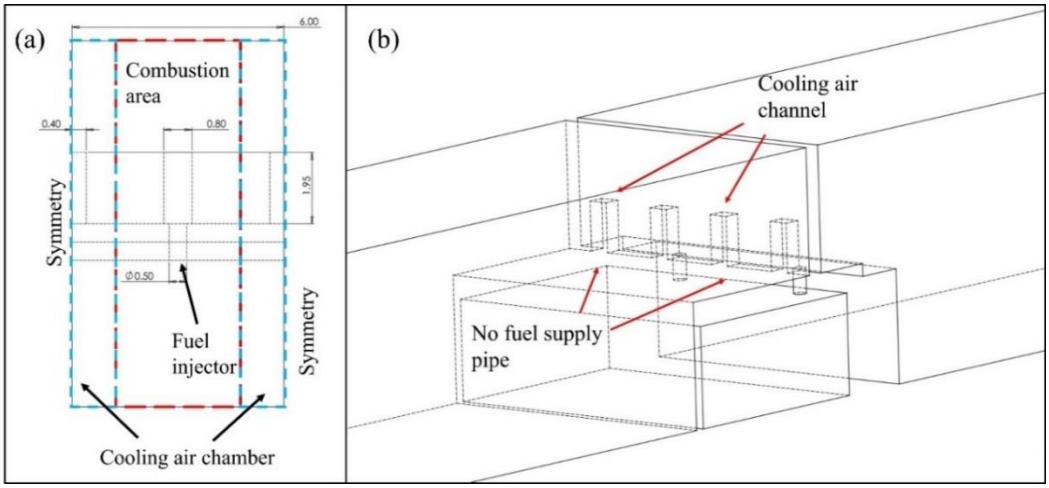

Figure 5-18. Schematic drawing of side cooling design on multi-injection elements.

To verify the function of this design, the simulation work has been done for it. The modification has been done based on the geometry of the basic burner. The geometry of the test multi-injection elements with cooling air design (MIC) is shown in Figure 5-18 (a), the single injection element is 3*10mm2. For the air gate design, the original design is applied to this MIC case, the hydrogen pipe diameter is enlarged to 0.5mm. Because the side boundaries are set as a symmetry plane, two halves of the cooling air chamber are used in the simulation work in order to save the computational costs.

For the boundary conditions, the numerical calculation is under the overall equivalence ratio of 0.54, due to the modification of the cooling air chamber, to maintain the energy input as the same density, the fuel inlet amount would be doubled compared to the basic burner case, as 2.35×10^{-6} kg/s.

In the micromix combustor, the flow field in each individual combustion element can be considered that the flow exists independently and ideally does not interfere with each other. Therefore, for the calculation of the air inlet conditions, the air inlet of the basic burner is 3.88m/s at the 3*10mm2 inlet, for this case, to ensure the amount of air in the middle combustion chamber, the air inlet velocity is doubled as well, which is 7.77m/s. Under this condition, the amount of air flow through the air gate could mix with the fuel at $\phi = 0.54$ conditions.

5.3.2 Simulation results

Figure 5-19 below demonstrates the flow stream behaviour inside the MIC burner, the pathline clearly shows that the air gas flows through the air gate in the middle, mixes with the fuel stream and forms a large inner vortex. From the top view can see the inner vortex formed by the mid-gas stream is larger than the other gas streams. It's because there is no fuel jet into the other air flow, the air flow through the cooling air channels partially participates in the vortices formation, the major cooling air flowing down the sides of the flame cools the hot area of the chamber and then exits from the outlets.

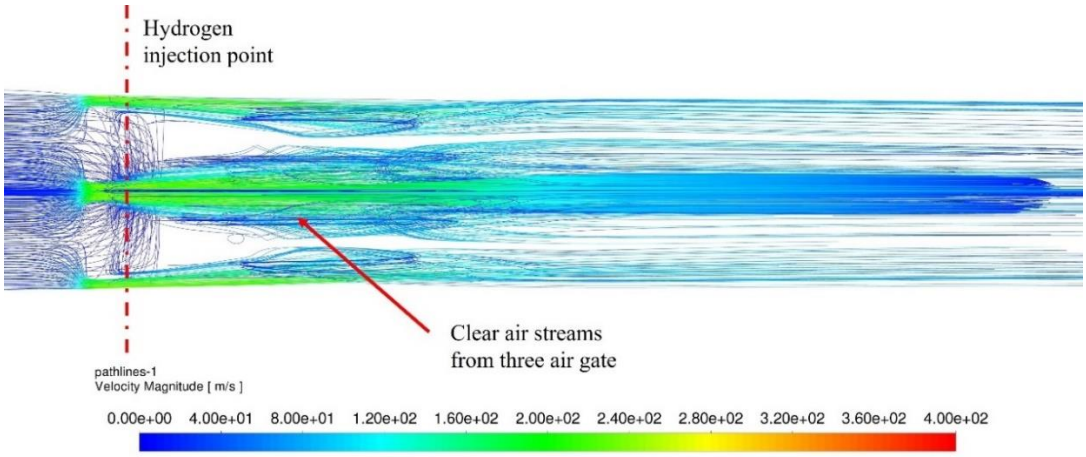

Figure 5-19. Velocity pathline of MIC burner from the top view.

An iso-surface was created for H_2O species shown in Figure 5-20 below. It could be found that H_2O was mainly formed in the middle gas stream as the red dash line circled which means the reaction between hydrogen and air occurred in the middle flow stream, the adjacent air stream doesn't participate in the combustion reaction. The function of those two air streams is cooling primarily. The capacity of the cooling air can be observed in the temperature contour in Figure 5-21.

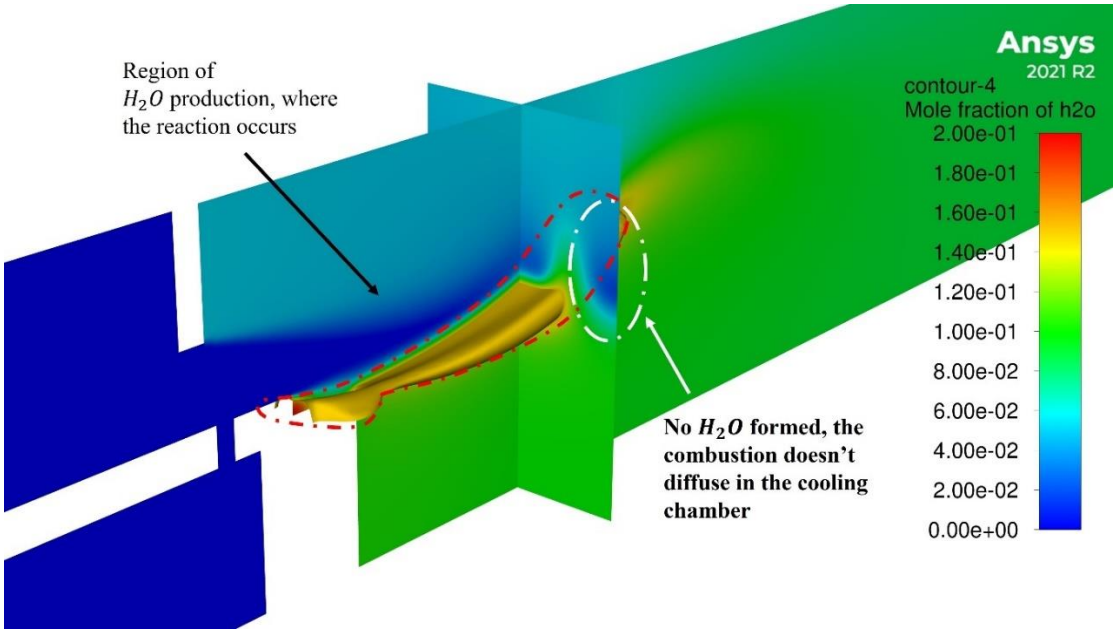

Figure 5-20. Iso-surface of H_2O production in MIC burner.

As Figure 5-21 shows below, even if the fuel inlet amount is doubled the combustion flame in the chamber presents a very clear shape and keeping far away from the adjacent flame. From the cross-section at Z=-11mm position, it could be found that in the original basic burner, the high temperature diffused into the outer vortex, the entire lower part of the combustion zone is full filled with high-temperature gases, under this situation, the flame would mostly like to merge. In terms of contrast, the flame stabilized in the centre of the MIC burner and the hot temperature only present in the middle. The cold air from two cooling air channels flows through greatly cooling down the chamber temperature and wrapping the flame laterally with an exceptionally low temperature. Compared to the combustion temperature in the basic burner, the flame temperature is effectively reduced, especially in the near wall region, because the hot temperature didn't diffuse to the inner and outer vortex, the temperature near the H2 segment is in an acceptable range which may increase the lifespan of the wall material.

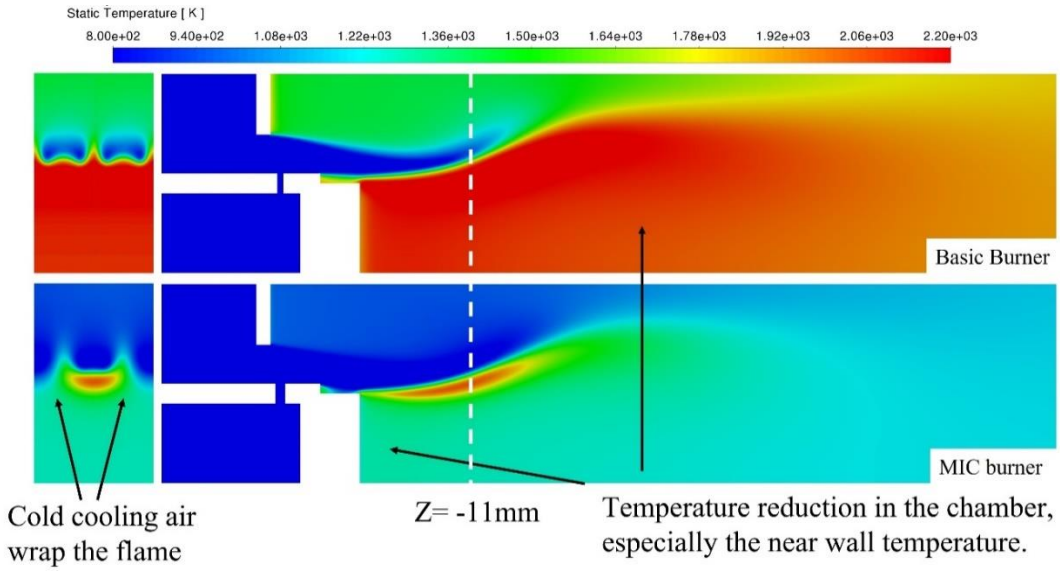

Figure 5-21. Temperature contour comparison between MIC burner and Basic burner $\Phi = 0.54$.

The NOx formation level in the MIC burner decreases exponentially compared to the basic burner. At the outlet of the burner, the NOx is 16.7ppm and 0.23ppm respectively for the basic burner and MIC burner. From the numbers, the huge gap of NOx reduction capacity could be clearly observed, the NOx distribution in Figure 5-22 corroborates it. Firstly, the colourmap of these two contours is different, the NOx emission in the basic burner is 10 times higher than the MIC burner. From the NOx distribution, it could be found the NOx formed in the outer vortex of basic burner disappeared in the MIC burner, as the temperature contour above displayed, in MIC burner the outer vortex temperature is much lower compared to the critical NOx formation temperature, it resulted in the great NOx reduction in MIC burner.

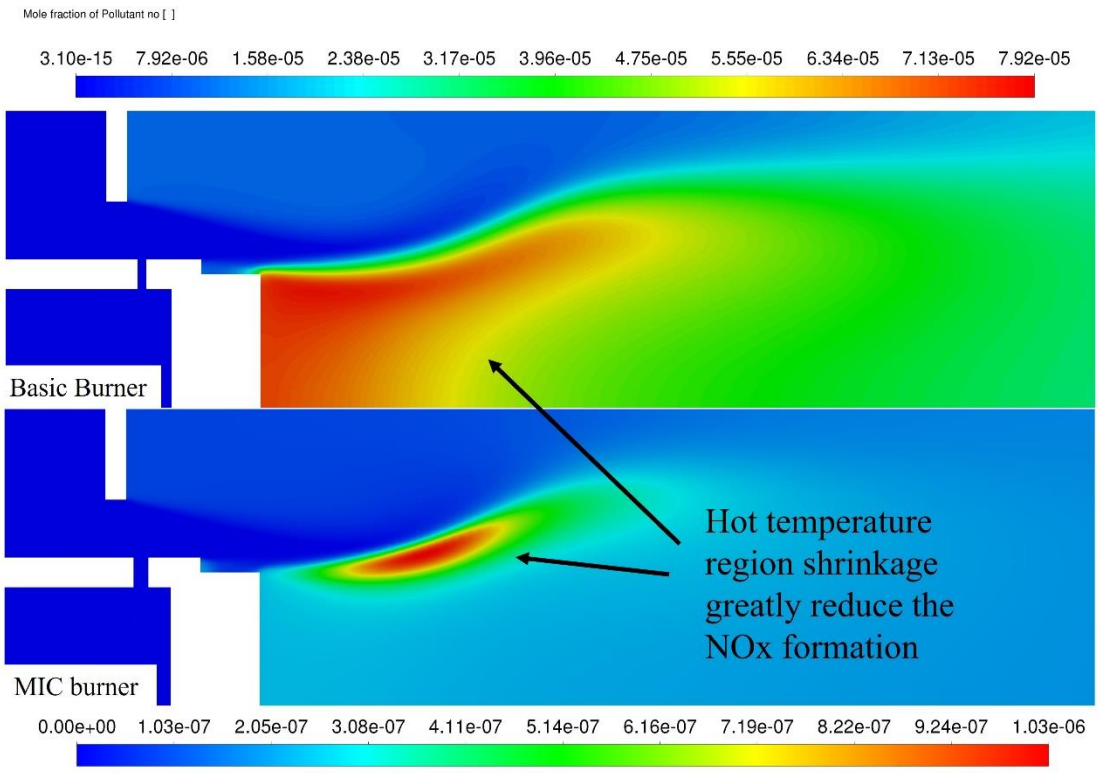

Figure 5-22. NOx formation distribution contour comparison.

The results demonstrated above indicate that the function of this MIC burner design is successful, at the condition that the total energy input remains the same, the combustion temperature is greatly reduced, meanwhile, the risk of the flame merging is eliminated. The shape of the flames is very clearly represented, keeping an absolutely safe distance from neighbouring flames. At the same time, in the new MIC burner, the NOx emissions have been drastically reduced – the value of 0.23ppm is undoubtedly a very desirable result. Of course, further study on this design is required especially the experiment study.

5.4 Summary of Enlarged Micromix Combustion Element Study

In the micromix combustor, thousands of micromix combustion elements are used to instead of conventional large-scale combustor. Therefore, increasing the single

combustion elements but maintaining the same energy density has an essential meaning for the further development of micromix combustor. It is important to the micromix combustor's practical usage, with the smaller number of elements and larger dimensions, the manufacturing cost could be reduced greatly. The main target of this chapter is to increase the burner size by widening the burner and reduce the potential risk of merged flame. The effects of combustion element width variation were focused.

Initially, the basic burner design of 3mm*10mm resulted in a flame size that was too large at high equivalence ratios. To prevent flame merging, the burner was enlarged by 1.5 times, increasing the width to 4.5mm. To maintain constant energy density, the hydrogen fuel mass flow rate was also increased by 1.5 times. Simulation results demonstrated that enlarging the burner width successfully prevented flame contact. However, the original design of the micromix combustor had drawbacks when the burner reference area increased, leading to rapidly increased hydrogen velocity and downward flame swing. To address this, the hydrogen injector diameter was increased to 0.5mm to reduce hydrogen velocity to an appropriate range. This adjustment caused the air stream velocity to become excessively high compared to the slowed hydrogen flow, resulting in ineffective injection of hydrogen fuel into the air stream, reduced injection depth, and atypical micromix combustion.

The following research focused on the increasing air gate size. The burner width has been modified from 1mm to 1.8mm, the results of this study show that although by increasing the width the penetration of hydrogen improved the flame angle moved up, and the flame width increased with the gate width increasing until the flame merged at width 1.8mm. It indicates that the enlargement of air gate is necessary, but the width of the gate needs to be controlled to prevent the flame contact with adjacent flames.

The air gate was subsequently redesigned with various sizes, including different areas and aspect ratios. Upon analysing the results, it was concluded that the NOx emissions and flame size were primarily influenced by the size of the air gate. Similar air gate

areas resulted in similar emissions and flame sizes. The studies demonstrated that a gate area below 1.8 mm^2 was acceptable to prevent flame merging. Specifically, design AG 5 with an area of 1.6 mm^2 yielded satisfactory results, with a distinct flame observed within an equivalence ratio range of 0.4 to 0.54. Further investigation of case AG 5 revealed that variations in width and height did not affect emissions but could influence flow behaviour. This finding could be utilized to combine the discoveries from the gate height study in section 4.2 and enhance combustion performance.

The multi-injection elements interaction has also been studied in another approach, a new design MIC burner is proposed to reduce the risk of flame merge and NOx reduction. The adjacent injection elements have been modified to the air-cooling chamber, the results show that this design could significantly reduce the NOx emission and eliminate the flame merging problem. On another hand, this modification could also reduce the costs of manufacturing by reducing the number of hydrogen pipes, only half the number of hydrogen pipes require which undoubtedly decreases the production costs.

This chapter shows that the enlargement of the micromix combustion element is available, the large elements could provide the same power output but with lower manufacturing and maintenance costs. A series of studies of air gate pointed out a simple way of air gate design which is defining the air gate size first and then improve combustion by adjusting the aspect ratio. The design of the MIC burner also pointed out another path to improve single element and reduce NOx.

However, there are lots of further studies required for the micromix combustion design, the relationship between emissions and air gate needs more work on it. The most important point is that all the study about multi-injection elements and flame behaviour is based on the Fluent simulation, for more practical situations the experimental works are necessary to verify the presumption established in this chapter.

CHAPTER 6: MICROMIX COMBUSTION WITH H2/NH3 BLENDED FUEL

The micromix combustion concept in the past decades was mostly studied with pure hydrogen fuel. The research has shown that the micromix burner has the great ability to burn hydrogen fuel with low NOx emissions, the risks of burning hydrogen are well avoided as well. In the last chapters, the designs of micromix combustion elements geometry have been studied and the NOx emissions reduction capability development has been proved with the geometric optimisations.

For alternative fuels, ammonia has also been researched from different aspects, it has been proven that ammonia has a great ability as the hydrogen carrier. On the other hand, ammonia has also been widely used as an additive fuel [130]–[132]. The hydrogen/ammonia fuel blend could effectively reduce the risk compared to pure hydrogen combustion.

In the existing studies, the ammonia/hydrogen mixed fuel has been studied with some different types of combustors. However, for micromix combustion burner, this field has not been studied for the mixing of hydrogen with ammonia.

In this chapter, a very basic ammonia/hydrogen fuel mixture combustion will be demonstrated. Due to the lack of practical experiments and experience with H_2/NH_3 combustion in a burner of such micro dimensions, the numerical results may not be very accurate and realistic. In addition, because of the limitation of computational power and time, there is still room for improvement in the use of mechanisms, turbulence models, and combustion models. Therefore, the results of this chapter could be considered as a start for future works, to provide a very accurate numerical prediction of H_2/NH_3 combustion there are still more works required.

6.1 Introduction of H_2/NH_3 Fuel Combustion

As introduced previously, ammonia (NH_3) has a bright future as a clean energy because it doesn't contain carbon and results in clean combustion [133]. Ammonia has demonstrated great potential as a sustainable energy source, with several advantages compared to other alternative fuels. Liquid ammonia has a comparable energy density to liquid hydrogen, but it is much easier to store due to its low vapour pressure and high boiling point. However, pure ammonia is not a good choice as an alternative fuel instead of conventional fossil fuels because of its properties. The low burning speed and high ignition conditions pose a challenge to the flammability of pure ammonia, limiting its feasibility as a combustion fuel[131][134].

Therefore, ammonia has been researched for many years as an additive fuel in different types of combustors. Ammonia-blended fuel has shown that, when mixed with other fuels, the flammability problem of ammonia could be effectively solved [113]. The fuel mixture paves the way for alternative fuel development, especially ammonia/hydrogen fuel. In this project, hydrogen has been studied extensively. As a carbon-free fuel, it's a good choice for ammonia-blended fuel, given that hydrogen has a high flame speed that can be used to promote ammonia combustion. Additionally, hydrogen can be produced by cracking ammonia, making ammonia a great energy carrier. The combustion of H_2/NH_3 fuel avoids the emissions of greenhouse gases such as CO and CO_2, etc. The only emission problem that needs to be overcome is the massive NOx emissions due to the nitrogen atom carried by ammonia.

6.2 Fuel Properties of H_2/NH_3 Mixed Fuel & Boundary Conditions

The fuel which will be tested on the micromix combustor is the H_2/NH_3 blended fuel, compare to the pure single fuel type, the density, energy contain and molar mass all these properties would be varied with the mixture composition changes.

For these two fuels, their fuel properties are listed in Table 6-1, all these properties of fuel gases are under operation temperature 300K.

Properties	Units	Hydrogen	Ammonia
Low heating value	MJ/kg	120.1	18.8
Flame speed	m/s	3.15	0.15
Auto-ignition temperature	℃	571	651
Density	Kg/m^3	0.0808	0.69

Table 6-1. Fuel properties comparison between ammonia/hydrogen.

In the combustion process, the lower heating value (LHV) is an important property of the fuel thermal power; it represents the heat released from a specified quantity of fuel during combustion. With different fuel mixture ratios, the lower heating value will vary. In this thesis, the LHV of H_2/NH_3 mixture will range between 18.8 MJ/kg (LHV of ammonia) and 120 MJ/kg (LHV of hydrogen).

The LHV of the blended fuels need to be defined by the mass fraction of the fuels, in the equation, the LHV of NH_3/H_2 mixture fuel could be calculated.

$$LHV_{\frac{NH3}{H2}} = g_{NH3} \times LHV_{NH3} + g_{NH3} \times LHV_{H2} \tag{6.1}$$

Where g_{NH3} and g_{H2} represent the mass fraction of respective fuel. For the fuel mixture, the compositions of the fuel are recorded in volumetric ratio. Therefore, to calculate the LHV of the fuel mixture, the mole fraction has to be converted to the mass fraction. The conversion is shown below:

$$\begin{cases} g_{NH3} = \dfrac{M_{NH3} \times x_{NH3}}{M_{NH3} \times x_{NH3} + M_{H2} \times x_{H2}} \rightarrow \dfrac{17x_{NH3}}{17x_{NH3} + 2x_{H2}} \\ g_{H2} = \dfrac{M_{H2} \times x_{H2}}{M_{NH3} \times x_{NH3} + M_{H2} \times x_{H2}} \rightarrow \dfrac{2x_{H2}}{17x_{NH3} + 2x_{H2}} \end{cases} \tag{6.2}$$

Where x_{NH3} is the mole fraction of ammonia in the fuel mixture, x_{H2} is the mole fraction of hydrogen. And M_i is the molar mass of the fuels, for ammonia the molar mass is 17 and 2 for hydrogen fuel. In addition, in this section, only two fuels are mixed, hence, $x_{H2} + x_{NH3} = 1$.

To calculate the density $\rho_{NH3/\mathrm{H2}}$, the fuel mixture composition can be used as shown in equation (6.3), the gases are assumed to be ideal gas.

$$\rho_{\frac{NH3}{H2}} = \rho_{H2} \times x_{H2} + \rho_{NH3} \times x_{NH3} \tag{6.3}$$

For the global stoichiometric combustion of NH_3/H_2/air is shown below:

$$(1 - x_{NH3})H_2 + x_{NH3} * NH_3 + \left(0.5 + \frac{x_{NH3}}{4}\right)(O_2 + 3.76N_2) \rightarrow \left(1 + \frac{x_{NH3}}{2}\right)H_2O + (1.88 + 1.44x_{NH3})N_2 \tag{6.4}$$

The air-fuel ratio could be expressed as:

$$\left(\frac{A}{F}\right)_{mass} = \frac{4.76 \times \left(0.5 + \frac{x_{NH3}}{4}\right) \times 28.8}{2 \times (1 - x_{NH3}) + 17x_{NH3}} \tag{6.5}$$

The blended fuel is combusted with different ratios, the percentage of hydrogen in the fuel mixture will be started from 1 and decrease by 10% to 0.5 ($x_{H2} = 1, 0.9, 0.8, 0.7, 0.6, 0.5$). For these fuel mixture compositions, the fuel properties would be different under different compositions.

In this chapter, the basic burner design was used to simulate the combustion of blended fuels. The basic burner has the overall dimensions of $3mm \times 10mm$ and the air gate size is $0.8mm \times 1.95mm$, the hydrogen pipe diameter is 0.3mm. Because of the density and LHV differences, at the same equivalence ratio to keep the energy input as a constant the inlet velocity of fuel would change for composition differences, as well as the air inlet velocity.

The initial numerical study about different fuel mixture compositions is at the equivalence ratio of 0.4 which is the original design point of the micromix hydrogen combustor. For this load condition, the fuel properties and the boundary conditions are listed in Table 6-2 below:

Properties / $H2$ mix fraction	LHV_{mix} $/MJ\ Kg^{-1}$	ρ_{mix} $/kgm^{-3}$	$(A/F)_{mass}$	$V_{air}/m/s$	V_{fuel}/m $/s$
1	120.00	0.081	34.27	5.23	1.213
0.8	70.85	0.142	20.56	5.32	1.172
0.6	51.18	0.203	15.08	5.40	1.134
0.4	40.60	0.264	12.13	5.47	1.100
0.2	33.98	0.324	10.28	5.54	1.067
0	29.45	0.385	9.02	5.61	1.036

Table 6-2. Fuel mixture properties and boundary conditions with different fuel compositions at $\boldsymbol{\Phi = 0.4}$.

The application of ammonia/hydrogen-blended fuel on a micromix combustor is based on the basic burner studied before. Therefore, for comparison purposes, the operating conditions will remain the same. The inlet temperature of the air is 550K, and 300K for the fuel, and combustion is conducted under a pressure of 1 bar.

In this chapter, the micromix burner design has been modified; the step gap structure has been removed to adopt the combustion of blended fuel. For the numerical settings, in this chapter, from the paper[135], the Large Eddy Simulation (LES) model showed good performance in calculation. However, limited by computational power, the turbulence model used will be the Realizable $k-\varepsilon$ model, and the combustion will be predicted by the species transport model with the Finite Rate/Eddy Dissipation model. For the mechanism used, after a series of studies about hydrogen/ammonia combustion, the mechanism from Hua Xiao et al. is applied for the numerical study of NH3/H2

micromix combustion[113]. Hua Xiao's team conducted a comprehensive study on ammonia/hydrogen fuel blends under gas turbine conditions. In their research, the existing mechanism was studied and optimized; the mechanism was reduced to save computational costs but provides a reliable prediction at the same time.

6.3 Comparison Between Hydrogen Fuel & Blended Fuel

To study blended fuel, the comparison between pure hydrogen fuel and blended fuel on the same basic micromix combustor is necessary. For comparison purposes, the combustion in the new geometry burner will be simulated for 100% hydrogen and 80% hydrogen-20% ammonia respectively, the inlet pressure and temperature for fuel and air were kept the same. At the same thermal power input and the equivalence ratio of 0.4, the combustion performance and emission level of H2 composition 80% and 100% were compared to investigate the difference between pure hydrogen fuel and NH_3/H_2 fuel.

The initial comparison between these two cases is the temperature profile. Figure 6-1 shown below demonstrates the combustion temperature difference between pure hydrogen and blended fuel. The maximum facet temperature on the cross-section panel along the Z-axis of the burner was recorded; those panels were established every 2mm from 4mm to 40mm, covering the flame region and downstream area of the combustion zone. As the temperature curves show, it can be found that with ammonia added to the hydrogen, the peak temperature reduced from approximately 2200K to 2130K. At the downstream of the combustion zone, the temperature reduction is more obvious. The temperature curve of the 80% H_2 case shifted down about 20K at each recorded position. This finding is interesting and will be further studied with different composition groups later.

The NOx emission produced has a huge difference between pure hydrogen and mixed

fuel. Because of the NH_3 molecules in the blended fuel, the large amount of nitrogen atoms in ammonia causes a significant number of nitrogen atoms to participate in the combustion reaction when it occurs, resulting in a sharp increase in the NOx of the combustion product. In the numerical study, the NOx emission calculation of 100% hydrogen cases uses post-processing by the extended Zeldovich mechanism, primarily based on the temperature of combustion. The level of NOx emission is mainly calculated for thermal NOx and prompt NOx. For the blended fuel cases, detailed mechanisms about nitrogen atoms are included, and emissions such as NO and NO_2 are calculated by the reaction equations. Therefore, the prediction of NOx emission for blended fuel is directly calculated from the species that participate in the reaction.

The numerical calculation results shown in Figure 6-1. In this comparison, the NOx emission in the pure hydrogen case is predicted in post process method, because the turbulence model changed to Realizable $k-\varepsilon$ model, also the burner geometry was changed, the NOx emission calculated along the chamber remains below 1ppm, at the outlet of burner NOx produced is 0.13ppm.

With the addition of 20% NH_3 fuel, the NOx emission at the burner greatly increased to approximately 450 ppm. This increase is attributed to the nitrogen atoms in ammonia fuel participating in the reactions. The NOx distribution starts to rise from the 6mm position where the fuel ignites, reaching a peak of 449 ppm at the position Z=14mm, which is the tail of the flame. In the region before this, the mixed fuel reacts with oxygen, and a large amount of ammonia is involved in the combustion.

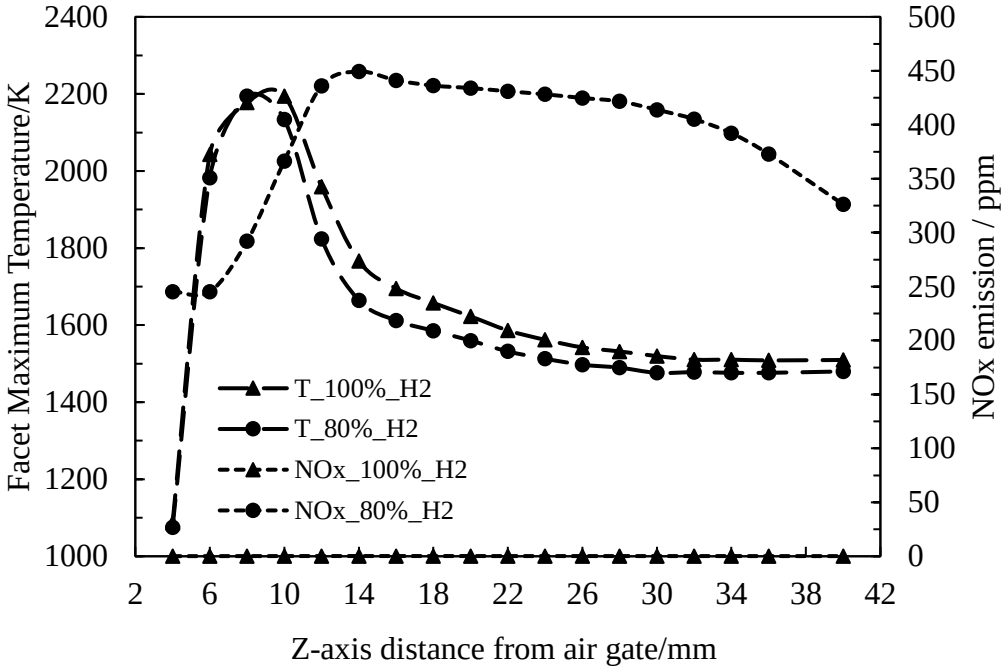

Figure 6-1.Temperature and NOx comparison along Z-axis at ϕ=0.4.

The results presented above show that the addition of ammonia may decrease the combustion temperature. For pure hydrogen combustion, this has a positive impact because a lower combustion temperature can result in lower thermal NOx produced during combustion. However, with the addition of ammonia, the NOx emission level has increased exponentially because of the large amount of nitrogen contained in ammonia. During combustion, the huge amount of fuel NOx produced leads to this result. The findings presented by Ariemma et al. and Ilbas et al. corroborate this assertion [136], [137]. In their respective studies on the combustion of ammonia mixed with Kerosene and Methane, it was observed that the introduction of ammonia led to a substantial increase in the levels of NOx. The positive impact of a lower temperature is no longer enough to offset the NOx produced by ammonia fuel. Additionally, the reduced temperature would lead to a decrease in power output. On the other hand, if the reduction of combustion temperature is within a controllable range, lowering the temperature may extend the life of components and reduce maintenance costs.

6.4 Study of Different Fuel Composition

To study the effect of different fuel mixing ratios on combustion performance, various molar fractions of NH_3 groups were tested. The composition of hydrogen in the fuel was decreased from 100% to 50%, and the detailed boundary conditions are listed in Table 6-2 above. As the fraction of ammonia added increases, the flammability of the blended fuel decreases. With the numerical models used in this project, the flameout problem occurs when the molar fraction of hydrogen fuel is lower than 50%. Therefore, in this section, only 50%_H_2 to 90%_H_2 cases will be discussed.

For different fuel composition cases, the flame temperature was compared. The temperature contour with the range of 1200~2000K is demonstrated in Figure 6-2 below. From the contour, it can be clearly observed that with the proportion of ammonia increasing in the fuel mixture, the temperature in the chamber decreases accordingly. Comparing the temperature distribution in 90%_H_2 to 50%_H_2 cases, the hot region almost disappears, which proves that the addition of ammonia into hydrogen fuel would effectively reduce the flame temperature. In addition, the position of the peak temperature region reflects that with the increasing proportion of ammonia, the peak temperature slightly shifts right. In the case of 50%_H_2, the hot gases diffuse into the outer vortex, and the temperature in most areas of the combustion chamber is approximately 1400K. This might be due to the reaction products improving the radiation heat transfer. Although the flame temperature decreases, from the colour map, it can be found that at the end of the combustor, the hot gases' temperature is reduced to almost the same level. It can be said that the amount of introduced ammonia into the

chamber would not change the exit temperature of gases.

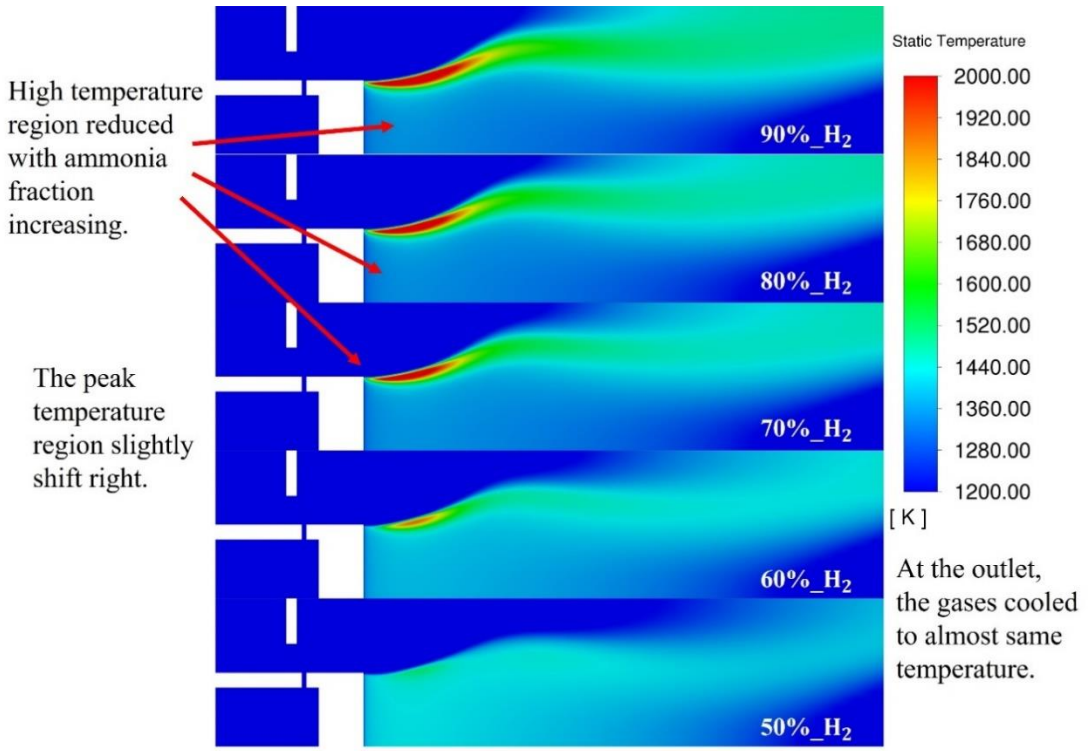

Figure 6-2. Temperature contour comparison with different fuel compositions.

The temperature distribution differences could be observed more directly from the curves plotted in Figure 6-3. The facet maximum temperature on the cross-panel set along the chamber is plotted for different fuel mix compositions. As shown by the curves, increasing the ammonia proportion from 10% to 50%, the peak temperature in the chamber reduces by more than 600K. At the downstream of the flame zone, the temperature decreases to a similar level for all cases, and the temperature differences are in the range of 90K. The result is very good for gas turbines; the lower the temperature in the combustion zone, the better, while ensuring that the temperature of gases entering the turbine stage is fixed. This ensures that the thermal output power is maintained and also reduces the temperature in the chamber, improving the reduction of thermal NOx.

In expectation, because of the lower burning velocity of ammonia, with ammonia added,

the flame location should shift further. With the help of the red dashed line on the curves, it can be said that the peak temperature point is shifting to the end of the chamber, which could prove that the addition of ammonia has the effect of decreasing burning velocity. Although the shifting is not considerable, there are two speculated reasons. Firstly, because the scale of the micromix combustor is too small, the entire chamber length is less than 5cm, so the shifting is not obvious. Another potential reason is the high air stream velocity; compared to the burning velocity of blended fuel, the air velocity entering the chamber is much higher than the velocity of fuel burning. This may contribute to the insignificant combustion shifting.

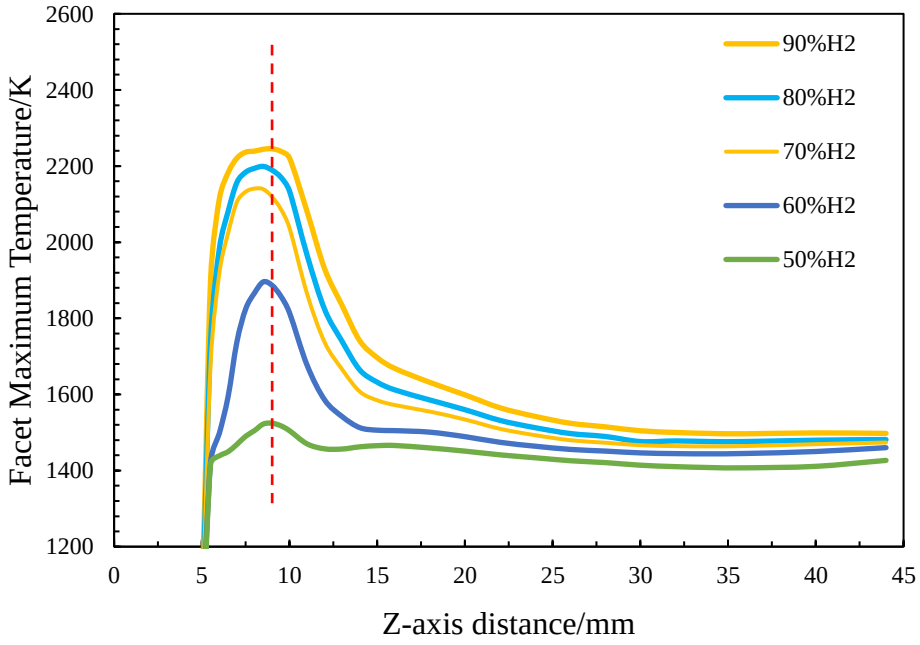

Figure 6-3.Temperature distribution along Z-axis of different fuel compositions.

Another indicator of measuring the combustion performance of different fuel compositions in this section is the NOx formation. As shown in Figure 6-4 shown below, the NOx emission, converted to PPM, is plotted. The NOx emission recorded on the curves starts from the ignition point to the outlet of the combustor. From the figure, it can be said that there is no clear tendency between NOx emission levels and fuel compositions. Although the 90%_H_2 cases have the highest NOx emission at the flame

position and outlet, the 50%_H_2 has the second-highest NOx, reflecting that the proportion of NH_3 blended may not directly affect the NOx formation during combustions.

From the curves, it could be found that the highest point of NOx generation is shifting further with the increase of ammonia molar fraction. This further supports the conclusion that the burning velocity was affected by ammonia additions. The curve of 50%_H_2 has the highest point at half of the combustor chamber, which can be said that the reaction of NO formation still occurs in that area; the chemical reaction is delayed with the addition of ammonia.

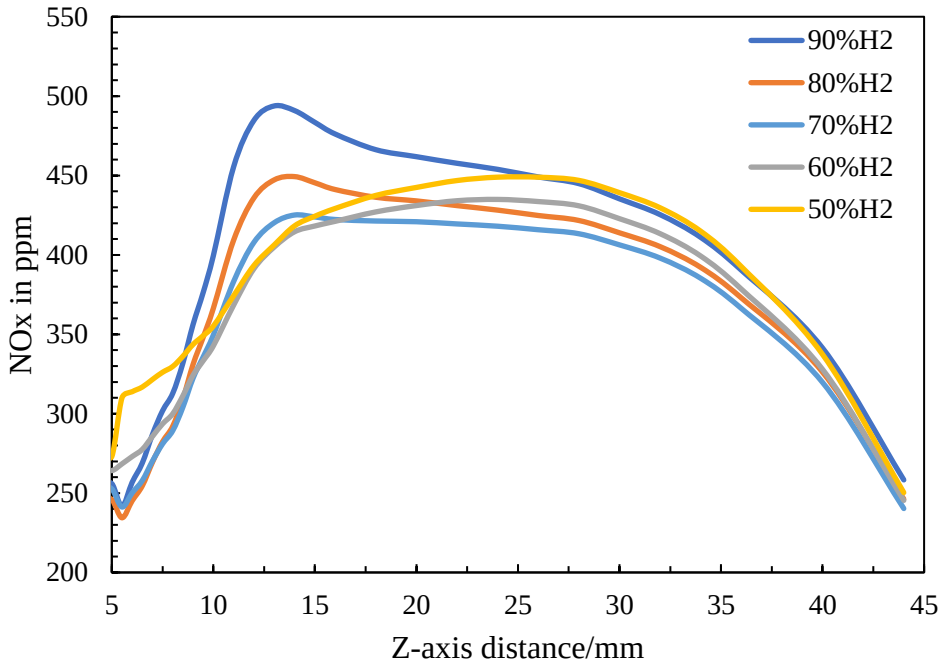

Figure 6-4.NOx distribution along Z-axis of different fuel compositions.

6.5 Conclusion

In conclusion, this chapter is simply a preliminary study for an ammonia/hydrogen combustion study, and many details have been left out; the discussion of the combustion performance of different fuel compositions has only concentrated on two elements, temperature, and NOx production. As a result, the conclusion given may not be full or

complete.

First, the addition of ammonia does effectively lower the flame temperature, as was found in several comparisons of different mixture fractions, but the overall temperature at the end of the combustion chamber is at a close level. The second point is that the addition of ammonia reduces the burning velocity of the fuel. Due to the fact that ammonia's burning velocity is much lower than hydrogen, adding ammonia to hydrogen will slow the combustion. This phenomenon is not very obvious in the results presented, but it could be confirmed from different aspects.

CHAPTER 7: CONCLUDING REMARKS AND FUTURE STUDY

7.1 Conclusion

In this thesis, the further optimization of NOx reduction capability was investigated on the basis of the micromix combustion principle. In the present work, a well-evaluated numerical method was used in FLUENT simulation studies to optimize the micromix combustor. The burner's internal geometric parameters were modified to improve the combustion. Also, the combustion of multiple injection elements was studied to further develop a micromix combustor. After a series of design optimisations, the project aim has been achieved.

7.1.1 Numerical settings study and validation

- The research from Ayed [66] was used for the validation purpose. A basic micromix burner case was established which has the same dimension as the test burner. FLUENT simulation has been conducted under the same boundary conditions to validate the numerical settings.

- Turbulence, NOx, and combustion models are thoroughly studied to select the most appropriate methods. Comparisons between different models indicate that the SST k-ω model provides acceptable flow dynamics, temperature prediction, and the closest NOx value with low computational cost.

- The NOx prediction relies on the extended Zeldovich mechanism to accurately estimate thermal NOx emissions. The selection of NOx settings in Fluent significantly affects the accuracy of NOx prediction. Compared to the NOx measure data from the reference paper, the approaches are selected as

"Instantaneous" which predicted NOx is 1.07ppm compared to the experimental 1.3ppm.

- Seven hydrogen combustion mechanisms are compared, and the Li-2015 and ELTE-2015 mechanisms demonstrate the best performance. ELTE-2015 is further validated for NOx emission prediction within a specific range of equivalence ratios, it shows a very agreement with the experimental results.
- For the combustion model, the EDC and FR/ED models are compared with ELTE-2015 and Li-2015 mechanisms. FR/ED model accurately predicts NOx emissions, while the EDC model shows discrepancies.
- As expected, EDC model should have better performance in combustion simulation. Regarding this result, speculation is due to the fact that hydrogen has high burning velocity, and the reaction steps of hydrogen are all forward reactions, therefore the FR/ED may be more suitable for the hydrogen micromix combustion.

7.1.2 The modification of the micromix burner geometry

The trends in the effects of geometry changes on NOx emission and other combustion performances were scrutinized and summarized. The numerical studies of modified internal geometric parameters of the micromix combustor prove that the reduction of NOx emission could be achieved by physical modification of burner geometry.

- The mixing distance has a great impact on the flow structure and NOx emission, in the comparison group the mixing distance was increased from 2mm to 6mm. The results reflected that with the longer mixing distance, the NOx emission could be reduced gradually.
- With the higher equivalence ratio, the NOx emission differences were bigger between varied mixing distances.

- The extension of the mixing distance has a limitation which is the NOx reduction capability becomes weaker with long mixing distance. In this situation, the combustor component would be thicker and heavier due to the long distance which is not expected in practical usage. Therefore, the mixing distance should be controlled in a suitable range.

- The air gate was designed with different heights to study the effect of air gate dimensions, the gate height varied from 1.5mm to 2.4mm. From the results, the lower air gate has the best performance. The airflow through accelerated due to the smaller air gate and resulted in the increasing mixing intensity, the structure of the vortex was affected as well.

- The temperature along the chamber was decreased with a lower air gate. For the smallest air gate, the temperature at the rear part of the burner is about 200 K lower than the basic burner.

- For the NOx reduction, the NOx was reduced by 80% in the 1.5mm air gate design compared to the original design.

- The hydrogen injection pipe diameter also has an impact on the combustion performance, Comparison between 0.24mm and 0.4mm diameter shows that with the smaller pipe diameter, the NOx emission decreased. Also, the flame size would be bigger in the larger pipe case. This conclusion is not that absolute, when the diameter increased to 0.5mm, the NOx produced was lower than the basic burner 0.3mm diameter. This may be because the larger pipe lifted more air gas in the vortex and improved the mixing.

As the points listed above, the trends in the effects of geometry changes have been concluded. The longer mixing distance would undoubtedly help the NOx reduction. The air gate height cases indicate that the lower the air gates, the better the combustion performance. The hydrogen diameter groups presented a confused result, generally, the

small hydrogen injection pipe could give the lower NOx formation. However, the hydrogen pipe cannot be too thin, it would cause the high injection velocity which has the risk of choking, also, the pipe is easier to block.

7.1.3 Further modifications of micromix burner and study of multi-injector combustion

This project also explores the perspective of micromix combustion research beyond single injection elements. The interaction of multi-injection elements is studied from a different angle. Increasing the size of injection elements while maintaining energy density is meaningful as it reduces manufacturing costs and helps with the pressure drop problem.

- Increasing the burner width from 3mm to 4.5mm successfully avoids the flame merge risk, however, the widening of the burner would increase the velocity of hydrogen injection velocity too high, so the hydrogen pipe diameter needs to be increased.

- The hydrogen pipe diameter has increased to 0.5mm. the high air flow speed with the 0.5mm hydrogen pipe results in untypical micromix flames and a rapid increase in NOx emissions.

- To lower the airspeed, the air gate width has been studied in the range from 1mm to 1.8mm, the results show that the enlargement of the air gate is useful, but the flame would contact when the gate is getting overly wide. With the fixed height, the wider air gate, larger flame size and more NOx produced.

- The air gate was further adjusted with different areas and aspect ratios, the results reflected that the gate area greatly affected the combustion. The combustion performance and NOx formation level are determined by the air

gate area, the smaller air gate provided better performance, this is mainly because the mixing intensity improved due to higher air velocity.

- As the conclusion, for this enlarged burner, the air gate should be kept smaller than 1.8 mm^2. Because the overly high air velocity would cause the flame blow-off problem.

- Although the air gate area is a prerequisite for determining emissions, with the same area, the gate aspect ratio would affect the flow dynamics inside the burner, the flame angle, flame position.

- MIC burner design was proposed to avoid the fame merging danger and reduce NOx. The micromix combustion elements are spaced out and a cooling chamber is inserted between adjacent combustion elements. The results indicated that this modification effectively eliminated the flame merging problem and greatly reduced the NOx emission by over 90%.

7.1.4 Micromix combustion with H2/NH3 blended fuel

A preliminary study of hydrogen/ammonia micromix combustion has been conducted. The discussion of combustion performance of different fuel compositions just focused on two aspects, temperature and NOx production.

- Compared to pure hydrogen combustion and H_2/NH_3 combustion, the addition of ammonia could reduce the combustion temperature. Due to the N atoms contained in ammonia, NOx emissions level rapidly increased.

- Several comparisons of different fuel mixture fractions indicate that the addition of ammonia does effectively lower the flame temperature. But the overall temperatures at the exit of the burner are close.

- The NOx emission variation does have a clear trend, 50%_H_2 case have higher NOx distribution in the chamber than 80%_H_2 but lower than 90%_H_2. The

NOx emissions at the outlet are at a similar level for different fuel compositions.

- The burning velocity of blended fuel decreases with the ammonia addition. The peak temperature point shift further proves this finding. Because the ammonia burning velocity is much lower than hydrogen, the ammonia added to the hydrogen will slow the combustion.

Because only basic simulation works were conducted in this chapter, to study the micromix combustion with blended fuel in detail, more research is required for it.

7.2 Future Work

In this project, due to the restriction of experimental conditions, the validation has been done based on the experimental data from reference papers. However, this validation is not comprehensive, the data validated is only the NOx emission and flame shape. In future studies, experiments are required to validate with different data, such as the combustion temperature, the burning velocity, the species distribution. With all these data, the numerical settings could be studied in detail and more comprehensively, which could better help the following researchers on numerical studies about micromix hydrogen combustion. In addition, the combustion model EDC and FR/ED need more work on it to find out why FR/ED could provide a better prediction of NOx emissions.

For the micromix burner geometry optimization, there is still a large research potential regarding burner configuration. The geometric studies presented in this thesis are mainly based on the design of a basic burner from H.Funke's work [65], [138]. Improvements in geometric shapes are restricted to the existing design, the overall geometric appearance of the micromix burner has not changed much.

In prospective investigations, additional modifications to the configuration could be implemented, including the incorporation of multiple fuel injection pipes, alteration of the air gate's shape, and exploration of diverse injection methods. These adaptations

hold the potential for yielding more significant positive impacts on NOx reduction. Furthermore, there remains a need for further exploration into the hydrogen pipe diameter. The specific reasons underlying the superior performance of a 0.5mm hydrogen diameter compared to a 0.3mm diameter remain unclear. To elucidate the effects of diameter variations, extensive simulations and experimental studies are warranted. By conducting such comprehensive research, a deeper understanding of the combustion dynamics and NOx reduction mechanisms can be attained, thereby contributing to advancements in clean and efficient combustion technologies.

In Chapter Five, the simulation results demonstrate that the modification of injection elements proves effective in achieving the intended design objectives. However, to validate these design improvements in practical applications, experimental testing becomes essential. Moreover, numerous unresolved issues persist, particularly regarding the flow dynamics' impact on combustion performance.

The influence of the air gate area on flame size and NOx emissions has been established, but further investigation is needed concerning the gate aspect ratio. The dimensions of the gate, including height and width, significantly affect flow structure and vortex formation, potentially resulting in varied flame shapes. The current turbulence model may not capture subtle flow field variations adequately. In the future, the availability of computational resources could enable the use of Large Eddy Simulation (LES) and Direct Numerical Simulation (DNS) to study the effects of different air gate designs on flow structure at a finer level.

Additionally, the design of the MIC burner exhibits promising NOx reduction capability and addresses flame merging concerns. However, being a novel concept, this design requires extensive scrutiny under practical conditions. Verification of its effectiveness is paramount, followed by evaluation of combustion efficiency, thermal power output, and other relevant aspects. A comprehensive examination of various aspects of the MIC burner is necessary to ascertain its practicability fully.

The combustion of H_2/NH_3 blends presented a promising avenue, but substantial future research is still required to facilitate practical application in micromix combustors. In this project, only basic aspects such as combustion temperature and NOx emissions were compared and analysed. However, for the blended fuel's successful integration into micromix combustors, a more comprehensive understanding of other crucial characteristics is imperative.

To enable the practical implementation of hydrogen/ammonia mixed fuel, detailed investigations into various factors are warranted. Key areas for future study include the reaction production rate, burning velocity, and the combustion efficiency of different fuel mixture fractions. These aspects play a critical role in determining the viability of hydrogen/ammonia blends for micromix combustors.

In addition to simulation work, experimental investigations are essential for validating the accuracy of numerical predictions. The numerical settings employed in Chapter Six were largely based on evaluations from existing literature, which might not always be suitable for practical micromix combustor applications. Hence, a combined approach of simulation studies and experimental work is required in future research to comprehensively explore the potential of hydrogen/ammonia fuel.

Overall, all the works that have been done in this thesis are based on numerical studies. The results provided by FLUENT initially gave help to the research on hydrogen micromix combustion in this thesis, but for more research based on real-life conditions, experimental cooperation is still essential in subsequent studies.

REFERENCE

[1] D. Cecere, E. Giacomazzi, and A. Ingenito, “A review on hydrogen industrial aerospace applications,” *Int. J. Hydrogen Energy*, vol. 39, no. 20, pp. 10731–10747, 2014, doi: 10.1016/j.ijhydene.2014.04.126.

[2] J. Li *et al.*, “A Review on Combustion Characteristics of Ammonia as a Carbon-Free Fuel,” *Front. Energy Res.*, vol. 9, no. October, pp. 1–15, Oct. 2021, doi: 10.3389/fenrg.2021.760356.

[3] G. D. Brewer, *Hydrogen Aircraft Technology*, Illustrate. New York: Routledge, 1991. doi: 10.1201/9780203751480.

[4] The Engineering toolbox, “Energy Storage Density,” 2017.

[5] “Hydrogen Compared with Other Fuels,” *Hydrogen Tools*.

[6] B. Khandelwal, Y. Li, P. Murthy, V. Sethi, and R. Singh, “Implication of different fuel injector configurations for hydrogen fuelled micromix combustors,” in *Proceedings of the ASME Turbo Expo*, Jan. 2011, vol. 4, pp. 293–298. doi: 10.1115/GT2011-46845.

[7] A. M. Abdalla, S. Hossain, O. B. Nisfindy, A. T. Azad, M. Dawood, and A. K. Azad, “Hydrogen production, storage, transportation and key challenges with applications: A review,” *Energy Conversion and Management*, vol. 165, no. April. pp. 602–627, 2018. doi: 10.1016/j.enconman.2018.03.088.

[8] J. L. Sloop, “LIQUID HYDROGEN AS A PROPULSION FUEL, 1945-1959.,” *NASA Spec Publ*, no. 4404, 1978, doi: 10.2307/3104021.

[9] C. M. Stoots, J. E. O’Brien, K. G. Condie, and J. J. Hartvigsen, “High-temperature electrolysis for large-scale hydrogen production from nuclear

energy - Experimental investigations," *Int. J. Hydrogen Energy*, vol. 35, no. 10, pp. 4861–4870, 2010, doi: 10.1016/j.ijhydene.2009.10.045.

[10] O. Bendaikha and S. Larbi, "Hydrogen production system analysis using direct photo-electrolysis process in Algeria," in *Proceedings of 2013 International Conference on Renewable Energy Research and Applications, ICRERA 2013*, 2013, pp. 1123–1128. doi: 10.1109/ICRERA.2013.6749921.

[11] R. Boudries, A. Khellaf, A. Aliane, L. Ihaddaden, and F. Khida, "PV system design for powering an industrial unit for hydrogen production," *Int. J. Hydrogen Energy*, vol. 39, no. 27, pp. 15188–15195, 2014, doi: 10.1016/j.ijhydene.2014.04.166.

[12] D. Verstraete, P. Hendrick, P. Pilidis, and K. Ramsden, "Hydrogen fuel tanks for subsonic transport aircraft," *Int. J. Hydrogen Energy*, vol. 35, no. 20, pp. 11085–11098, 2010, doi: 10.1016/j.ijhydene.2010.06.060.

[13] H. Dagdougui, R. Sacile, C. Bersani, and A. Ouammi, "Hydrogen Storage and Distribution: Implementation Scenarios," in *Hydrogen Infrastructure for Energy Applications*, 2018, pp. 37–52. doi: 10.1016/b978-0-12-812036-1.00004-4.

[14] C. Koroneos and N. Moussiopoulos, "Cryoplane - Hydrogen vs. Kerosene as Aircraft Fuel," in *7th International Conference on Environmental Science and Technology*, 2001, no. June 2014, pp. 484–493.

[15] G. D. Brewer, R. E. Morris, R. H. Lange, and J. W. Moore, "STUDY OF THE APPLICATION HYDROGEN SUBSONIC FUEL TO LONG-RANGE TRANSPORT AIRCRAFT," 1975.

[16] D. Verstraete, "An assessment of the potential of hydrogen fuelled large long-range transport aircraft," in *ICAS Secretariat - 26th Congress of International Council of the Aeronautical Sciences 2008, ICAS 2008*, 2008, vol. 5, pp. 840–849.

[17] M. Bellis, “The History and Invention of the Jet Engine,” *ThoughtCo.*, 2019.

[18] S. Harsha, “Liquid hydrogen as aviation fuel and its relative performance with commercial aircraft fuel,” *Int. J. Mech. Eng. Robot. Res.*, vol. 1, pp. 73–77, 2014, doi: 10.13140/2.1.5168.9927.

[19] C.-J. WINTER, “HYDROGEN IN HIGH-SPEED AIR TRANSPORTATION,” vol. 15, no. 8, pp. 579–595, 1990.

[20] R. Kaufnnan, “High-Altitude Performance Investigation of J65-13-3 Turbojet Engine with Both JP-4 and Gaseous-Hydrogen Fuels,” 1957.

[21] A. Contreras, “HYDROGEN AS AVIATION FUEL : A COMPARISON WITH HYDROCARBON FUELS,” *Int. J. Hydrogen Energy*, vol. 22, no. 10–11, pp. 1053–1060, 1997.

[22] Airbus Deutschland GmbH, “Liquid Hydrogen Fuelled Aircraft - System Analysis,” *Cryoplane*, no. May 2003, pp. 1–80, 2003.

[23] H. Z. Cui *et al.*, “Iron-based composite nanostructure catalysts used to produce COx-free hydrogen from ammonia,” *Sci. Bull.*, vol. 61, no. 3, pp. 220–226, 2016, doi: 10.1007/s11434-015-0991-9.

[24] R. Can Seyfeli and D. Varisli, “Ammonia decomposition reaction to produce COx-free hydrogen using carbon supported cobalt catalysts in microwave heated reactor system,” *Int. J. Hydrogen Energy*, vol. 45, no. 60, pp. 34867–34878, 2020, doi: 10.1016/j.ijhydene.2020.01.124.

[25] R. F. Service, “Liquid sunshine,” *Science (80-.).*, vol. 361, no. 6398, pp. 120–123, 2018, doi: 10.1126/science.361.6398.120.

[26] Y. Kojima, H. Miyaoka, and T. Ichikawa, “Ammonia-Based Hydrogen Storage Materials,” in *Advanced Materials for Clean Energy*, 2015.

[27] J. H. Lee, S. I. Lee, and O. C. Kwon, "Effects of ammonia substitution on hydrogen/air flame propagation and emissions," *Int. J. Hydrogen Energy*, vol. 35, no. 20, pp. 11332–11341, 2010, doi: 10.1016/j.ijhydene.2010.07.104.

[28] N. A. Hussein, A. Valera-Medina, and A. S. Alsaegh, "Ammonia- hydrogen combustion in a swirl burner with reduction of NOx emissions," *Energy Procedia*, vol. 158, no. 2018, pp. 2305–2310, 2019, doi: 10.1016/j.egypro.2019.01.265.

[29] G. Issayev *et al.*, "Combustion behavior of ammonia blended with diethyl ether," *Proc. Combust. Inst.*, vol. 38, no. 1, pp. 499–506, 2021, doi: 10.1016/j.proci.2020.06.337.

[30] H. Kobayashi, A. Hayakawa, K. D. K. A. Somarathne, and E. C. Okafor, "Science and technology of ammonia combustion," *Proc. Combust. Inst.*, vol. 37, no. 1, pp. 109–133, 2019, doi: 10.1016/j.proci.2018.09.029.

[31] C. H. Christensen, T. Johannessen, R. Z. Sørensen, and J. K. Nørskov, "Towards an ammonia-mediated hydrogen economy?," *Catal. Today*, vol. 111, no. 1–2, pp. 140–144, 2006, doi: 10.1016/j.cattod.2005.10.011.

[32] E. Morgan, J. Manwell, and J. McGowan, "Wind-powered ammonia fuel production for remote islands: A case study," *Renew. Energy*, vol. 72, pp. 51–61, 2014, doi: 10.1016/j.renene.2014.06.034.

[33] A. Valera-Medina, H. Xiao, M. Owen-Jones, W. I. F. David, and P. J. Bowen, "Ammonia for power," *Prog. Energy Combust. Sci.*, vol. 69, pp. 63–102, 2018, doi: 10.1016/j.pecs.2018.07.001.

[34] J. R. Bartels, "A feasibility study of implementing an Ammonia Economy," Iowa State University, 2008. doi: https://doi.org/10.31274/etd-180810-1374.

[35] M. G. Bull, "Development of an Ammonia-Burning Gas Turbine Engine," vol.

824, no. September 1964, p. 56, 1968, [Online]. Available: https://apps.dtic.mil/sti/citations/AD0671667

[36] D. T. Pratt and E. S. Starkman, "Gas Turbine Combustion of Ammonia," *SAE Trans.*, vol. 76, pp. 3160–3168, 1968.

[37] N. Iki *et al.*, "Micro Gas Turbine Firing Kerosene and Ammonia," in *Volume 8: Microturbines, Turbochargers and Small Turbomachines; Steam Turbines*, Jun. 2015, pp. 1–5. doi: 10.1115/GT2015-43689.

[38] A. Hayakawa, Y. Arakawa, R. Mimoto, K. D. K. A. Somarathne, T. Kudo, and H. Kobayashi, "Experimental investigation of stabilization and emission characteristics of ammonia/air premixed flames in a swirl combustor," *Int. J. Hydrogen Energy*, vol. 42, no. 19, pp. 14010–14018, 2017, doi: 10.1016/j.ijhydene.2017.01.046.

[39] O. Kurata *et al.*, "Development of a wide range-operable, rich-lean low-NOx combustor for NH3 fuel gas-turbine power generation," *Proc. Combust. Inst.*, vol. 37, no. 4, pp. 4587–4595, 2019, doi: 10.1016/j.proci.2018.09.012.

[40] M. C. Franco, R. C. Rocha, M. Costa, and M. Yehia, "Characteristics of NH3/H2/air flames in a combustor fired by a swirl and bluff-body stabilized burner," *Proc. Combust. Inst.*, vol. 38, no. 4, pp. 5129–5138, 2021, doi: 10.1016/j.proci.2020.06.141.

[41] R. Ju *et al.*, "Experimental study on burning velocity, structure, and NOx emission of premixed laminar and swirl NH3/H2/air flames assisted by non-thermal plasma," *Appl. Energy Combust. Sci.*, vol. 14, no. May, p. 100149, 2023, doi: 10.1016/j.jaecs.2023.100149.

[42] A. Cappelletti and F. Martelli, "Investigation of a pure hydrogen fueled gas turbine burner," *Int. J. Hydrogen Energy*, vol. 42, no. 15, pp. 10513–10523, 2017, doi: 10.1016/j.ijhydene.2017.02.104.

[43] Shelil N, "Flashback Studies with Premixed Swirl Combustion," Cardiff University, 2009.

[44] G. Dahl and F. Suttrop, "Engine control and low-nox combustion for hydrogen fuelled aircraft gas turbines," *Int. J. Hydrogen Energy*, vol. 23, no. 8, pp. 695–704, 1998, doi: 10.1016/s0360-3199(97)00115-8.

[45] F. Haglind and R. Singh, "Design of aero gas turbines using hydrogen," *J. Eng. Gas Turbines Power*, vol. 128, no. 4, pp. 754–764, 2006, doi: 10.1115/1.2179468.

[46] M. Sato and T. Hasegawa, "Reaction of fuel NOx formation for gas turbine conditions," *J. Eng. Gas Turbines Power*, vol. 120, no. 3, pp. 474–480, 1998, doi: 10.1115/1.2818169.

[47] C. J. Marek, T. D. Smith, and K. Kundu, "Low Emission Hydrogen Combustors for Gas Turbines Using Lean Direct Injection," *41st AIAA/ASME/SAE/ASEE Jt. Propuls. Conf. Exhib.*, pp. 1–27, 2005, doi: 10.2514/6.2005-3776.

[48] D. Crunteanu and R. Isac, "Investigation of low emission combustors using hydrogen lean direct injection," *INCAS Bull.*, vol. 3, no. 3, pp. 45–52, 2011, doi: 10.13111/2066-8201.2011.3.3.5.

[49] J. Li, X. Sun, Y. Liu, and V. Sethi, "Preliminary aerodynamic design methodology for aero engine lean direct injection combustors," *Aeronaut. J.*, vol. 121, pp. 1087–1108, 2017, doi: 10.1017/aer.2017.47.

[50] C. M. Heath, Y. R. Hicks, R. C. Anderson, and R. J. Locke, "Optical characterization of a multipoint lean direct injector for gas turbine combustors: Velocity and fuel drop size measurements," *Proc. ASME Turbo Expo*, vol. 2, no. PARTS A AND B, pp. 791–802, 2010, doi: 10.1115/GT2010-22960.

[51] J. D'Entremont, R. M. Gejji, P. Venkatesh, and S. P. M. Bane, "Plasma Control

of Combustion Instability in a Lean Direct Injection Gas Turbine Combustor," in *52nd Aerospace Sciences Meeting*, Jan. 2014, no. January. doi: 10.2514/6.2014-0622.

[52] A. H.Lefebvre and D. R.Ballal, *GAS Turbine Combustion Alternative Fuels and Emissions*. 2010.

[53] J. Li, L. Yuan, and H. C. Mongia, "Simulation of combustion characteristics in a hydrogen fuelled lean single-element direct injection combustor," *Int. J. Hydrogen Energy*, vol. 42, no. 5, pp. 3536–3548, Feb. 2017, doi: 10.1016/j.ijhydene.2016.10.159.

[54] J. E. Little *et al.*, "Fuel-Flexible Gas Turbine Combustor Flametube Facility," 2004.

[55] J. D. Holdeman and R. E. Walker, "Mixing of a row of jets with a confined crossflow," *AIAA J.*, vol. 15, no. 2, pp. 243–249, 1977, doi: 10.2514/3.60622.

[56] J. D. Holdeman, "Mixing of a Row of Jets with a Confined Crossflow," *AIAA J.*, vol. 15, no. 2, 1977, doi: 10.2514/3.60622.

[57] J. Goldmeer, *Turbomachinery International - Special report : The race for 100% Hydrogen*, vol. 424, no. November/December. 2020.

[58] L. Miniero, K. Pandey, G. De Falco, A. D'Anna, and N. Noiray, "Soot-free and low-NO combustion of Jet A-1 in a lean azimuthal flame (LEAF) combustor with hydrogen injection," *Proc. Combust. Inst.*, vol. 39, pp. 4309–4318, 2022, doi: 10.1016/j.proci.2022.08.006.

[59] P. M. de Oliveira, L. Miniero, K. Pandey, N. Noiray, and E. Mastorakos, "A novel ultra-low NOx hydrogen combustor based on the Lean Azimuthal Flame concept," Jan. 2023. doi: 10.2514/6.2023-1488.

[60] CLEAN AVIATION, "A new 100% hydrogen combustor for aviation," 2022.

https://www.clean-aviation.eu/media/news/a-new-100-hydrogen-combustor-for-aviation

[61] S. Börner and H. Funke, "Modification and testing of an engine and fuel control system for a hydrogen fuelled gas turbine," *rogress Propuls. Phys.*, vol. 2, pp. 475–486, 2011, doi: 10.1051/eucass/201102475.

[62] Y. B. Zel'dovich, "The Oxidation of Nitrogen in Combustion Explosions," *Acta Physicochim. U.S.S.R.*, vol. 21, pp. 577–628, 1946.

[63] S. Boerner, H. H. Funke, P. Hendrick, and E. Recker, "Development And Integration of A Scalable Low NOx Combustion Chamber For A Hydrogen-fulled Aerogas Turbine," *Prog. Propuls. Phys.*, vol. 4, pp. 357–372, 2013, doi: 10.1051/eucass/201304.

[64] A. H. Ayed, K. Kusterer, H. H. Funke, and J. Keinz, "Improvement study for the dry-low-NO x hydrogen micromix combustion technology," *Propuls. Power Res.*, vol. 4, no. 3, pp. 132–140, 2015, doi: 10.1016/j.jppr.2015.07.003.

[65] H. H. W. Funke *et al.*, "Experimental and numerical study on optimizing the dry low NOx micromix hydrogen combustion principle for industrial gas turbine applications," *J. Therm. Sci. Eng. Appl.*, vol. 9, no. 2, pp. 1–10, 2017, doi: 10.1115/1.4034849.

[66] A. Haj Ayed, K. Kusterer, H. H. W. Funke, J. Keinz, C. Striegan, and D. Bohn, "Experimental and numerical investigations of the dry-low-NOx hydrogen micromix combustion chamber of an industrial gas turbine," *Propuls. Power Res.*, vol. 4, no. 3, pp. 123–131, 2015, doi: 10.1016/j.jppr.2015.07.005.

[67] J. Ziemann *et al.*, "Low-NOx combustors for hydrogen fueled aero engine," *Int. J. Hydrogen Energy*, vol. 23, no. 4, pp. 281–288, 1998, doi: 10.1016/s0360-3199(97)00054-2.

[68] A. H. Ayed, K. Kusterer, H. H. W. Funke, J. Keinz, and D. Bohn, "CFD based exploration of the dry-low-NOx hydrogen micromix combustion technology at increased energy densities," *Propuls. Power Res.*, vol. 6, no. 1, pp. 15–24, 2017, doi: 10.1016/j.jppr.2017.01.005.

[69] A. H. Ayed *et al.*, "Numerical study on increased energy density for the DLN Micromix hydrogen combustion principle," *Proc. ASME Turbo Expo*, vol. 4A, no. x, pp. 1–12, 2014, doi: 10.1115/GT2014-25848.

[70] T. Weydahl, M. Poyyapakkam, M. Seljeskog, and N. E. L. Haugen, "Assessment of existing H2/O2 chemical reaction mechanisms at reheat gas turbine conditions," *Int. J. Hydrogen Energy*, vol. 36, no. 18, pp. 12025–12034, 2011, doi: 10.1016/j.ijhydene.2011.06.063.

[71] T. Tura, "Development and Testing of a Comprehensive Chemical Mechanism for," 2001.

[72] M. A. Mueller, T. J. Kim, R. A. Yetter, and F. L. Dryer, "Flow reactor studies and kinetic modeling of the H2/O2 reaction," *Int. J. Chem. Kinet.*, vol. 31, no. 2, pp. 113–125, 1999, doi: 10.1002/(SICI)1097-4601(1999)31:2<113::AID-KIN5>3.0.CO;2-0.

[73] N. Marinov, "DETAILED AND GLOBAL CHEMICAL KINETICS MODEL FOR," *Transp. Phenom. ...*, no. October, 1996, [Online]. Available: https://books.google.com/books?hl=en&lr=&id=75moKYUYmPcC&oi=fnd&pg=PA118&dq=IMPORTANCE+CHEMICAL+KINETICS&ots=ok9W-kMT3Y&sig=xA8LanYuHWX5BBnpK3yU3tFZNZU

[74] M. Ó Conaire *et al.*, "A comprehensive modeling study of hydrogen oxidation," *Int. J. Chem. Kinet.*, vol. 36, no. 11, pp. 603–622, 2004, doi: 10.1002/kin.20036.

[75] J. Li, Z. Zhao, A. Kazakov, and F. L. Dryer, "An updated comprehensive kinetic model of hydrogen combustion," *Int. J. Chem. Kinet.*, vol. 36, no. 10, pp. 566–

575, 2004, doi: 10.1002/kin.20026.

[76] J. Ströhle and T. Myhrvold, “An evaluation of detailed reaction mechanisms for hydrogen combustion under gas turbine conditions,” *Int. J. Hydrogen Energy*, vol. 32, pp. 125–135, 2007, doi: 10.1016/j.ijhydene.2006.04.005.

[77] G. Del Álamo, F. A. Williams, and A. L. Sánchez, “Hydrogen-oxygen induction times above crossover temperatures,” in *Combustion Science and Technology*, 2004, vol. 176, no. 10, pp. 1599–1626. doi: 10.1080/00102200490487175.

[78] G. Balakrishnan, M. D. Smooke, and F. A. Williams, “A numerical investigation of extinction and ignition limits in laminar nonpremixed counterflowing hydrogen-air streams for both elementary and reduced chemistry,” *Combust. Flame*, vol. 102, no. 3, pp. 329–340, 1995, doi: 10.1016/0010-2180(95)00031-Z.

[79] Z. Hong, D. F. Davidson, and R. K. Hanson, “An improved H2/O2 mechanism based on recent shock tube/laser absorption measurements,” *Combust. Flame*, vol. 158, no. 4, pp. 633–644, Apr. 2011, doi: 10.1016/j.combustflame.2010.10.002.

[80] A. A. Konnov, “Remaining uncertainties in the kinetic mechanism of hydrogen combustion,” *Combust. Flame*, vol. 152, no. 4, pp. 507–528, 2008, doi: 10.1016/j.combustflame.2007.10.024.

[81] J. LI, Z. ZHAO, A. KAZAKOV, F. L. D. MARCOS CHAOS, and J. JAMES J. SCIRE, “A comprehensive kinetic mechanism for CO, CH2O, and CH3OH combustion,” *Int. J. Chem. Kinet.*, vol. Vol.39, no. 3, pp. 109–136, 2007, doi: 10.1002/kin.

[82] I. G. Zsély, J. Zádor, and T. Turányi, “Uncertainty analysis of updated hydrogen and carbon monoxide oxidation mechanisms,” *Proc. Combust. Inst.*, vol. 30, no. 1, pp. 1273–1281, 2005, doi: 10.1016/j.proci.2004.08.172.

[83] R. A. YETTER, F. L. DRYER, and H. RABITZ, "Flow Reactor Studies of Carbon Monoxide/Hydrogen/ Oxygen Kinetics," *Combust. Sci. Technol.*, vol. 79, no. 1–3, pp. 129–140, 1991, doi: 10.1080/00102209108951760.

[84] C. Olm *et al.*, "Comparison of the performance of several recent hydrogen combustion mechanisms," *Combust. Flame*, vol. 161, no. 9, pp. 2219–2234, 2014, doi: 10.1016/j.combustflame.2014.03.006.

[85] A. Kéromnès *et al.*, "An experimental and detailed chemical kinetic modeling study of hydrogen and syngas mixture oxidation at elevated pressures," *Combust. Flame*, vol. 160, no. 6, pp. 995–1011, 2013, doi: 10.1016/j.combustflame.2013.01.001.

[86] T. Varga *et al.*, "Optimization of a hydrogen combustion mechanism using both direct and indirect measurements," *Proc. Combust. Inst.*, vol. 35, no. 1, pp. 589–596, 2015, doi: 10.1016/j.proci.2014.06.071.

[87] D. Miller and M. Frenklach, "Sensitivity analysis and parameter estimation in dynamic modeling of chemical kinetics," *Int. J. Chem. Kinet.*, vol. 15, no. 7, pp. 677–696, 1983, [Online]. Available: https://doi.org/10.1002/kin.550150709

[88] T. Turányi *et al.*, "Determination of rate parameters based on both direct and indirect measurements," *Int. J. Chem. Kinet.*, vol. 44, no. 5, pp. 284–302, 2012, doi: 10.1002/kin.20717.

[89] M. Ilbas, I. Yilmaz, T. N. Veziroglu, and Y. Kaplan, "Hydrogen as burner fuel: Modelling of hydrogen-hydrocarbon composite fuel combustion and NOx formation in a small burner," *Int. J. Energy Res.*, vol. 29, no. 11, pp. 973–990, 2005, doi: 10.1002/er.1104.

[90] M. G. Michaud, P. R. Westmoreland, and A. S. Feitelberg, "Chemical mechanisms of NOx formation for gas turbine conditions," *Symp. Combust.*, vol. 24, no. 1, pp. 879–887, 1992, doi: 10.1016/S0082-0784(06)80105-0.

[91] A. Frassoldati, T. Faravelli, and E. Ranzi, "A wide range modeling study of NOx formation and nitrogen chemistry in hydrogen combustion," *Int. J. Hydrogen Energy*, vol. 31, no. 15, pp. 2310–2328, 2006, doi: 10.1016/j.ijhydene.2006.02.014.

[92] R. C. Steele, A. C. Jarrett, P.C.Malte, J.H. Tonouchi, and D. G. Nicol, "VARIABLES AFFECTING NOx FORMATION IN LEAN-PREMIXED COMBUSTION," 2018.

[93] T. Nakata, M. Sato, T. Ninomiya, T. Abe, S. Mandai, and N. Sato, "Experimental evaluation of a low NOx LBG combustor using bypass air," in *Proceedings of the ASME Turbo Expo*, 1990, vol. 3, no. June 1990. doi: 10.1115/90-GT-380.

[94] A. H. Lefebvre, "The Role of Fuel Preparation in Low-Emission Combustion," *J. Eng. Gas Turbines Power*, vol. 117, no. 4, pp. 617–654, Oct. 1995, doi: 10.1115/1.2815449.

[95] D. Anderson, "EFFECTS OF EQUIVALENCE RATIO AND DWELL TIME ON EXHAUST EMISSIONS FROM AN EXPERIMENTAL PREMIXING PREVAPORIZING BURNER.," in *American Society of Mechanical Engineers (Paper)*, 1975, vol. 75, no. 75-GT-69.

[96] S. J. Lee, J. G. Yun, H. M. Lee, J. Y. Kim, J. H. Yun, and J. G. Hong, "Dependence of n2o/no decomposition and formation on temperature and residence time in thermal reactor," *Energies*, vol. 14, no. 4, 2021, doi: 10.3390/en14041153.

[97] T. Rutar, D. C. Horning, J. C. Y. Lee, and P. C. Malte, "NOx Dependency on Residence Time and Inlet Temperature for Lean-Premixed Combustion in Jet-Stirred Reactors," Jun. 1998. doi: 10.1115/98-GT-433.

[98] C. P. Fenimore, "Formation of nitric oxide in premixed hydrocarbon flames," *Symp. Combust.*, vol. 13, no. 1, pp. 373–380, 1971, doi: 10.1016/S0082-

0784(71)80040-1.

[99] T. D. Canonsburg, *ANSYS Fluent Theory Guide*, vol. 15317, no. November. 2013. [Online]. Available: http://www.afs.enea.it/project/neptunius/docs/fluent/html/th/main_pre.htm

[100] J. A. Miller and C. T. Bowman, "Mechanism and modeling of nitrogen chemistry in combustion," *Prog. Energy Combust. Sci.*, vol. 15, no. 4, pp. 287–338, Jan. 1989, doi: 10.1016/0360-1285(89)90017-8.

[101] R. P. LINDSTEDT, F. C. LOCKWOOD, and M. A. SELIM, "Detailed Kinetic Modelling of Chemistry and Temperature Effects on Ammonia Oxidation," *Combust. Sci. Technol.*, vol. 99, no. 4–6, pp. 253–276, Sep. 1994, doi: 10.1080/00102209408935436.

[102] Y. B. Zeldovich and J. Zeldovich, "The oxidation of nitrogen in combustion and explosions," *Eur. Phys. J. A. Hadron. Nucl.*, vol. 21, pp. 577–628, 1946, doi: https://doi.org/10.1515/9781400862979.364.

[103] C. Duynslaegher, H. Jeanmart, and J. Vandooren, "Ammonia combustion at elevated pressure and temperature conditions," *Fuel*, vol. 89, no. 11, pp. 3540–3545, 2010, doi: 10.1016/j.fuel.2010.06.008.

[104] C. Duynslaegher, F. Contino, J. Vandooren, and H. Jeanmart, "Modeling of ammonia combustion at low pressure," *Combust. Flame*, vol. 159, no. 9, pp. 2799–2805, Sep. 2012, doi: 10.1016/j.combustflame.2012.06.003.

[105] J. Li, H. Huang, N. Kobayashi, C. Wang, and H. Yuan, "Numerical study on laminar burning velocity and ignition delay time of ammonia flame with hydrogen addition," *Energy*, vol. 126, no. x, pp. 796–809, 2017, doi: 10.1016/j.energy.2017.03.085.

[106] Ø. Skreiberg, P. Kilpinen, and P. Glarborg, "Ammonia chemistry below 1400 K

under fuel-rich conditions in a flow reactor," *Combust. Flame*, vol. 136, no. 4, pp. 501–518, Mar. 2004, doi: 10.1016/j.combustflame.2003.12.008.

[107] Z. Tian, Y. Li, L. Zhang, P. Glarborg, and F. Qi, "An experimental and kinetic modeling study of premixed NH3/CH4/O2/Ar flames at low pressure," *Combust. Flame*, vol. 156, no. 7, pp. 1413–1426, Jul. 2009, doi: 10.1016/j.combustflame.2009.03.005.

[108] T. Mendiara and P. Glarborg, "Ammonia chemistry in oxy-fuel combustion of methane," *Combust. Flame*, vol. 156, no. 10, pp. 1937–1949, Oct. 2009, doi: 10.1016/j.combustflame.2009.07.006.

[109] H. Nozari and A. Karabeyoğlu, "Numerical study of combustion characteristics of ammonia as a renewable fuel and establishment of reduced reaction mechanisms," *Fuel*, vol. 159, pp. 223–233, Nov. 2015, doi: 10.1016/j.fuel.2015.06.075.

[110] A. A. Konnov, "Implementation of the NCN pathway of prompt-NO formation in the detailed reaction mechanism," *Combust. Flame*, vol. 156, no. 11, pp. 2093–2105, 2009, doi: 10.1016/j.combustflame.2009.03.016.

[111] R. Li, A. A. Konnov, G. He, F. Qin, and D. Zhang, "Chemical mechanism development and reduction for combustion of NH3/H2/CH4 mixtures," *Fuel*, vol. 257, no. June, p. 116059, 2019, doi: 10.1016/j.fuel.2019.116059.

[112] O. Mathieu and E. L. Petersen, "Experimental and modeling study on the high-temperature oxidation of Ammonia and related NOx chemistry," *Combust. Flame*, vol. 162, no. 3, pp. 554–570, 2015, doi: 10.1016/j.combustflame.2014.08.022.

[113] H. Xiao, A. Valera-Medina, and P. J. Bowen, "Modeling Combustion of Ammonia/Hydrogen Fuel Blends under Gas Turbine Conditions," *Energy and Fuels*, vol. 31, no. 8, pp. 8631–8642, 2017, doi:

10.1021/acs.energyfuels.7b00709.

[114] Y. Zhang, O. Mathieu, E. L. Petersen, G. Bourque, and H. J. Curran, "Assessing the predictions of a NOx kinetic mechanism on recent hydrogen and syngas experimental data," *Combust. Flame*, vol. 182, no. x, pp. 122–141, 2017, doi: 10.1016/j.combustflame.2017.03.019.

[115] H. Huitenga and E. R. Norster, "Development Approach to the Dry Low Emission Combustion System of," in *ASME Turbo Expo 2014: Turbine Technical Conference and Exposition*, 2014, pp. 1–10. [Online]. Available: https://doi.org/10.1115/GT2014-25164

[116] T. Nurettin, A. Mitsugu, A. Horikawa, and F. Harald, "Enhancement of fuel flexibility of industrial gas turbines by development of innovative hydrogen combustion stystem," *REPORTS Gas Turbines*, vol. gas for en, no. 2, pp. 18–22, 2018.

[117] G. Lopez-Ruiz, I. Alava, and J. M. Blanco, "Study on the feasibility of the micromix combustion principle in low NOx H2 burners for domestic and industrial boilers: A numerical approach," *Energy*, vol. 236, p. 121456, 2021, doi: 10.1016/j.energy.2021.121456.

[118] A. Haj Ayed, "Numerical Characterization and Development of the Dry Low NOx High Hydrogen Content Fuel Micromix Combustion for Gas Turbine Applications," *PhD Thesis*, no. March 2017, pp. 1–14, 2017.

[119] P. Kosky, R. Balmer, W. Keat, and G. Wise, "Chapter 7 - Chemical Engineering," in *Exploring Engineering*, Fifth., 2021, p. Pages 129-145.

[120] I. Sadrehaghighi, "Unstructured Meshing for CFD," 1993.

[121] F. Galeazzo, G. Donnert, P. Habisreuther, N. Zarzalis, R. Valdes, and W. Krebs, "Measurement and Simulation of Turbulent Mixing in a Jet in Crossflow," 2021.

doi: 10.1115/GT2010-22709.

[122] M. P. Burke, M. Chaos, Y. Ju, F. L. Dryer, and S. J. Klippenstein, "Comprehensive H 2/O 2 kinetic model for high-pressure combustion," *Int. J. Chem. Kinet.*, vol. 44, no. 7, pp. 444–474, 2012, doi: 10.1002/kin.20603.

[123] X. Li, X. You, F. Wu, and C. K. Law, "Uncertainty analysis of the kinetic model prediction for high-pressure H2/CO combustion," *Proc. Combust. Inst.*, vol. 35, no. 1, pp. 617–624, 2015, doi: 10.1016/j.proci.2014.07.047.

[124] H. H. W. Funke, N. Beckmann, and S. Abanteriba, "An overview on dry low NO x micromix combustor development for hydrogen-rich gas turbine applications," *Int. J. Hydrogen Energy*, vol. 44, no. 13, pp. 6978–6990, 2019, doi: 10.1016/j.ijhydene.2019.01.161.

[125] E. Recker and W. Bosschaerts, "Experimental study of a round jet in cross-flow at low momentum ratio," *15th Int Symp Appl. Laser Tech. to Fluid Mech.*, vol. 1, no. x, pp. 5–8, 2010, [Online]. Available: http://files.instrument.com.cn/FilesCenter/20120406/201246114555/1671_wrcwsy_3.2.3.Full_1671.pdf%5Cnhttp://ltces.dem.ist.utl.pt/LXLASER/LXLASER2010/upload/1671_wrcwsy_3.2.3.Full_1671.pdf

[126] J. Berger, "Scaling of an Aviation Hydrogen Micromix Injector Design for Industrial GT Combustion Applications," *Aerotec. Missili Spaz.*, vol. 100, no. 3, pp. 239–251, 2021, doi: 10.1007/s42496-021-00091-5.

[127] C. Devriese, S. Snijders, W. De Paepe, and R. Bastiaans, "The Design and Optimisation of a 100% Hydrogen Micro Gas Turbine Micromix Combustor: Preliminary Hydrogen Injection Depth Characterisation Using Cold Flow Steady RANS," pp. 1–10, 2022, doi: 10.1115/gt2022-80805.

[128] E. Yamada, M. Shinoda, H. Yamashita, and K. Kitagawa, "Experimental and numerical analyses of magnetic effect on OH radical distribution in a hydrogen-

oxygen diffusion flame," *Combust. Flame*, vol. 135, no. 4, pp. 365–379, 2003, doi: 10.1016/j.combustflame.2003.08.005.

[129] Z. S. Li, B. Li, Z. W. Sun, X. S. Bai, and M. Aldén, "Turbulence and combustion interaction: High resolution local flame front structure visualization using simultaneous single-shot PLIF imaging of CH, OH, and CH2O in a piloted premixed jet flame," *Combust. Flame*, vol. 157, no. 6, pp. 1087–1096, 2010, doi: 10.1016/j.combustflame.2010.02.017.

[130] C. S. Mørch, A. Bjerre, M. P. Gøttrup, S. C. Sorenson, and J. Schramm, "Ammonia/hydrogen mixtures in an SI-engine: Engine performance and analysis of a proposed fuel system," *Fuel*, vol. 90, no. 2, pp. 854–864, 2011, doi: 10.1016/j.fuel.2010.09.042.

[131] A. J. Reiter and S. C. Kong, "Combustion and emissions characteristics of compression-ignition engine using dual ammonia-diesel fuel," *Fuel*, vol. 90, no. 1, pp. 87–97, 2011, doi: 10.1016/j.fuel.2010.07.055.

[132] S. M. Grannell, D. N. Assanis, S. V. Bohac, and D. E. Gillespie, "The fuel mix limits and efficiency of a stoichiometric, ammonia, and gasoline dual fueled spark ignition engine," *J. Eng. Gas Turbines Power*, vol. 130, no. 4, pp. 1–8, 2008, doi: 10.1115/1.2898837.

[133] C. Zamfirescu and I. Dincer, "Using ammonia as a sustainable fuel," *J. Power Sources*, vol. 185, no. 1, pp. 459–465, 2008, doi: 10.1016/j.jpowsour.2008.02.097.

[134] A. Hayakawa, T. Goto, R. Mimoto, Y. Arakawa, T. Kudo, and H. Kobayashi, "Laminar burning velocity and Markstein length of ammonia/air premixed flames at various pressures," *Fuel*, vol. 159, pp. 98–106, 2015, doi: 10.1016/j.fuel.2015.06.070.

[135] K. Bioche, L. Bricteux, A. Bertolino, A. Parente, and J. Blondeau, "Large Eddy

Simulation of rich ammonia/hydrogen/air combustion in a gas turbine burner," *Int. J. Hydrogen Energy*, vol. 46, no. 79, pp. 39548–39562, 2021, doi: 10.1016/j.ijhydene.2021.09.164.

[136] G. B. Ariemma, G. Sorrentino, R. Ragucci, M. de Joannon, and P. Sabia, "Ammonia/Methane combustion: Stability and NOx emissions," *Combust. Flame*, vol. 241, no. x, p. 112071, Jul. 2022, doi: 10.1016/j.combustflame.2022.112071.

[137] M. Ilbas, O. Kumuk, and S. Karyeyen, "Numerical study of a swirl gas turbine combustor for turbulent air and oxy-combustion of ammonia/kerosene fuels," *Fuel*, vol. 304, no. June, p. 121359, Nov. 2021, doi: 10.1016/j.fuel.2021.121359.

[138] H. H.-W. Funke *et al.*, "Experimental and Numerical Characterization of the Dry Low NOx Micromix Hydrogen Combustion Principle at Increased Energy Density for Industrial Hydrogen Gas Turbine Applications," in *Volume 1A: Combustion, Fuels and Emissions*, Jun. 2013, no. X, pp. 1–10. doi: 10.1115/GT2013-94771.